STUDIES ON $SiO_2\text{-}BaO\text{-}ZnO\text{-}(M_2O_3)_x\text{-}(B_2O_3)_{1-x}$ (M= Al, Mn, Y, La) BASED GLASS SEALANTS

A
THESIS
SUBMITTED FOR THE AWARD OF THE DEGREE OF

DOCTOR OF PHILOSOPHY

BY

ANU ARORA

SCHOOL OF PHYSICS AND MATERIALS SCIENCE
THAPAR UNIVERSITY
PATIALA-147004
INDIA
April 2009

CERTIFICATE

This is to certify that the thesis entitled **"Studies on SiO_2-BaO-ZnO-$(M_2O_3)_x$-$(B_2O_3)_{1-x}$ (M= Al, Mn, Y, La) Based Glass Sealants"** which is being submitted by Ms. Anu Arora in fulfillment of the requirements for the award of the degree of Doctor of Philosophy in the School of Physics & Materials Science, Thapar University, Patiala, is a record of candidate's own work carried out by her under our supervision and guidance. The matter presented in this thesis has not been submitted in part or full for the award of any degree in any other University or Institute.

Date: 7/4/09

Place: Patiala

Dr. O.P.Pandey
Professor & Head
School of Physics & Materials Science
Thapar University
Patiala-147004 (INDIA)

Dr. Kulvir Singh
Assistant Professor
School of Physics & Materials Science
Thapar University
Patiala-147004 (INDIA)

ACKNOWLEDGEMENTS

At this momentous occasion of binding my thesis I would like to acknowledge the contribution of all those benevolent people, I have been blessed to associate with. Behind every student, there stand a myriad of people whose help and contribution makes things successful. Since such a list can be a prohibitively long, I may be excused for any omissions. My first and foremost offering of thanks goes to my supervisors **Dr. O. P. Pandey** (Prof. & Head) and **Dr. Kulvir Singh** (Astt. Prof.) for providing me a chance to work under their guidance and supervision, assisting with all kinds of support and inspiration, wide counsel, constant encouragement, sincere criticism, valuable suggestions, expertise and fruitful advice which they proffered throughout this investigation and preparation of the thesis.

I am profound obliged to **Prof. K.K. Raina**, School of Physics and Materials Science and presently, Deputy Director, Thapar University, Patiala for his constant encouragement and needful help during various stages of the work.

I am very thankful to **Prof. N. K. Verma**, former Head, School of Physics and Materials Science for his whole hearted support and blessings.

My special thanks to **Prof. J.M.F. Ferriera** and his student **Ashutosh Goel** for the help they provided in getting some of our characterizations done. I am also thankful to **Dr. E. R. Shaaban** for mathematical modeling of differential thermal curves.

I am highly obliged to **Dr. Puneet Sharma** and **Dr. Pankaj Kumar** for their insightful and helpful assistance, comments and views.

Words are inadequate in expressing my sincere thanks to my friend **Mr. Vishal Kumar** for his support in every moment of difficulty. His skills, fruitful discussion, constructive suggestions and constant inspiration in this work helped me to fulfil this effort.

I would also like to give my thanks to Research Scholars **Kamalpreet Kaur, Jasmeet Kaur, Manoj Kumar, Shefali Kanwar, Zinki Jindal, Akshay Kumar, Sanjeev Kumar, Ravi Shukla and Bhupinder Kaur** for their kind help and valuable suggestions whenever I needed. I am grateful to Materials Science & Engineering program students **Sarita Sharma, Indu Bala, Vishal Sharma, Alok Jain, Sanjay Kumar and Yousuf Pathan** for providing me a friendly atmosphere and encouraging me throughout this research.

My special thanks to **Mr. Indermani Kumar, Mr. Jant Singh, Mr. Purushottam** and **Mr. V. Kothari** for providing all kind of help for creating a healthy environment.

All the faculties and staff of School of Physics and Materials Science are acknowledged who never turn me down whenever I approached for any help.

I would also like to acknowledge **Mr. C.P. Khatter**, Director MSME, Jalandhar for providing all possible technical help during course of investigation

My husband **Mr. Yogender Arora** and **my family** deserve the special thanks and great appreciation for their patience, persistent moral support and capability to rejuvenate me during the course of the Ph.D. work at each step. Their faith made me confident at every time.

Last but not least my father **Mr. Satish Kumar** and my mother **Mrs. Sanjeev Arora** are the two guiding pillars of my success. Especially my father whose constant motivation and financial assistance during thick and thin has been the sole source of inspiration and strength to carry on my work.

Above all, hidden force by **Almighty God** steered me in the right direction to achieve the goal.

(Anu Arora)

CONTENTS

LIST OF FIGURES

Page No.

Chapter 1

Chapter 2

Chapter 3

Chapter 4

Chapter 5

LIST OF TABLES

Page No.

Chapter 1

Chapter 2

Chapter 3

Chapter 4

Chapter 5

PUBLICATIONS

1. Non-isothermal crystallization kinetics of ZnO-BaO-B_2O_3-SiO_2 glass, **Anu Arora**, E.R. Shaaban, K. Singh and O.P. Pandey, Journal of Non-Crystalline Solids, 354 (33), p.3944-3951, Sep 2008.

2. Crystallization kinetics of BaO-ZnO-Al_2O_3-B_2O_3-SiO_2 glass, **Anu Arora**, A. Goel, E.R. Shaaban, K. Singh, O.P. Pandey and J.M.F Ferreira, Physica B: Condensed Matter, 403 (10), p.1738-1746, May 2008.
3. Studies on thermal and structural properties of glasses as sealants for solid oxide fuel cells, Vishal Kumar, **Anu Arora**, O.P. Pandey and K. Singh, International Journal of Hydrogen Energy, 33 (1), p.434-438, Jan 2008.
4. Studies on thermal and structural properties of glasses as sealants for solid oxide fuel cells, Vishal Kumar, **Anu Arora**, O.P. Pandey and K. Singh, International Workshop on Hydrogen Energy, University of Rajasthan, Jaipur, Nov 2006.
5. Solid Oxide Fuel Cell: An Overview, Vishal Kumar, **Anu Arora**, O.P.Pandey and K. Singh, National seminar on Physics & Society, NREC College, Khurja, U.P., India, p. 23, 2006.
6. Thermal behaviour of SiO_2-BaO-ZnO-B_2O_3 glass, **Anu Arora**, Vishal Kumar, K. Singh and O.P.Pandey, National conference of emerging trends in engineering materials, Thapar University, Patiala, Feb 2007.
7. Influence of Y_2O_3 on structural and thermal properties of SiO_2-BaO-ZnO based glass systems (communicated in Acta Materialia).
8. Thermal, structural and crystallization kinetics of ZnO-BaO-SiO_2-Mn_2O_3 based glass sealants for solid oxide fuel cells (communicated in Journal of Non Crystalline Solids).

PREFACE

The search of alternate energy source has led to development of secondary energy generating units. Among these, fuel cell is one, which is in demand to supply energy at source. Depending upon need and requirement, several types of fuel cells have been developed.

Based on electrolyte used, fuel cells have been categorized in five different categories. Among these solid oxide fuel cell (SOFC) has a number of advantages when compared with other categories of fuel cells (environmentally friendly, fuel flexibility, cost effectiveness and higher efficiency). Apart from these the corrosion problem in SOFC is reduced to minimum extent because of the use of ceramic solid-phase electrolyte. On the other hand, SOFC has number of disadvantages like high operating temperature (800^oC-1000^oC) and because of this there is less capability with other components used in SOFC. The current need is to lower the operating temperature (550^oC-850^oC) of SOFC. SOFC consists of electrodes, electrolyte, interconnect and sealant as its components. Among the four designs of SOFC the flat plate and tubular design have been studied in detail because of its better properties as compared to segmented-cell-in-series and monolithic design. As is evident from the name, sealless tubular design needs no seals; therefore, the problems with the gastight seals for ceramics at high temperatures are eliminated. The disadvantage of sealless tubular design is that it has relatively long current path through the cell, resulting in greater resistive loss. On the other hand the flat-plate design offers simpler fabrication and in plane conduction. However, the need of effective and high temperature seal to prevent the fuel leakage and air mixing is the urgent requirement of the planar design. The present study is done on sealant as it is important part of SOFC which is used to seal all components of SOFC. In other words it comes in direct contact with all the other components of SOFC. The purpose of sealing is to separate fuel gases from oxidizing gases at SOFC operating temperature.

There are three general categories of joining process viz. mechanical (through the mechanical interlocking of components), direct bonding (in which components are bonded by solid-state process) and indirect joining. The rigid bonding technique has some advantages as compared to others as our requirement is minimization of device weight and volume, so rigid seals are good choice. Glass and glass-ceramics are used as rigid sealants. However, these glass sealants when used at higher temperature fail at several occasions. There are several ways in which a rigid seal can fail during operation e.g. failure by fracture under pressure, failure during rapid thermal cycling and failure upon thermal aging. These failures occur because of variation in coefficient of thermal expansion in glasses. The variation occurs due to nucleation of certain phases in the matrix of glass. Despite of these problems, glasses and glass-ceramics have been focused as the potential sealing materials with major emphasis on alkaline earth aluminosilicates, borosilicates, and lanthanide alumino borosilicates.

The present study focuses on development of suitable glass material for SOFC application, which can act as a good sealant and have compatibility with the other components of SOFC. In order to fulfill the desired requirement for glass to be used as a sealing material, a glass series SiO_2-BaO-ZnO-$(M_2O_3)_x$-$(B_2O_3)_{1-x}$ (M= Al, Mn, Y, La) where x= 0, 0.25, 0.5, 1 has been selected. Glasses of above mentioned series were synthesized using different stoichiometric compositions of constituent oxides. Various experiments were performed to check their suitability. The study includes the development of glasses, their characterization, heat-treatment and study of crystallization kinetics for various phases formed during heat treatment and their compatibility with the other components like interconnect and electrolyte of SOFC.

Chapter 1 describes the introduction about various categories of fuel cells, their properties and in particular the properties of SOFC. The different constituents of SOFC are also described in detail and a comparison between tubular and planar design of SOFC is given. This chapter also describes the properties of glasses which are used as sealant materials for the other components of fuel cell. The properties of different series of glasses like thermal expansion coefficient which should be in matching with all the other components are discussed in detail. After reviewing the work of different authors and considering the fact that glass and glass-ceramics offer better properties to be used as sealants as their bonding with other components the SOFC is better, selection criteria for selecting this glass series is explained.

Chapter 2 presents a detailed literature review on SOFC seals. Factors affecting nucleation and growth of different phases, development of microstructure, transition temperature, formation, and suppression of various phases formed by adding different constituents and nucleating agents have been described. Also the role of different nucleating agents like TiO_2 which suppresses the formation of cordierite phase, which is detrimental for SOFC because of its very low TEC value is discussed. Similarly, the effect of B_2O_3/SiO_2 ratio is described in detail as it is very dominating factor in achieving glass transition temperature.

Chapter 3 gives the experimental techniques used to synthesize the glass series of different stoichiometric composition by conventional melt quenching technique. Homogeneous mixtures of different oxide constituents were melted in a high resistance heating furnace using high purity alumina crucibles. The glass so obtained was characterized through XRD to check its glassy structure i.e. to confirm its amorphous nature. Then these glasses were annealed and heat treated at different temperatures for 1, 10, 100 hrs and were further characterized with XRD and SEM/EDX to study the formation of crystalline phases induced during different heat treatments. The as prepared glass samples were also analyzed in DTA to know the transition temperature. TEC values and softening temperature was observed by dilatometer. The as prepared glasses were coated with silver paste and their conductivity measurement was done using two probe method. A suitable join of glass powder with commercially available interconnect (Crofer 22 APU) and electrolyte (bismuth vanadate) was made. The entire mass was heat treated for 100 hrs at 800 ^{o}C to see its reactivity with the components used in SOFC. This heterogeneous junction was analyzed under SEM to observe the reactivity of glass.

Chapter 4 describes the results and discussion of the study done for these glasses. Based on less percentage weight loss in glass samples during TGA analysis four glass samples out of seventeen samples where chosen for detailed investigation. This includes alumina series sample with composition $40SiO_2$-$30BaO$-$20ZnO$-$2.5B_2O_3$-$7.5Al_2O_3$ and lanthanum series sample with composition $40SiO_2$-$30BaO$-$20ZnO$-$2.5B_2O_3$-$7.5La_2O_3$. Variations in their microstructures and phase formation with thermal aging are discussed in detail. Further, these glasses are characterized by DTA and shift of their transition temperature value with heating rate is discussed. A value of TEC obtained by dilatometer is given. Resistivity values obtained by two probe set up is tabulated and has been confirmed that its value lies in MΩ range. On the similar track, glass with composition $40SiO_2$-$30BaO$-$20ZnO$-$10Mn_2O_3$ from manganese series and $40SiO_2$-$30BaO$-$20ZnO$-$5.0B_2O_3$-$5.0Y_2O_3$ from yttrium series is taken and the above discussed analysis was again done on these two glass samples.

Chapter 5 describes the detailed discussion on the interaction study among the lanthanum and yttrium doped glass samples with interconnect (Crofer 22 APU); electrolyte (bismuth vanadate) during thermal aging for 100 hrs at 800 ^{o}C. SEM study of these heat treated samples is done in detail and due to thermal aging the various effects on all the three surfaces is discussed. The interaction among other components of SOFC is studied. After taking commercially used 8YSZ (electrolyte) the XRD study of yttrium doped sample is done. The formation of different phases during this heat treatment is analyzed and discussed.

Chapter 6 concludes the entire work done and highlights the important interpretations of the experimental results. Highly fascinating results have opened a new vista for us to carry on this work further.

Chapter 1

SOLID OXIDE FUEL CELL: AN INTRODUCTION

Overview

This chapter reviews the history and origin of glass forming. It describes different methods of glass preparation starting from ancient civilizations to modern age describing new scientific methods. The application of glass as a promising sealing material for solid oxide fuel cell is described. In this chapter various categories of fuel cells, their properties and in particular the properties of SOFC are discussed in detail. The various components of SOFC have been described along with different types of sealing techniques. This chapter elaborates the reason for selecting glass as a sealing material over other prevalent sealing techniques.

1.1 Introduction to Glasses

The history of glass is quite old. Glass was formed naturally from common elements in the earth's crust long before anyone ever thought of experimenting with its composition, molding to give it shape or putting it to the myriad of uses that it enjoys in the world today. Obsidian was the first naturally occurring combination of oxides fused by intense volcanic heat and vitrified (made into glass) by rapid air-cooling.

Humans have been producing glasses by melting of raw materials for thousands of years. "Faience" was the first synthetic glass made by the Egyptians who molded figurines from sand (SiO_2). They coated them with natron, the residue left by the flooding nile river which was composed of calcium carbonate ($CaCO_3$), soda ash (Na_2CO_3), salt (NaCl) and copper oxide (CuO). Heating below $1000^{o}C$ produced a glassy coating by the diffusion of the fluxes, CaO and Na_2O into the sand and their subsequent solid-state reaction with the sand. The copper oxide gave the article an appealing blue colour.

Apart from Egyptians, Romans also did lot of work to spread the glass making technology. They developed varieties of glasses for different applications. During 15th century, the first clear glass called "cristallo" was developed in Venice. In 1675, George Ravenscroft invented lead crystal glass by adding lead oxide to venetian glass of high refractive index.

German scientist Otto Schott (1851-1935) did systematic study to see the effects of different chemical elements on the optical and thermal properties of glass. Towards the end of 19th century, Michael Owens (1859-1923), an American engineer invented an automatic bottle blowing machine which led to wide spread applications of glasses. The development of flat glass (1905), sheet glass (1914), float process (1959) have further enhanced the applicability of glasses.

Today glass making in hi-tech industry has acquired a position in the global market where quality, design and service levels are of high standard. Glasses have become part of our life as they feature in almost every aspect of lives starting from homes, cars, drinking bottle, eating plates, packing of wires, sprit, bears, medicines, cooking ware, laboratory apparatus, cosmetics, and foodstuffs. These widespread applications are because of the environment friendly and its ability to be recycled.

Despite of all these applications its brittle nature and poor thermal properties have compelled the scientific community to develop specific glasses by selecting different ingredients to achieve better thermal expansion coefficient (TEC) to make them suitable material for several devices.

One of the possible applications of glasses is as sealing material in solid oxide fuel cell where it is used to seal different components of solid oxide fuel cell. In order to understand the need and properties required for a glass to be used as seal it is essential to have a description of different types of solid oxide fuel cell and their components and most importantly the role of these components to produce electricity which is described in subsequent sections.

1.2 Fuel Cell

The steady depletion of the world's limited fossil fuel reserves calls for the development of new energy technology for power generation, which is more environment friendly with better efficiency. Fuel cells have been identified as one of the most promising and potential energy source, which can meet the future requirements for the energy. It has been proposed to use hydrogen as one of the energy sources to fulfill the requirement of energy. The use of hydrogen in fuel cell is considered as clean and efficient means of energy conversion device for power generation. The hydrolysis of water may generate hydrogen and oxygen. Hydrogen so produced can be used in SOFC and the byproduct oxygen can be utilized for other purposes. It is also observed that methane yields the lowest carbon-dioxide production among the hydrocarbon family of fuels due to the highest hydrogen to carbon ratio of its molecular structure. Therefore, a sustainable future energy system will include fuel cells, with hydrogen, methane and methanol derived from renewable sources, to produce electricity in areas where and in times when power is needed or electricity is in demand.

1.3 Fuel Cell vs. Battery

A fuel cell is an electrochemical device that converts chemical energy of reactants (fuel and oxidant) directly into electrical energy or in simple words fuel cell is an energy conversion device for power generation. A fuel cell can produce electric energy output for as long as the fuel and oxidant are supplied. The lifetime of fuel cell is unlimited in principle, as long as the reactants are supplied and products are removed continuously. In addition, electrodes in a fuel cell are stable during the energy conversion process. The electrodes facilitate the electrochemical reaction and keep their physical and chemical characteristics. On the other hand, a battery is an energy storage device. The maximum amount of useful energy available from a battery is determined by the amount of chemical reactants stored within the battery itself. The lifetime of battery is quite limited, often depending on the amount of reactants stored. The electrode of a battery not only participates in the electrochemical reactions producing electric energy, but also is consumed in the process. Therefore, the electrode in a battery is not stable during the energy conversion process. The lifetime of battery really depends upon the lifetime of its electrode.

However, batteries and fuel cells have a number of similarities like both are electrochemical devices, can produce electric energy directly from electrochemical reaction of fuel and oxidant and more importantly both have similar components called electrodes and electrolytes.

1.4 Working of Fuel Cell

The main function of the electrode is to promote the reaction between the fuel and the oxygen through oxidation-reduction reaction at electrode-electrolyte interfaces without being consumed or corroded. In a typical fuel cell, gaseous fuels are fed continuously to the anode (negative electrode) compartment and an oxidant (oxygen from air) is fed continuously to the cathode (positive electrode) compartment. The electrochemical reactions take place at the electrodes to produce an electric current as shown in figure 1.1. The various reactions taking place at anode and cathode are as follows:

Anode: $O_2 + 2e^- \Longrightarrow 2O^-$

Cathode: $2O^- + 2H_2 \Longrightarrow 2H_2O$

These steps are particularly true for the systems using oxide ion conducting electrolytes.

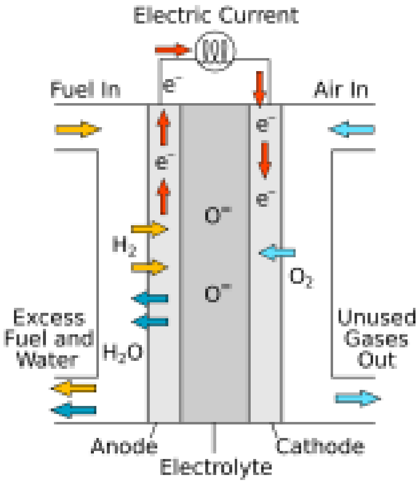

Figure 1.1: Schematic diagram of an acid electrolyte fuel cell

Overall cell reaction: $2H_2 + O_2 \Longrightarrow 2H_2O + W$

where 'W' stands for useful electric energy output from the fuel cell.

1.5 Classification of Fuel Cells

Fuel cells are primarily named by the nature of their electrolyte used. There are several types of fuel cells that are being developed for applications as small as a cellular phone (0.5 Watts) to as large as a small power plant for an industrial facility or a small town (10 Megawatts). Based on electrolyte used, fuel cells are categorized in five types [1].

- Alkaline Fuel Cells (AFC)
- Phosphoric Acid Fuel Cell (PAFC)
- Molten Carbonate Fuel Cell (MCFC)
- Solid Oxide Fuel Cell (SOFC)
- Proton or polymer Exchange Membrane Fuel Cell (PEMFC)
- Direct Methanol Fuel Cell (DMFC): It is the only fuel cell that is not categorized based on the electrolyte used; instead, it is categorized on the type of the fuel used in it.
- Regenerative Fuel Cell

1.5.1 Alkaline Fuel Cells (AFC)

Alkaline fuel cells (AFC) are one of the most developed technologies and have been used since the mid-1960s by NASA in the Apollo and Space Shuttle programs. Alkaline fuel cells use an electrolyte that is an aqueous (water-based) solution of potassium hydroxide (KOH) retained in a porous stabilized matrix. The concentration of KOH can be varied with the fuel cell operating temperature, which ranges from 65°C to 220°C. The charge carrier for an AFC is the hydroxyl ion (OH^-) that migrates from the cathode to the anode where they react with hydrogen to produce water and electrons. Water formed at the anode migrates back to the cathode to regenerate hydroxyl ions. The chemical reactions at the anode and cathode in an AFC are shown below. This set of reactions in the fuel cell produces electricity and by-product heat.

Anode Reaction: $2\,H_2 + 4\,OH^- \Rightarrow 4\,H_2O + 4\,e^-$

Cathode Reaction: $O_2 + 2\,H_2O + 4\,e^- \Rightarrow 4\,OH^-$

Overall Net Reaction: $2\,H_2 + O_2 \Rightarrow 2\,H_2O$

One characteristic of AFCs is that they are very sensitive to CO_2 that may be present in the fuel or air. The CO_2 reacts with the electrolyte, poisoning it rapidly, and severely degrading the fuel cell performance. Therefore, AFCs are limited to closed environments, such as space and undersea vehicles, and must be run on pure hydrogen and oxygen. Furthermore, molecules such as CO, H_2O and CH_4, which are harmless or even work as fuels to other fuel cells, are poisons to an AFC.

1.5.2 Phosphoric Acid Fuel Cells (PAFC)

Phosphoric Acid Fuel Cells (PAFC) were the first fuel cells developed in the mid-1960s and field-tested since the 1970s. The PAFC uses an electrolyte that is phosphoric acid (H_3PO_4) that can approach 100% concentration. The ionic conductivity of phosphoric acid is low at low temperatures, so PAFCs are operated at the upper end of the temperature range 150ºC–220ºC. The charge carrier in this type of fuel cell is the hydrogen ion (H^+, proton). The protons migrate through the electrolyte and combine with the oxygen, usually from air, at the cathode to form water. The electrons are routed through an external circuit where they can perform useful work. This set of reactions in the fuel cell produces electricity and heat as by-product.

Anode Reaction: $2\,H_2 \Rightarrow 4\,H^+ + 4\,^{e-}$

Cathode Reaction: $O_2(g) + 4\ H^+ + 4\ ^{e-} \Longrightarrow 2\ H_2O$

Overall Cell Reaction: $2\ H_2 + O_2 \Longrightarrow 2\ H_2O$

The PAFC operates at greater than 40% efficiency in generating electricity. Furthermore, at the operating temperature of PAFCs, the waste heat is capable of heating hot water or generating steam at atmospheric pressure. CO_2 does not affect the electrolyte or cell performance and can therefore be easily operated with reformed fossil fuel.

1.5.3 Molten Carbonate Fuel Cells (MCFC)

Molten Carbonate Fuel Cells (MCFC) is in the class of high-temperature fuel cells. The higher operating temperature allows them to use natural gas directly without the need for a fuel processor. Developed in the mid 1960s; improvements have been made in fabrication methods, performance and endurance. MCFCs work quite differently from other fuel cells. These cells use an electrolyte composed of a molten mixture of carbonate salts. Two mixtures are currently used: lithium carbonate and potassium carbonate, or lithium carbonate and sodium carbonate. To melt the carbonate salts and achieve high ion mobility through the electrolyte, MCFCs operate at high temperatures (650ºC). When heated to a temperature of around 650ºC, these salts melt and become conductive to carbonate ions (CO_3^{2-}). These ions flow from the cathode to the anode where they combine with hydrogen to give water, carbon dioxide and electrons. These electrons are routed through an external circuit back to the cathode, generating electricity and by-product heat.

Anode Reaction: $CO_3^{2-} + H_2 \Longrightarrow H_2O + CO_2 + 2e^-$

Cathode Reaction: $CO_2 + 1/2O_2 + 2e^- \Longrightarrow CO_3^{2-}$

Overall Cell Reaction: $H_2(g) + \frac{1}{2}O_2(g) + CO_2\ (\text{cathode}) \Longrightarrow H_2O(g) + CO_2\ (\text{anode})$

The higher operating temperature of MCFCs has both advantages and disadvantages compared to the lower temperature PAFC and PEFC. At the higher operating temperature, fuel reforming of natural gas can occur internally, eliminating the need for an external fuel processor. Additional advantages include the ability to use standard materials for construction, such as stainless steel sheet, and allow use of nickel-based catalysts on the electrodes. The by-product heat from an MCFC can be used to generate high-pressure steam that can be used in many industrial and commercial applications. The high temperatures and the electrolyte chemistry also have disadvantages. The high temperature requires significant time to reach operating conditions and responds slowly to changing power demands. These characteristics make MCFCs more suitable for constant power applications. The carbonate electrolyte can also cause electrode corrosion problems.

1.5.4 Solid Oxide Fuel Cell (SOFC)

The Solid Oxide Fuel Cell (SOFC) is currently the highest-temperature fuel cell in development and can be operated over a wide temperature range from 600ºC–1000ºC allowing a number of fuels to be used. To operate at such high temperatures, the electrolyte is a thin, solid ceramic material (solid oxide) that is conductive to oxygen ions (O^{2-}). The charge carrier in the SOFC is the oxygen ion (O^{2-}). At the cathode, the oxygen molecules from the air are split into oxygen ions with the addition of four electrons. The oxygen ions are conducted through the electrolyte and combine with hydrogen at the anode, releasing four electrons. The electrons travel an external circuit providing electric power and producing by-product heat.

Anode Reaction: $2\,H_2 + 2\,O^{2-} \Longrightarrow 2\,H_2O + 4\,e^-$

Cathode Reaction: $O_2 + 4\,e^- \Longrightarrow 2\,O^{2-}$

Overall Cell Reaction: $2\,H_2 + O_2 \Longrightarrow 2\,H_2O$

The operating efficiency in generating electricity is the highest for fuel cells (about 60%). Combining a high-temperature fuel cell with a turbine into a hybrid fuel cell further increases the overall efficiency of generating electricity with a potential of an efficiency of more than 70%. It is therefore considered to be a leading candidate for high-power applications including industrial and large-scale central-electricity generating-stations. The very high operating temperature of the SOFC has both advantages and disadvantages. The high temperature enables them to tolerate relatively impure fuels, such as those obtained from the gasification of coal or gasses from industrial process and other sources. However, the high temperature requirement brings more expensive materials for their construction.

1.5.5 Proton Exchange Membrane Fuel Cells (PEMFC)

Proton Exchange Membrane Fuel Cells (PEMFC) are believed to be the best type of fuel cell as the vehicular power source to eventually replace the gasoline and diesel internal combustion engines. First used in 1960s for the NASA Gemini program, PEMFCs are currently being developed and demonstrated for systems ranging from 1W to 2kW. PEM fuel cells use a solid polymer membrane (a thin plastic film) as the electrolyte. This polymer is permeable to protons when it is saturated with water, but it does not conduct electrons.

The fuel for the PEMFC is hydrogen and the charge carrier is the hydrogen ion (proton). At the anode, the hydrogen molecule is split into hydrogen ions (protons) and electrons. The hydrogen ions permeate across the electrolyte to the cathode while the electrons flow through an external circuit and produce electric power. Oxygen, usually in the form of air, is supplied to the cathode and combines with the electrons and the hydrogen ions to produce water. The reactions at the electrodes are as follows:

Anode Reactions: $2H_2 \Rightarrow 4H^+ + 4e^-$
Cathode Reactions: $O_2 + 4H^+ + 4e^- \Rightarrow 2\,H_2O$
Overall Cell Reactions: $2H_2 + O_2 \Rightarrow 2\,H_2O$

Compared to other types of fuel cells, PEMFCs generate more power for a given volume or weight of fuel cell. This high-power density characteristic makes them compact and lightweight. In addition, the operating temperature is less than 100ºC, which allows rapid start-up. Other advantages result from the electrolyte being a solid material, compared to a liquid. The sealing of the anode and cathode gases is simpler with a solid electrolyte, and therefore, less expensive to manufacture. The solid electrolyte is also more immune to difficulties with orientation and has fewer problems with corrosion, compared to many of the other electrolytes, thus leading to a longer cell and stack life. One of the disadvantages of the PEMFC for some applications is that the operating temperature is low. Temperatures near 100ºC are not high enough to perform useful cogeneration. Also, since the electrolyte is required to be saturated with water to operate optimally, careful control of the moisture of the anode and cathode streams is important.

1.5.6 Direct Methanol Fuel Cells (DMFC)

The technology behind Direct Methanol Fuel Cells (DMFC) is still in the early stages of development, but it has been successfully demonstrated powering mobile phones and laptop computers—potential target end uses in future years.

DMFC is similar to the PEMFC in that the electrolyte is a polymer and the charge carrier is the hydrogen ion (proton). However, the liquid methanol (CH_3OH) is oxidized in the presence of water at the anode generating CO_2, hydrogen ions and the electrons that travel through the external circuit as the electric output of the fuel cell. The hydrogen ions travel through the electrolyte and react with oxygen from the air and the electrons from the external circuit to form water at the anode completing the circuit.

Anode Reaction: $CH_3OH + H_2O \Longrightarrow CO_2 + 6H+ + 6e-$
Cathode Reaction: $3/2\ O_2 + 6\ H+ + 6e- \Longrightarrow 3\ H_2O$
Overall Cell Reaction: $CH_3OH + 3/2\ O_2 \Longrightarrow CO_2 + 2\ H_2O$

Initially developed in the early 1990s, DMFCs were not embraced because of their low efficiency and power density, as well as other problems. Improvements in catalysts and other recent developments have increased power density 20-fold and the efficiency may eventually reach 40%.

These cells have been tested in a temperature range from about 50ºC-120ºC. This low operating temperature and no requirement for a fuel reformer make the DMFC an excellent candidate for very small to mid-sized applications, such as cellular phones and other consumer products, up to automobile power plants.

One of the drawbacks of the DMFC is that the low-temperature oxidation of methanol to hydrogen ions and carbon dioxide requires a more active catalyst, which typically means a larger quantity of expensive platinum catalyst is required than in conventional PEMFCs. This increased cost is, however, expected to be more than outweighed by the convenience of using a liquid fuel and the ability to function without a reforming unit.

One other concern driving the development of alcohol-based fuel cell is the fact that methanol is toxic. Therefore, some companies have embarked on developing a Direct Ethanol Fuel Cell (DEFC). The performance of the DEFC is currently about half that of the DMFC, but this gap is expected to narrow with further development.

1.5.7 Regenerative Fuel Cells (RFC)

Regenerative fuel cells (RFC) are attractive as a closed-loop form of power generation. Water is separated into hydrogen and oxygen by a solar-powered electrolyzer. The hydrogen and oxygen are fed into the fuel cell which generates electricity, heat and water. The water is then recirculated back to the solar-powered electrolyzer and the process begins again. These types of fuel cells are currently being researched by NASA and others worldwide.

However, currently the infrastructure for hydrogen delivery does not exist. In addition, the cost of electricity would be high, but will decrease as cost decreases for each of the components: fuel cells, hydrogen storage, and delivery, renewable energy collection, etc.

Among different categories of fuel cells, solid oxide fuel cell (SOFC) is one, which is currently in demand. Due to its better output with ease of handling and manufacturing, this third generation fuel cell, is attracting substantial interest among the scientific community as it is considered to be the most efficient and versatile power generation system, particularly for dispersed power generation [2]. SOFC is also known as one kind of green energy in the 21st century. It has the potential to directly utilize a wide variety of commercial fuels, such as natural gas, methanol, coal gas liquid hydrocarbons, all at significant reduction in pollution emissions relative to present-day combustion power plants [3].

Since its invention, different modifications in SOFC design have been suggested and implemented. This has brought a complete change into its stacking sequence and ultimately, a change in design of complete system. According to the stacking design and fabrication, at present, four common stack configurations have been proposed and fabricated for SOFCs: sealless tubular design, segmented-cell-in-series design, monolithic design and flat-plate design. The designs differ in the extent of dissipative losses within the cells, in the manner of sealing between fuel and oxidant channels, and in the manner of making cell-to-cell electrical connections in a stack of cells. Articles describing various aspects of these designs had been published [4, 5]. Out of these four designs, the flat plate (planar) and seal-less tubular [Fig. 1.2 and Fig. 1.3] designs have been seen with alacrity. As evident from the name, sealless tubular design has a distinct feature that it has no seals; therefore, the problems with the gastight seals for ceramics at high temperatures are eliminated. In addition, this design has the advantage that each single cell is built as a unit structure. This allows some freedom of thermal expansion and minimizes the problem of cracking caused by undue thermally induced stresses in a monolithic pack of connected cells. Along with these positive points, some negative points accompany this design too, which severely hamper the performance of a fuel cell, and thus cannot be ignored. The sealless tubular design has a relatively long current path through the cell. The current path is long in the plane of the electrodes, resulting in greater resistive loss. The support tube is a limitation on cell performance. The thick support tube restricts the amount of oxygen, which can be transported to the cathode/electrolyte interface. Thus gas diffusion through the tube can become the rate-limiting step and sets the limiting current for the cell. Even below the limiting current, gas transport represents the loss in cell performance. On the other hand, the flat plate design [6] offers improved performance and improved power density relative to the tubular and segmented-cell-in-series design. Because of in-plane conduction, internal resistance losses of flat-plate SOFCs are independent of cell area.

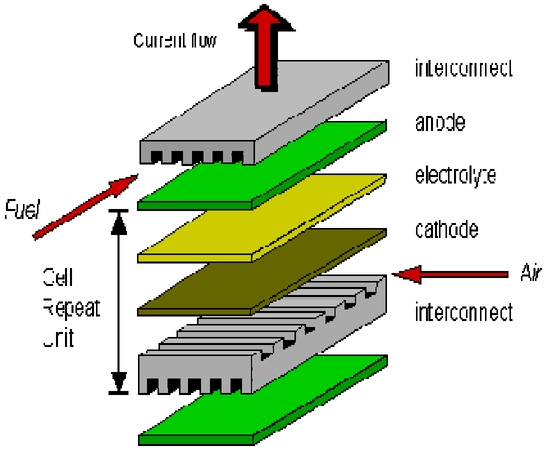

Figure 1.2 Planer Stack for SOFC

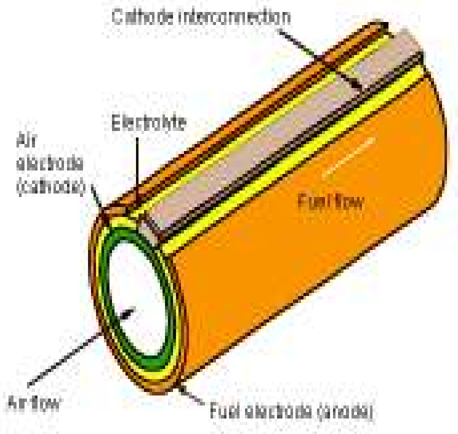

Figure 1.3 Tubular design for SOFC

Thus, cell components can be made very thin to minimize the electrical resistance. The flat-plate design also offers simpler fabrication. The two dense components, the electrolyte and the interconnect, can be fabricated independently. This avoids the difficulties in co-sintering of the ceramic interconnect and provides multiple processing options. Furthermore, the fabrication of flat-plate SOFC allows cell components to be assessed individually, thus, ensuring better quality control [4]. However, the flat-plate (planar) design must overcome a significant challenge, which does not apply to tubular systems. The need for effective, high temperature seals to prevent fuel leakage and air mixing at high temperature along with to seal the electrolyte against the metallic body of the device, in order to create a hermetic, rugged and stable stack is the urgent requirement of the planar design [Fig. 1.4]. Any leakage of fuel into the air (or air into the fuel) will lead to direct combustion of fuel and may cause local overheating (hot spots) and sometimes may burst. To prevent the fuel gas and air from mixing during the operation it is necessary to seal the electrodes properly.

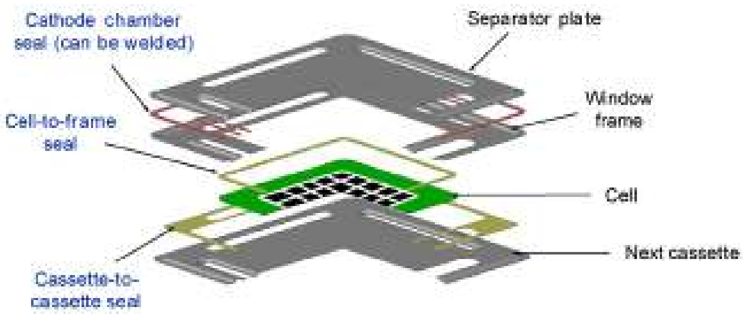

Figure 1.4 Seal in Planar SOFC [7]

The cathode is required to be sealed on the fuel inlet and outlet side while the anode is to be sealed on the air inlet and outlet side. Typical conditions under which the SOFC is expected to operate and to which the seal will be exposed include [8, 9]:

- An average operating temperature of 750°C.
- Continuous exposure to an oxidizing atmosphere on the cathode side and a wet reducing gas on the anode side.
- An average oxygen partial pressure in the range from 2×10^{4} to 1×10^{-13} Pa.
- An anticipated device lifetime of more than 10,000 hours.

1.6 Parts of Solid Oxide Fuel Cell

Solid Oxide Fuel Cell consists the following components:

- Electrodes (Cathode and Anode)
- Solid Electrolyte
- Interconnect or separator and
- Sealants

The details of their functioning are described below:

1.6.1 Electrodes

SOFC exhibit two electrodes. These are cathode and anode. The functioning of these electrodes are given below:

1.6.1.1 Cathode

Cathode is made to be porous in order to allow oxygen molecules to reach electrode/electrolyte interface. The most commonly used cathode material is Lanthanum manganite ($LaMnO_3$). Typically it is doped with rare alkaline earth elements (e. g. Sr, Ce, Pr) to enhance its conductivity. Most often it is doped with strontium and referred to as LSM ($La_{1-x}Sr_xMnO_3$). The conductivity of these Perovskite structured (Fig. 1.5, ABO_3 Type, A atom in the center, B atoms at the corners and oxygen atoms at the midpoints of the edges) materials is electronic in nature which is a desirable feature since the electrons from the open circuit flow back through the cell via the cathode.

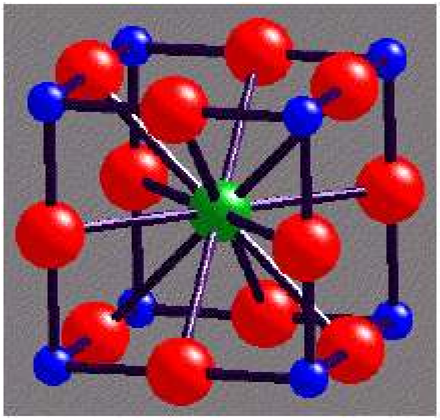

Figure 1.5 Perovskite Structure

1.6.1.2 Anode

The anode must meet the same requirements as the cathode for electrical conductivity, thermal expansion compatibility and porosity, and it must be chemically stable due to steep change in oxygen partial pressure (reducing atmosphere). Most developments have focused on nickel owing to its abundance and affordability. Pure Ni has high thermal expansion coefficient (13.3x10^{-6}/C). Making the anode with Ni-Yttria Stabilized Zirconia composite has solved these problems. The YSZ provides structural support for separated Ni particles, preventing them from sintering together while matching the thermal expansions.

The main function of the electrode is to promote the reaction between the fuel and the oxygen through oxidation-reduction reaction at electrode-electrolyte interfaces without themselves being consumed or corroded.

The diagrammatic representation of the reactions taking place in solid oxide fuel cell operated on hydrogen is as shown in Fig. 1.6.

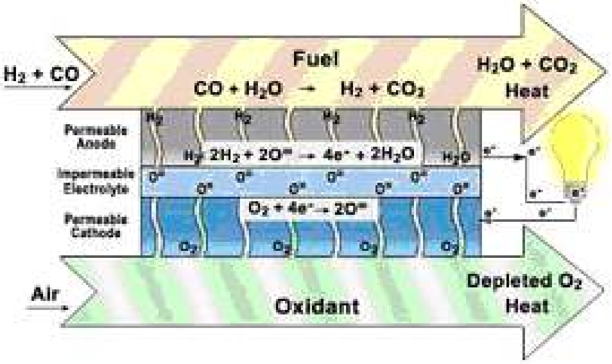

Figure 1.6: Working of Solid Oxide Fuel Cell

The by-products of these reactions are water, CO_2 and heat. For oxide ion conducting electrolytes the by-products are formed at the anode side, whereas for proton conducting electrolytes, they are formed at the cathode side. Due to the difference in oxygen activity at the electrodes, an electrical potential is developed, the magnitude of which depends on temperature and oxygen partial pressures at the electrodes [10].

1.6.2 Electrolyte

Once the molecular oxygen has been converted to oxygen ions it must migrate through the electrolyte to the fuel side of the cell. In order for such migration to occur, the electrolyte must possess a high ionic conductivity (>0.05 Scm^{-1}) and ionic transport number of the order of one at operating temperature of SOFC. It must be dense enough to prevent mixing of reacting gases and minimize resistive losses in the cell. As with the other materials, it must be chemically, thermally and structurally stable across a wide temperature range.

YSZ has emerged as the most suitable electrolyte material. Yttria serves the dual purpose of stabilizing zirconia into the cubic structure at high temperatures and also providing oxygen vacancies. A typical dopant level is 10 mol% yttria.

Cerium oxide has also been considered as a possible electrolyte. Its advantage is that it has high ionic conductivity in air but can operate effectively at much lower temperatures (under 700°C). This temperature range significantly broadens the choice of materials for the other components, which can be made of much less expensive and more readily available materials. The problem is that this electrolyte is susceptible to reduction on the anode (fuel) side.zzzzzzzz

1.6.3 Interconnect or separator

Interconnect is used to connect single unit of cell to the other unit of fuel cell so that enough voltage could be achieved in outer circuit of the stacks. The interconnect also functions as the separator to prevent the mixing of fuel gases and oxidizing gases. Interconnect material should be stable because it will be exposed simultaneously to the reducing environment of the anode and the oxidizing atmosphere of the cathode.

Presently, three materials have been used as a interconnect such as high chrome steel, oxygen deficient steel and $LaCrO_3$ the material of the choice is $LaCrO_3$ doped with alkaline earth elements (Ca, Mg, Sr etc) to improve its conductivity. Ca-doped yttrium chromite is also being considered because it has better thermal expansion compatibility.

1.6.4 Sealant

The selection of sealing materials/techniques is closely related to the specific application in which stack will be used. The various factors that affect the seal performance are individual cell and stack materials and geometries, stack assembly sequence, thermal gradients expected across the seal and other stack components, maximum weight and/or volume of the power plant, anticipated external forces, and required heating and/or cooling rate of the device. Table 1.1 gives a detailed list of generic set of requirements for the SOFC seals [8].

Table 1.1 Requirements for planar SOFC seals

Mechanical	**Chemical**
• Hermetic/marginal leak rate • TEC matching • Acceptable bond strength or compressive loading requirement (i.e. load frame design) • Resistant to degradation due to thermal cycling/thermal shock • Robustness under external static and dynamic forces	• Long –term chemical stability under simultaneous oxidizing/wet fuel environments • Long-term chemical compatibility with the adjacent sealing surfaces • Resistance to hydrogen embrittlement
Design/fabrication	**Electrical**
Low cost Facile application/processing High reliability with respect to achieving initial hermeticity (i.e. seal conforms to non-flat substrate surfaces) Design flexibility	Non-conductive (non-shorting configuration)

1.7 Methods of sealing

Many techniques are available for joining ceramics to other ceramics or to metals. There are three general categories or types of joining processes. In the first, attachment is mechanical and is achieved through the use of mechanical interlocking of components. Provided that the materials are refractory and chemically compatible, this approach should provide high strength at high temperatures. However, it has been pointed out that the lack of ductility in ceramics severely limits the temperature range over which the method is applicable because of the high local tensile stresses that can develop in systems with thermal expansion mismatches, causing failure in the ceramics [11]. Moreover, it has been observed that successful application of mechanical attachment in demanding environments is difficult to achieve, especially if leak tight joints are required or if the joint will be subjected to thermal cycling [12]. The second approach is direct joining, in which components are bonded either by solid – state process or by fusion. Direct joining or solid-state pressure bonding has been applied to joining of ceramics to ceramics and ceramics to metals [13-16]. Successful pressure bonding relies upon the achievement of adequate interfacial contact and subsequent diffusion or plastic flow to eliminate interfacial porosity. The advantages of solid-state pressure bonding include a simple fabrication procedure, a one-step process, and potentially very high joint strength. However, there are also several limitations and disadvantages: high cost; only flat specimens can be joined; a vacuum/inert atmosphere is required; and a pressure must be applied. The need to apply pressure during diffusion bonding imposes restrictions on the joint geometry; most joints are of face seal type and are not well suited for accommodating thermal expansion mismatch. As a result, the bonded components must either be small, one component must be thin or the TEC of the components must be well matched. The third approach could be referred to as indirect joining in the sense that an intermediate layer of material, such as an adhesive, cement, or braze is used to bond two components. The use of a liquid, a glass, or a solid foil readily under low applied stress to join materials can have advantages. Flow of a wetting liquid or glass or of the ductile solid can fill irregularities in the surface and therefore imposes less stringent demands on surface preparation and degree or extent of surface mating required. Ductile metal interlayers can undergo plastic flow and thus reduce the stress that builds up in the ceramic during thermal cycling [17-19]. Based on these three approaches, various high temperature-sealing techniques, which are being considered for SOFC application, have been tried. These include:

- Diffusion bonding
- Reaction bonding
- Active metal brazing
- Air brazing
- Bonded compliant sealing
- Compressive sealing
- Rigid bonding or glass joining

However, there are some inherent advantages and limitations of each technique. The salient features and drawbacks of the above mentioned sealing methods are discussed in brief with special emphasis on compressive seals and rigid bonding.

1.7.1 Diffusion bonding

Diffusion bonding is a solid-state welding process wherein coalescence of contacting surfaces is produced with minimum macroscopic deformation by diffusion-controlled processes, which are induced by applying heat and pressure for a finite interval [20]. By means of diffusion bonding, it is possible to bond all materials whose chemical and metallurgical properties are compatible. Since bonding of advanced materials using the classical welding methods [21] is not possible due to unexpected phase propagation at the bond interface [22], the diffusion bonding technique can be employed to bond such materials. This technique is dependent on a number of parameters, in particular, time, applied pressure, bonding temperature and method of heat application. Diffusion bonding usually takes place in an uniaxial press (hot isostatic pressing can be used but requires more complex fixturing) heated via elements or induction units. This also presents a restriction on the size of components that is to be processed. However, a more recent innovation uses microwave heating and this has been shown to produce excellent bonds in a matter of minutes, but still for components no bigger than a shoe box. Ceramic-ceramic diffusion bonding is difficult to achieve unless either diffusion aids or secondary phases are present. These second phases are most typically glassy phases at grain boundaries. Moreover, there is usually an added complication when joining dissimilar materials - the differences in thermal expansion coefficient (TEC). This can cause strains to develop at the interface, which can cause premature failure of the bond.

The extreme conditions required for diffusion bonding generally make this technique incompatible with the planar stack fabrication.

1.7.2 Reaction bonding

Reaction Bonding (RB) is a ceramic casting process. Silicon carbide grains are mixed with water and binding agents to form slurry, cast into a mold and then freeze dried to remove the water. This part is then sintered to form a porous alpha SiC structure. A high temperature process then introduces silicon into the porous structure and results in a 100% dense structure consisting of a bonded network of silicon carbide with isolated regions of free silicon (10-30%). The reaction bonding process has shrinkage of less than 0.5%. Use of a fugitive core allows substrates to be cast with integral backs. While the reaction bonding has been used to join non-oxide ceramics like SiC, less success has been demonstrated with forming hermetic ceramic-to-metal joints. The joints formed by this technique often contain residual porosity, shrinkage-induced cracks, unconverted reactants, and undesired secondary product phases, each of which can reduce the overall joint strength [23].

1.7.3 Active metal brazing

Brazing is a process in which two or more closely fitting parts are joined via an intermediate metallic material, which melts and wets the surface being joined. The melt reacts with the surface and gets solidified. The joining of an assembly of two or more metal parts into a structure is achieved by heating the assembly to a temperature high enough to melt the filler metal but not the parts. The molten filler metal spreads into the joint and wet the base-metal surfaces. Dissimilar metals that cannot be joined by a traditional welding process, because of their metallurgical incompatibilities or complex geometry, can be brazed successfully. Two basic mechanisms are involved in bond formation, by wetting the surfaces with the braze alloy, and consequent interface reaction with the two surface layers of some micrometer thickness. If these layers increase in thickness the bond strength of the joints may be degraded, promoting failure by interfacial stresses due to thermal expansion mismatch [24]. The technique of active metal brazing utilizes filler metal that when heated above its liquidus temperature will flow and fill the gap between the two joining pieces by capillary action. Unlike metal-to-metal brazes, this particular family of braze alloys contains one or more reactive metals, often titanium, which will chemically reduce the ceramic at the interface with the braze, thus greatly improving wetting and adherence between the two materials [25, 26]. However, two problems are encountered when using this technique to solid-state electrochemical devices:

- The joint is not sufficiently resistant to oxidation, and will degrade under high-temperature operation [27].
- Joining must be conducted in a high-temperature, reducing gas environment, a condition that is too demanding for many of the p_{O2} –sensitive oxides used in the fuel cell [28].

1.7.4 Air brazing

This is a new concept under investigation at Pacific Northwest National Laboratory (PNNL), USA [29]. It is a method of ceramic-to-metal brazing specifically for fabricating high-temperature solid-state devices such as oxygen generators in which braze pastes are formulated by mixing appropriate ratio of copper and silver powders with a standard screen printing binder. Disc -shaped bilayer coupons of requisite dimensions are fabricated by traditional tape casting and co-sintering techniques and are tested on SOFC components.

This technique differs from the metal brazing in two important ways [8]:

- It uses a liquid-phase oxide/noble metal melt as the basis for joining, and therefore exhibits high-temperature oxidation resistance.
- The process is conducted directly in air without the use of fluxes and/or inert cover gases.

1.7.5 Bonded compliant seal

This is another sealing concept being tried at PNNL, which can employ a number of high temperature alloys for use as the foil membranes i.e. to seal metal and ceramic component. Experiments are being conducted using commercial alumina-forming ferritic steel as the foil membrane: DuraFoil (22% Cr, 7% Al, 0.1% La+Ce, balance Fe, manufactured by Engineered Materials Solutions Inc, Attleboro, MA) [8].

However, the research on the concept of air brazing and bonded compliant seals is at initial stages and their long-term durability, as well as the potential for scale up and prototype use in demonstration stacks is still to be proved.

1.7.6 Compressive sealing

Compressive seals utilize materials such as sheet structure silicates, which do not bond to the SOFC components; instead the sealing material acts as a gasket and the seal is achieved by applying a compressive force to the stack. In comparison to the rigid seals (discussed in the next section), compressive seals potentially offer several advantages. Since, they are not bonded rigidly to the cells; the need for matching thermal expansion coefficient (TEC) of all the stack components is reduced or eliminated. The cells and the interconnects are allowed to expand and contract freely during thermal cycling which exists in routine operation. Elimination of the need of matching TEC greatly expands the list of candidate interconnect materials, whether ceramic or metallic [30]. However, the use of compressive seals bring new challenges to the SOFC stack design- a load frame must be included to maintain a desired level of compressive load during operation, and the stack components must be able to withstand the compressive load required for adequate sealing for the lifetime of the stack [31]. The commercial derivatives of mica (class = phyllosilicates; general formula = $AB_{2\text{-}3}(X,Si)_4O_{10}(O,F,OH)_2$) like muscovite ($KAl_2(AlSi_3O_{10})(F,OH)_2$), phlogopite ($KMg_3(AlSi_3O_{10})(OH)_2$) are being considered as a potential base material in compressive seals [32-36]. Researchers at PNNL, [30, 31, 33-36] and Forschungszentrum Jülich, Germany [37] are actively engaged in assessing the potential of mica as a compressive seal for intermediate temperature (~800°C) SOFC. Fig. 7 shows the various types of mica seals.

Simner and Stevenson [31] examined micas in paper form as well as the cleaved single crystal form. The results showed the cleaved natural mica sheets to be far superior as compared to mica papers, however, the coupon leak rate shown by the latter was also not acceptable for actual SOFC stacks, in which, multiple, full size components would be stacked together with the mica gaskets between each component. The problem of reducing the leak rates as admissible to the actual stack conditions led to the birth of a novel hybrid mica-based seal in which the leak rate can be reduced ~4300 times by simply adding the glass interlayers between the mica and the adjacent stack components [Fig. 1.7] [30].

For an ideal hermetic seal, the leak rate should be zero. Practically, the actual low leak rates were limited by the system's background. Low fuel leak rate are required if SOFC stacks are to operate safely and economically. Although, the allowable leak rate remain to be determined and will be somewhat offering leak rates as low as possible at compressive stress as low as possible. The hybrid seal based on muscovite single crystal mica appears to be a viable candidate [39].

The use of compressive seals brings several new challenges to SOFC stack design- a load frame must be included to maintain the desired level of compressive load during operation, and the stack components must be able to withstand the compressive load required for adequate sealing for the lifetime of the stack. The problems have been found with the natural variance in thickness of mica sheets and relative non-compressibility of the mica. Also, it has been found that mica may leach minerals into the cell and poison the catalyst. [40]. These factors prevent an effective seal from forming.

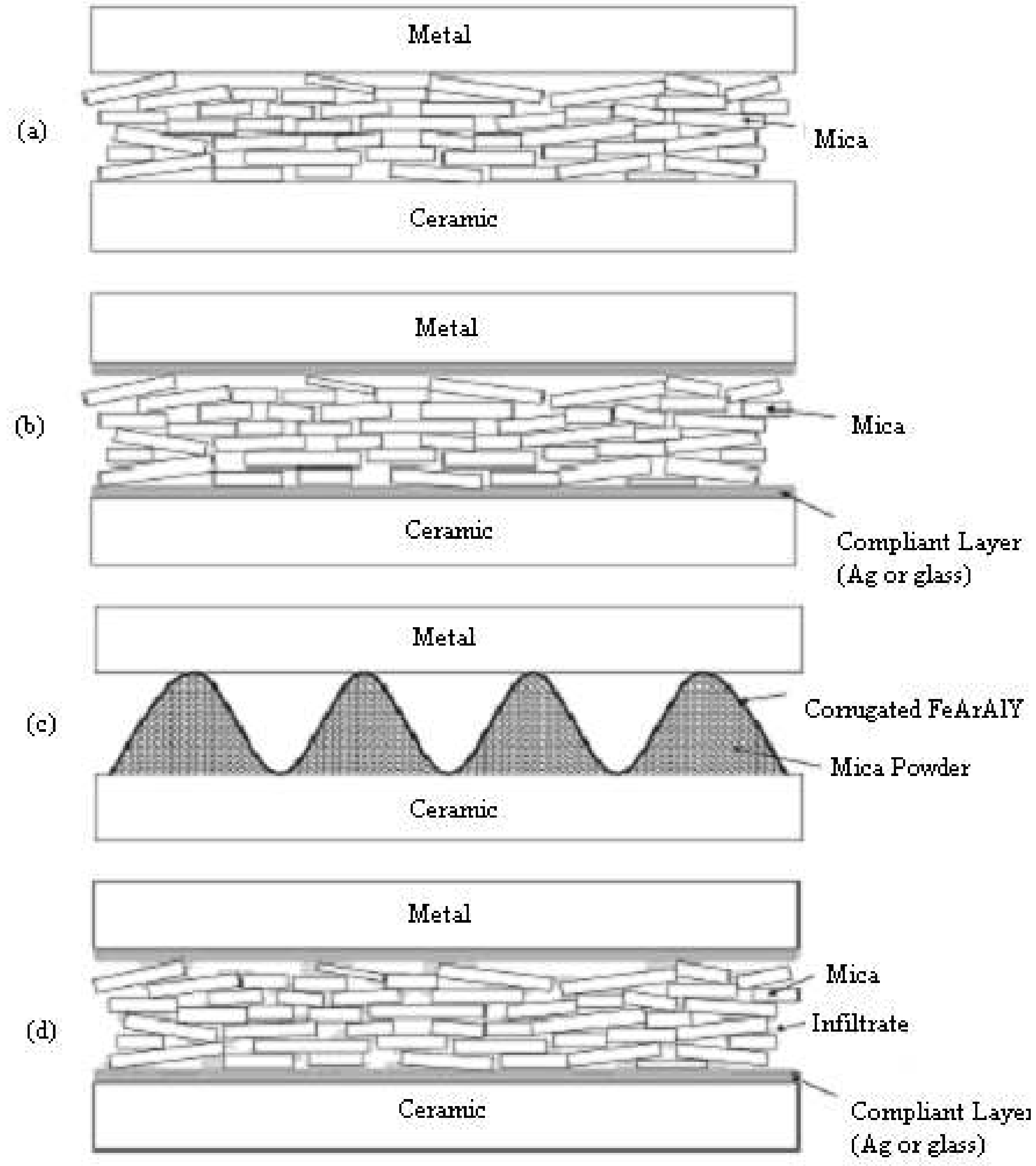

Figure 1.7 Mica seals: (a) plain mica seal [30, 38], hybrid mica seal with compliant layer (glass or metal) [30, 38], (c) mica powder with corrugated alloy [37] and (d) hybrid mica seal with compliant layer and infiltrated mica [35].

At present, however, this technology remains incomplete due to the lack of reliable high temperature sealing material that would form the basis of the compressive seal.

1.7.7 Rigid bonding or glass joining

A number of materials have been considered for compressive sealing, including, mica, nickel and copper, but each has been found deficient for several reasons, including the oxidation resistance in the case of metals to poor hermiticity and also the seal leakage in the case of mica [32]. Material oxidation and load relaxation due to creep, as well as added expense and additional thermal mass that must be heated, cooled and maintained at temperature under the equilibrium operation are all issues that require particular attention with this type of cell design. Due to these constraints and specifically because our application is an auxiliary power unit (APU) where minimization of device weight and volume are critical, rigid seals are good choice such as glass sealants [41]. The majority of SOFC seal development has focused on bonded, rigid seals; primarily glass and glass-ceramics, which essentially "glue" the stack components together. Many glass seals are deigned to soften, and viscously flow above the SOFC operating temperature to provide hermetic seals by mechanical/chemical bonding. On cooling back down to operating temperature, the glass crystallizes to form a rigid, bonded seal. A principal advantage of glass seals is that the glass composition can be tailored to optimize some of the physical properties, such as thermal expansion coefficient (TEC).

1.7.7.1 Requirements for a suitable glass sealants

A sealing material has to fulfill some critical requirements as described above, because the operation temperature of the SOFC is almost 850°C and the operation period must be more than 5 years. Other major requirements are [42]:

- no chemical reaction with the joining components and solder stability in oxidizing and wet reducing atmospheres;
- viscosity: 10^5 Pa-s at joining temperature (1000°C) and $>10^9$ Pas at operating temperature (850°C);
- only a small thermal expansion mismatch with respect to SOFC components (TEC=7-11X10^{-6} K^{-1});
- leakage rate of joining should be less than 10^{-7} mbar $1s^{-1}$ per cm joined length;
- resistivity more than 2 KΩ cm .

However, several challenges remain with respect to the use of glass seals in SOFCs. The brittle nature of glasses below the glass transition temperature makes the seals vulnerable to crack formation, and glasses tend to react with other cell components, such as electrodes, at SOFC operating temperatures. Glass seals can affect electrode performance over a short range (via solid state diffusion or viscous flow) or over longer distances (via gaseous transport of glass constituents).

1.7.7.2 Problems with glass sealants

Potentially there are several ways in which a rigid glass seal can fail during operation, including the following:

- *Failure by fracture under pressure.* The glass seal can be viewed essentially as a multicomponent laminate composite composed of the electrolyte, the sealing glass and the oxide scale that naturally forms on the metal substrate during stack sealing and operation. Each of these layers is a brittle material and as such, each is susceptible to failure by brittle fracture. Thus, if a large enough flaw exists in any of the materials with in the seal or if the residual tensile stresses of a minimum critical value develop due to thermal expansion mismatch between components or warping due to non-uniform heating with in a given component, fracture can occur [43].
- *Failure during rapid thermal cycling.* Thermal gradients arising during rapid heating or cooling can generate out-of-plane bending stresses that may lead to failure in one of the brittle components in the ceramic-to-metal joint. In addition, thermal cycling may lead to fatigue problems in both the metals and ceramic components. Specifically in ceramic materials, this can occur due to a critical size under even small thermally generated stresses [44].
- *Failure upon thermal aging.* As the glass begins to crystallize, its carefully engineered thermal expansion properties will change and continue to evolve with time at operating temperature, which can ultimately limit the number of thermal cycles and the rate of cycling at which the joints are capable of surviving [45]. In addition, compositional and microstructural changes induced by long term thermal diffusion are likely to take place at the seal/substrate interfaces, which may also lead to seal degradation and subsequent failure.

Despite of the above-discussed problems, glasses and glass-ceramics have been focused on as the potential sealing materials with major emphasis on alkaline earth aluminosilicates [45-48], borosilicates, and lanthanide alumino borosilicates [11, 42, 49-52]. Of course, the effect of many other glass additives have been evaluated and the glasses have been tailored using various additives in accordance with the required properties [42, 45, 52, 53].

The main aim of present study is to synthesis a glass composition which can be used as a sealant at a low working temperature SOFC i.e. at 800^{o}C. In order to fulfill this requirement glass series comprising of 40mol% SiO_2, which will act as a main glass former, thus increasing the glass forming range and also the transition temperature. In order to reduce the glass transition temperature due to high content of SiO_2 the addition of 10mol% B_2O_3 is done. The viscosity of the glass at the operating temperature of SOFC is contained within the permissible limit i.e. 10^7-10^9 Pa.s by addition of 20mol% ZnO and 30mol% of alkaline earth. BaO acts as a modifier. B_2O_3 is replaced by Al_2O_3, La_2O_3, Mn_2O_3 and Y_2O_3 to study the effects of these intermediates on the properties of parent glass series. The heat treatment was done at a temperature range lying between T_g and T_m i.e. at 800^{o}C.

References

[1] http://www.fctec.com/fctec_basics.asp

[2] S. P. S. Badwal and K. Foger, Ceram. Int. 22 (1996) 257.

[3] T. L. Wen, D. Wang, M. Chen, H. Tu, Z. Lu, Z. Zhang, H. Nie and W. Huang, Solid State Ionics 148 (2002) 513.

[4] N. Q. Minh, J. Am. Ceram. Soc. 76 (1993) 563.

[5] L. Carrette, K. A. Friedrich, U. Stimming, ChemPhysChem 1 (2000) 162.

[6] W. Dönitz, E. Erdle, W. Schäfer, R. Schamm, R. Späh, in Proceedings of 2nd International Symposium on SOFC Athens, 1991, Commission Europe Communities, Luxemberg.

[7] K.S. Weil and B.J. Koeppel International Journal of Hydrogen Energy 33 (2008) 3976.

[8] K. S. Weil, C. A. Coyle, J. S. Hardy, J. Y. Kim and G.-G. Xia, Fuel Cells Bull. May 2004, p. 11.

[9] P. H. Larsen and P. F. James, J. Mater. Sci. 33 (1998) 2499.

[10] P. Sujatha Devi, A. Das Sharma, H. S. Maiti, Trans. Ind. Cer. Soc. 63 [2] (2004) 75.

[11] R. W. Rice, in "Advances in Joining Technology" edited by J. J. Burke, A. E. Gorum, and A. Tarpinian, (Brook Hill Publishing, Chestnut Hill, MA 1976).

[12] M. G. Nicholas, "Joining Structural Ceramics" In Designing Interfaces for Technological Applications, edited by S. D. Peteves, (Elsevier Appl. Science, Amsterdam, 1989) p. 49.

[13] K. Suganuma, T. Okamoto, M. Shimada and M. Koizumi, J. Am. Ceram. Soc. 66 (1983) C117.

[14] M. Koizumi, T. Okamoto, M. Shimada, K. Suganuma, Am. Ceram. Soc. Bull. 63 (1984) 1173.

[15] K. Suganuma, T. Okamoto, M. Koizumi and M. Shimada, J. Am. Ceram. Soc. 67 (1984) C256.

[16] K. Suganuma, T. Okamoto, M. Koizumi, M. Shimada, J. Am. Ceram. Soc. 68 (1985) C334.

[17] K. Suganuma, T. Okamoto, Y. Miyamoto, M. Shimada and M. Koizumi, Mater. Sci. Tech. 2 (1986) 1156.

[18] K. Suganuma, T. Okamoto, M. Koizumi, M. Shimada, J. Mater. Sci. 22 (1987) 1359.

[19] W. G. Nicholas and D. A. Mortimer, Mater. Sci. Tech. 1 (1985) 657.

[20] W. A Owczarski, D. F Paulonis, Welding J. 62 (1981) 22.

[21] B. Alman, I. Guterrez, J. Urcola, Scripta Mater. 36 (1997) 509.

[22] D. R. Askeland, in “The science and engineer of materials” (Hong Kong: Nan Nostrand Reinhold; 1989).

[23] E. Pippel, J. Woltersdorf, P. Colombo and A. Donato, J. Eur. Ceram. Soc. 17 (1997) 1259.

[24] M. M. Schwartz, Brazing ASM International, Metals Park, Ohio p. 47

[25] C. W. Fox and G. M. Slaughter, Welding J. 43 (1964) 591.

[26] O. M. Akselsen, J. Mater. Sci. 27 (1992) 1989.

[27] J. P. Rice, D. M. Paxton and K. S. Weil, in Proceedings of 26th Annual Conference on Composites, Advanced Ceramics, Materials and Structures: B, edited by H.-T. Lin and M. Singh, (American Ceramic Society, Westerville, OH, USA, 2002).

[28] J. W. Stevenson, T. R. Armstrong, R. D. Carneim, L. R. Pederson and W. J. Weber, J. Electrochem. Soc. 143 (1996) 2722.

[29] J. S. Hardy, J. Y. Kim and K. S. Weil, J. Electrochem. Soc. 151 (2004) J43.

[30] Y. S. Chou, J. W. Stevenson and L. A. Chick, J. Power Sources 112 (2002) 130.

[31] S. P. Simner, J. W. Stevenson, J. Power Sources 102 (2001) 310.

[32] J. Kim, A. Virkar, in, “Solid Oxide Fuel Cells-VI” , edited by S. Singhal, M. Dokiya (Electrochemical Society, Pennington, NJ, PV 99-19, 1999) p. 830.

[33] Y. S. Chou and J. W. Stevenson, J. Power Sources 115 (2003) 274.

[34] Y. S. Chou and J. W. Stevenson, J. Power Sources 124 (2003) 473.

[35] Y. S. Chou and J. W. Stevenson, J. Power Sources 135 (2004) 72.

[36] Y. S. Chou and J. W. Stevenson, J. Power Sources 140 (2005) 340.

[37] M. Bram, S. Reckers, P. Drinovac, J. Mönch, R. W. Steinbrech, H. P. Buchkremer and D. Stöver, J. Power Sources 138 (2004) 111.

[38] Y. S. Chou, J. W. Stevenson, L. A. Chick, J. Am. Ceram. Soc. 86 (2003) 1003.

[39] Y. S. Chou and J. W. Stevenson, J. Power Sources 112 (2002) 376.

[40] D. Ghosh, S. Thompson, U. S. Pat, 6902798 (June7, 2005)

[41] K. Scott Weil, John E Deibler, John S Hardy, Dong Sang Kim, Guan Guang Xia, L A Chick and Chris A Coyle, J. Mat. Eng. Perf. 13[3] (2004) 316.

[42] K. Eichler, G. Solow, P. Otschik and W. Schaffrath, J. Eur. Ceram. Soc. 19 (1999) 1101.

[43] G. Qian, T. Nakamura and C. C. Berndt, Mech. Mater. 27 (1998) 91-110.

[44] G. Kirchoff, M. Holzherr, U. Bast and U. Rettig, Key Eng. Mater. 89-91 (1994) 605-10.

[45] N. Lahl, K. Singh, L. Singheiser, K. Hilpert, D. Bahadur, J. Electrochem. Soc. 149 (2002) A607.

[46] N. Lahl, L. Singheiser, K. Hilpert, K. Singh, D. Bahadur, in "Solid Oxide Fuel Cells-VI" edited by S. Singhal, M. Dokiya (Electrochemical Society, Pennington, NJ, PV 99-19, 1999) p. 1057.

[47] Z. Yang, J. W Stevenson and K. D. Meinhardt, Solid State Ionics 160 (2003) 213.

[48] D. Bahadur, N. Lahl, K. Singh, L. Singheiser, K. Hilpert, D. Bahadur, J. Electrochem. Soc. 151 (2004) A558.

[49] K. Ley, M. Krumplet, R. Kumar, J. Meiser, I. Bloom, J. Mat. Res. 11 (1996) 1489.

[50] S.B. Sohn, S.Y. Choi, G.-H. Kim, H.-S. Song and G.-D. Kim, J. Am. Ceram. Soc., 87 [2] (2004) 254.

[51] S.B. Sohn, S.Y. Choi, G.-H. Kim, H.-S. Song and G.-D. Kim, J. Non-Cryst. Solids 297 (2002) 103.

[52] N. Lahl, K. Singh, L. Singheiser, K. Hilpert, D. Bahadur, J. Mater. Sci. 35 (2000) 3089.

[53] T. Schwickert, R. Sievering, P. Geasee and R. Conradt, Mat.-wiss.u. Werkstofftech. 33 (2002) 363.

Chapter 2

Literature Review

Overview

In this chapter the development in the field of glass sealants has been reviewed. A detailed study of the effect of various elements on glass formation and its crystallization kinetics has been studied. The importance of B_2O_3/SiO_2 in deciding the glass transition temperature, viscosity and the role played by various additives in modifying different properties of glass such as wettability and thermal expansion coefficient has been discussed. Different glass systems such as Mg, Ca, Ba, Sr, and specially Zn based glass systems were thoroughly investigated. Recently published literature for interaction studies has also been documented to include the latest work in this field.

2.1 Role of various constituents of glasses

In this chapter the development in the field of glass sealants has been reviewed. Basically, the composition of raw materials used for glass making plays an important role in the formation of glass and its crystallization kinetics to form the various crystalline phases during SOFC operation. Therefore, the role of initial constituents and their molar ratio is also discussed in this chapter.

2.1.1 B_2O_3/SiO_2 ratio

Independent studies of glass-ceramics have shown that the B_2O_3/ SiO_2 ratio is a dominant factor in determining the glass transition temperature, T_g and the viscosity. Glasses with high B_2O_3/ SiO_2 ratios have T_g at the lower end while those with low B_2O_3/ SiO_2 ratios increase glass transition temperature [1, 2, 3]. This can be explained on the basis of the property of the formation of boron-oxygen triangle by B_2O_3, which loosened the tetrahedral Si-O network. Thus viscosity of glass decreases which leads the inhancement in wetabbility property of glasses. Ley *et al.* [1] have observed that small amount of La_2O_3 have a stronger influence on viscosity than the B_2O_3/ SiO_2 ratio. An increase in La_2O_3 amount leads to decrease in viscosity of the glass. Similarly, Sohn *et al.* [2] studied the controlled effect of La_2O_3 on the viscosity of glass. They reported that higher content of BaO increases the thermal expansion coefficient (TEC). On the other hand, Al_2O_3 content in glass components to prevent the rapid crystallization of glass during heat-treatment. Lara *et al.* [3] have also reported decrease in TEC of the glasses on increasing the SiO_2 content. Additionally, in borosilicate glasses, boron reacts with a humidified hydrogen atmosphere to form the gaseous species $B_2(OH)_2$ and $B_2(OH)_3$ at the operating temperature of SOFC. Therefore, any high boron glass may corrode in a humidified hydrogen environment. Glasses containing B_2O_3 have shown upto 20% weight loss in the humidified hydrogen environment and extensive interactions with other components of SOFC in both air and wet fuel gas [4].

2.1.2 Crystallization of glasses

Understanding the fundamental mechanisms involved in the creation and destruction of glassy state is impossible without the understanding of nucleation and crystallization kinetics [5-10]. Glass–Ceramics, glass contents in glass ceramics during cell operation at high temperature possess superior mechanical properties and have very different thermal expansion coefficients (TEC), due to nucleation of different crystalline phases in different volume fraction. The crystallization behavior of the glass-ceramics can be classified into two types. One behavior consists of relatively slow and, consequently, stable crystallization with the long-term operation. The other type of behavior consists of relatively rapid crystallization that occurs progressively for up to 1000 h. The latter behavior is thought to be unsuitable for long-term operation of SOFC. Rapid and progressive crystallization of a glass-ceramic sealant during cell operation can deteriorate the fluidity of the glass-ceramic because of a significant decrease of the residual glass matrix. It can lead thermal expansion mismatch, especially if the TEC value of the increasing crystalline phase differs significantly from that of the parent glass. To develop a good sealant, it is therefore, necessary to understand the crystallization kinetics both from the point of view of their sealing properties and their chemical interactions when in contact with other components of the cell [11, 12].

2.1.3 Effect of additives

Several additives are used to optimize the properties of the glass sealants. However, the choice of additives is restrictive as they do not influence just one property of the sealant but they also affect the other properties of glasses. Al_2O_3, for instance, improves flux, thus making for better joining behavior. On the other hand, higher content of Al_2O_3 decreases the thermal expansion, as it promotes the formation of a detrimental crystalline phase, which exhibit low thermal expansion coefficient [13]. Similarly, Na_2O acts as the most effective flux, but it makes the glass soluble in water. Na_2O can be replaced by K_2O but K^+ cations enhance the volatility of chromium [8, 14] thus, poisoning the cathode and also react vigorously with the other fuel cell components leading to the formation of undesirable low TEC phases [3, 9, 10, 15]. Bloom *et al.* [16] evaluated a commercial glass, Corning 0080, for possible use as sealants for the SOFC. It is a soda-lime glass, with TEC of 9.35×10^{-6} /^{o}C. However, it produced good bonds with YSZ but exhibited unacceptable chemical and/or physical interactions with the various interconnect materials. The effects of various additives on the properties of sealants are listed in Table 2.1.

Table 2.1 Effect of additives on various properties of glasses [1, 7, 12, 14, 15, 17-20, 36]

Additive	Effect
Al_2O_3	Improves flux. Prevents rapid crystallization of glass during heat treatment and also increase surface tension of glass. Too much Al_2O_3 decreases thermal expansion as it promotes the formation of crystalline phase with low TEC.
Na_2O, K_2O	Act as effective flux but the alkali cations react vigrously with the fuel cell components like cathodes; have undesirable TEC. Increases conductivity
La_2O_3, Nd_2O_3, Y_2O_3	Increase TEC, T_g, T_M
B_2O_3	Improves flux, reduces T_g, surface tension and stability of glass
ZnO, PbO	Improves flux, reducing agent
Cr_2O_3, V_2O_5	Reduces surface tension
NiO, CuO, CoO, MnO	Improves adhesion
TiO_2, ZrO_2, SrO, MgO, Cr_2O_3, Ni	Stimulates crystallization
Sb_2O_5	Oxidizing agent
P_2O_5	P_2O_5 decreases volatilization, reduce TECs and mechanical strength

The effect of small additions of TiO_2 and P_2O_5 has been studied. These agents enhance the nucleation of crystals in the glasses and induced phase separation in glasses. Tomozawa [21] explained the greater tendency of phase separation of P_2O_5 over TiO_2 as a result of higher ionic potential (Z/r) of phosphorous than titanium ions. TiO_2 is quite soluble in silicate glasses and lowers their viscosity considerably. A number of other oxides have been used as nucleating agents. Among these are zirconium, chromium, vanadium, iron, zinc and nickel. Their field strength played important role in the phase separations among the glasses.

Larsen *et al.* [17] revealed a number of challenging problems with glasses particularly P_2O_5 rich glasses. At high temperature, the phosphate volatilized and reacted with the Ni/yttria-stabilized zirconia-based anode to form nickel phosphide and zirconium oxyphosphate. Additionally, when de-vitrified these phosphate glasses typically form meta- or pyrophosphates, both of which exhibit low stability in humidified fuel gas at temperatures greater than 700°C.

The heat-treatment of glasses containing nucleation agents is often carried out in two stages. First the glass is given a "nucleation treatment" at a temperature just above the annealing temperature; it is then crystallized at a higher temperature. The separation between these two processes is not sharp since some crystallization probably occurs during nucleation treatment [22].

At least three different mechanisms have been proposed for the action of nucleating agents. Their role can be classified such as agent crystallization, catalysts of phase separation, and reduction of interfacial tension. However, very few reports have appeared in the literature on the role of first two actions of nucleating agents. After rejecting the other possibilities, Hillig [23] suggested that these agents lower the interfacial tension, ν between the crystal and the glass, thus increasing the rate of nucleation. This idea has been confirmed by measurements of crystal numbers as a function of time in lithium aluminosilicate glasses containing different amounts of titania as nucleating agent [24]. The change in titania concentration was too small to change the heat of fusion appreciably, so the increase in nucleation rates must result from a reduction in the interfacial energy. Ions of high field strength can possibly act as "surface active agents" to lower the interfacial energy. Barry *et al.* [25] have extended this idea in developing a detailed model for the enhancement of crystalline nucleation by titania in lithium aluminosilicate glasses. According to them, Ti^{4+} ions associate with the non-bridging oxygen ions, causing these ions and alkalis to concentrate at the edge of domains enclosing bridging oxygens. Based on this hypothesis, the effect of initial composition can be explained on nucleation of the glasses.

2.1.4 Wettability

The surface of any phase has associated free energy. That energy, ε (J/m^2), is always positive and is equivalent to the energy required to create a unit area of new surface of the material. The adhesive energy or work of adhesion between two phases is given as follows:

$$W_{AB} = \varepsilon_A + \varepsilon_B - \varepsilon_{AB},$$

Where the subscripts A and B indicate the free surfaces of phase A and B, and AB indicates their common interface. Two materials form a stable bond when the energy of adhesion is negative, that is, when creating the AB interface gives a net decrease in the free energy of the system by eliminating the high positive free energy of the interface [26].

When one of the phases is a liquid during the sealing process, for example, molten glass, the liquid phase generally must wet the solid to form the bonding. There is a general agreement that wetting is an essential prerequisite for making a good bond. Wetting occurs when the surface energy of the solid exposed to the atmosphere is greater than that of the liquid and the driving force for the wetting. When using a glass-ceramic as a sealant, the glass should wet the surfaces so that its sinterability increases in presence of liquid phase before crystallization, which decreases the viscosity of the glass [27-30]. Crystallization is facilitated by low value of the activation enthalpy for atom transfer across the interface. Activation enthalpy is approximately proportional to the logarithm of viscosity of the liquid. A low activation enthalpy is the characteristic of a low viscosity of the sealant. The characteristics of various glass systems and their properties are given in the following section.

2.2 MgO-Al_2O_3-SiO_2 system (MAS)

The crystallization of glass in this system is extremely complex because of the large number of phases, many of them metastable, which can be crystallized to form the glass. Barry *et al.* [31] demonstrated that the sequence of crystallization can vary from non stoichiometric to stoichiometric cordierites depending upon the nucleating agents (i.e. titania or titania plus zirconia).

A typical sequence of crystallization for a near-stoichiometric cordierite glass-ceramic containing approximately 11 wt. % TiO_2 as the nucleating agent would proceed in the following manner. During heat-treatment of the glass, initially glass undergoes amorphous phase separation preceding the precipitation of nucleating phase [(Mg, Al)(Ti, $Al)_2O_5$], a pseudobrookite structure. Further heat treatment of the glass (900^oC), form a metastable silicate, a stuffed derivative of the β-quartz solid solution phase. Subsequently, this solid solution phase breaks down to a very fine mixture of siliceous quartz and spinel and at slightly higher temperatures than 900^oC, it forms sapphirine, cordierite and rutile phases. Cordierite and rutile form very rapidly near 1200°C through a solid-state reaction between quartz, sapphirine, and pseudobrookite. These formed phases are stable at temperatures above 1250°C.

When mixtures of TiO_2 and ZrO_2 are employed as nucleating agents, the sequence of crystallization differs in that β-quartz and magnesium petalite are observed in the early stages of crystallization and a minor amount of cristobalite occurs at higher temperatures, which delays the conversion to cordierite. The influence of alkaline earth metals A (A=Ba, Ca, Mg) and nucleating agents (TiO_2, ZrO_2, Cr_2O_3 and Ni) on the crystallization kinetics of $AO-Al_2O_3-SiO_2-B_2O_3$ glasses has been studied by thermal and microstructural studies [12, 13, 14, 19, 32]. The activation energy of crystal growth, E_a, was shown to be varying between 330 and 622 kJ/mol. It was observed that E_a increases with nucleating agents except ZrO_2. Cr in the hexavalent state and Ti^{4+} ion posses a high field strength imparting a marked ordering effect in $MgO-Al_2O_3-SiO_2-B_2O_3$ glasses. These may be the reasons for higher E_a values for the glasses containing ZrO_2 or without nucleating agent. An increase of the Al_2O_3 concentration induced phase separation and decrease in E_a. Also, chemical interactions of the candidate sealants with 8 mol% yttria stabilized zirconia (8YSZ), Ni and the oxide dispersion strengthened (ODS) alloy was studied. It was observed that MgO base sealants exhibit superior properties as compared to BaO and CaO base sealants because of higher activation energy of crystal growth thereby hindering crystallization and moderate chemical interactions with other components of SOFC. On the other hand, magnesium aluminosilicates without barium oxide form cordierite phase ($Mg_2Al_4Si_5O_{18}$). Also it was reported that glasses with TiO_2 as nucleating agent are known to have a high tendency for the formation of ordered zones with high TiO_2 content due to high field strength of Ti^{4+}, which can cause phase separation in these glasses. The most encouraging result was the complete absence of cordierite phase in all powder mixtures composed of the sealant with Cr_2O_3 as the nucleating agent. A high value of T_g, T_c, and the activation energy of crystal growth is obtained if Cr_2O_3 (0.6 mol%) is used as nucleating agent. The chromium seemed to have a thermodynamic affinity to magnesium, which favours spinel formation and suppresses the formation of the cordierite phase.

2.3 BaO-Al_2O_3-SiO_2 system (BAS)

Many researchers [2, 11, 15, 33, 34, 35] have targeted their search of sealing material on barium aluminosilicate glass and some related systems. Eichler *et al.* [34] characterized the crystallization properties of commercially available BAS (BaO. Al_2O_3. SiO_2) glass in order to test their suitability as sealing glass for SOFC, while Sohn *et al.* [2, 11] studied the thermal and chemical compatibility of glasses with yttria stabilized zirconia (YSZ) electrolyte. These systems formed two major phases during heat treatment. There phases are hexacelsian and monocelsian. The details of these two phases are given in Table 2. Bansal *et al.* [43, 44] reported that the BaO. Al_2O_3. $2SiO_2$ (BA2S) glass always crystallizes to the hexacelsian first than monocelsian. However, the transformation from the hexacelsian to monocelsian is very sluggish. These glasses (BA2S) were prepared by melting at 2000°C. The as prepared glasses were completely crystallized to pure hexacelsian phase when heated at 1000°C for 1h. After increasing heat treatment time duration (10hrs) and temperature (1100°C), the hexacelsian phase began to transform to the monocelsian. The BA2S glass powders heated even at 1400°C for 10h showed formation of both the hexacelsian and monocelsian phases although the amount of monocelsian phase was increased relative to the hexacelsian.

Sung *et al.* [45] fabricated non-stoichiometric celsian glass-ceramics having a composition of 50wt% BaO. $2SiO_2$–50wt%BaO. Al_2O_3. $2SiO_2$ (B2S-BA2S). The B2S-BA2S glass powders showed a much lowered melting temperature of ~1500°C and high sintering ability as compared to earlier reported systems. The glass pellets sintered at 850°C for 2h and crystallized at 1100°C for 4h showed formation of two equilibrium phases of β-BaO.$2SiO_2$, monocelsain, and metastable hexacelsian phase. The glass ceramic pellets crystallized at 1400°C for 4h showed the formation of β-BaO.$2SiO_2$ and monocelsian with only a trace of the hexacelsian [46].

In the case of barium containing glass-ceramics, the crystallization increases thermal expansion. The increase in the TEC is due to the formation of barium silicate ($BaSiO_3$), which has large TEC ($9\text{-}13 \times 10^{-6}$ /°C) [47, 48-52]. On the other hand, MgO based glass ceramic exhibits the TEC in the range of $7\text{-}9 \times 10^{-6}$/°C due to formation of enstatite ($MgSiO_3$). Strontium forms solid solutions with barium in the celsian crystal structures and has been shown to stabilize the monocelsian phase [51]. Other alkaline earth oxides do not dissolve in the celsian phase, but rather form other phases. Calcium oxide is often added to form barium calcium aluminosilicate (BCAS) sealants. In this case an additional phase, barium calcium orthosilicate ($Ba_3CaSi_2O_8$), with a desirably large TEC is formed during crystallization [53, 54-56].

The interaction of the sealing glasses with the metallic interconnects has been studied in detail by different researchers [15, 57]. $BaCrO_4$ has been observed the primary crystalline reaction product of barium calcium aluminosilicate (BCAS) glass and interconnect. However, extent and nature of their interaction depends on the exposure conditions and/or proximity of the interface of the sealing glass and ferritic stainless steel to the ambient air. At or near the edges, where oxygen is accessible, the chromia scale grows on the steel and its vapor species react with BaO from glass ceramic, leading to formation of $BaCrO_4$. In the interior regions where oxygen or air access is blocked, chromia dissolves into BCAS sealing glass to form Cr rich solid solutions. In addition to this, the stainless steel also reacts with the residual species in the sealing glass-ceramic along the interior region of interface. It has been observed by Pio Jinhua [58] that in La doped BCAS glasses T_g and T_c values increase greatly with an increase in CaO content and decrease in the BaO content. It can be attributed due to higher field strength of Ca^{+2} ion as compared to Ba^{+2} ion. The TEC values of these glass samples decrease with reduced Ba^{+2} content and increase in the Ca^{+2} content. The interaction study between glass and LSGM (lanthanum strontium manganese with gadolinium doped interconnect) has also been done and reported that one glass composition showed minimum weight loss (approximately zero) after heat treatment at 800°C for 500 hrs. Weil *et al.* [59] used FeCrAlY (82.8 Fe, 22% Cr, 5% Al, 0.2% Y) alloy as a model metal for sealing by brazing to YSZ. In this study, Ag-CuO braze materials were used. Lewinsohn *et al.* [60] presented an idea of using polymers of Si-C-N to make seals to SOFC components. Potentially these polymers can be used as a paste to join two surfaces, but these materials are inherently unstable against oxidation in air at high temperatures or in humidified air.

Table 2.2 Dominant phases formed in glass sealants and their effects on the different properties

S.No.	Phase formed	Properties
1.	Hexacelsian and Celsian ($BaAl_2Si_2O_8$)	Hexacelsian has proved to be stable. It always crystallizes out first with thermal treatment in BaO. Al_2O_3 $2SiO_2$ system glass. Because hexacelsian is more compatible with the parent glasses than the celsian, in terms of TEC mismatch, hexacelsian crystallization is considered desirable in preparation of glass-ceramic sealants for SOFCs, whereas progressive celsian crystallization is considered undesirable. TEC of the hexacelsian is relatively close to that of the stainless steel and reaction zone is quite thin, therefore, thermal expansion mismatch is not as problematic as in the case of $BaCrO_4$ formation. Thus the crystallization of celsian impairs the long term thermal stability of sealant [2, 11, 32]
2.	Cristobalite, Quartz (SiO_2)	Quartz is thermodynamically stable at the operating temperature where as cristobalite acts detrimentally in the case of thermal cycling procedures with respect to a volume change of about 8 %, caused by the change of the crystal structure of cristobalite at 200°C [36]. Imanaka *et al.* [37] examined the effect of ceramic additions containing Al, such as alumina, cordierite based ceramics, aluminium nitride, mullite and spinel into the borosilicate glass for suppression of cristobalite precipitation. The results showed that formation of cordierite, mullite or aluminium nitride suppress cristobalite formation more effectively than alumina or spinel. The common factor for this suppression is the Al^{3+}. It has also been demonstrated that cristobalite prevention depends on the amount of alumina present in the composite.
3.	Cordierite ($Mg_2Al_4Si_5O_{18}$)	Transparent to microwave, resistant to thermal shock and erosion. It is suggested that in the early stages of crystallization, a solid solution rich in SiO_2 crystallizes. In the later stage, an isomorphic substitution of Mg^{2+} and Al^{3+} occurs, that composition approaches to cordierite [38]. Due to low thermal expansion coefficient, it is very harmful for SOFC operation. It can be suppressed with the addition of various additives like TiO_2, Cr_2O_3 [39, 40, 41].
4.	Barium calcium orthosilicate ($Ba_3CaSi_2O_8$)	Thermal expansion of this phase is compatible to other components of SOFC. Highly desirable phase.
5.	Forsterite (Mg_2SiO_4)	Forsterite has no alkali ions in vitreous phase so that it has higher resistivity (> 10^{12} ohm.m). Formation of forsterite phase suppresses the formation of cordierite phase when the alumina content is low (5%). It has been demonstrated that Ni promotes the forsterite formation in MgO-CaO-Al_2O_3 glass system [42]. Ni in the ionic state substitutes the Mg^{2+} ion in the octahedral site of the forsterite structure.

The interaction of the sealing glasses with the metallic interconnects has been studied in detail by different researchers [15, 57]. $BaCrO_4$ has been observed the primary crystalline reaction product of barium calcium aluminosilicate (BCAS) glass and interconnect. However, extent and nature of their interaction depends on the exposure conditions and/or proximity of the interface of the sealing glass and ferritic stainless steel to the ambient air. At or near the edges, where oxygen is accessible, the chromia scale grows on the steel and its vapor species react with BaO from glass ceramic, leading to formation of $BaCrO_4$. In the interior regions where oxygen or air access is blocked, chromia dissolves into BCAS sealing glass to form Cr rich solid solutions. In addition to this, the stainless steel also reacts with the residual species in the sealing glass-ceramic along the interior region of interface. It has been observed by Pio Jinhua [58] that in La doped BCAS glasses T_g and T_c values increase greatly with an increase in CaO content and decrease in the BaO content. It can be attributed due to higher field strength of Ca^{+2} ion as compared to Ba^{+2} ion. The TEC values of these glass samples decrease with reduced Ba^{+2} content and increase in the Ca^{+2} content. The interaction study between glass and LSGM (lanthanum strontium manganese with gadolinium doped interconnect) has also been done and reported that one glass composition showed minimum weight loss (approximately zero) after heat treatment at 800^{o}C for 500 hrs. Weil *et al.* [59] used FeCrAlY (82.8 Fe, 22% Cr, 5% Al, 0.2% Y) alloy as a model metal for sealing by brazing to YSZ. In this study, Ag-CuO braze materials were used. Lewinsohn *et al.* [60] presented an idea of using polymers of Si-C-N to make seals to SOFC components. Potentially these polymers can be used as a paste to join two surfaces, but these materials are inherently unstable against oxidation in air at high temperatures or in humidified air.

They also suggested using ceramic and metallic fillers to control the thermal expansion coefficient (TEC) to match expansion of SOFC components. Loehman [61] has suggested the use of viscous seals for attaching SOFC components. Chou and Stevenson [62-64] used a novel approach of mica and mica-glass hybrid compressive seals with promising results, but these seals require compression loads. Moreover, issues related to interface reactions and crystallization of some of the glasses are also addressed. Chou [65] presented another idea based on infiltrated mica for seals with promising results. In this case mica was infiltrated by with Bi, B and glass-forming materials. The main problem is requirement of the load. Also it may pose stability issues (evaporation) at high temperatures when used over extended times. Taniguchi *et al.* [66] reported using a combination of glass/YSZ and Fiberfax (essentially alumina fiber) fiber matte to seal the SOFC components. The fiber layer was porous and compliant and provided stress reduction on the electrolyte electrode assembly via compliance of the fiber layer. A recent study done by S. Ghosh [67] on BCAS glasses found that higher the BaO content, higher the density of glasses and the value of TEC and T_g increases and viscosity decreases with increase in BaO content. The increase in CTE with increasing BaO content, observed under the present investigation, is believed to be associated with the highest ionic radius of Ba^{+2} among all the alkaline-earth elements in this group of the periodic table [68]. Glass series synthesized by them is found to have low T_g and least mismatch with Crofer 22 APU (steel interconnect) even after 100 hrs of heat treatment at 800^{o}C. SEM study of the same glass series showed that it has most excellent sealing with Crofer 22 APU and have a mixture of amorphous glassy and needle like crystallized phases after heat treatment at 800^{o}C for 20 hrs. In another study done by S. Ghosh [69] on BAS glasses with lanthanum doping shows that it has good compatibility and less TEC mismatch with YSZ and Crofer 22 APU which ultimately leads to the thermal and thermo-mechanical stability of the sealant during long term operation. The XRD pattern of this glass shows the formation of hexacelsian phase which is desirable for SOFC because of its TEC matching within 30-1000^{o}C with other components of SOFC. Therefore, crystallization of hexacelsian is always desirable in the preparation of glass sealant for SOFCs, whereas, rapid and progressive transformation from hexacelsian to celsian is considered undesirable because of less value of TEC in celsian. Fortunately, the transformation of hexacelsian to celsian is very sluggish. According to Drummond *et al.* [70] the crystal structure of hexacelsian contains infinite two dimensional hexagonal sheets consisting of two layers of $(Al,Si)O_4$ tetrahedra. Celsian consists of three dimensional feldspar structure in which all four corners of silica tetrahedra are shared forming a three dimensional network. The transformation of hexacelsian to celsian would require the creation of a three dimensional network from a two dimensional structure of hexacelsian as well as rearrangement of the Ba-sites. This would require breaking and forming of Al–O and Si–O bonds. Due to this kinetic barrier, the transformation of hexacelsian to celsian is very slow. In another work done by Meinhardt *et al.* [71] the glass ceramic resulting from glass sealing displays little interaction with the YSZ electrolyte layer on the cell. However, a reaction zone does develop between the sealant and the situ formed oxide scales of both chromia and alumina forming stainless steels.

In an another study on barium aluminosilicate glasses (BAS) [2], it was found that BAS glasses exhibit the lowest transition temperature, T_g and crystallization temperature, T_c as well as more than two exothermic peaks [Fig. 2.1]. Moreover, glass BAS showed 100% crystallization when heated at ≥800°C. Obviously, the crystallization energy of glass BAS is significantly smaller that that of the other glasses.

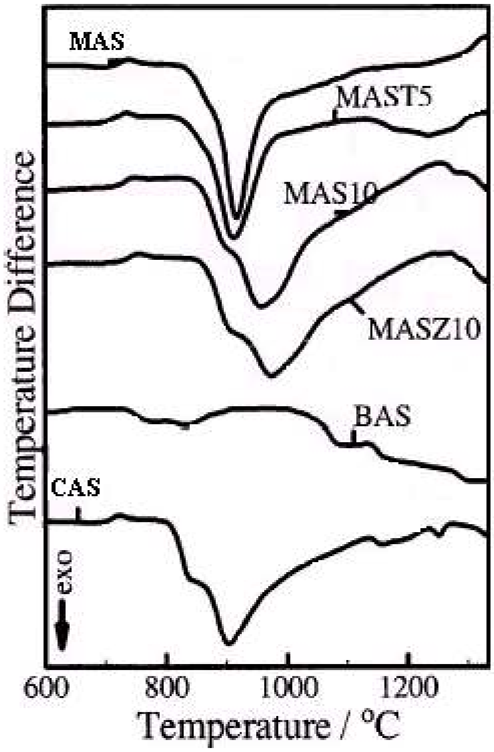

Fig. 2.1 DTA thermograms determined with a heating rate of 10 $Kmin^{-1}$ for samples BAS, CAS, MAS, MAST5, MAS10, MASZ10 [2].

2.6 CaO-Al_2O_3-SiO_2 (CAS) and SrO-Al_2O_3-SiO_2 systems

Many researchers have investigated the crystallization of CAS glass system. According to Lahl *et al.* [12], the sealant CAS shows a lower thermal expansion coefficient than the sealant MAS though the field strength of Mg^{2+} exceeds that of Ca^{2+}. They attributed this result to the higher degree of crystallization of sealant CAS as compared to sealant MAS. Also, it has been observed [12] that activation energy increases significantly as the alkaline earth metal changes from Ba to Ca and to Mg. The reason to this observation has been explained on the basis of field strength. Monterio *et al.* [49] realized that the glasses crystallize in the whole body when the SiO_2 content in CAS glasses is low. Kingery's research [72] showed that the glasses crystallize only on the surface if the content of SiO_2 is high but, if some nucleating agents such as TiO_2, Cr_2O_3, etc., are added to the glasses, they can crystallize in the whole body. Larsen and James [73] reported that presence of Cr (VI) in the form of $CaCrO_4$ might cause pore formation inside the seal if severe reaction takes place at the inrterconnect-seal interface. Lahl *et al.* [32] showed that CaO base glasses in contact with 8YSZ give rise to the formation of m-ZrO_2, which is detrimental to SOFC. This may not only create leakage in the seal but will also reduce the mechanical strength. Gunther *et al.* [74] and Ley *et al.* [1] reported promising results for high B_2O_3 glasses in the SrO-La_2O_3-Al_2O_3-B_2O_3-SiO_2 system. Boron undergoes significant reaction with humidified hydrogen to form several gaseous species including $B_2(OH)_2$ and $B_2(OH)_3$ at operating temperature. Therefore, it can be concluded that high boron containing glass will likely undergo measurable corrosion over time in a humidified fuel environment. However, the softening temperature of these glasses was too low for SOFCs operating above 700°C [75]. Also, glass compositions based on B_2O_3 tend to exhibit excessive volatilization in the SOFC environment.

Several studies of the interconnect alloys in oxidizing atmosphere have demonstrated that Cr vaporization might present a long-term reliability issue [8, 35]. Apart from this other studies on interconnect alloys have focused on the contact resistance of the alloys both with and without ceramic coating [34, 73, 76]. In general, the long term stability of the interconnect is critical parameter for electrical performance. But the chemical reaction for the sealing glass with an oxide scale appears to be critical for the hermiticity requirement [1].

To date, the best results have been obtained using compositions rich in silica. While alkali silicate glasses tend to be very reactive towards SOFC components [13], alkaline-earth aluminosilicate glasses have yielded promising results [12, 44, 19, 32].

Although silicates are the most common ceramic glass sealants, non-oxide systems synthesized from the polymer precursors have also been developed [77, 78]. However, the stability of such systems in the oxidizing environment of the SOFC cathode creates as additional challenge to their implementation as a sealing material.

Nonetheless, barium calcium aluminosilicates have been used successfully in operating fuel cells [79]. In addition, the success of glass sealants has led to their use for bonding the interconnects to the frames [80].

In another study done by F. Smeacetto [81] to join Crofer 22 APU alloy to YSZ by glass ceramic seal in planer SOFCs, they have designed a new barium and boron free glass of composition SiO_2-Al_2O_3-CaO-Na_2O and successfully used that glass to join YSZ to Crofer 22 APU alloy. The pressure less joining process at 900^oC causes the partial surface induced crystallization of the glass, resulting in a glass–ceramic seal, still having a matched TEC with both YSZ and Crofer 22 APU alloy. The wettability of the seal was determined to be very good on both YSZ and as received and preoxidised Crofer 22 APU substrates. Thermal ageing in air (800 ^oC,400 h) caused a Cr-diffusion from Crofer 22 APU alloy to the seal only when the alloy is in the as received condition, whereas the preoxidised one did not result in migration of Cr ions through the seal.

F. Smeacetto *et al.* [82] have also studied the performance and characterization of glass-ceramic sealant to join metallic interconnect to YSZ and anode-supported-electrolyte in planer solid oxide fuel cell. The designed glass-ceramic taken by them was barium-free silica-based glass, which crystallizes by heat treatment after being deposited on substrate by the slurry technique. The joined ceramic/seal/metal sample was characterized and tested for 400 h in air and hydrogen atmosphere at fuel cell operating temperature i.e 800^oC. The glass sealant made by them was successful in joining the ceramic electrolyte to the metallic interconnect and also prevented the corrosion at the interface.

In a theoretical study A. Pramuanjaroenkij *et al.* [83] have developed the mathematical transport model for planar solid oxide fuel cells. In this model SOFC being operated at 500, 600, 800 & 1000^{o}C and reversible cell voltage is obtained by the use of modified nernst equation. They have also compared the electrolyte material i.e. YSZ and CGO (gadolinium-doped ceria) and found that YSZ electrolyte shows higher power density than the CGO electrolyte at higher temperatures than 750^{o}C.

In another study by Zhang *et al.* [84] thermodynamic calculations and experimental results of volatility of borate glass for SOFC have been reported. They have observed that the glasses containing 20 mol% B_2O_3 have 10 times greater weight loss than the glass containing 2 mol% of B_2O_3 under the same condition. The activation energy of volatilization was calculated to be 371 ± 86 and 372 ± 65 kJ/mol for this category of glasses.

2.7 ZnO containing systems

C. Lara *et al.* [54] have investigated the effect of ZnO on the properties of glass sealants which are used in SOFC. Glass containing ZnO gives TEC value 9-11 X $10^{-6}/^{o}C$ which is comparable to the other components of SOFC. Glasses containing ZnO shows small value of expansion with increase in temperature, which is desirable for its application in SOFC. During crystallization process Ca and Mg containing glass samples exhibits undesirable expansion whereas Zn containing glass best fits the sealing requirement. In another study done by C. Lara *et al.* [3] transition and softening temperatures decrease with increase in ZnO content and the glasses containing Zn best fulfill the dilatometric requirement of SOFC sealant and present sintering before crystallization, this allowing dense and homogeneous glass-ceramics to be obtained. In another work performed by Lara *et al.* [85] have shown the electrical properties of glasses containing ZnO and calculated its electrical resistance value which is much higher than 10^4 Ωcm in the range of studied temperature. A study done by Wang *et al.* [86] on PbO and ZnO containing glass shows good adherence with YSZ electrolyte at some particular angle under a suitable pressure and it also avoids the spreading of glass freely on the surface of electrolyte. A study done by Tkalcec *et al.* [87] conclude that nanocrystalline transparent glass-ceramic with gahnite as the single phase could be achieved by controlled heat treatment of bulk glasses with composition of SiO_2-Al_2O_3-ZnO and TiO_2 as nucleating agents. The crystallization of metastable zinc-aluminosilicate occurred on the surface of particles, whereas gahnite crystallized by volume crystallization mechanism.

Based on the literature review a glass series with composition $40SiO_2$-30BaO-20 ZnO-(10-x)B_2O_3-xM_2O_3 (M=Al, La, Y, Mn) has been selected. SiO_2 is selected on the basis of its large glass forming range and its ability to decrease TEC value. BaO has property to enhance TEC value. ZnO will again increases the glass forming range, increases T_g value, controls viscosity and decreases TEC of glass. B_2O_3 will lower the T_g, decreases viscosity value and increases TEC value. Addition of Al_2O_3 increases the surface tension leading to lowering of crystallization. This further results in lowering of T_g and an increase in TEC value. La_2O_3 controls the viscosity value whereas Y_2O_3 suppresses the formation of cordierite phase. Mn_2O_3 has not been studied yet in the literature.

References:

[1] K. Ley, M. Krumplet, R. Kumar, J. Meiser, I. Bloom, J. Mat. Res. 11 (1996) 1489.

[2] S.-B. Sohn, S.-Y. Choi, G.-H. Kim, H.-S. Song and G.-D. Kim, J. Non-Cryst. Solids 297 (2002) 103.

[3] C. Lara, M. J. Pauscal, A. Duran, J. Non-Cryst. Solids 348 (2004) 149.

[4] K. D. Meinhardt, J. D.Vienna, T. R. Armstrong, L. R.. Pederson, U. S. Pat. 6430966 (Aug. 13, 2002).

[5] D. R. Uhlmann, J. Non-Cryst. Solids 38 & 39 (1980) 693.

[6] U. Schiffner and W. Panhorst, Glastech. Ber., 60 (1987)239.

[7] I. Gutzow and J. Schmelzer, The Vitreous State (Springer, Berlin, 1995).

[8] S. P.Jiang, L. Christiansen, B. Hughan, K. Foger, J. Mater. Sci. Lett. 20 (2001) 695.

[9] D. Stolen, E. Monreal, W. Miller in Fuel Cell Seminar Abstracts, Tucsan, AZ, November 29th - December 2nd, 1992, p. 53.

[10] Y. Harufuji, Jpn Kokai Tokyo JP 04-47, 672 (Feb. 17, 1992).

[11] S.-B. Sohn, S.-Y. Choi, G.-H. Kim, H.-S. Song and G.-D. Kim, J. Am. Ceram. Soc., 87 [2] (2004) 254.

[12] N. Lahl, K. Singh, L. Singheiser, K. Hilpert, D. Bahadur, J. Mater. Sci. 35 (2000) 3089.

[13] D. Bahadur, N. Lahl, K. Singh, L. Singheiser, K. Hilpert, D. Bahadur, J. Electrochem. Soc. 151 (2004) A558.

[14] N. Lahl, L. Singheiser, K. Hilpert, K. Singh, D. Bahadur, in "Solid Oxide Fuel Cells-VI" edited by S. Singhal, M. Dokiya (Electrochemical Society, Pennington, NJ, PV 99-19, 1999) p. 1057.

[15] Z. Yang, J. W Stevenson and K. D. Meinhardt, Solid State Ionics 160 (2003) 213.

[16] I. D. Bloom, K. L. Ley, U.S. Pat. 5453331 (Sept. 26, 1995).

[17] P. H. Larsen, F. W. Poulsen, R. W. Berg, J. Non-Cryst. Solids 244 (1999) 16.

[18] Robert A Meyers "Encyclopedia of Physical Science and Technology" (Academic Press Inc. 1987) Vol. 6.

[19] N. Gupta, K. Singh, O. P. Pandey in Proceedings of the National Conference on Materials and Related Technologies held at Thapar Institute of Engineering & Technology, Patiala during September 19-20, 2003 p. 141.

[20] K. Singh, N. Gupta, O. P. Pandey, J. Mater. Sci. 42 (2005) 6426.

[21] M. Tomozawa, in "Advances in Crystallization and Nucleation in Glasses"(American Ceramic Society, 1971) p. 41.

[22] Robert H. Dooremus in Glass Science (Second Edition) (John Wiley & Sons, Inc., New York, NY, 1994) p. 85.

[23] W. B. Hillig, in Proceedings of Symposium on Nucleation and Crystallization in Glasses and Melts (American Ceramic Society, Columbus, OH, 1962) pp. 77.

[24] U. Schiffner and W. Panhorst, Glastech. Ber., 60 (1987)239.

[25] T. J. Barry, D. Clinton, L. A. Ray, R. A. Mercer, and R. P. Miller, J. Mater. Sci. 4 (1969) 496; 5 (1970) 117.

[26] A. Adamson in, "Physical Chemistry of Surfaces, 4th Ed." (John Wiley, New York, 1982).

[27] K. A. Nielsen, M. Solvang, F. W. Poulsen, P. H. Larsen, Ceram. Eng. Sci. Proc. 25 (2004) 309.

[28] S. Ohara, K. Mukai, T. Fukui, Y. Sakaki, M. Hattori, Y. Esaki, J. Ceram. Soc. Japan 109 (2001) 186.

[29] Y. Sakaki, M. Hattori, Y. Esaki, S. Ohara, T. Fukui, K. Kodera, Y. Kubo, Proc. Electrochem. Soc. 97-408 (SOFC V) (1997) 652.

[30] T. W. Kueper, I. D. Bloom, in, Proceedings of International Conference on Heat Resistant Materials 2nd edited by: K. Natesan, P. Ganesana, G. Y. Lai (ASM International, Materials Park, OH, 1995) p. 545.

[31] T. I. Barry, J. M. Cox and R. Morell, J. Mater. Sci. 13 (1978) 594.

[32] N. Lahl, K. Singh, L. Singheiser, K. Hilpert, D. Bahadur, J. Electrochem. Soc. 149 (2002) A607.

[33] M. G. Nicholas, "Joining Structural Ceramics" In Designing Interfaces for Technological Applications, edited by S. D. Peteves, (Elsevier Appl. Science, Amsterdam, 1989) p. 49.

[34] K. Eichler, G. Solow, P. Otschik and W. Schaffrath, J. Eur. Ceram. Soc. 19 (1999) 1101.

[35] Z. Yang, K. D. Meinhardt, J. W. Stevenson, J. Electrochem. Soc. 150 (2003) A1095.

[36] T. Schwickert, R. Sievering, P. Geasee and R. Conradt, Mat.-wiss.u. Werkstofftech.

33 (2002) 363.

[37] Yoshihiko Imanaka, Shigenori Akoi, Nobuo Kamehara and Koichi Niwa, J. Am.

Ceram. Soc. 78 (1995) 1265.

[38] W. Zdaniewski, J. Am. Ceram. Soc. 58 (1975) 163.

[39] J. W. Stevenson, T. R. Armstrong, R. D. Carneim, L. R. Pederson and W. J. Weber, J. Electrochem. Soc. 143 (1996) 2722.

[40] J. S. Hardy, J. Y. Kim and K. S. Weil, J. Electrochem. Soc. 151 (2004) J43.

[41] J. Kim, A. Virkar, in, "Solid Oxide Fuel Cells-VI" , edited by S. Singhal, M. Dokiya (Electrochemical Society, Pennington, NJ, PV 99-19, 1999) p. 830.

[42] L. Barbieri, A. M. Ferrari, C. Leonelli, T. Manfredini, G. C. Pellacani, S. Bruni and F. Cariatti, Phys. Chem. Glasses 36 (1995) 176.

[43] C. H. Drummond III and N. P. Bansal, Ceram. Eng. Sci. Proc. 11 (1990) 1072.

[44] M. J. Hyatt and N. P. Bansal, J. Mater. Sci. 31 (1996) 172.

[45] Y.-M. Sung, J. Mater. Sci. 35 (2000) 4913.

[46] N. A. Toropov, F. Y. Galakhov and I. A. Bondar, Izvest. Akad. Naak S.S.S.R, Otdel. Khim. Naak 5 (1954) 756.

[47] Y.-S Chou and J. W. Stevenson, J. Power Sources 140 (2005) 340.

[48] W. Holland, G. Beall in "Glass-Ceramics Technology" (The American Ceramic Society, Westerville, OH, 2002).

[49] Y. S. Touloukian (Ed.), Thermophysical Properties of High Temperature Solid Materials, vol. 4, Oxides and Their Solutions and Mixtures, (The MacMillan Co., New York).

[50] N. H. Menzler, M. Bram, H. P. Buchkremer, D. Stoever, J. Eur. Ceram. Soc. 23 (2002) 445.

[51] N. P. Bansal, M. J. Hyatt, C. H. Drummond III, Ceram. Eng. Sci. Proc. 12 (1991) 1222.

[52] D. Bahat, J. Mater. Sci. 7 (1972) 198.

[53] K. Scott Weil, John E Deibler, John S Hardy, Dong Sang Kim, Guan Guang Xia, L A Chick and Chris A Coyle, J. Mat. Eng. Perf. 13[3] (2004) 316.

[54] C. Lara, M. J. Pascual, J. M. Prado, A. Duran, Solid State Ionics 170 (2004) 201.

[55] K. S. Weil, J. Mater. Eng. Perf. 13 (2003) 309.

[56] N. P. Bansal, E. A. Gamble in Proceedings of Electrochemical Society 2005-07 (SOFC IX).

[57] Z. Yang, G. Xia, K. D. Meinhardt, K. Scott Weil and J. W. Stevenson, J. Mat. Eng. and Perf. 13 (2004) 327

[58] P. Jinhua, S. Kening, Z. Naiqing, C. Xinbing and Z. Derui J. Rare Earths 25 (2007) 434.

[59] K.S. Weil, J.S. Hardy, and J.Y. Kim, The Joining of Advanced and Specialty Materials, Vol V, ASM, 2003.

[60] C. Lewinsohn, S. Quist, and S. Elangovan, SECA Core Technology Program Review, October 1, 2003, Albany, NY.

[61] R. Loehman, SECA Core Technology Program Review, October 1, 2003, Albany, NY.

[62] Y.S. Chou, SECA Core Technology Program Review, October 1, 2003, Albany, NY

[63] Y.S. Chou, J.W. Stevenson, and L.A. Chick, J. Power Sources, 2002, 112**,** 130.

[64] Y.S. Chou and J.W. Stevenson, J. Power Sources, 2003, 115**,** 274.

[65] S. Tanaguchi, M. Kadowaki, T. Yasuo, Y. Akiyamu, Y. Miyaki, and K. Nishio, J. Power Sources, 2000, 90,163.

[66] I.W. Donald, J. Mater. Sci., 1993, 28**,** 2841.

[67] S. Ghosh, A.D. Sharma, P. Kundu, S. Mahanty and R. N. Basu, J. Non-Cryst. Solids xxx(2008)xxx-xxx

[68] S. Ghosh, A. Das Sharma, P. Kundu, R.N. Basu, H.S. Maiti, Electrochem. Soc. Trans. 7 (2007) 2443.

[69] S. Ghosh, P. Kundu, A.D. Sharma, R. N. Basu, H. S. Maiti, J. Eur. Ceram. Soc. 28 (2008) 69.

[70] C. H. Drummond, W. E. Lee, N. P. Bansal, and M. J. Hyatt, Ceram. Eng. Sci. Proc., 10(9-10) (1989) 1485.

[71] K. D. Meinhardt, D. S. Kim, Y. S. Chou and K. S. Weil, J. Power Sources 182 (2008) 188.

[72] W. D. Kingery, P. B. Vandiver, I. W. Huang, J. Non-Cryst. Solids 54 (1983) 163.

[73] P. H. Larsen and P. F. James, J. Mater. Sci. 33 (1998) 2499.

[74] C. Gunther, G. Hofer, W. Kleinlein, Proceedings of the Fifth International Symposium on Solid Oxide Fuel Cells, vol. 97-18, The Electrochemical Society, 1997, p. 746.

[75] F. Teitz, Ionics 5 (1999) 129.

[76] S. P. Simner, J. W. Stevenson, J. Power Sources 102 (2001) 310.

[77] C. A. Lewinsohn, S. Elangovan, S. M. Quist, Ceram. Eng. Sci. Proc. 25 (2004) 315.

[78] C. A. Lewinsohn, S. Elangovan, Ceram. Eng. Sci. Proc. 24 (2003) 317.

[79] L. G. J. de Haart, I. C. Vinke, A. Janke, H. Ringel, F. Tietz in, Proceedings of Electrochemical Society 2001-16 (SOFC VII) (2001) 111.

[80] L. Blum, H. P. Buckhkremer, L. G. J. de Haart, H. Habielek, J. W. Quadakkers, U. Reisgen, R. Steinbrech, F. Tietz, I. Vinke, Ceram. Eng. Sci. Proc. 25 (2004) 219.

[81] F. Smeacetto, M. Salvo, M. Ferraris, J. Cho and A.R. Boccaccini, J. Eur. Ceram. Soc. 28 (2008) 61.

[82] F. Smeacetto, M. Salvo, M. Ferraris, V. Casalegno, P. Asinari and A. Chrysanthou, J. Eur. Ceram. Soc. 28 (2008) 2521.

[83] A. Pramuanjaroenkij, S. Kakac and Xiang Yang Zhou International Journal of Hydrogen Energy, 33 (2008) 2547.

[84] T. Zhang, W. G. Fahrenholtz, S. T. Reis and R. K. Brow, J. Am. Ceram. Soc. 91 (2008) 2564.

[85] C. Lara, M. J. Pascual, R. Keding and A. Dur´an, J. Power Sources 157 (2006) 377.

[86] Ruifang Wang, Zhe Lu, Chaoqian Liu, Ruibin Zhu, Xiqiang Huang, Bo Wei, na Ai and Wenhui Su, J. Alloys Comp. 432 (2007) 189.

[87] Emilija Tkalcec, Stanislav Kurajica and Hrvoje Ivankovic J. Non-Cryst. Solids 351 (2005)149.

Chapter 3

Experimental Techniques

Overview

This chapter describes the details of experimentation. The experimental procedures followed to prepare glasses of different compositions and their melting schedule is given. The characterization procedures along with instruments used to generate and analyze the data has been given. The details about each of the instrument, its model number, working and operating conditions have been given. The steps followed for different experiments have been schematically shown with the help of flow chart. This chapter sums up the whole scheme of events leading to successful completion of experimental work.

The detail about sample processing methodology, which we followed during the course of the investigation, is presented in this chapter. Conventional techniques were used for the measurement of thermal properties of glass sealants viz. transition temperature, crystallization temperature, melting temperature, softening temperature, percentage change in length with temperature and thermal expansion coefficient. SEM used for microstructural investigation. XRD was used to confirm the amorphous nature of glass and further used to have information about the various phases formed during different heat-treatments. Two-probe method was used to confirm the high resistance of glass samples.

3.1 Raw Materials

In the present study, raw materials used for preparing the samples were SiO_2 (99%, CDH), $BaCO_3$ (99%, Sdfine), ZnO (99.5%, Sdfine), B_2O_3 (99%, Sdfine), Al_2O_3 (99.9%, CDH), La_2O_3 (99.9%, CDH), Mn_2O_3 (99%, Sigma Aldrich), and Y_2O_3 (99.995%, Sigma Aldrich). All these materials were used without any further purification.

3.1.1 Sample Preparation

Glass samples were prepared by grinding the raw materials using conventional techniques followed by melting. Each batch was prepared by taking an appropriate mole fraction of well-desired initial ingredients and grinding them in mortar and pestle. Sample compositions with their label are given in table 3.1. The followed process for making of sample is shown in Fig. 3.1.

Table 3.1 : Glass compositions (mol %) with their label

Sample Label	**SiO_2**	**BaO**	**ZnO**	**B_2O_3**	**Al_2O_3**	**La_2O_3**	**Mn_2O_3**	**Y_2O_3**
INA1	40	30	20	10	0	0	0	0
INA 2	40	30	20	7.5	2.5	0	0	0
INA 3	40	30	20	5.0	5.0	0	0	0
INA 4	40	30	20	2.5	7.5	0	0	0
INA 5	40	30	20	0	10	0	0	0
INL-1	40	30	20	7.5	0	2.5	0	0
INL-2	40	30	20	5.0	0	5.0	0	0
INL-3	40	30	20	2.5	0	7.5	0	0
INL-4	40	30	20	0	0	10	0	0
INM-1	40	30	20	0	0	0	2.5	0
INM-2	40	30	20	0	0	0	5.0	0
INM-3	40	30	20	0	0	0	7.5	0
INM-4	40	30	20	0	0	0	10	0
INY-1	40	30	20	0	0	0	0	2.5
INY-2	40	30	20	0	0	0	0	5.0
INY-3	40	30	20	0	0	0	0	7.5
INY-4	40	30	20	0	0	0	0	10

Fig. 3.1 Process of pouring the glass in graphite mould at 1550°C

For each system, required amount of raw materials as per the stoichiometric ratio were taken. The mixture was grinded to break agglomerate particles. After grinding the mixture was further transformed to ball mill and grinded for two hours in a ball mill in wet medium (acetone). The ball milling was done using porcelain balls in porcelain jar (Retsch, Germany, Model S 1000). The mass to ball ratio for each system was 1:2 which was kept constant for each milling. The resulting mixture was dried in air. The mixed dried powder of the homogenous mass was transformed in recrystallized alumina crucible and heated in an automized Molybdenum Disilicide ($MoSi_2$) electric high resistance furnace in oxidizing atmosphere. The powder of the samples were initially heated to achieve a temperature of 1000 ºC in 2 hrs i.e. at a heating rate of 8K/min. The temperature was maintained at 1000 °C for 45 minutes to facilitate the calcination. During heating process moisture is released and the calcinations occurs. After that the temperature was increased upto 1200 °C at a rate of 3K/min and kept at this temperature for 30 minutes to facilitate the fusion and melting process. Then, system was reheated at 1550 ºC by keeping constant heating rate and kept at this temperature for 1 hour 45 minutes in order to achieve the homogeneous molten glass. The schedule followed for sample melting is also shown in Fig. 3.2. The molten mass was poured in a preheated graphite mold. The remaining melt was poured on the flat copper plate and quenched by other copper plate in air to obtain flakes. All the samples were prepared using the same route as described above. Before melting, the furnace was calibrated and in hot zone fluctuation in temperature was within ± 2 °C. In order to check the percentage weight loss of volatile substances (B_2O_3, ZnO) after the formation of glass, glass compositions are studied by AAS (atomic absorption spectroscopy) and wet chemical analysis and results obtained by them is given in next chapter. The details of the sample preparation and other relevant information about preparation and characterization are summarized in the Fig. 3.3.

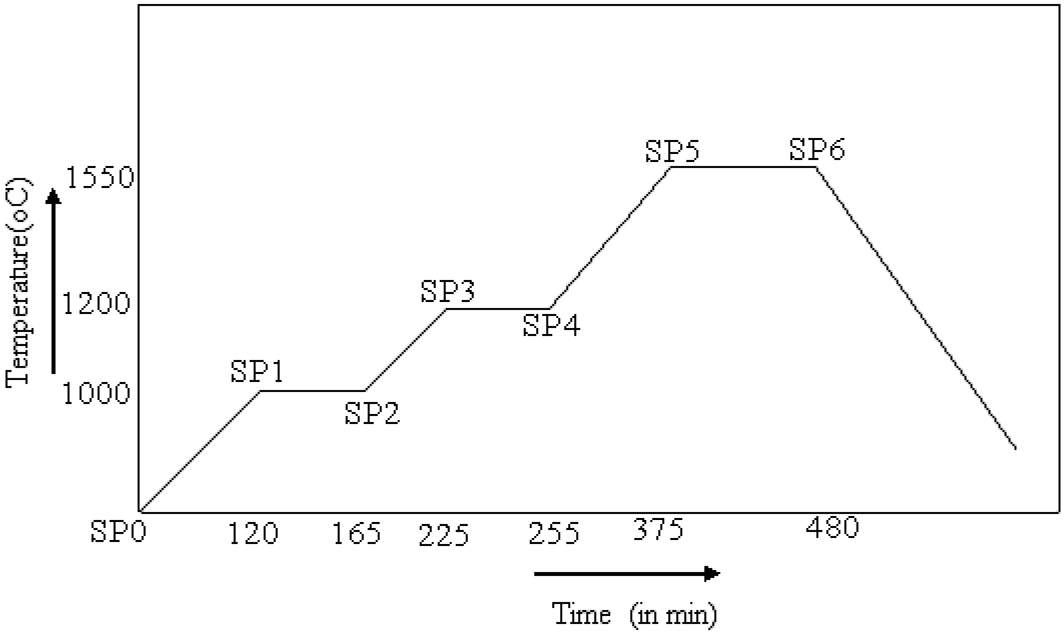

Fig. 3.2 Typical schedule followed for the melting of the glass samples.

3.1.2 Annealing

The obtained frits were annealed at 500 °C (below T_g, glass transition temperature) for 10 hours in air in a calibrated resistance heating furnace. The annealing process is done to remove the internal stresses generated during quenching process.

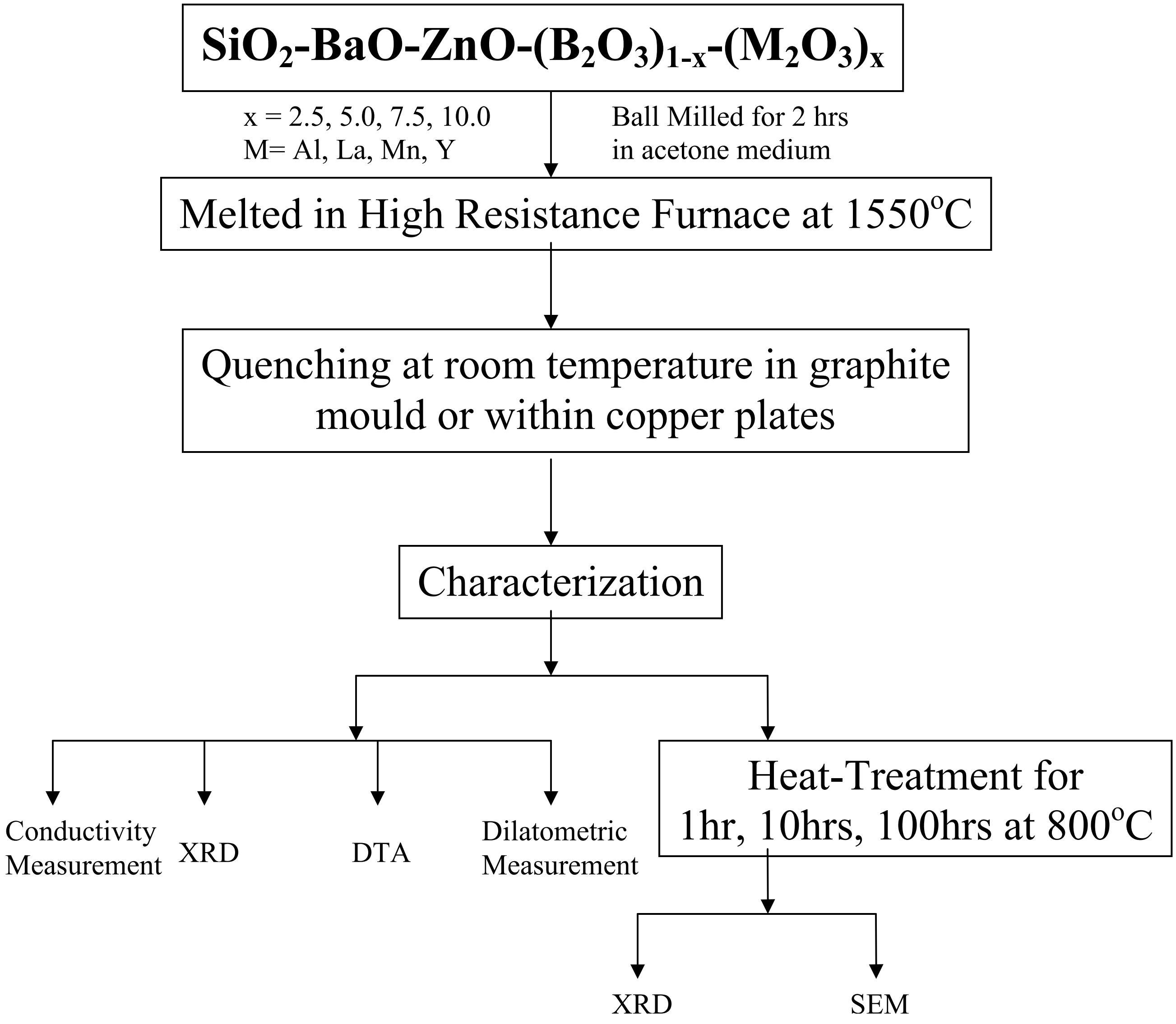

Figure 3.3 Flow chart of the procedure followed throughout the work

3.2 Characterization of Materials

The materials obtained following the above procedure is then characterized to know the initial structure and transformation during various heat-treatments. Different transition temperatures (T_g, T_c), percentage change in length with respect to temperature and conductivity measurement were also done. For the analysis of above parameters, the obtained glass samples were characterized through X-ray diffraction (XRD), differential thermal analysis (DTA), scanning electron microscopy (SEM), dilatometry and conductivity measurement. The long time duration heat treatment temperature (800°C) is selected on the basis of results obtained by DTA study. The details of these techniques are given below:

3.2.1 X-Ray Diffraction

X-ray diffraction (XRD) is a versatile, non-destructive technique that reveals detailed information about the chemical composition and crystallographic structure of natural and manufactured materials. X-ray powder diffractogram was recorded at room temperature by Philips Xpert Powder diffractometer using monochromatic CuK_α radiation (λ = 1.5418 Å) at a scan speed of 1°/minutes. Monochromatic X-rays are used to determine the interplanar spacing of the unknown samples. Samples are analyzed as powders with grains in random orientations to insure that all crystallographic directions are sampled by the beam. When X-rays are scattered from a crystal lattice (fig. 3.4), peaks of scattered intensity are observed which correspond to the following conditions:

1. The angle of incidence = angle of scattering.
2. The pathlength difference is equal to an integer number of wavelengths.

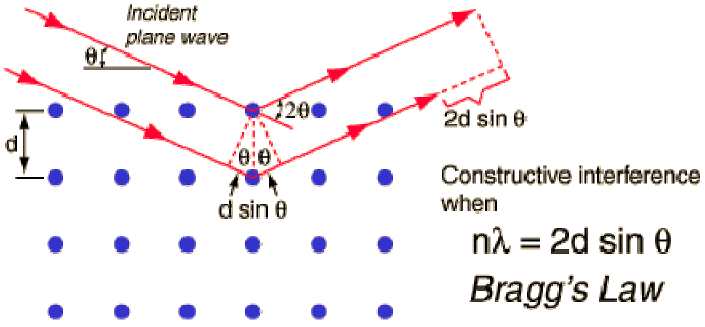

Figure 3.4 Geometric derivation of Bragg's law

The condition for maximum intensity contained in Bragg's law above allow us to calculate details about the crystal structure, or if the crystal structure is known, to determine the wavelength of the x-rays incident upon the crystal.

$$2d\text{Sin}\theta = n\lambda$$

where d = interplanar spacing, λ = wavelength of incident x-ray, θ = diffraction angle, n = integer

The data obtained from XRD is indexed by standard powder diffraction files provided by International Centre for Diffraction Data -ICDD (formerly known as JCPDS).

3.2.2 Scanning Electron Microscopy (SEM)

The scanning electron microscope (SEM) is a type of electron microscope that images the sample surface by scanning it with a high-energy beam of electrons. The electrons interact with the atoms that make up the sample producing signals that contain information about the sample's surface topography, composition and other properties such as electrical conductivity. The types of signals produced by the SEM include secondary electrons (SE), back scattered electrons (BSE), characteristic x-rays, light (cathodoluminescence), specimen current and transmitted electrons. These types of signals require specialized detectors for their detection that are not usually present on a single machine. The signals result from interactions of the electron beam with atoms at or near the surface of the sample.

In the present study, scanning electron micrographs of the selected samples were taken by SEM (EVO, 50) in order to understand the crystal growth in samples during various heat-treatments.

3.2.3 Differential Thermal Analysis (DTA)

Differential thermal analysis (DTA) is a thermoanalytic technique, similar to differential scanning calorimetry. In DTA, the material under study and an inert reference are heated (or cooled) under identical conditions, while recording any temperature difference between sample and reference. This differential temperature is then plotted against time, or against temperature (DTA curve). Changes in the sample, either exothermic or endothermic, can be detected relative to the inert reference. Thus, a DTA curve provides data on the transformations that have occurred, such as glass transitions, crystallization and melting.

In the present work differential thermal analysis of the powdered samples was done by DTA, Perking Elmer (Diamond TG/DTA) in nitrogen atmosphere (Fig. 3.5) using platinum crucibles at different heating rates from room temprature to 1000 ^{o}C. The reference sample taken was α-alumina. Thermographs has been taken between temperature and endotherm showing the endothermic (transition and melting) and exothermic (crystallization) peaks.

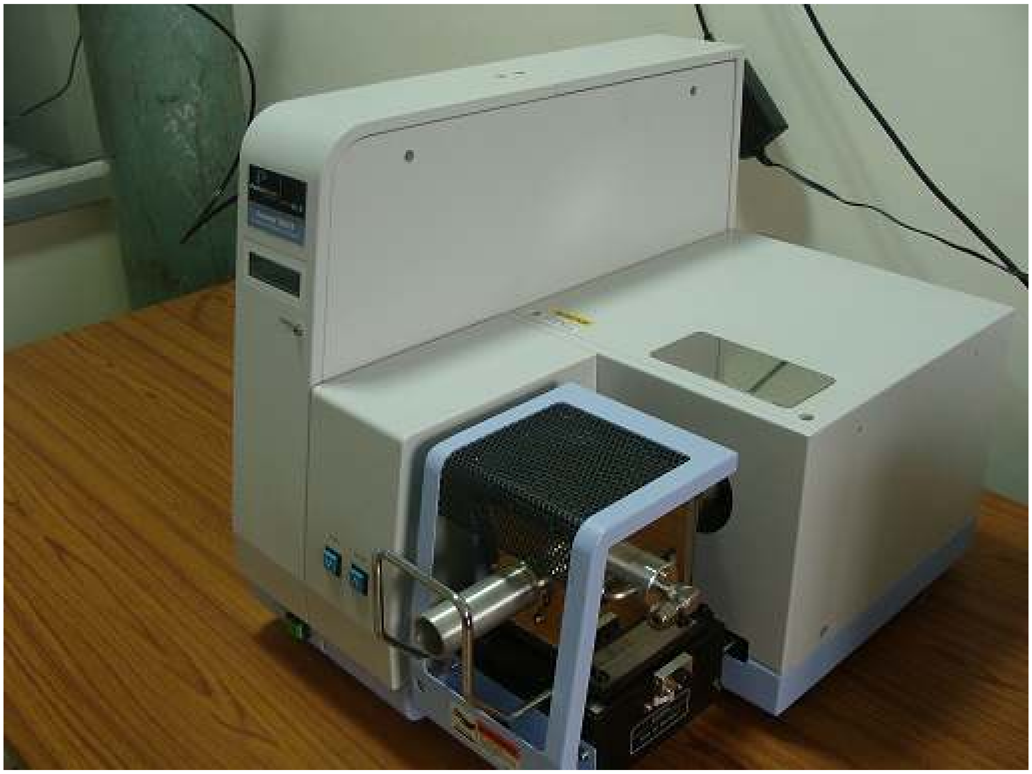

Figure 3.5 Differential Thermal Analyzer (DTA)

3.2.4 Dilatometric Measurement

Thermal dilatometric analysis (TDA), often called "dilatometry", measures the dimensional change of a material (ceramics, glasses, metals, composites and others) as a function of temperature or time. This test determines both reversible and irreversible changes in length (expansion and shrinkage) during heating and cooling, and pinpoints where reactions occur that cause expansion or contraction. The dilatometer is used to determine Coefficient of Thermal Expansion (CTE), softening point, glass transition temperature, curie point, crystalline transformation, phase transition, shrinkage, warping, bloating, sintering rate, isothermal creep and stress relaxation.

In the present work dilatometery of the well polished glass frits was done by dilatometer, Netzsch (DIL 402 PC) in air using alumina kit including alumina push rod at a heating rate of 5^{o}C/min (Fig. 3.6) from room temprature to a specific temperature depending upon the sample requirement. Thermographs has been taken between temperature and percentage change in length of the sample. Thermal expansion coefficient of all the glass samples was measured at various temperature ranges.

Figure 3.6 Thermal Dilatometric Analyzer (TDA)

3.2.5 Conductivity Measurement

Electrical conductivity of a material was measured directly by imposing a dc current [1] in which voltage drop is measured across the material according to ohm's law. In case of ionic conductors, it is not so straight forward as dc voltage will cause the flow of current due to both ions and electrons. The material will become polarized as electrodes blocks the ion movement and voltage drops to zero. In case of glasses, being insulators, they have very low value of conductivity and high value of resistivity i.e. of MΩ range.

In the present study, resistivity measurement of glass samples was done by using programmable automatic RCL meter, Fluke (PM6306) at room temperature by taking circuit in parallel. Glass being insulators have very high value of resistivity. For this purpose glasses need to be conducting, so selected glass samples are given very fine coating by silver paint and observed value of resistivity was lying in the MΩ range as per our requirement.

References

[1] CRC Handbook of Solid State Chemistry, Eds P. J. Gellings and H. J. M. Boumeester (CRC press Inc. , USA, 1997)

Chapter 4

Results and Discussion

Overview

In this chapter the experimental results of different series of glasses are presented. The entire work has been done to achieve the properties of glasses which can make it suitable as glass sealant in SOFC. The properties which are required for making the glass suitable as sealant material are glass transition temperature (T_g) and thermal expansion coefficient (TEC). Apart from these its long term behavior under different reducing and oxidizing atmosphere with other components of SOFC is also important. In this chapter the study on different glass series is presented. The results obtained by XRD (X-Ray Diffraction), SEM (Scanning Electron Microscopy), DTA (Differential Thermal Analysis), TDA (Thermal Dilatometric Analysis) and conductivity measurement of all the prepared glass samples are analyzed.

The as prepared glass samples were given different heat treatments for various time durations and the phases formed during heat-treatments was studied by XRD and SEM. In this study the glass series $40SiO_2$- $30BaO$-$20ZnO$- (10-x) B_2O_3- x M_2O_3 (M= Al, La, Mn, Y) was selected because of better properties of various constituents used in it. SiO_2 being an excellent glass-former is taken to be 40 mol% and it increases glass forming range also. BaO acts as glass modifier and it also lowers the melting temperature of the glass. ZnO acts as an intermediate which controls the viscosity of glass and increases glass-forming range. B_2O_3 helps to lower the T_g value and improves fluxing phenomenon. The elements chosen for replacement of B_2O_3 will act at network modifiers and helps to control values of T_g, T_c and TEC. After confirming that all the glasses made from these compositions are amorphous in nature. The subsequent study was taken in detail.

4.1 INA-Series

In this series $40SiO_2$-$30BaO$-$20ZnO$-$(10-x)B_2O_3$–xAl_2O_3 (x=0, 2.5, 5.0, 7.5, 10.0) five samples have been prepared and studied which is described in subsequent sections.

4.1.1 Differential Thermal Analysis (DTA)

Thermal analysis of prepared glass series was carried out by differential thermal analysis at different heating rates of 10 ^{o}C/min, 20 ^{o}C/min, 30 ^{o}C/min and 40 ^{o}C/min from 50 ^{o}C to 1000 ^{o}C by taking α-alumina as reference. For this study the amount of sample taken was approximately 20 mg. The plots of INA-1, INA-2, INA-3, INA-4 and INA-5 glass samples at different heating rates are shown in figures 4.1, 4.2, 4.3, 4.4 and 4.5 respectively.

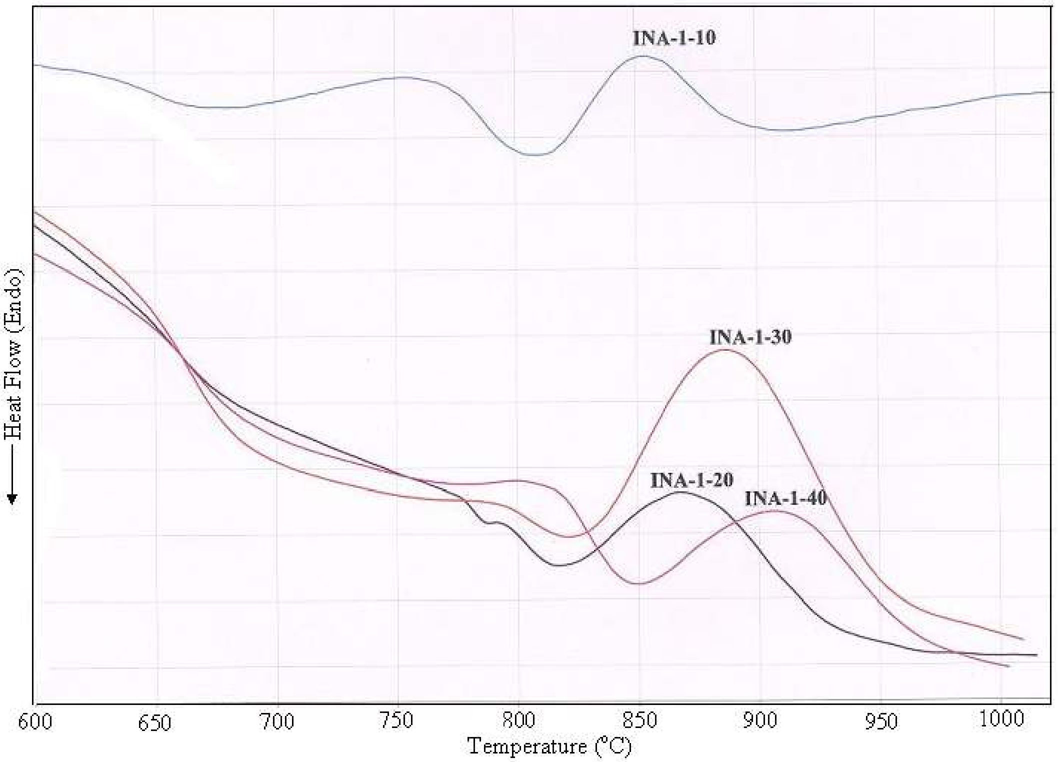

Figure 4.1 DTA plot of INA-1 glass sample at 10, 20, 30, 40^{0}C/min from 600-1000^{o}C

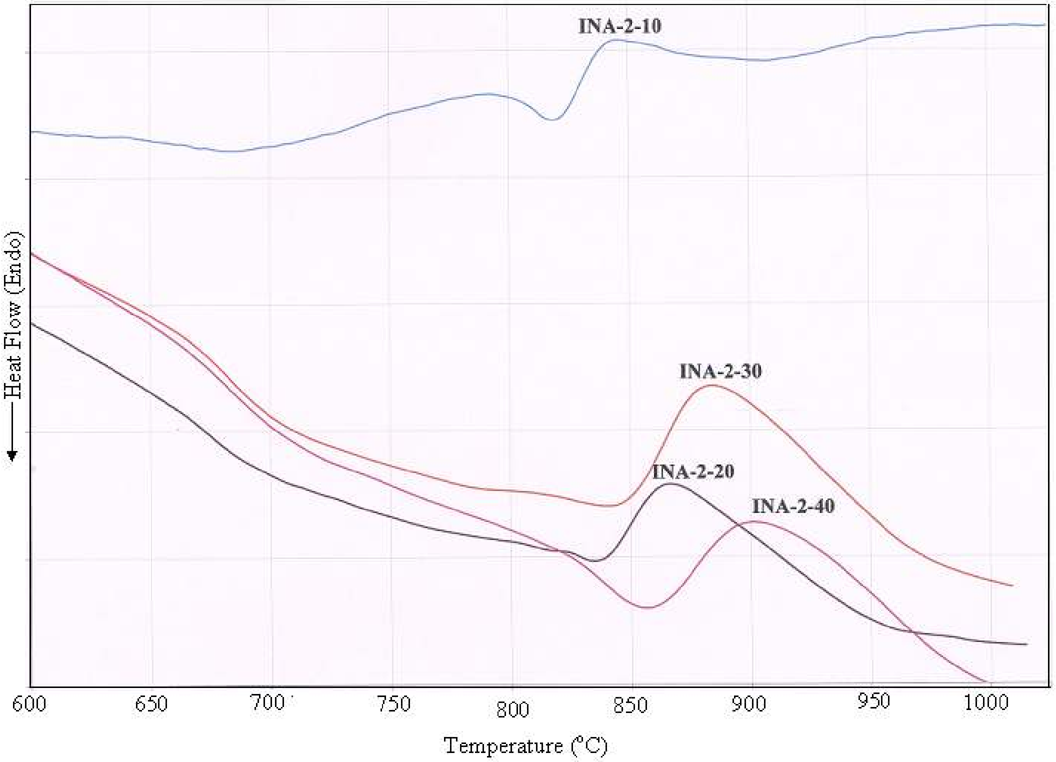

Figure 4.2 DTA plot of INA-2 glass sample at 10, 20, 30, 40^{0}C/min from 600-1000^{o}C

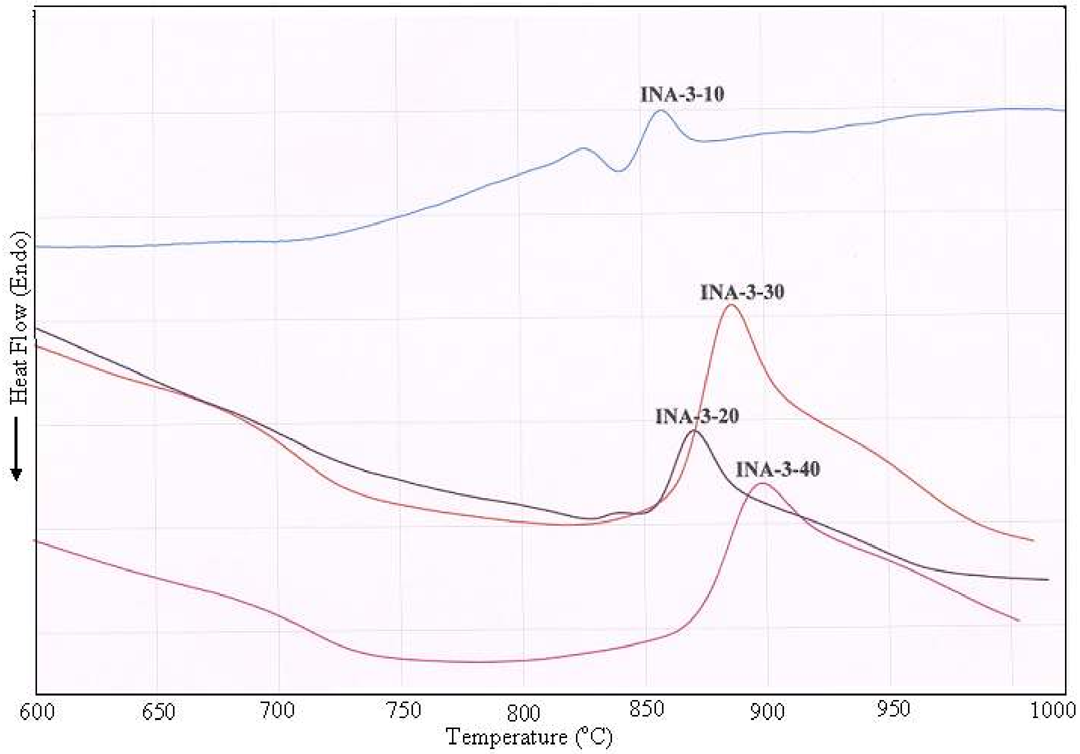

Figure 4.3 DTA plot of INA-3 glass sample at 10, 20, 30, 40^0C/min from 600-1000°C

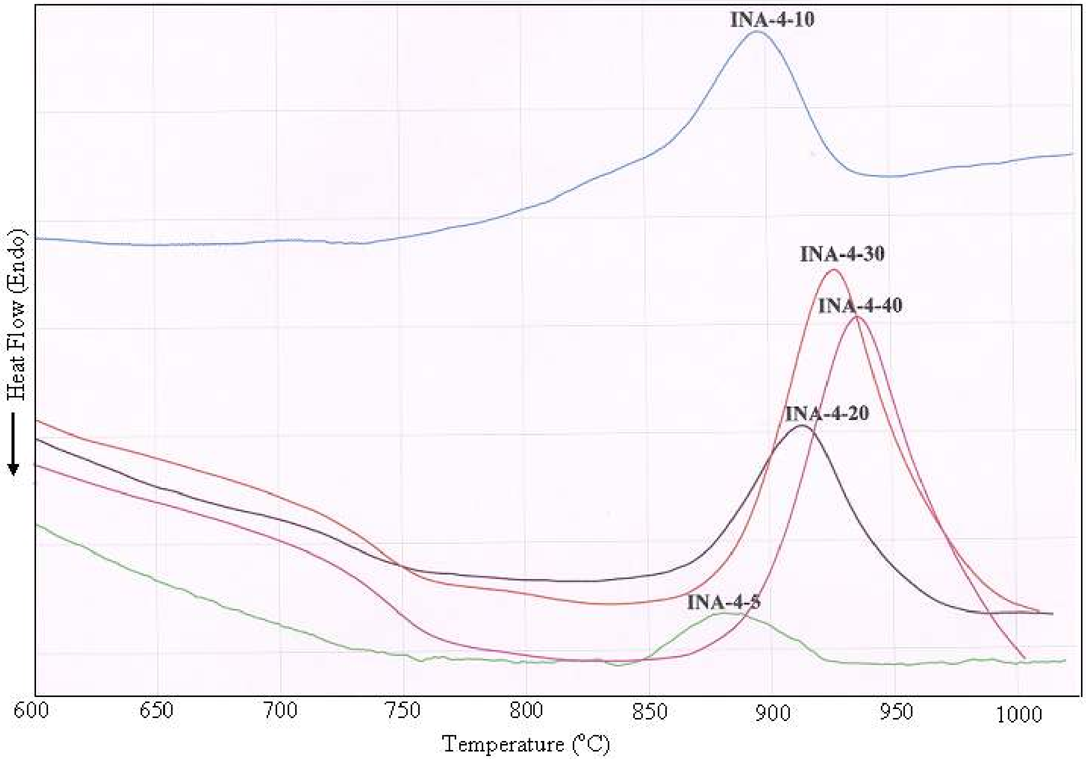

Figure 4.4 DTA plot of INA-4 glass sample at 5, 10, 20, 30, 40^0C/min from 600-1000°C

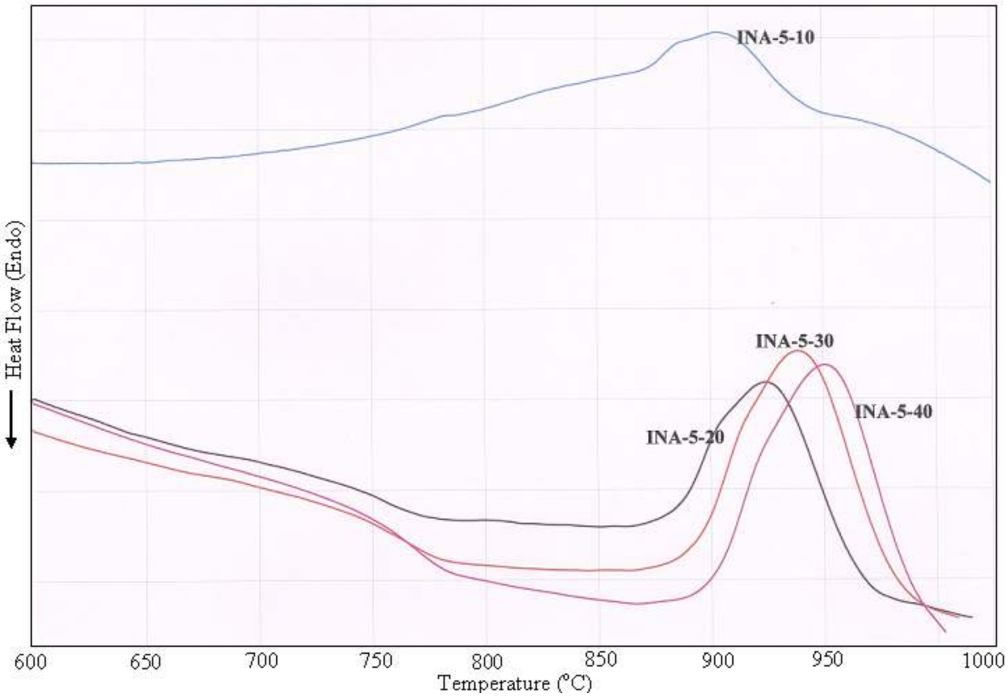

Figure 4.5 DTA plot of INA-5 glass sample at 10, 20, 30, 40^0C/min from 600-1000^oC

The values of T_g (glass transition temperature), T_c (crystallization temperature) and T_{pc} (peak crystallization temperature) as obtained from the DTA study at various heating rates are given in table 4.1.

Table 4.1 T_g, T_c and T_{pc} values of INA series

COMPOSITION	$T_g(^oC)$	$T_c(^oC)$	$T_{pc}(^oC)$
INA-1-10	627	816	853
INA-1-20	676	819	868
INA-1-30	684	822	887
INA-1-40	693	848	909
INA-2-10	644	819	844
INA-2-20	698	834	866
INA-2-30	707	846	881
INA-2-40	717	863	902
INA-3-10	688	841	858
INA-3-20	723	851	871
INA-3-30	730	857	886
INA-3-40	732	865	898
INA-4-5	700	837	870
INA-4-10	710	850	897
INA-4-20	752	858	913
INA-4-30	760	873	927
INA-4-40	764	886	937
INA-5-10	730	871	903
INA-5-20	777	876	925
INA-5-30	781	886	939
INA-5-40	789	898	951

The glass transition and crystallization temperature increase with increase in Al_2O_3 content as Al_2O_3 here is acting as glass former and hence there is increase in T_g and T_c value. Many researchers have reported that Al^{3+} acts as network former and network modifier that depends upon whether it is forming AlO_4 or AlO_6 network in the glass matrix. In the present glasses the amount of modifier is high owing to the existence of a large number of non-bridging oxygen ions, Al^{3+} cations can attain a co-ordination number of 6, so non-bridging oxygen converts into bridging oxygen with the addition of Al_2O_3 by replacing B_2O_3 in these samples. Therefore the conversion of non bridging oxygen to bridging oxygen leads to increase in T_g, T_c and T_m of these glasses. Moreover, the addition of Al_2O_3 in glass matrix is known to prevent the crystallization. However, the field strength of B^{3+} is higher than Al^{3+} [22]. The crystallization peak maximum is seen to increase with increase in heating rate (table 4.1). The crystallization peak maximum in DTA scan corresponds to the temperature at which the rate of transformation of the viscous liquid into crystals become maximum. When the crystallization phase has the same composition as the liquid, the transformation rate will depend on the density of crystallization sites. However, when the composition of crystalline phase is different from that of the liquid, as in our case, the rate of transformation will be controlled by the rate of diffusion through the viscous liquid and the number of crystallization sites to which diffusion can occur. If the number of nucleation sites is increased, e.g. by using slower heating rates, the peak maximum will occur at a temperature at which the melt viscosity is higher, i.e. at a lower temperature. This explains the increase in T_{pc} with the heating rate in the present study. Out of five synthesized glass samples designated as INA-1, INA-2, INA-3, INA-4 and INA-5 as x varies from 0, 2.5, 5.0, 7.5, 10.0 respectively, sample INA-4 shows better results (fig. 4.6) as it has minimum weight change in percentage as compared to other glass samples (table 4.2) in above glass series during heat-treatment from room temperature to 1000 °C at a heating rate of 10 °C/min as confirmed by TGA.

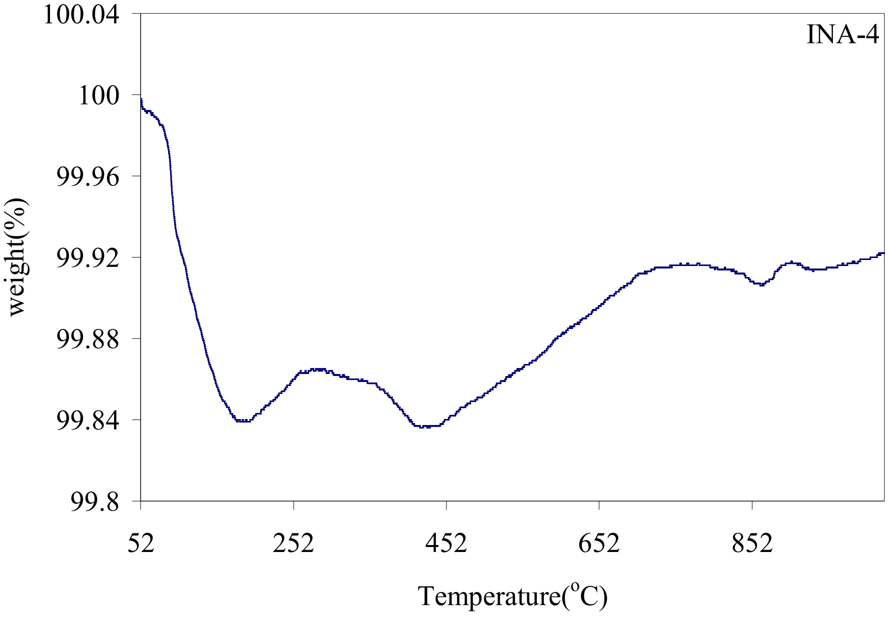

Figure 4.6 Change in weight % of INA-4 sample

Table 4.2 change in weight % in INA glass samples

Sample ID	Change in weight (%)
INA-1	-0.14
INA-2	-0.29
INA-3	-0.19
INA-4	-0.08
INA-5	-0.33

Based on TGA results, sample INA-4 is selected for further characterization. From DTA data we have also calculated the activation energy of INA series using Kissinger equation [1] as given in equation (i) by plotting a graph between $\ln(T_p^2/\beta)$ versus $10^3/T_p$ for crystallization of glass (fig 4.7).

$$\ln\left(\frac{\beta}{T_p^{\,2}}\right) = -\frac{E_a}{RT_p} + const \qquad \text{(i)}$$

here β is the heating rate, R is gas constant and T_p is peak crystallization temperature. The plot of $\ln(T_p^2/\beta)$ versus $1000/T_p$ is a straight line, whose slope corresponds to E_a.

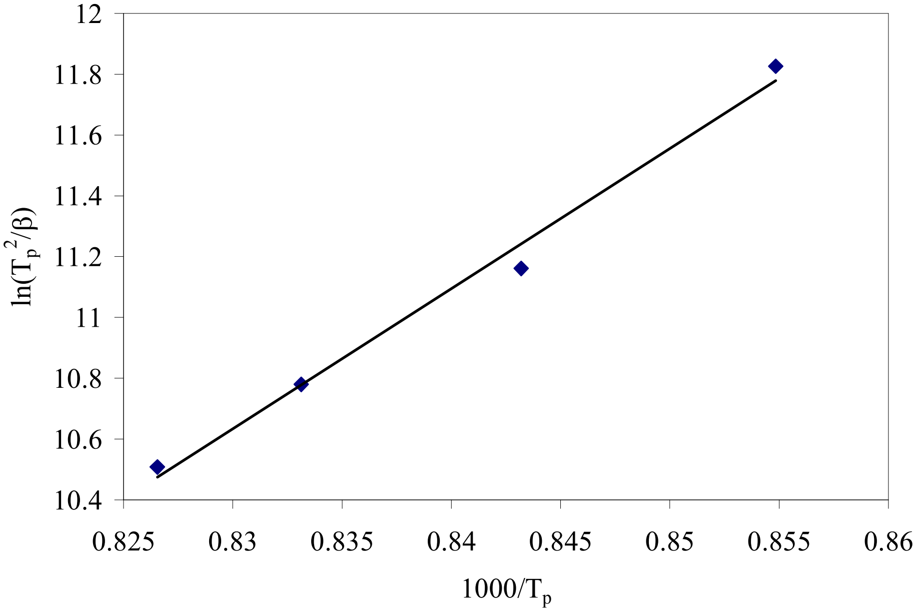

Figure 4.7 Plot of $\ln(T_p^2/\beta)$ vs. $10^3/T_p$ for INA-4 glass powder

Values of kinetic parameter i.e activation energy of peak crystallization E_a obtained from least square fitting of the experimental data from samples INA-1 to INA-5 is listed in table 4.3. It is clear from the data of activation energy that with the increase in alumina content from 2.5 to 7.5 activation energy is increasing. However, when alumina content is 10 mol%, activation energy of sample is decreased. As the number of constituents is increased more competition to attract the non bridging oxygen takes place. At the same time intraforce among cations within glass matrix is also disturbed. Therefore, in INA-5 glass sample where B_2O_3 is absent has less competition among the cations which might be responsible for lower E_a in this sample [20, 21]. This can be explained on the basis that higher amount of alumina may lead to weakening of the network and thus decreases the activation energy value.

Table 4.3 Activation energy values of INA glass samples determined by DTA

Sample ID	E_a(kJ/mol)
INA-1	246
INA-2	247
INA-3	353
INA-4	383
INA-5	327

Large difference in activation energy of the INA-4 glass as compared to other glasses may be due to the formation of different crystalline phases in these glasses. The detailed study of nucleation and growth of crystalline phases due to heat treatments is given in section 4.4.

4.1.1.1 Hruby Parameter Calculations

Hruby proposed a parameter, K_H (eq. ii), obtained from DTA that measures the glass stability against crystallization on heating of glasses [2]. The Hruby parameter is defined by

$$K_H = \frac{T_c - T_g}{T_m - T_c} \qquad \text{(ii)}$$

where T_c, T_g and T_m are the onset crystallization (on heating), the glass transition and melting temperatures respectively, estimated from DTA. According to Hruby, the larger K_H of a certain glass, the greater is its stability against crystallization on heating. In our case, data obtained by DTA to calculate the Hruby parameter is given in table 4.4.

Table 4.4 Hruby parameter value obtained from DTA for INA series

Sample ID	$T_m(^oC)$	$K_H = (T_c-T_g)/T_m-T_c$
INA-1	1127.43	0.6055
INA-2	1162.45	0.5100
INA-3	1190.1	0.4374
INA-4	1254.61	0.3463
INA-5	1287.79	0.3377

Figure 4.8 gives us the graphical representation of Hruby parameter with respect to Al_2O_3 (mol%), which clearly indicate that INA-1 glass has maximum stability against crystallization on heating.

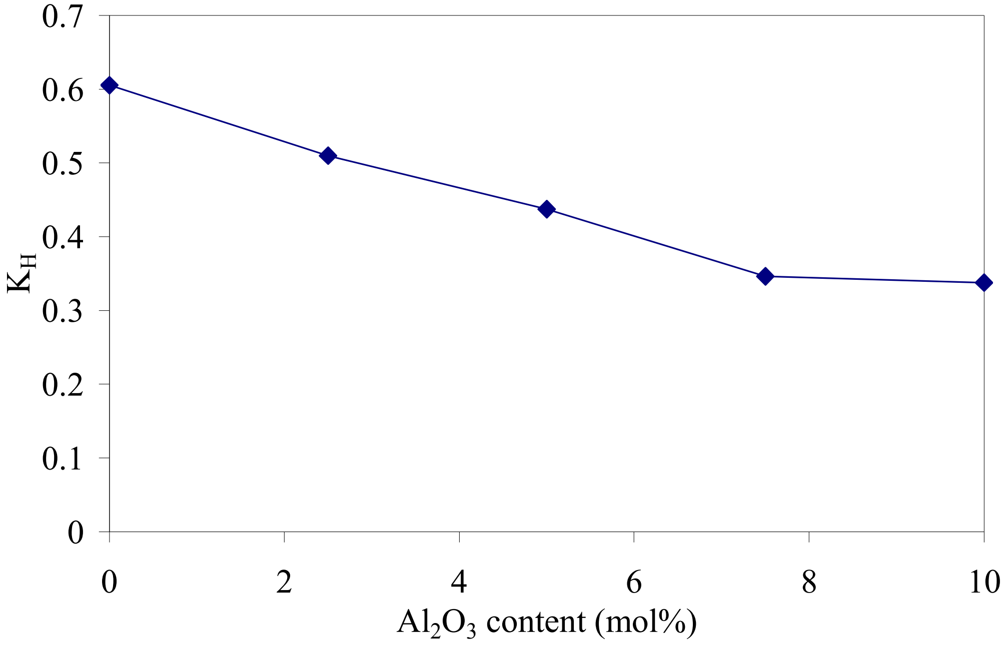

Figure 4.8 Variation of K_H vs. Al_2O_3 (mol %) for INA series

4.1.1.2 Thermal Stability Parameter (S)

A parameter usually employed to estimate the glass stability is the thermal stability (ΔT) [3], which is defined by the following equation

$$\Delta T = T_c - T_g \qquad \text{(iii)}$$

The bigger difference between T_c and T_g indicates the most thermally stable glass.

Saad and Poulain [4] obtained another criterion, the thermal stability parameter:

$$S = \frac{(T_p - T_c)(T_c - T_g)}{T_g} \qquad \text{(iv)}$$

The thermal stability parameter, S, reflects the resistance to devitrification after the formation of the glass. In Eq. (iv), (T_p-T_c) is related to the rate of devitrification transformation of the glassy phases. On the other hand, a high value of (T_c-T_g) delays the nucleation process. The values of thermal stability (ΔT) and thermal stability parameter (S) are as given in table 4.5.

Table 4.5 Values of ΔT and S from DTA data for INA glass series

Sample ID	**Thermal Stability (ΔT)**	**Thermal stability parameter (S)**
INA-1	156	6.2
INA-2	175	4.8
INA-3	153	2.7
INA-4	140	6.7
INA-5	141	4.5

This is clear from the calculated values of ΔT and S for INA glass series that glass sample INA-4 exhibits highest thermal stability as compared to other samples present in the series.

4.1.1.3 Fragility index (F)

Structural relaxation is a general phenomenon occurring when a glass is maintained at a temperature below its glass transition temperature (T_g). Glass forming liquids that exhibit an approximately Arrhenius temperature dependence of the viscosity are defined as strong glass formers and those, which exhibit a non-Arrhenius behavior are declared fragile glass formers [5]. Fragile glasses are usually substances with nondirectional, interatomic/intermolecular bonds. Strong glasses are those which show resistance to structural degradation in the liquid state.

The fragility index can be calculated using the following relation [6, 7]:

$$F = \frac{E_t}{RT_g \ln 10} \qquad \text{(v)}$$

Where E_t is the activation energy for glass transition.

It was found that the limit for kinetically strong-glass-forming (KS) liquids is reached for a low value of F ($F \approx 16$) [8], while the limit for kinetically fragile-glass-forming (KF) liquids is characterized by a high value of F ($F \approx 200$) [9].

Table 4.6 Values of Fragility Index for INA glass series calculated from DTA data

Sample ID	Fragility Index (F)
INA-1	13.78
INA-2	14.07
INA-3	19.19
INA-4	20.36
INA-5	17.03

The above calculated data indicates that INA-3, INA-4 and INA-5 glasses approach the limit for kinetically strong-glass-forming liquids (table 4.6).

4.1.1.4 Crystallization kinetics of INA-1 glass sample

Representative DTA thermographs of INA -1 glass sample taken at different heating rates exhibited one well defined broad crystallization exotherm, which might have formed by the overlapping of two exothermic crystallization curves. Typical scan at heating rates of 30 K/min is shown in Fig. 4.9 (a) while the crystallization exotherm and the overlapping of the crystallization curves for the DTA scan at $\beta = 5$ K/min are shown in Fig. 4.9 (b) and 4.9 (c). Influence of the scan rate on the peak temperature of crystallization (T_p) is given in Table 4.7. These results of INA-1 glass sample are published in our paper [10] and DTA study of this particular glass sample was done at DTA-TG (Labsys Setaram, France) by taking sample amount to be 50 mg with α alumina as reference.

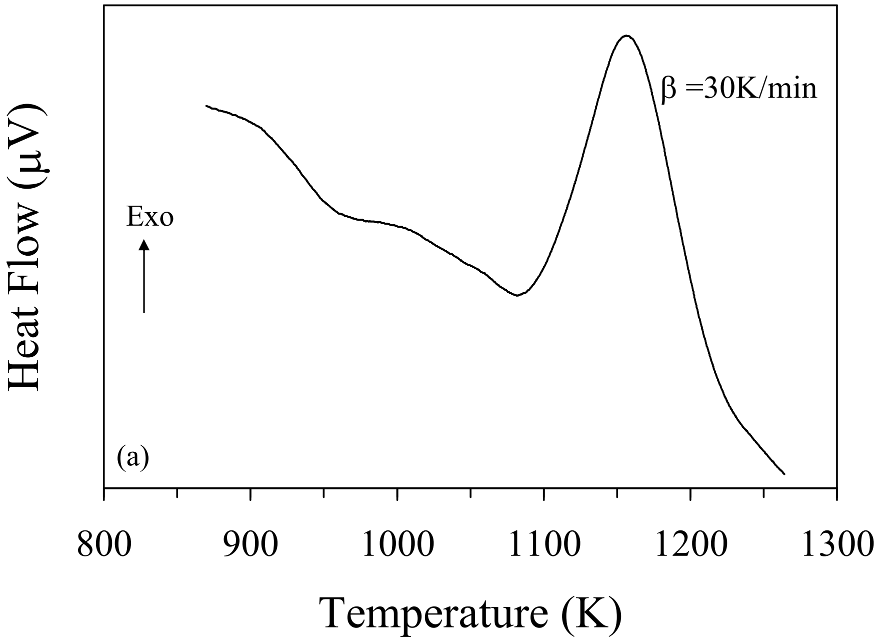

Figure 4.9 (a) DTA thermograph for glass powder at heating rate 30K/min.

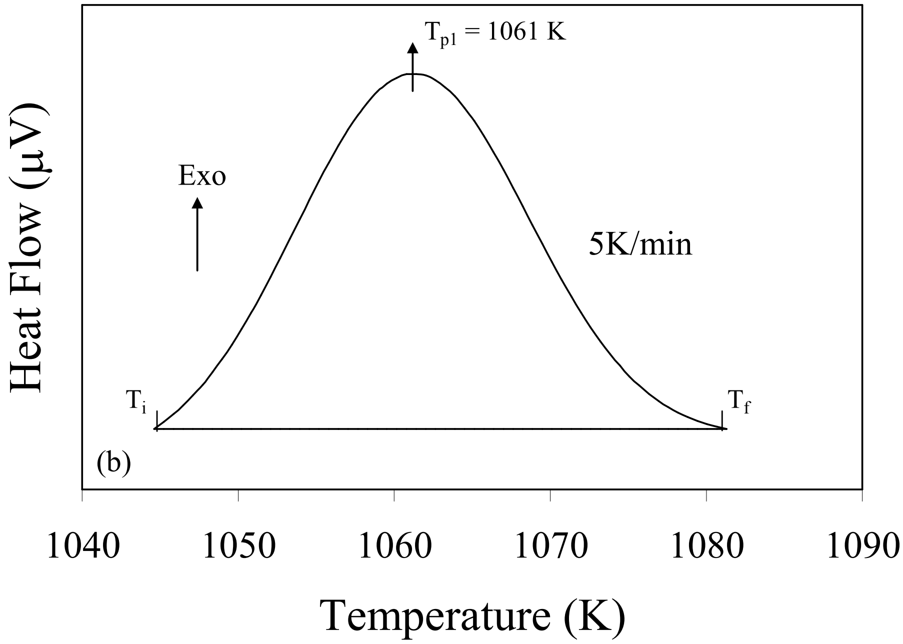

Figure 4.9 (b) Crystallization curve obtained from DTA (β = 5K/min) showing area A_T between T_i and T_f.

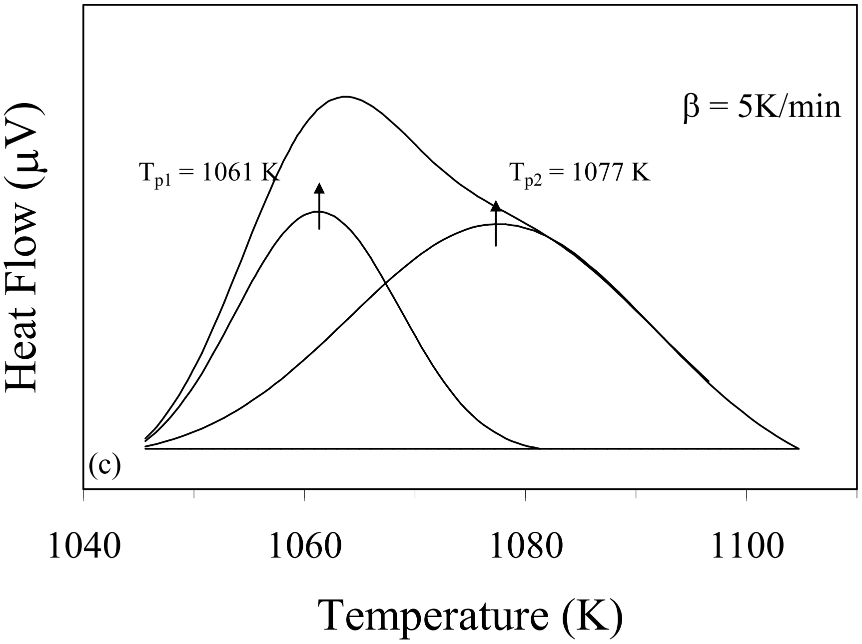

Figure 4.9 (c) Separation of two overlapped crystallized peaks (β=5K/min)

Table 4.7 Peak temperature of crystallization, maximum crystallization rate, corresponding maximum crystallization temperature, and kinetic exponent for the different heating rates

	First crystallization curve				Second crystallization curve			
β (K/min)	T_{p1} (K)	$10^3(d\chi/dt)(s^{-1})$	n_1	$<n_1>$	T_{p2} (K)	$10^3(d\chi/dt)(s^{-1})$	n_2	$<n_2>$
5	1061	0.0014	2.034	2.1257	1077	0.0019	3.149	3.125
10	1086	0.0027	2.0548		1112	0.0035	3.092	
20	1120	0.0053	2.145		1149	0.0067	3.159	
30	1138	0.0080	2.2285		1169	0.0094	3.059	
40	1153	0.0101	2.1661		1182	0.0127	3.169	

Fig. 4.10 (a) and 4.10 (b) shows the fraction, χ, crystallized at a given temperature, T and is given by $\chi = A_T/A$, where A is the total area of the exotherm between the temperature, T_i, where crystallization just begins and the temperature, T_f, where the crystallization is completed, and A_T is the area between T_i and T. The graphical

representation of the volume fraction crystallized for both the exothermic curves shows the typical sigmoid curve as a function of temperature for different heating rates.

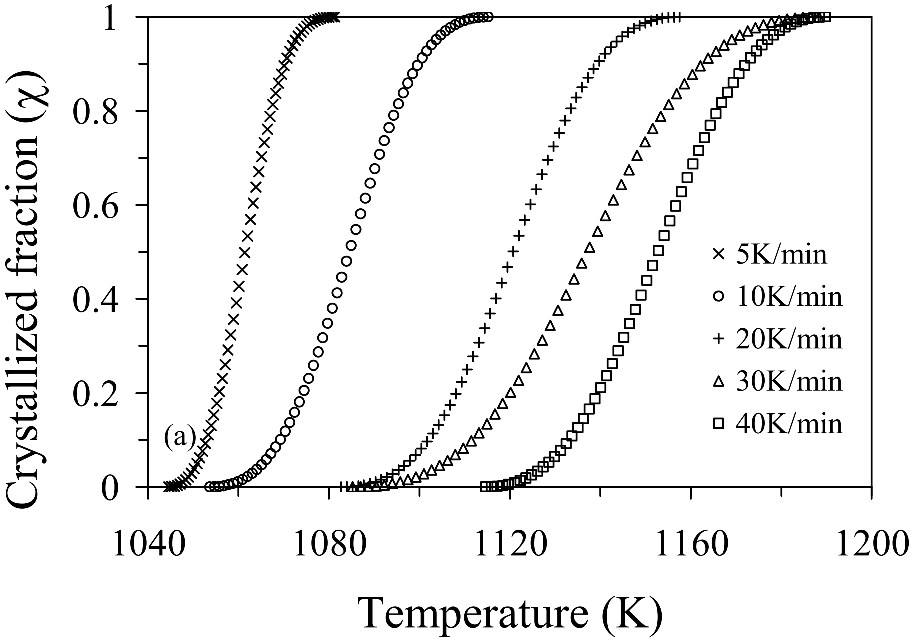

Figure 4.10 (a) Crystallized fraction as a function of temperature at different heating rates for first crystallization curve.

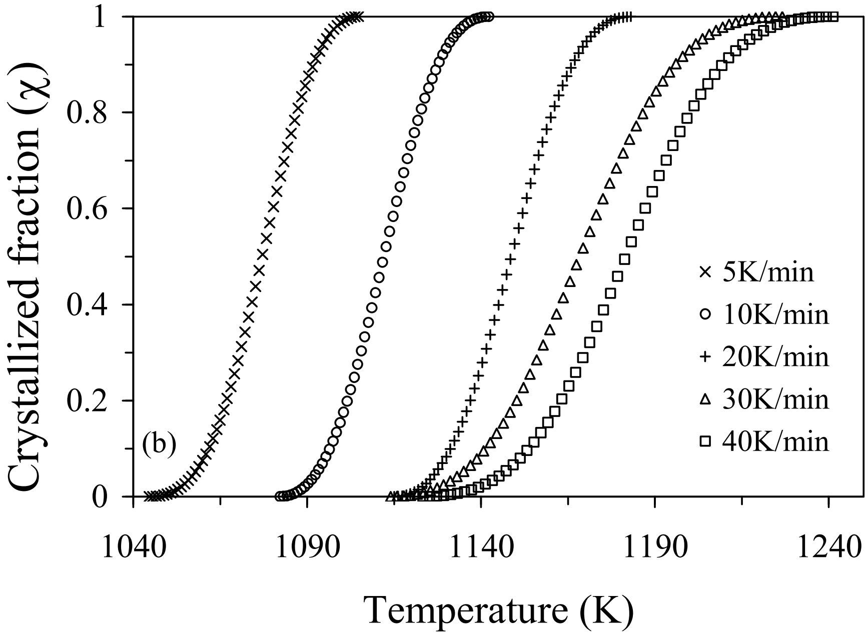

Figure 4.10 (b) Crystallized fraction as a function of temperature at different heating rates for second crystallization curve.

The theoretical basis for interpreting DSC results is provided by the formal theory of transformation kinetics as developed by Johnson and Mehl [11] and Avrami [12, 13]**.** The ratio between the ordinates of the DSC curve and the total area of the peak gives the corresponding crystallization rates, which makes it possible to build the curves of the exothermal peaks represented in Fig. 4.11 (a, b). It may be observed that, the $(dx/dt)_p$ values increases as well as the heating rate, a property which has been widely discussed in the literature [14]**.** From the experimental values of the $(dx/dt)_p$ one can calculate the kinetic exponent n by using the following Equation

$$\left(d\chi/dt\right)_p = n(0.37\beta E_c)/(RT_p^2) \tag{vi}$$

The n values for the present glass are calculated and is listed in Table (4.7).

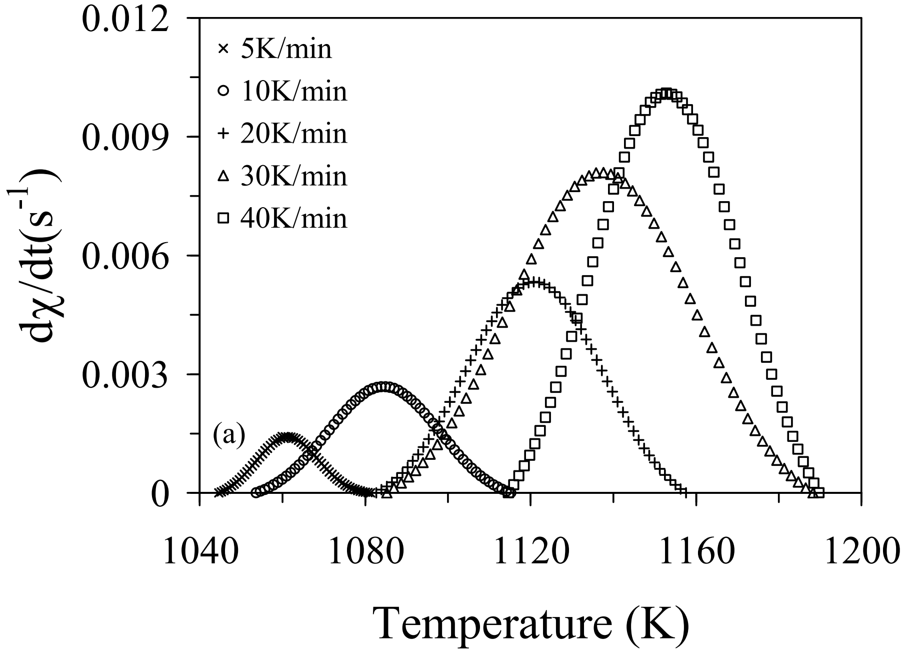

Figure 4.11 (a) Crystallization rate vs. Temperature for first exothermic curve at different heating rates.

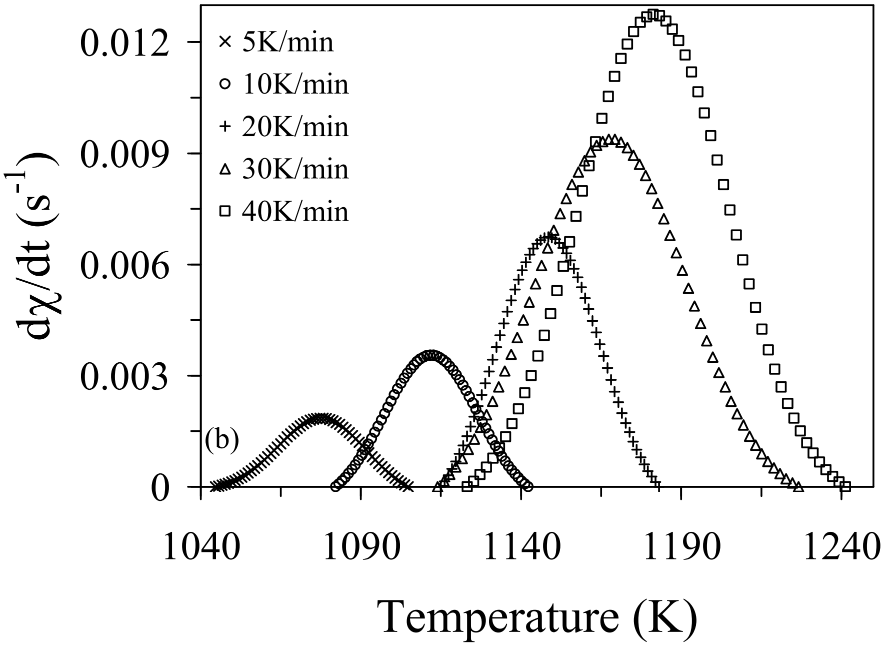

Figure 4.11 (b) Crystallization rate vs. Temperature for second exothermic curve at different heating rates.

For the evaluation of activation energy for crystallization (E_c) by using the variation of T_p with β Vázquez et al. [14] developed a method for non-isothermal analysis of devitrification as follows:

$$\ln[T_p^2/\beta] \quad = \quad E_c/RT_p \; + \; \ln q \qquad \text{(vii)}$$

where q is the pre-exponential factor.

Finally, the experimental data, T_p, and $(dx/dt)_p$, shown in table 4.7 and the above mentioned value of the activation energies of crystallization process for two peaks, make it possible to determine, through relationship (eq. vi), the kinetic exponent, n, for each of the experimental heating rates for two groups of peaks, whose values are also given in table 4.7, the mean value being, $\langle n \rangle =$(2.1257) for the first peaks and (3.125) for the second peaks. Allowing for experimental error, value of $\langle n \rangle$ is close to 2 for the first phase and close to 3 for the second phase. The kinetic exponent was deduced based on the mechanism of crystallization [15]**.** The $\langle n \rangle$ value of the kinetic exponent of the as quenched glass is consistent with the mechanism of volume nucleation with two-dimensional growth for the first phase and one-dimensional growth for the second phase [16].

In the non-isothermal crystallization, the volume fraction of crystallites, χ, precipitated in a glass heated at constant rate, β is related to the crystallization activation energy, E_a through the following expression [17]

$$\ln[-\ln(1-\chi)] = -n\ln\beta - 1.052(mE/RT) + const. \qquad \text{(viii)}$$

where m and n are integers or half-integers which depend on the mechanism of the growth and the dimensionality of the crystal [18]. Mahadevan et al. [3] have shown that n may be 4, 3, 2, or which are related to different glass-crystal transformation mechanisms: n = 4, volume nucleation, three-dimensional growth; n = 3, volume nucleation, two-dimensional growth, n = 2, volume nucleation, one-dimensional growth; n = 1, surface nucleation, one-dimensional growth from surface to the inside.

The kinetic parameter n, for both the crystallization exotherms can also be calculated using eq. viii by plotting of $\ln[-\ln(1-\chi)]$ versus 1/T for the all heating rates.

The crystallization maximum temperature is seen to increase with the increase in heating rate (Table 4.7). The crystallization maximum in DTA or DSC scans corresponds to the temperature at which the rate of transformation of the viscous liquid into crystals becomes maximum. When the crystalline phase has the same composition as that of the liquid, the rate of the transformation will depend on the density of the crystallization sites. However, when the composition of the crystalline phase is different from that of the liquid, as in the present case, the rate of transformation will be controlled by the rate of diffusion through the viscous liquid and the number of crystallization sites to which diffusion can occur. If the number of nucleation sites is increased, e.g. by using slower heating rates, the peak maximum will occur at a temperature at which the melt viscosity is higher, i.e. at lower temperature. This explains the increase in T_p with the heating rate (Table 4.7) observed in the present study.

The ratio between the ordinates of the DTA curve and the total area of the exothermal peak gives the corresponding crystallization rates, which makes it possible to build the curves of the exothermal peaks represented in Fig. 4.11(a and b). The activation energy values obtained for this glass sample from Kissinger equation are considerably lower in comparison to the activation energies of the zinc aluminosilicate glasses as mentioned in the earlier studies [19]. This indicates that the three dimensional connectivity decreases in the glass due to the presence of B^{3+} ions and the diffusion of the ions in the glass became too easy to form a crystalline phase. Since the three dimensional connectivity becomes weak due to the addition of B_2O_3, the nucleation can be completed before the crystal growth occurs at around a glass transition temperature. Effect of B_2O_3 on the lowering of activation energy of crystallization is well documented in literature [20, 21]. Presence of Al_2O_3 has a marked effect in decreasing the extent of immiscibility. If Al_2O_3 concentration is less that 5 mol% it does not exhibit any phase separation. However, if Al_2O_3 content increases, it leads to phase separation. The structural role of Al^{+3} for its deviation in nature is because of variation in coordination number of Al^{+3}. Higher coordination number leads to phase separation [22] which is being observed when Al_2O_3 shifts from tetrahedral coordination to octrahedral. The experimental data T_p and $(dx/dt)_p$, for both the crystallization exotherms, shown in Table 4.7, along with their activation energies of crystallization, makes it possible to determine, through relationship Eq. (vii), the kinetic exponent n for both the phases at each of the experimental heating rates, whose values are also given in Table 4.7. The value of Avrami parameter, n depends on the mechanism of the transformation reaction. If the rate of nucleation is a function of time, so is n; n is higher for a constant nucleation rate than when the nucleation rate increases with time and lies between those for constant and zero nucleation rates when the nucleation rate decreases with time. The kinetic parameter n, for both the crystallization exotherms can also be calculated using Eq. (viii) by plotting of $\ln[-\ln(1-\chi)]$ versus $1/T$ for the all heating rates [Fig. 4.12 (a) and Fig. 4.13 (a)]. From the data obtained by Fig. 4.12 (b) and Fig. 4.13 (b), a plot of $\ln[-\ln(1-\chi)]$ versus $\ln\beta$ at constant temperature can be performed. Fig. 4.12 (b) and Fig. 4.13 (b) shows the relation between $\ln[-\ln(1-\chi)]$ with $\ln\beta$ at two fixed temperatures for both the crystallization exotherms. From the slope of this relation one can deduce the order of the crystallization mechanism (or Avrami index), n. Allowing for experimental error, the value of <n> is close to 2 for the first phase and 3 for the second phase. This confirms the value of n calculated from Eq. (8), thus corresponding to the one dimensional growth of the first crystalline phase and two dimensional growth for the second phase.

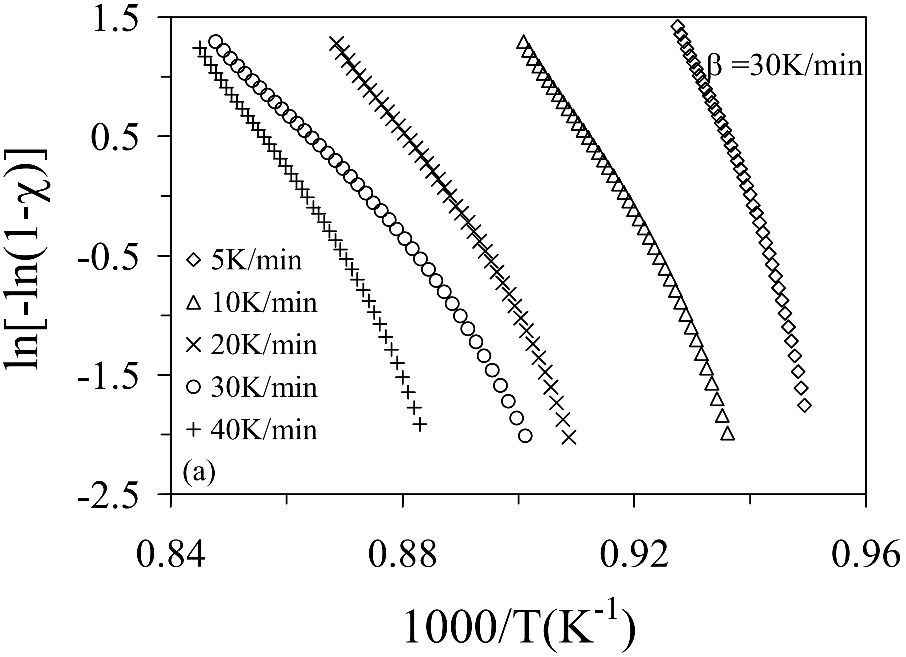

Figure 4.12 (a) Plot of ln[-ln(1-χ)] vs. 1000/T at for first crystallization curve at all the heating rates.

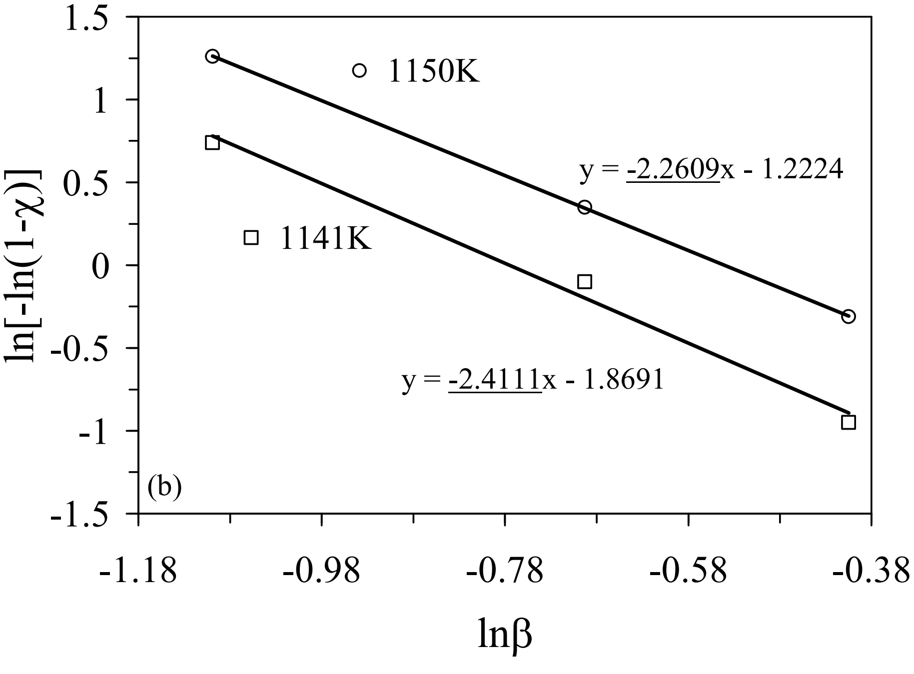

Figure 4.12 (b) Plot of ln[-ln(1-χ)] vs. lnβ for first crystallization curve at two constant temperatures (1141K and 1150K) (The underlined value is the Avrami index)

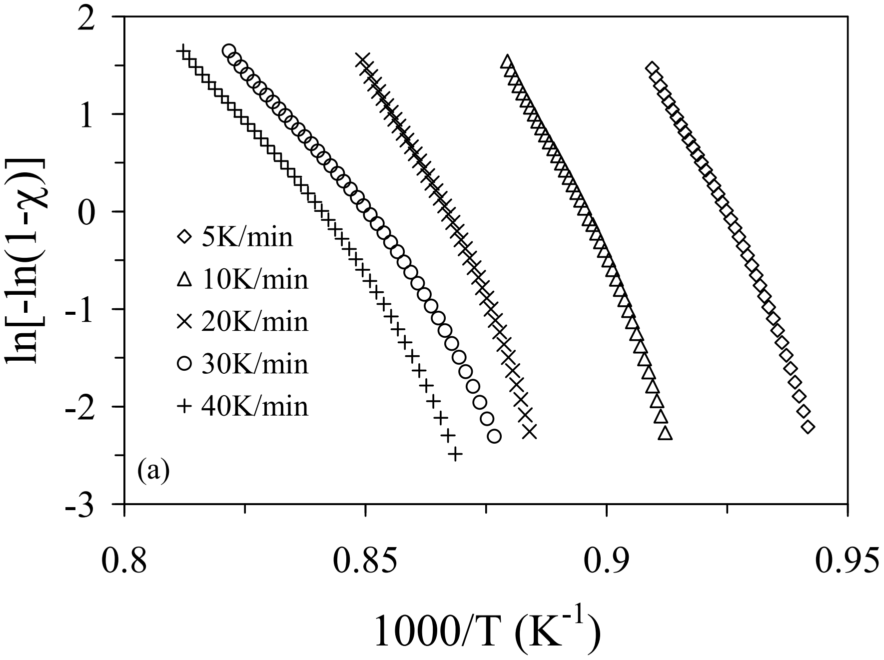

Figure 4.13 (a) Plot of ln[-ln(1-χ)] vs. 1000/T for second crystallization curve at all the heating rates.

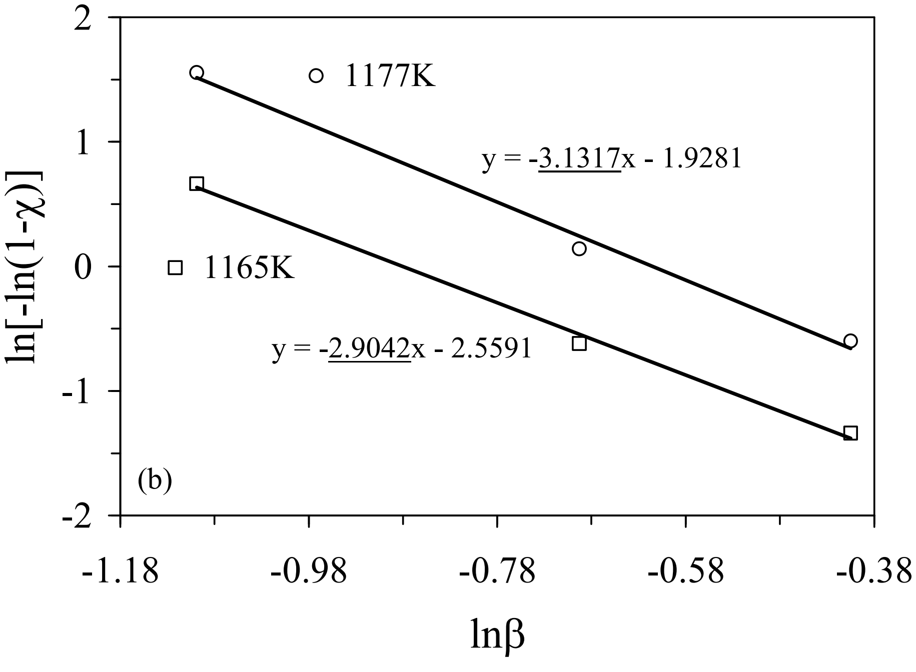

Figure 4.13 (b) Plot of ln[-ln(1-χ)] vs. lnβ at two fixed temperatures (1165K and 1177K) (The underlined value is the Avrami index).

4.1.1.5 Glass transition and crystallization kinetics by DTA of INA-2 glass sample

The data of INA-2 glass sample is published in another paper of our group [23] and the theoretical results are discussed follows:

The theoretical basis for interpreting DTA results is provided by the formal theory of transformation kinetics as developed by Johnson and Mehl [11] and Avrami [12, 13]. This theory describes the evolution with time, t, of the volume fraction crystallized, χ, in terms of the crystal growth rate u

$$\chi = 1 - \exp\left[-gN_0 \left(\int^{t} u(t') dt' \right)^m \right] \qquad \text{(ix)}$$

where N_0 being the number of pre-existing nuclei per unit volume, m is an exponent, which depends on the dimensionality of the crystal growth. In the considered case, "site saturation" [14], the kinetic exponent is $n = m$. Assuming an Arrhenian temperature dependence for $u = u_0 e^{E/RT'}$, and a heating rate, $\beta = \mathrm{d}T/\mathrm{d}t$, Eq. (i) becomes as

$$\chi = 1 - \exp\left[-gN_0 u_0^n \beta^{-n} \left(\int_{T_0}^{T} e^{-E/RT'} dT' \right)^n \right] = 1 - \exp\left(-qI^n \right) \qquad \text{(x)}$$

where E being the effective activation energy for crystal growth.

By using the substitution $y' = E/RT'$ the integral I can be represented, according to the literature [24], by the sum of the alternating series

$$S(y') = \frac{-e^{-y'}}{y'^2} \sum_{k=0}^{\infty} \frac{(-1)^k (k+1)!}{y'^k}$$

Considering that in this type of series the error produced is less than the first term neglected and bearing in mind that in most crystallization reactions $y' = E/RT' >> 1$ (usually $E/RT' \geq 25$), it is possible to use only the first term of this series, without making any appreciable error, and the above-mentioned integral becomes:

$$I = \left(\frac{E}{R} \right) e^{-y} y^{-2} = RT^2 E^{-1} \exp\left(-\frac{E}{RT} \right) \qquad \text{(xi)}$$

if it is assumed that $T_0 = T$ (T_0 is the starting temperature), so that y_0 can be taken as infinity. This assumption is justifiable for any thermal treatment that begins at a temperature where crystal growth is negligible, i.e. below the glass transition temperature, T_g [18].

Substituting Eq. (iii) into Eq. (ii), the volume fraction crystallized in a non-isothermal process is expressed as

$$x = 1 - \exp\left[-Q\left(K_R T^2 \beta^{-1}\right)^n\right] \qquad \text{(xii)}$$

where $Q = gN_0\left(R/E\right)^n$ and K_R is the reaction rate constant. It should be noted that Eq. (xii) is a general expression for all values of the parameter n, which, as it is well known, in the case of "site saturation" depends on the mechanism of the crystal growth.

With the aim of calculating the kinetic parameters, the crystallization rate has been obtained by deriving Eq. (xii) with respect to time, yielding

$$\frac{dx}{dt} = nQ\left(K_R T^2 \beta^{-1}\right)^{n-1}(1-x)\left(K_R E R^{-1} + 2K_R T\right) \qquad \text{(xiii)}$$

which has been assumed that the reaction rate constant is a time function through its Arrhenian temperature dependence.

The maximum crystallization rate is found by making $d^2x/dt^2 = 0$, thus obtaining the relationship

$$\left[(K_R|_P T_P^2 \beta^{-1}\right]^n = 1 - \left(\frac{2}{n}\right)\left(1 + \frac{E}{RT_P}\right)\left(2 + \frac{E}{RT_P}\right)^{-2} \qquad \text{(xiv)}$$

where the subscript p denotes the magnitude values corresponding to the maximum crystallization rate. Assuming the above mentioned hypothesis $E/RT_p >> 1$; the logarithmic form of Eq. (xiv) is written as

$$\ln\left(T_p^2/\beta\right) = \frac{E}{RT_P} - \ln q = 0$$

equation of a straight line, whose slope and intercept give the activation energy, E, and the pre-exponential factor, $q = Q^{\frac{1}{n}} K_{R0}$, respectively.

On the other hand, the quoted assumption, $E/RT_p >> 1$, according to Eqs. (iv-vi), allow us to express the maximum crystallization rate by the relationship:

$$\left.\frac{dx}{dt}\right|_p = 0.37\beta En\left(RT_p^2\right)^{-1} \qquad \text{(xv)}$$

which makes it possible to obtain, for each heating rate, a value of the kinetic exponent, *n*. The corresponding mean value may be taken as the most probable value of the quoted exponent.

In the similar way as discussed in section 4.1.1.4 for glass sample INA-1 in the non-isothermal crystallization, the volume fraction of crystallites, χ, precipitated in a glass heated at constant rate, β is related to the crystallization activation energy, E_c through the following expression [17]

$$\ln[-\ln(1-\chi)] = -n\ln\beta - 1.052(mE/RT) + const. \qquad \text{(viii)}$$

where *m* and *n* are integers or half-integers which depend on the mechanism of the growth and the dimensionality of the crystal [3]. Besides, from the mean value of the kinetic exponent, *n*, is possible to postulate a crystallization reaction mechanism for the aluminosilicate glasses.

To study the crystallization kinetics, glass powder of mean particle size 165.5μm (Fig. 4.14) was employed. Representative DTA thermographs taken at different heating rates exhibited one well defined broad crystallization exotherm, which was formed by the overlapping of two exothermic crystallization curves. Typical scans at heating rates of 10 and 40K/min are shown in Fig. 4.15 a and the separation of the two crystallization curves under the broad DTA curve is shown Fig. 4.15 b for β = 10K/min. Fig. 4.16 (a and b) shows the fraction, χ, crystallized for both the crystallization exotherms at a temperature, T. The graphical representation of the volume fraction crystallized for both the exothermic curves shows the typical sigmoid curve as a function of temperature for different heating rates.

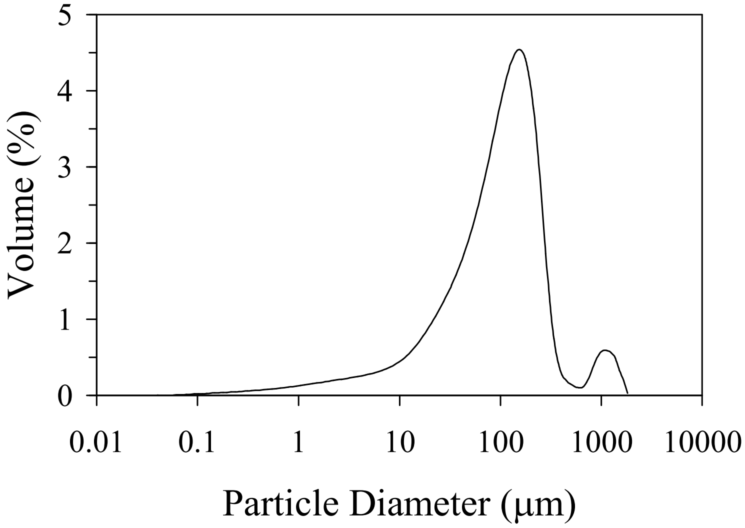

Figure 4.14 Particle size distributions of milled glass powder used for differential thermal analysis (DTA).

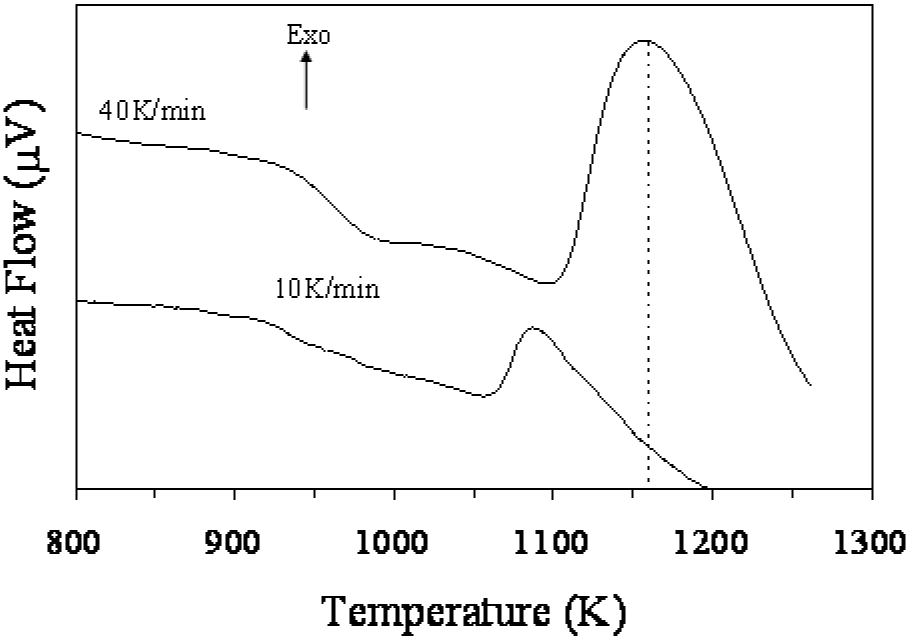

Figure 4.15 (a) DTA of the investigated glass BZAS from milled fine powders of glass-frits.

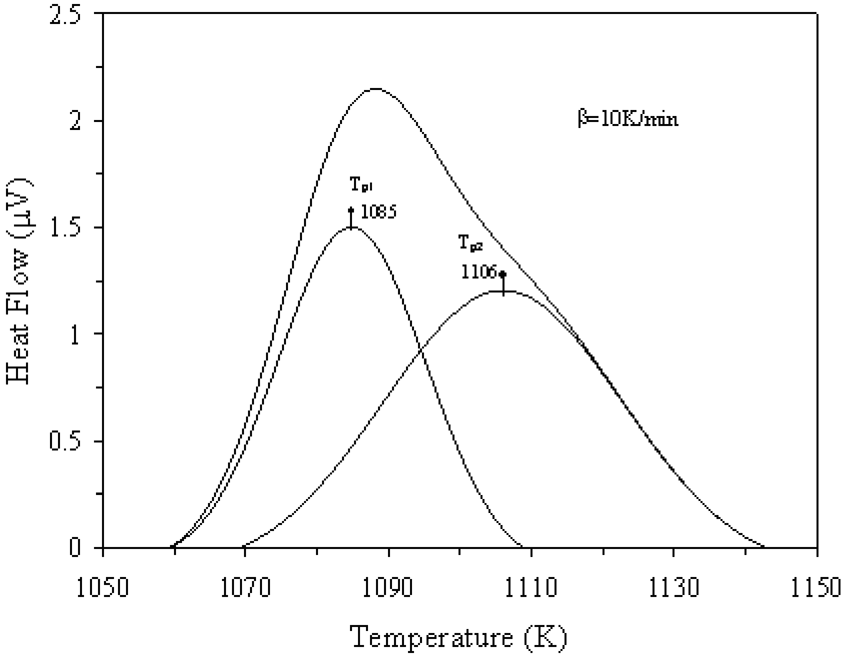

Figure 4.15 (b) Separation of overlapped crystallization exothermal curves.

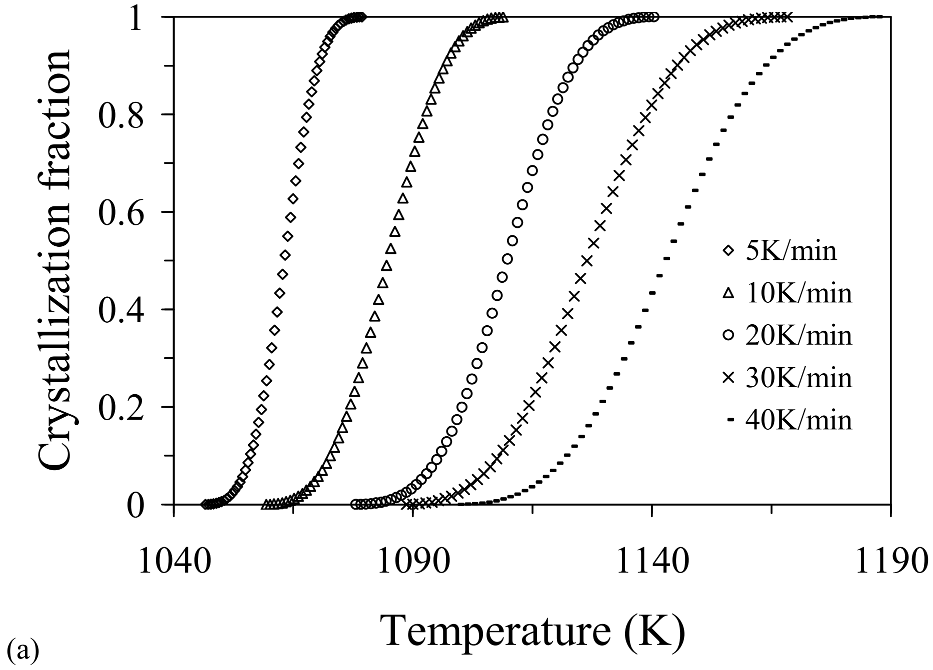

Figure 4.16(a) Crystallization fraction v/s temperature for first crystallization exotherm

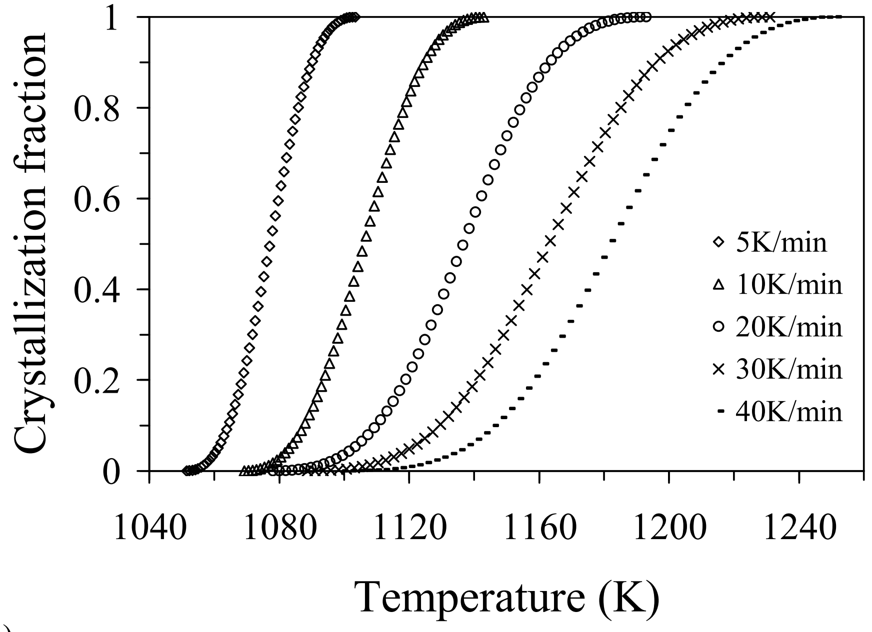

(b)

Figure 4.16 (b) Crystallization fraction v/s temperature for second crystallization exotherm

Glass devitrification is the result of two separate processes: nucleation and crystal growth. Nucleation in glass-forming systems can occur either in the volume or on the surface of the sample. Practically, surface crystal nucleation occurs more easily and is observed in most compositions. Addition of nucleating agents is often necessary to achieve internal crystal nucleation. However, certain glass systems nucleate internally without such additions. In the present study, crystallization maximum temperature is seen to increase with the increase in heating rate. The ratio between the ordinates of the DTA curve and the total area of the exothermal peak gives the corresponding crystallization rates, which makes it possible to build the curves of the exothermal peaks represented in Fig. 4.17 (a and b).

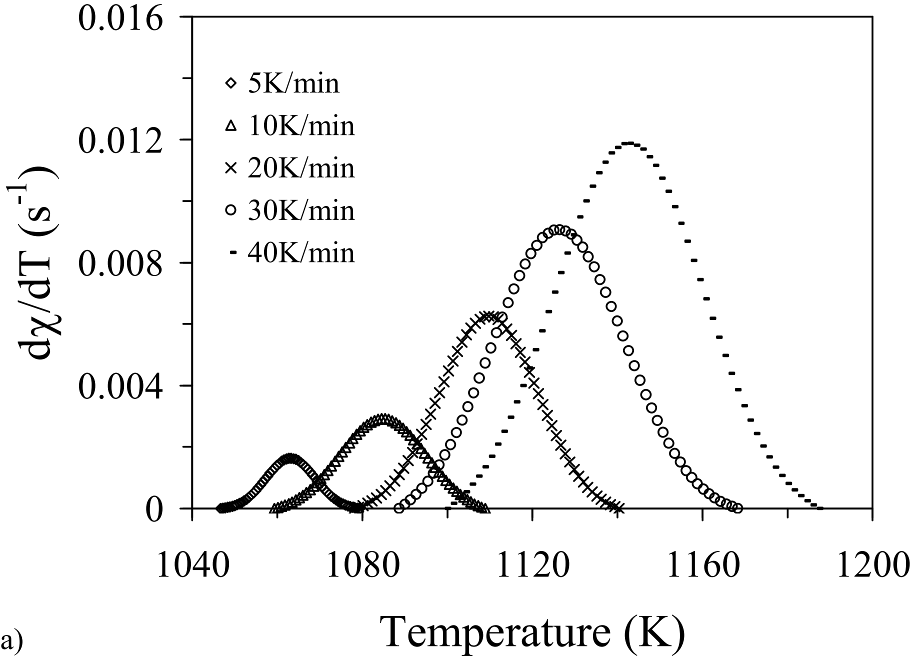

Figure 4.17(a) Crystallization rate vs. temperature for the first exothermic peak at different heating rates

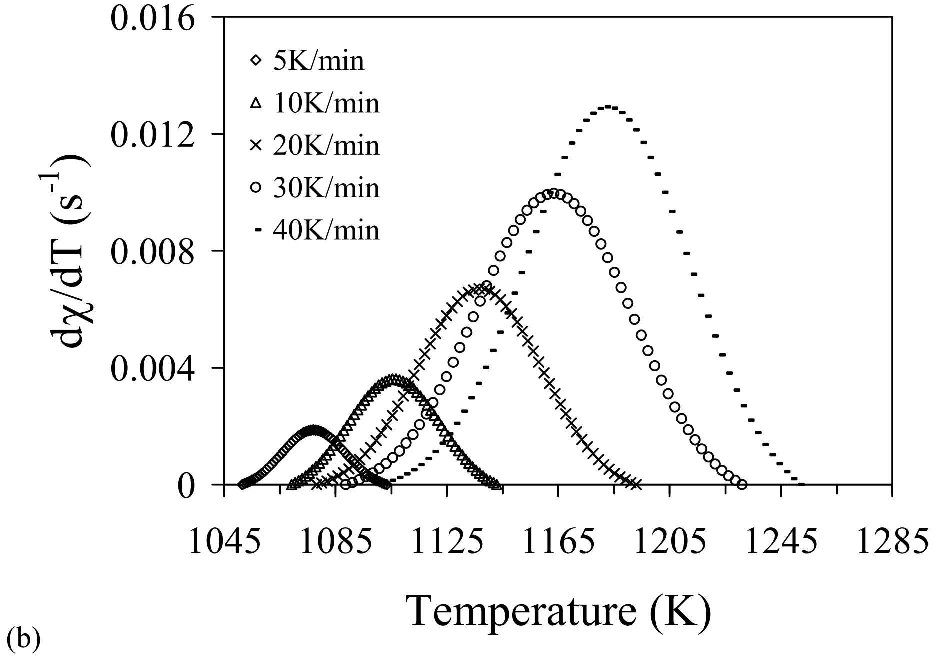

Figure 4.17(b) Crystallization rate vs. temperature for the second exothermic peak at different heating rates

The kinetic exponent, *n*, for both the crystalline phases can be calculated by using Eq. (viii). The *n* is the Avrami parameter which determines the crystallization mode. The value of *n* depends on the mechanism of the transformation reaction. If the rate of nucleation is a function of time, so is *n*; *n* is higher for a constant nucleation rate than when the nucleation rate increases with time and lies between those for constant and zero nucleation rates when the nucleation rate decreases with time. When surface crystallization dominates, n~1 and when the bulk crystallization dominates, $n \geq 3$. When both surface and bulk crystallization occur, *n* has value between 1 and 3. The kinetic parameter *n*, for both the crystallization exotherms can also be calculated using Eq. (viii) by plotting of $\ln[-\ln(1-\chi)]$ versus 1/T for the all heating rates [Fig. 4.18 (a) and Fig. 4.19 (a)]. From the data obtained by Fig. 4.18 (a) and Fig. 4.19 (a), a plot of $\ln[-\ln(1-\chi)]$ versus 1/T at constant temperature can be performed. Fig. 4.18 (b) and Fig. 4.19 (b) shows the relation between $\ln[-\ln(1-\chi)]$ with $\ln\beta$ at two fixed temperatures for both the crystallization exotherms. From the slope of this relation one can deduce the order of the crystallization mechanism (or Avrami index), *n*. Allowing for experimental error, the value of $\langle n \rangle$ is 2.05 and 3.08 for the first and the second crystalline phase respectively. The values of the Avrami index for both the phases are less than those obtained for the same crystalline phases in our previous study [10]. Thus, it can be said that the decrease in B_2O_3/Al_2O_3 ratio tends to increase the activation energy of crystallization and affects the mode of crystallization by shifting the nucleation mechanism from the bulk towards the surface.

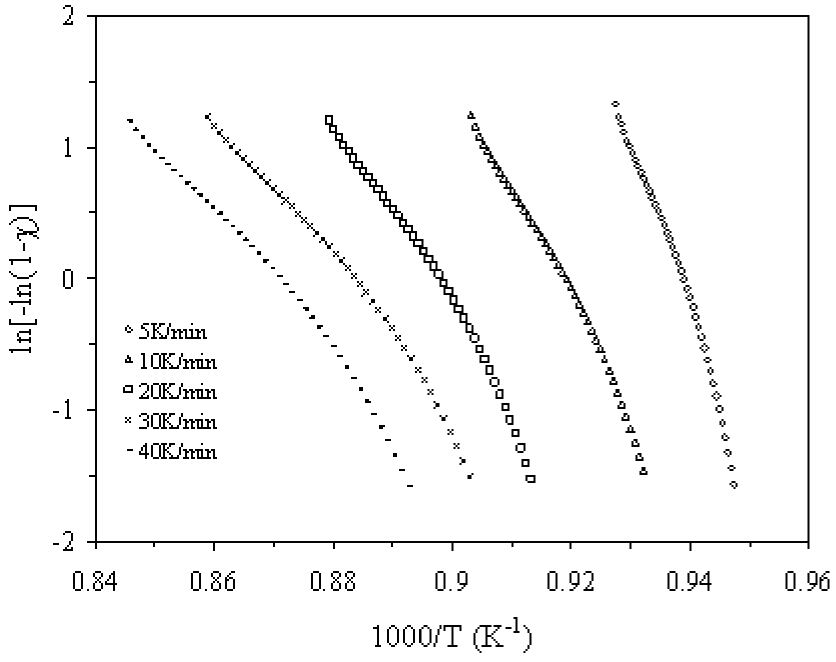

Figure 4.18 (a) Plot of ln[-ln(1-χ)] vs. 1000/T for first exothermic peak at different heating rates

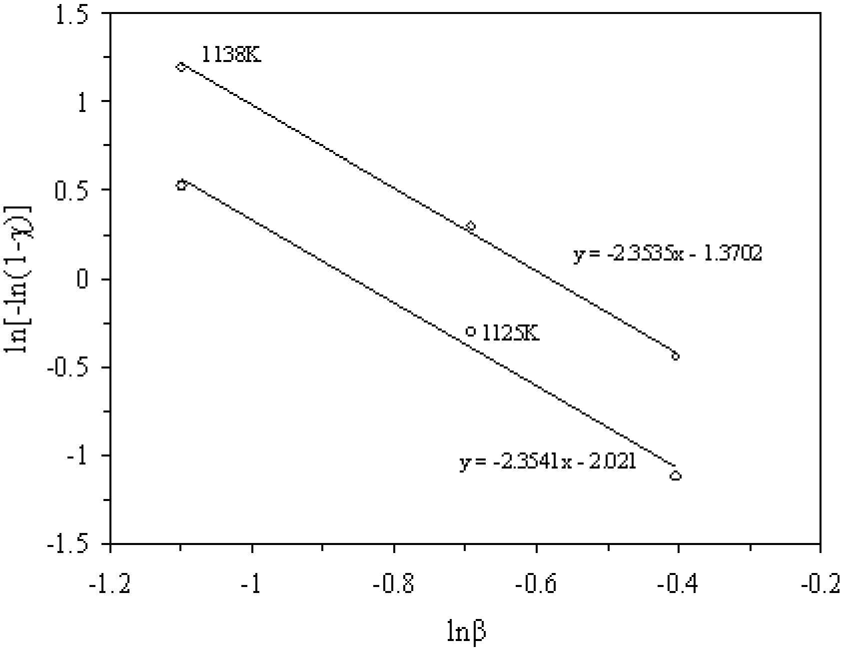

Figure 4.18 (b) Plot of ln[-ln(1-χ)] versus lnβ for first exothermic peak at two different temperatures

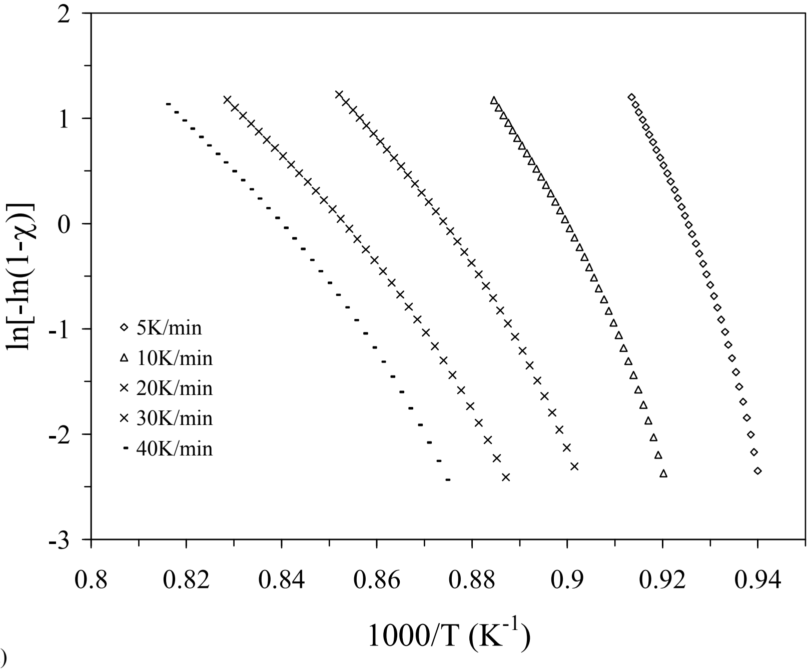

(a)

Figure 4.19 (a) Plot of ln[-ln(1-χ)] vs. 1000/T for second exothermic peak at different heating rates. (The underlined value is the Avrami index)

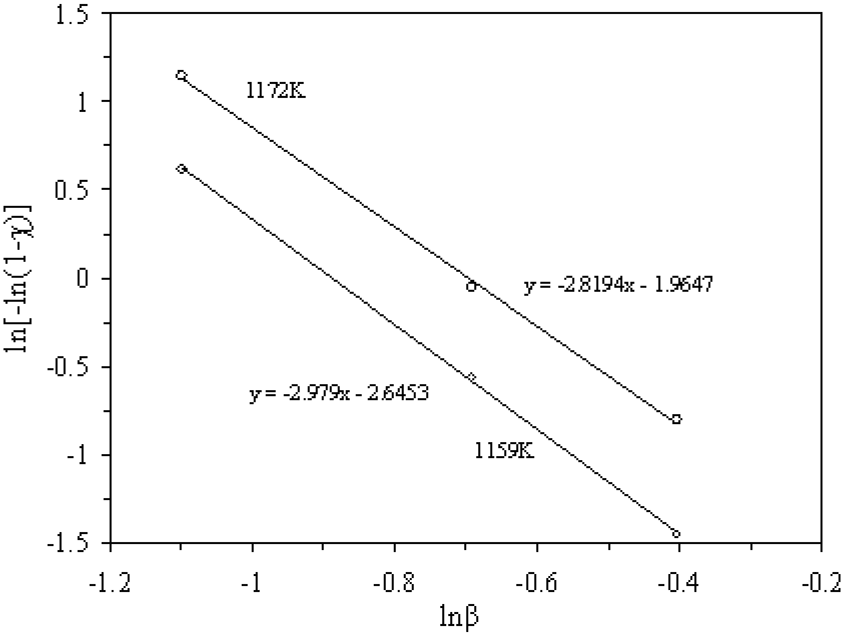

Figure 4.19 (b) Plot of ln[-ln(1-χ)] versus lnβ for second exothermic peak at two different temperatures. (The underlined value is the avrami index)

4.1.2 Thermal Dilatometric Analysis (TDA)

Thermal dilatometeric analysis also called dilatometery is done by taking polished glass samples (cylindrical shape) from 30 ^{o}C to the softening point of sample at a heating rate of 5 ^{o}C/min and values of softening temperature and thermal expansion coefficient are calculated for each sample. The plots obtained by dilatometer are shown in figure 4.20 for samples INA-1, INA-2, INA-3, INA-4 and INA-5.

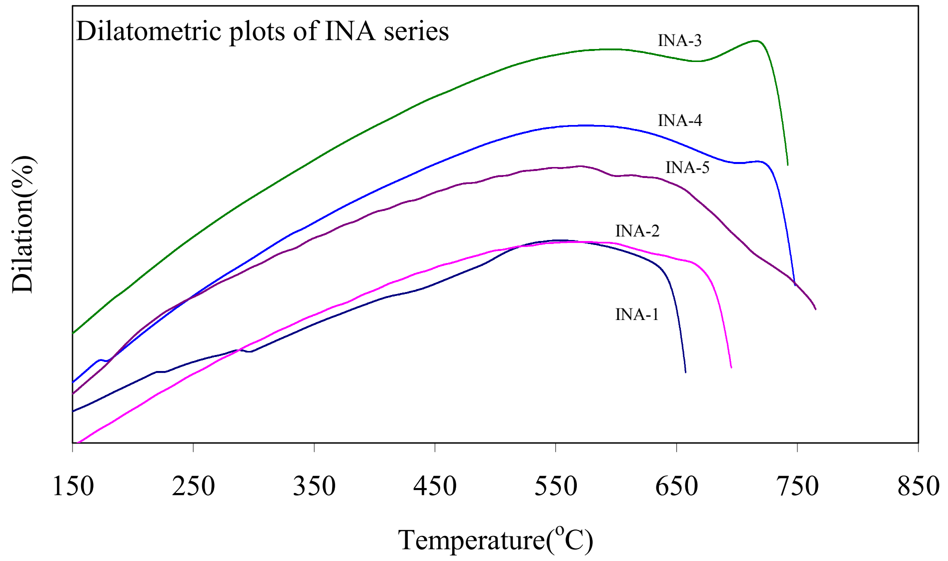

Figure 4.20 Plot of Dilatometer of INA-1 polished glass frit

It is clear from the above plot that with the increase in alumina contents from INA-1 to INA-5 the softening temperature value of glass frits are increasing. This is because of presence of Al_2O_3. Higher the concentration of Al_2O_3 in the glass it may lead to increase the softening temperature. The values obtained from the above plot of T_s (softening temperature) and TEC (thermal expansion coefficient) are given in table 4.8.

Table 4.8 T_s and TEC values obtained from dilatometer for INA series

Sample ID	T_s(°C)	TEC(10^{-6}/K)(200-600°C)
INA-1	657.5	7.9
INA-2	695.3	8.1
INA-3	742.0	8.3
INA-4	747.8	8.2
INA-5	765.1	8.1

Glass that best fulfills the cell requirement such as thermal expansion coefficient should lie in the range 8.5-12 X 10^{-6}/°C [31]. The values of TEC obtained in our glass samples are very near to this specified range so, they may act as suitable sealants for SOFC applications.

4.1.3 XRD & SEM of $40SiO_2$- $30BaO$-$20ZnO$- $(10-x)B_2O_3$- xM_2O_3 (M=Al, =0, 2.5, 5.0, 7.5, 10.0)

All the synthesized glass samples were characterized by XRD and all of them were found to be amorphous in nature. This observation was confirmed by a broad spectrum obtained in XRD pattern [fig. 4.21]. In order to understand the nucleation kinetics these glasses were heat treated at different temperatures for different time intervals. This study is presented in subsequent sections.

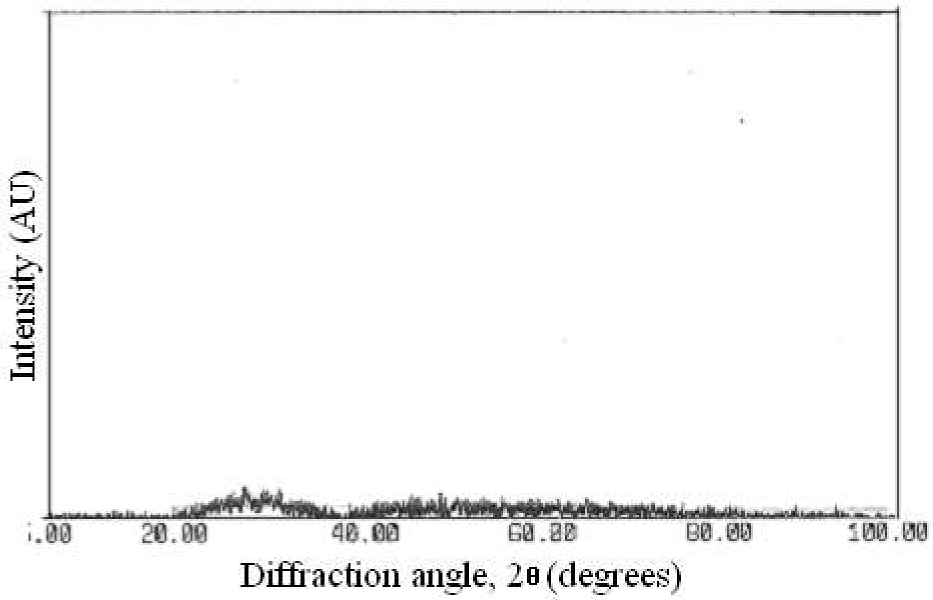

Figure 4.21 XRD pattern of as prepared glass

The X-ray diffraction pattern of glass sample INA-1 heat-treated at 800 °C and 850 °C for 1 hr is as shown in fig. 4.22. Fig. 4.23 shows the X-ray pattern of INA-1 glass sample heat treated at 850°C for 10 hrs.

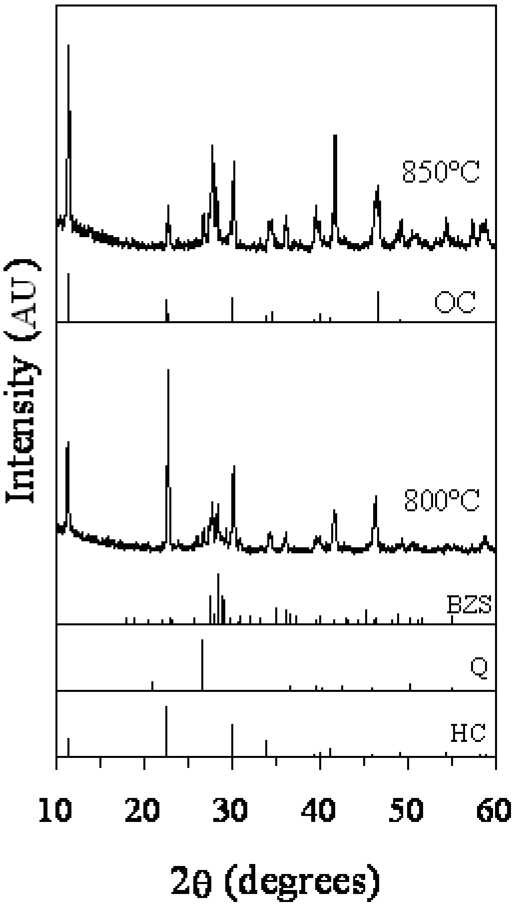

Figure 4.22 XRD pattern of INA-1 glass sample heat-treated at 800°C & 850°C for 1 hr (BZS= Barium Zinc Silicate, Q= Quartz, HC= Hexacelsian, OC= orthocelsian)

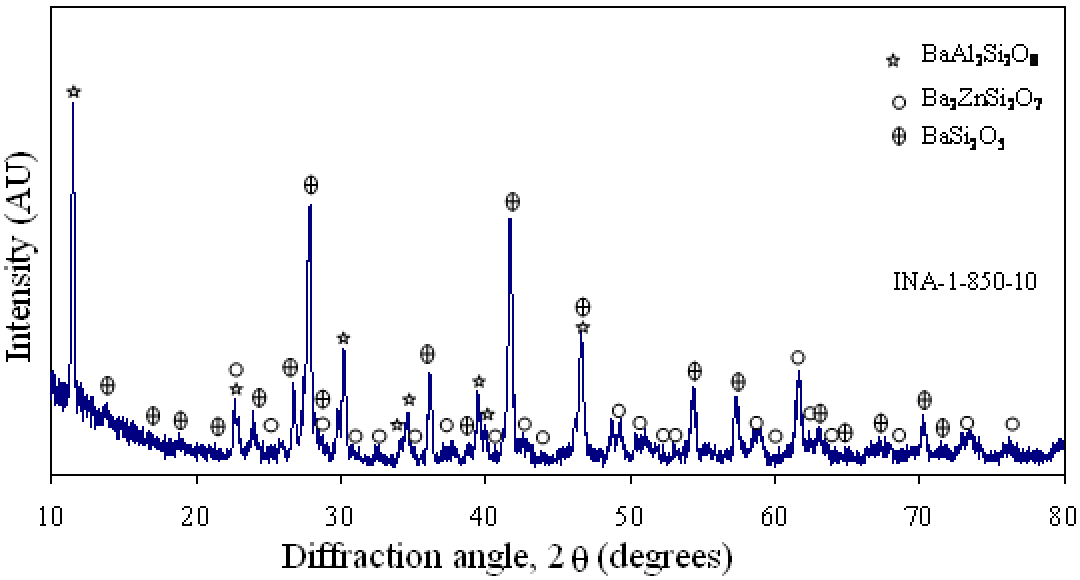

Figure 4.23 XRD pattern of INA-1 glass sample heat-treated at 850 °C for 10 hrs

When INA-1 glass sample is heat treated at 800 °C for 1 hr time duration formation of barium zinc silicate ($Ba_2Zn_3Si_3O_{11}$) (ICDD card no. 23-0844) (BZS), hexacelsian ($BaAl_2Si_2O_8$) (ICDD card no. 88-1048) (HC) and quartz (SiO_2) (ICDD card no. 46-1045) (Q) takes place. When temperature of heat treatment is increased from 800 to 850°C BZS and Q phase remains unchanged and HC is converted into orthocelsian (ICDD card no. 77-0185) (OC) phase. OC and HC are two polymorphs of this phase having different values of TEC i.e. 2.2 X $10^{-6}K^{-1}$ and 8.2 X $10^{-6}K^{-1}$ respectively [32-35]. The TEC value obtained in our case is 8.2 X $10^{-6}K^{-1}$ which gives a confirmation of hexacelsian phase after heat-treatment at 800 °C. Consequently, by increasing the time duration of heat treatment at 850 °C for 10 hrs, OC phase remains unchanged and BZS is converted into barium zinc silicate ($Ba_2ZnSi_2O_7$) (ICDD card no. 10-0047) and Q phase is converted into barium silicate ($BaSi_2O_5$) (ICDD card no. 10-0045) (BS) phase. Since Zn is volatile in nature it will have a tendency to migrate from the lattice. The vacant site created due to migration of Zn^{+2} is being occupied by Ba^{+2} ion by the mechanism of transformation of orthosilicate to pyrosilicate as the size of Ba^{+2} (1.43A°) is more than Zn^{+2} (0.84 A°). This mechanism can be explained by the following reaction.

$$10SiO_2 - 5BaO \rightarrow 5BaSi_2O_5$$
$$2SiO_2 - 2BaO - ZnO \rightarrow Ba_2ZnSi_2O_7$$
$$2SiO_2 - BaO - Al_2O_3 \rightarrow BaAl_2Si_2O_8$$
$$3SiO_2 - 2BaO - 3ZnO \rightarrow Ba_2Zn_3Si_3O_{11}$$

In order to understand the mode of nucleation of crystalline phase a detailed analysis of the microstructure has been done. The microstructures of samples which have been given heat treatment at 800 °C and 850 °C at heating rate of 5 °C/min indicate that the number of nucleation sites is more and peak maximum can occur at a temperature at which the melt viscosity is higher i.e. at lower temperature. This is also evident in our DTA analysis curve (fig 4.1). Fig. 4.24 (a & b) represents the micrographs of the samples INA-1 (without Al_2O_3) heat-treated at 800 °C for 1 hr time duration. All the samples are etched for same timing. The idea behind this analysis is to see the effect of Al_2O_3 addition on nucleation kinetics of glass-ceramics. Though Al_2O_3 was not added in this glass but it has picked up Al_2O_3 from the crucible during course of melting as described below where the characterization was done by EPMA analysis.

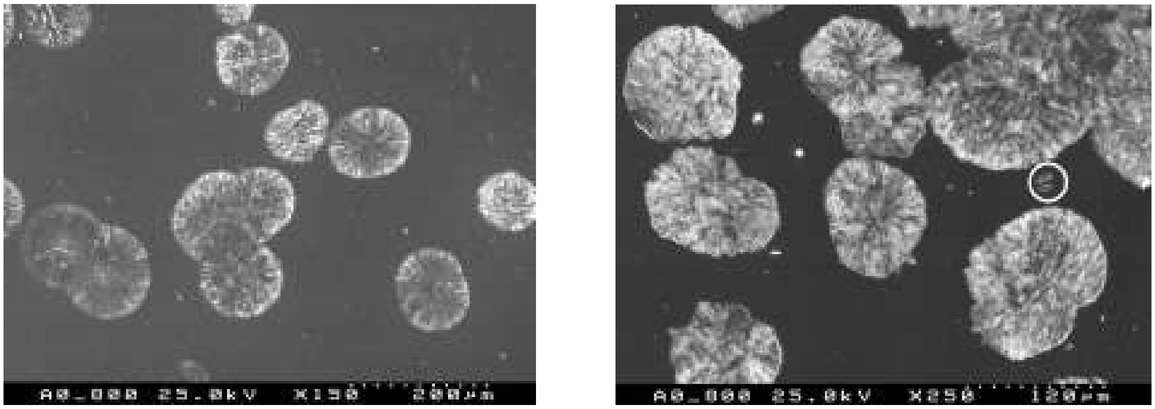

Figure 4.24 (a & b) SEM micrograph of INA-1 sample heat treated at 800°C for 1 hr

It can be seen that the nucleation and growth of crystalline phase has taken place in the glass matrix. This type of phases are developed during controlled crystallization by providing heat treatment between T_g and T_m. Structural features appear to be that of spherulite structure (Fig. 4.24 a & b). This structure gets derived when the crystallization rates are very slow. It is confocal arrays of fine fibrillar crystals which grow with preferred radial orientation. The large magnification view exhibit a feathery structure of the fibrillar crystal which can be designated as composite spherulites comprising of two phases [25]. One phase nucleates epitoxially and another phase grows laterally (Fig. 4.25).

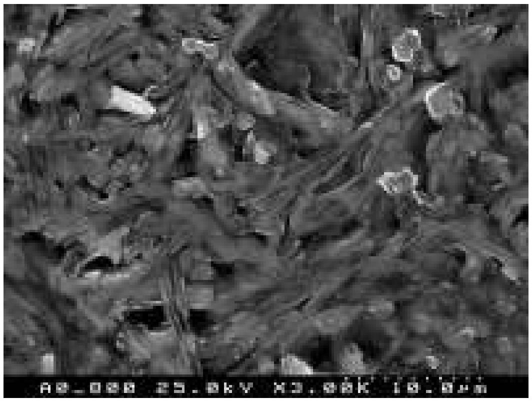

Figure 4.25 SEM image of INA-1 glass sample heat treated at 800 ^{o}C for 1 hr

However, when heat treated at higher temperature (at 850^{o}C) the fibrillar morphology gets recrystallized which leads to equilibrium phases with selective coarsening effect. Fig. 4.26 (a & b) corresponds to such microstructural features. It is evident from the micrograph that two types of equilibrium phases exist. One with faceted (sharp edges) morphology and another for ring type or ladder type features. A careful examination of the structure indicates that initially a solid solution phase has formed with faceted morphology and with in this phase the nucleation and growth of second phase has occurred as needle structure. The preferred growth morphology of this derived phase within the faceted phase can be seen in the structure. As per Jackson model [26,27] which is a relationship of relative change in surface free energy as a function of the fraction of surface sites which are occupied with variation in α, faceted structures are only possible when α lies in between 2 and 5. The α parameter depends on the latent heat and crystallographic factor which indicate the fraction of total binding energy which binds the atom in a layer parallel to the plane face to other atoms in the layer. The small differences in the free energy between two phases of similar composition may result in the kinetically preferred intermediate metastable phases. The variation in structure in layer chain type morphology can lead to secure anisotropy in surface energy. This further leads to variation in growth morphology of the phases [28]. This influences the interface type of growth kinetics leading to faceting tendency. The occurrence of liquid immiscibility in glasses also leads to a competition between phase separation and crystallization of metastable and equilibrium phases [29]. The structure derived from such interaction leads to equilibrium phase formation as can be seen in micrograph where the transition can be seen in the direction of arrow (Fig. 4.26 a & b). The structure comprises of a crystalline solid solution phase with faceted morphology. However, with passage of time the nucleation of another solid solution phase occurs in the matrix of faceted phase as needle. During heat treatment nucleation of the metastable crystalline solid solution along with other crystalline phase occurs in the beginning in the glass matrix. These crystalline phases are elongated in nature as can be seen in Fig. 4.24b marked in circles which further grow in the form of spherulite structure. The growth phenomenon continues till they merge in each other. As described above at higher temperature heat treatment metastable solid solution phase which nucleates in the glass matrix is further converted into crystalline phase within the glass matrix. This conversion of metastable phase into equilibrium phases is due to existence of miscibility gap and phenomenon is just like which occurs as lamellar structure in metallic system. The higher magnification micrographs reveal that these phases get derived from solid solution (Fig. 4.26a). The area above and below this lamellar structure (the variation in contrast) clearly indicate that the growth morphology is dominated by diffusion phenomenon. The separation between these derived phases is in between 500 nm and 900 nm. From all the microstructural features presented above, it is clear that for samples heat treated at 850 °C, three types of microstructural features exists. One with white contrast, another with grey contrast and third like needle with ladder features in the matrix of grey phase.

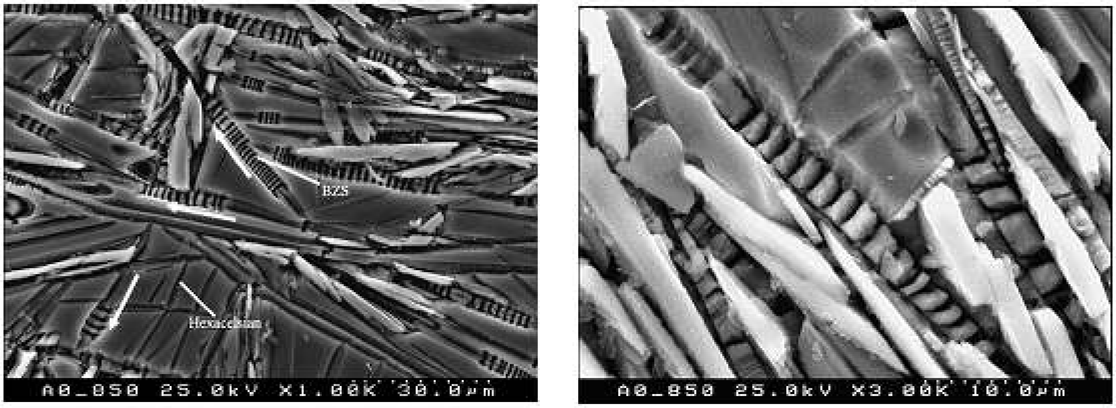

Figure 4.26 (a & b) SEM microstructure of INA-1 glass sample heat treated at 850 °C for 1 hr time duration

The EDS analysis done on these areas indicate that both white features and grayish features indicate the composition corresponding to hexacelsian. However, the white feature is derived from the fibrillar composite spherulite structure which gets converted to stable grey features with faceted morphology (Fig. 4.26b). However, the interesting feature is that the ladder like morphology corresponds to barium zinc silicate (Figs. 4.27 and 4.28). This micro crystalline phase comes out from the needle phase after it acquires certain critical width as it nucleates in the middle of the needle (marked as arrow in Fig. 4.26a). Our X-ray analysis also supports the existence of three crystalline phases which can be seen clearly in the micrographs (fig. 4.26).

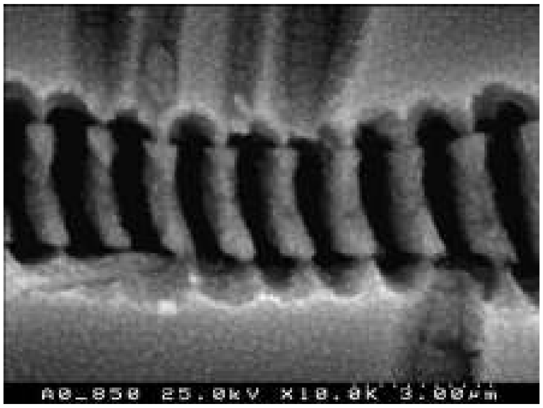

Figure 4.27 SEM micrograph of BZS phase in INA-1 sample heat treated at 850 °C for 1 hr time duration

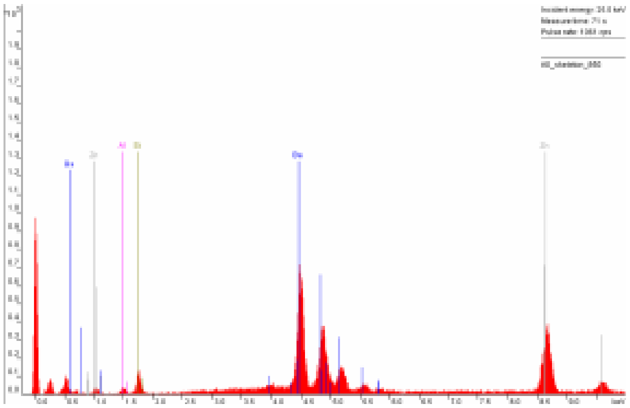

Figure 4.28 EDS analysis of BZS phase in INA-1 sample heat treated at 850 °C for 1 hr time duration

If the heat treatment is done at higher temperatures for longer time durations (10 hrs) these structural features transform to distorted faceted type of structure. A representative structure is shown in figure 4.29. Turnbull [30] in his work has demonstrated the process of nucleation and growth on the basis of homogenous and heterogeneous nucleation. In case of glass-ceramics similar theory with variation in viscosity can also be utilized as nucleation in glass-ceramic occurs from the glass which is a viscous liquid. The two interrelated but inherent features for glasses are the viscosity (which varies with temperature) and the crystallographic nature of growing silicate phase which nucleates in glass matrix. At higher viscosity when the heat treatment is done close to T_g, it may lead to localized segregation of solute or impurity at the crystal/ liquid interface. The interface controlled growth may become diffusion control leading to cellular transformation mechanism which may cause the equiaxed type of structure. Since there is vast variation in viscosity in glassy system as compared to metallic system a growth will occur like spherulite in glass-ceramic system which has been observed in our case (fig. 4.24 a & b).

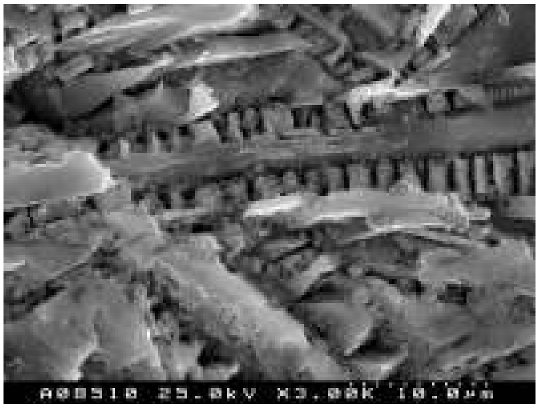

Figure 4.29 SEM micrograph of INA-1 sample heat treated at 850 ^{o}C for 10 hrs

Our DTA analysis followed by theoretical calculations indicated that there is simultaneous nucleation of two phases that is occurring with very small difference in their enthalpies [10]. This indicates that there is very small difference in their free energy of these two crystalline phases. It means that formation of probably metastable intermediate phase which is kinetically preferred with increase in temperature beyond T_g has occurred. Since the structural features observed at higher temperature (850 ^{o}C) heat treatment is different as compared to lower temperature (800 ^{o}C), this means that interface controlled mechanism is dominating at higher temperature. If growth kinetic is controlled by interface then facetating tendency is observed which can be seen in the sample heat treated at higher temperature (fig 4.29). Moreover, our X-ray diffraction pattern (fig. 4.23) corresponding to heat treatment at 850 °C for 10 hours shows the peak splitting which is an indication of internal distortion in the system. The transformation on mechanism observed in our SEM analysis confirms this configuration of the system. This splitting is more prominent for BZS phase. The SEM (fig 4.27) analysis shows the formation of drain like structure just above the lamellar feature. This further strengthens the idea of this metastable character causing straining effect in the crystalline lattice.

Like INA-1 glass, INA-2 glass was also given heat treatment. Since in INA-1 glass the Al_2O_3 was picked up from crucible during melting leading to formation of barium aluminum silicate phase. In order to know the nucleation in the glass matrix the INA-2 glass was given heat treatment in a different mode. Glass powder was heated upto 800 °C at a heating rate of 20K/min in air in DTA and hold for different time durations ranging from 1 to 30 seconds. Figure 4.30 presents the XRD pattern of heat treated powders at 800 °C for 12 sec and 30 sec of INA-2 glass.

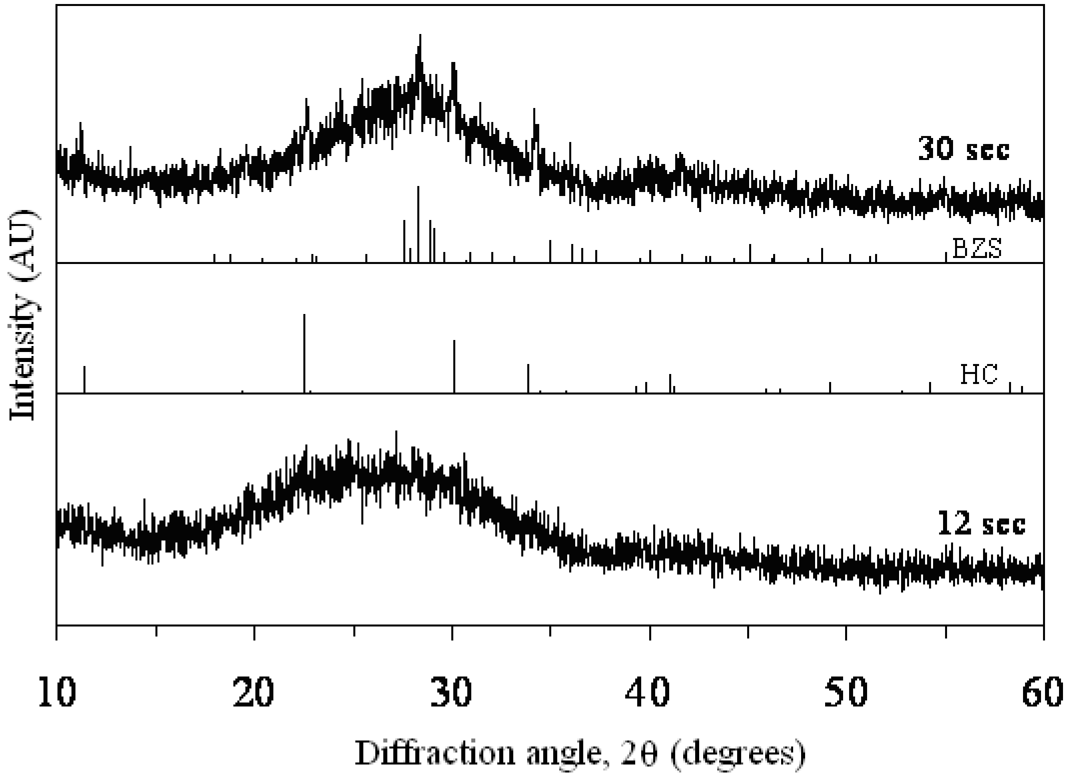

Figure 4.30 XRD pattern of INA-2 glass sample heat-treated at 800°C for 12 and 30 sec

Glass was amorphous after heat treatment at 800 ^oC for up to 12 s, however, two phases, namely hexacelsian (HC; ICDD card no. 01-077-0185), a hexagonal polymorph of barium aluminum silicate ($BaAl_2Si_2O_8$), and barium zinc silicate (BZS; $Ba_2Zn_3Si_3O_{11}$, ICDD card no. 00-023-0844) appeared after a dwell time of 30 s. These phases are nucleating side by side. On analyzing the intensity of peak it seems that BZS phase is nucleating first. Moreover, the enthalpy of formation of both the phases seems to be close to each other which can not be quantified due to non availability of data. Development of crystalline phases along with the study of the microstructure of the glass was made by heating the glass frits in the temperature range of 800–900 ^oC in air with a holding time of 1 h at each temperature. Heating rate was maintained at 5 K/min for each heating schedule. Figure 4.30 to 4.34 shows the X-ray diffratogram for the INA-2 glass sample heat treated at 800, 850 and 900 ^oC and figure 4.35 shows the variation of intensity of the maximum peak of the phases present after each heat treatment. As evident, BZS and barium aluminum silicate are the predominant phases in all XRD patterns, along with the presence of barium zinc borate ($BaZn_2(BO_3)_2$) at 800 ^oC and 850 ^oC. Barium aluminum silicate appeared in the form of its two polymorphs, namely HC and orthocelsian (OC; ICDD card no. 00-012-0725), an orthorhombic polymorph at different temperatures. From fig. 4.35 it is clear that the intensity of BZS increases with increase in temperature up to 850 ^oC while the OC reaches its maximum intensity at 900 ^oC. HC was observed only at 850 ^oC while the OC was absent at this temperature. Figs. 4.30 and 4.35 aim to shed light on these differences under the perspective of evolution of phases.

Figures 4.31 and 4.32 shows the formation of $BaZn_2(BO_3)_2$ and $Ba_3B_6Si_2O_{16}$ crystalline phases respectively when the sample INA-2 was heat treated from 800 to 850 ^oC for 1 hr time duration. The formation of $Ba_3B_6Si_2O_{16}$ (ICDD card no. 06-0351) can be explained on the basis of volatile nature of Zn as we have explained for sample INA-1. After that when this glass sample is further heat treated at 850 ^oC for 10 hrs (fig. 4.33) $Ba_3B_6Si_2O_{16}$ phase doesn't come into picture i.e. at this temperature this particular phase gets dissolved. When this glass sample is further heat treated at 900 ^oC for 1 hr (fig. 4.34) $BaAl_2Si_2O_8$ and $Ba_2Zn_3Si_3O_{11}$ remains as such and a new phase $Al_{13}B_7$ (hexagonal, ICDD card no. 29-0005) nucleates. On analyzing the entire heat treatment cycle and the resultant phases it can be concluded that nucleation and dissolution of crystalline phases in the glass matrix which behave like liquid is very complex process.

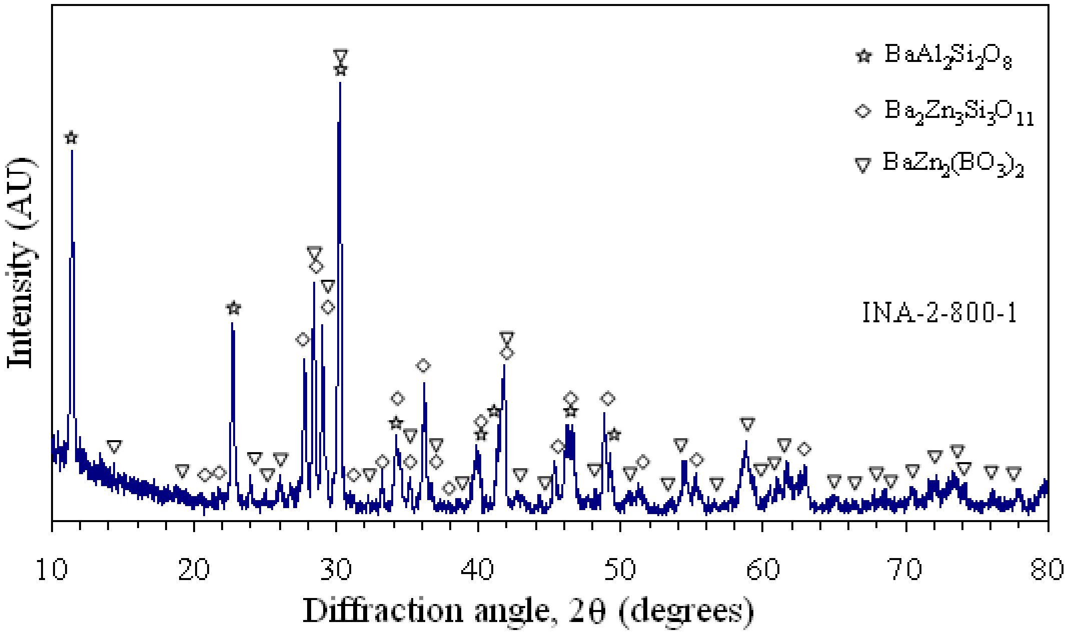

Figure 4.31 XRD pattern of INA-2 glass sample heat-treated at 800°C for 1 hr

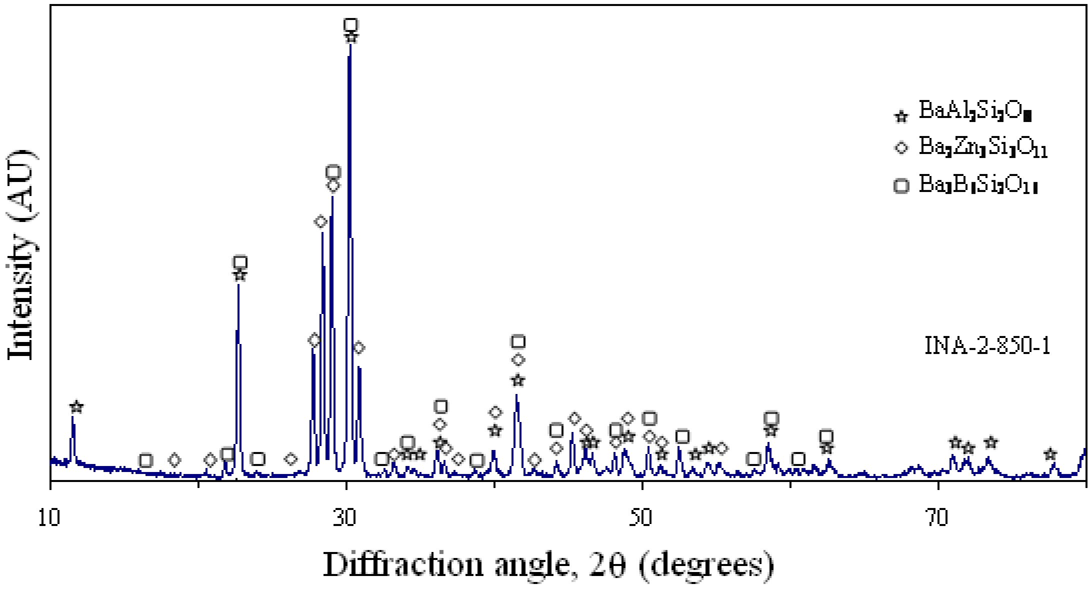

Figure 4.32 XRD pattern of INA-2 glass sample heat-treated at 850°C for 1hr

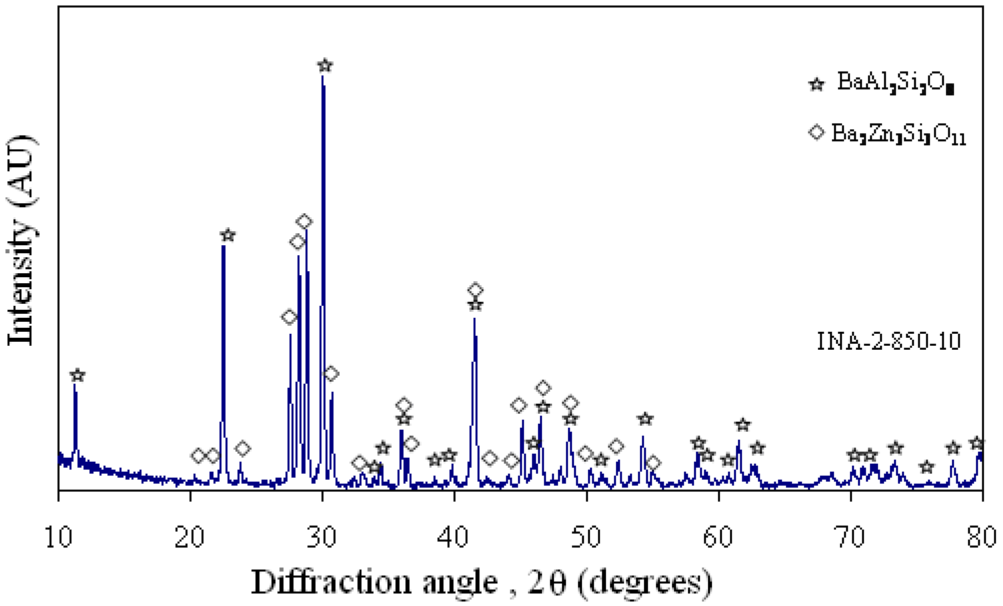

Figure 4.33 XRD pattern of INA-2 glass sample heat-treated at 850 °C for 10 hrs

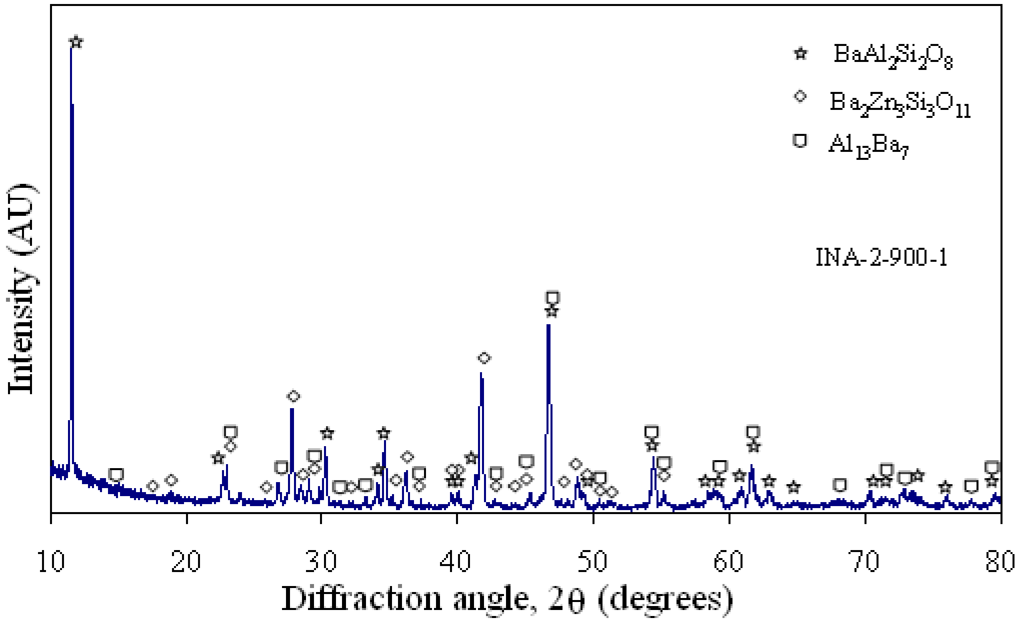

Figure 4.34 XRD pattern of INA-2 glass sample heat-treated at 900 °C for 1hr

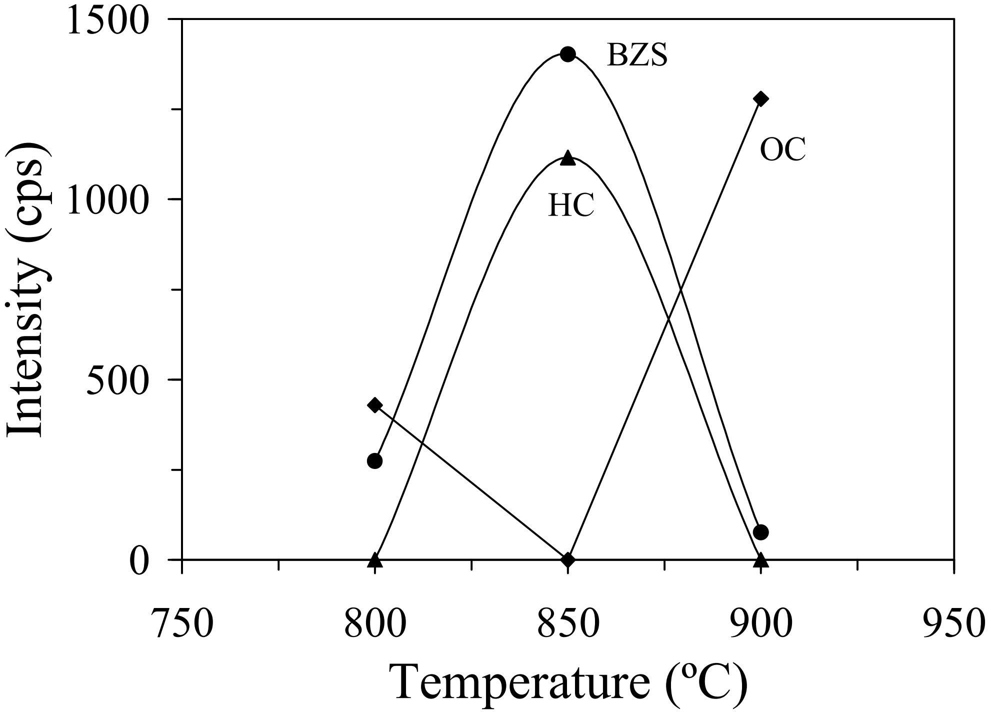

Figure 4.35 Change in intensity of different crystalline phases with increase in temperature

Fig. 4.36 shows the SEM micrograph for the glass specimen heated at 800 ^{o}C for 1 hr. Crystallization in the glass appears to start from the periphery of the glass, thus giving the signs of the dominance of surface crystallization mechanism for the crystallization process which occurs as time proceeds. The structure indicates that the growth of crystalline phase occurs from surface. The interface is planer type and is smooth in nature.

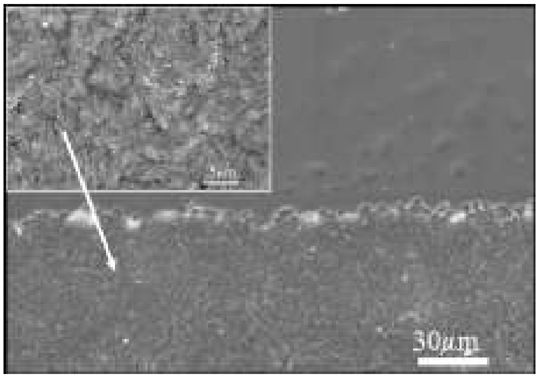

Figure 4.36 SEM image of INA-2 glass sample heat treated at 800 ^{o}C for 1 hr

No SEM image could be taken for the INA-2 glass sample heat treated at 850 ^{o}C as the resulting glass ceramic was highly transparent in nature. However when INA-2 glass sample was heat treated at 850 °C for 10 hrs (fig. 4.37) the growth of crystallites is same as we have observed in sample INA-1 heat treated at 850 °C for 10 hrs time duration (fig. 4.29). It seems that nucleation of crystalline phase(s) occurs in the preferred mode because of this the interface is smooth. However, a careful examination reveals that the glass matrix is in a strained condition as sharpness in the nucleated phase is not observed as in case of INA-1 glass. The conversion of $BaZn_2(BO_3)_2$ to $Ba_3B_6Si_2O_{16}$ phase from 800 °C to higher temperature heat treatment makes the glass matrix more strained as all the silicate tries to grow in a preferred direction. Because of this the elongated needle like structure is seen.

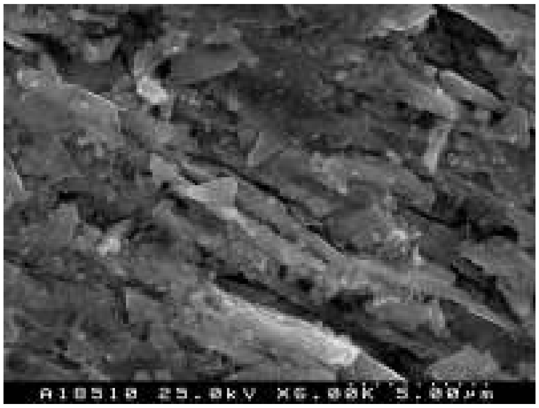

Figure 4.37 SEM micrograph of INA-2 sample heat treated at 850 °C for 10 hrs

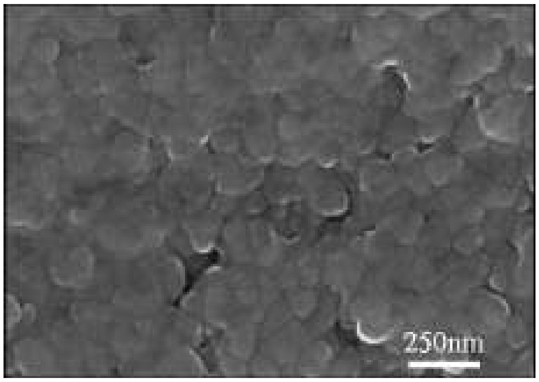

Figure 4.38 SEM image of INA-2 glass sample heat treated at 900 °C for 1 hr.

Fig. 4.38 is the SEM image of the INA-2 glass heat treated at 900 °C for 1 h. The resulting glass ceramic has very small size crystallites (~100 nm) which were not observable at lower magnifications. This is in accordance with the behavior of the transparent glass ceramic which resulted after heat treatment at 850 °C.

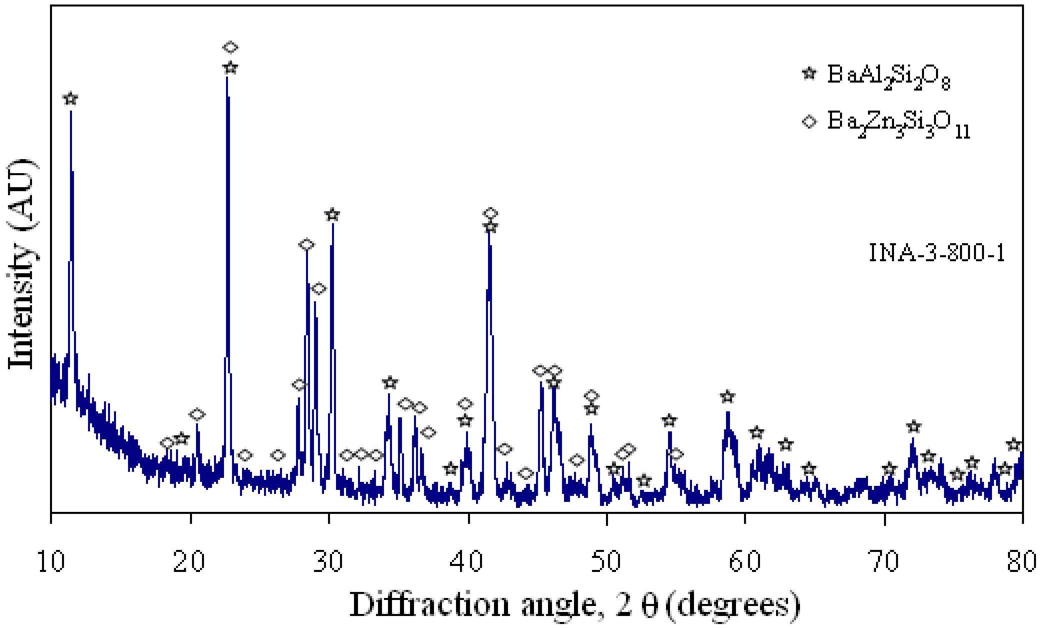

Figure 4.39 XRD pattern of INA-3 glass sample heat-treated at 800 °C for 1hr

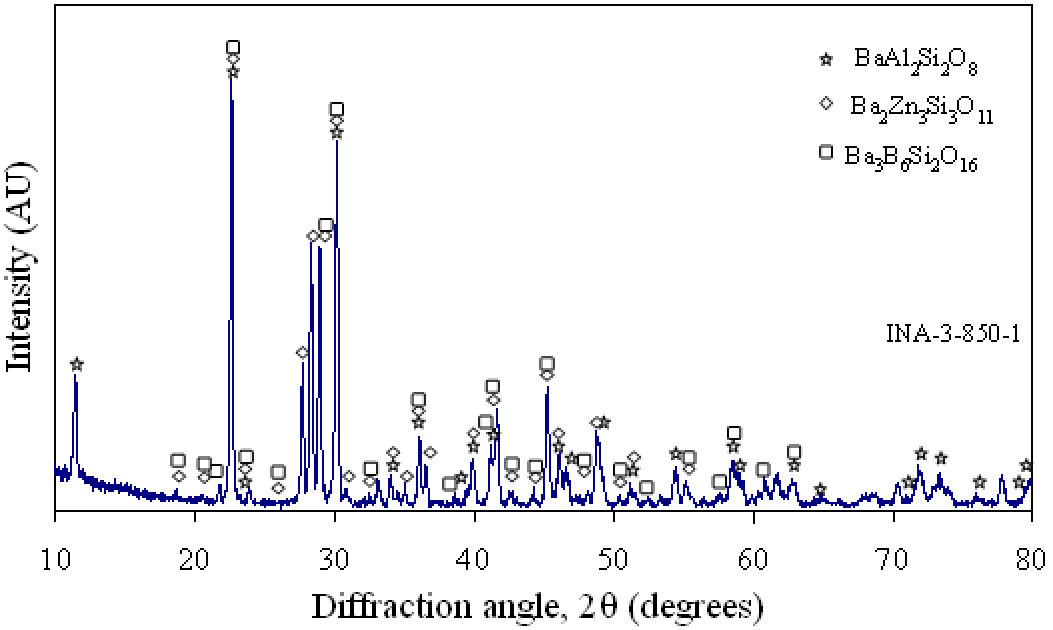

Figure 4.40 XRD pattern of INA-3 glass sample heat-treated at 850 °C for 1 hr

Figure 4.39 shows the formation of $BaAl_2Si_2O_8$ (HC, ICDD card no. 77-0185) and $Ba_2Zn_3Si_3O_{11}$ (ICDD card no. 23-0844) phase formation which nucleated at 800 ^oC when INA-3 glass sample is kept at this temperature for 1 hr. When this glass sample is further heat treated at 850 ^oC for 1 hr time duration formation of $Ba_3B_6Si_2O_{16}$ (ICDD card no. 06-0351) occurs along with the presence of $BaAl_2Si_2O_8$ and $Ba_2Zn_3Si_3O_{11}$ phases (fig. 4.40).

When this glass sample is further heat treated at 850 ^oC for longer duration i.e. for 10 hrs then $Ba_3B_6Si_2O_{16}$ phase gets dissolved and $BaAl_2Si_2O_8$ and $Ba_2Zn_3Si_3O_{11}$ phases remains as such (fig. 4.41). When the sample is given heat treatment for higher temperature i.e. for 900 ^oC it follows the same trend as we get in fig. 4.41 with an increase in intensity of $BaAl_2Si_2O_8$ phase (fig. 4.42). This indicates that the nucleation of other phase is restricted with addition of Al_2O_3 in higher concentration. $Ba_3B_6Si_2O_{16}$ phase gets dissolved in the glass matrix and more stable phase grows further.

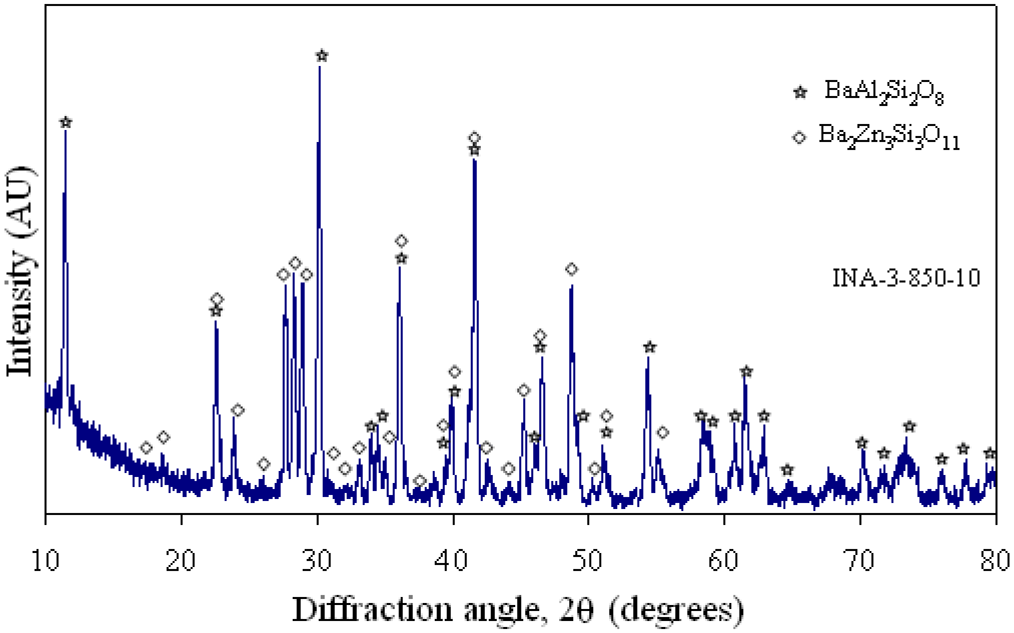

Figure 4.41 XRD pattern of INA-3 glass sample heat-treated at 850 ^oC for 10 hrs

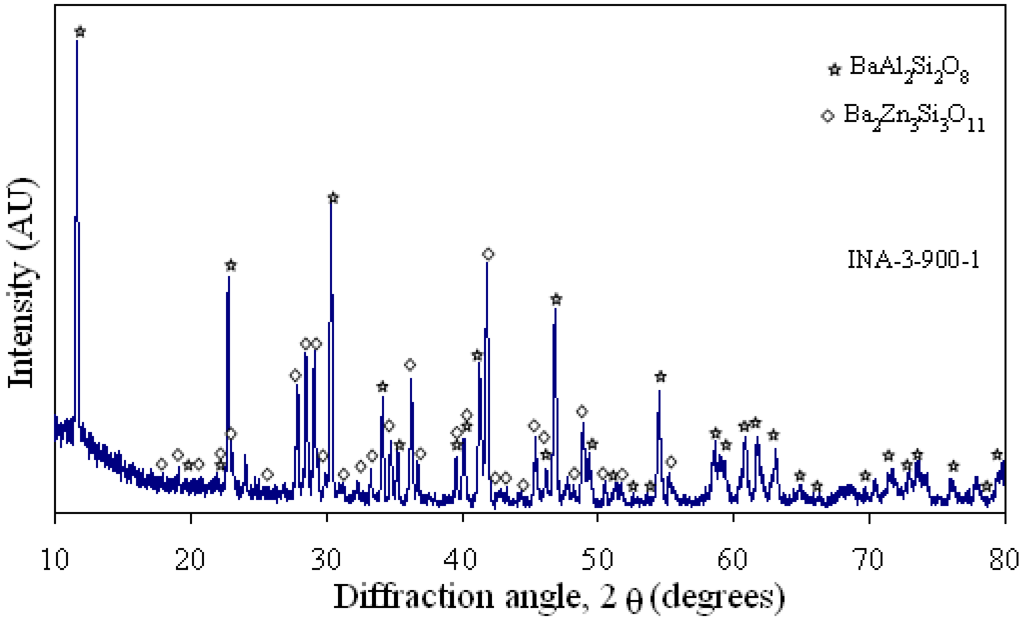

Figure 4.42 XRD pattern of INA-3 glass sample heat-treated at 900 ^{o}C for 1 hr

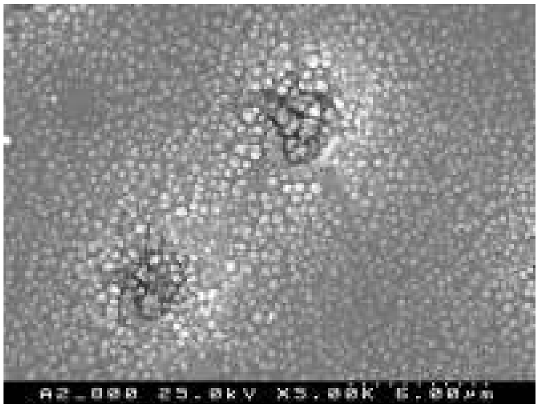

Figure 4.43 SEM micrographs of INA-3 glass sample heat treated at 800 ^{o}C for 1 hr

Figure 4.43 shows the micrograph of INA-3 glass sample which is heat treated at 800 ^{o}C for 1 hr. Since the nucleation can occur between T_g and T_m, the addition of Al_2O_3 further increases the glass transition temperature. The available thermal energy (temperature and time) is not sufficient enough for complete nucleation of crystalline phases in the glass matrix if the heat treatment is performed near T_g temperature. In our study we could find some defect sites also as can be seen in fig. 4.38, which provide active centre for nucleation to occur.

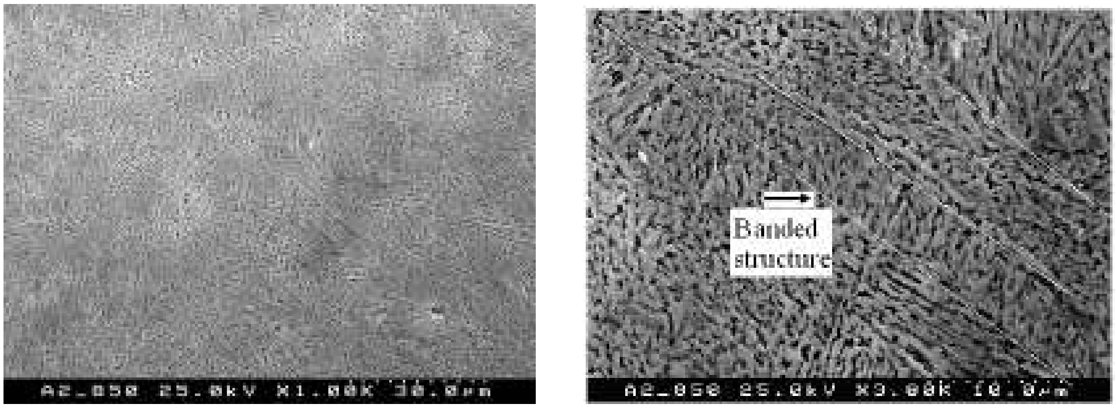

Figure 4.44 (a & b) SEM micrograph of INA-3 sample heat treated at 850 °C for 1 hr

Figures 4.44 (a & b) are the SEM images of INA-3 glass sample which is heat treated at 850 °C for 1 hr. In sample INA-3 crystallization process starts uniformly and crystalline growth is taking place in lateral and epitaxial direction. The feature resembles with dendritic structure which is stable one. The structure grows in different bands. These banded features are observed when the substance is in the highly undercooled state.

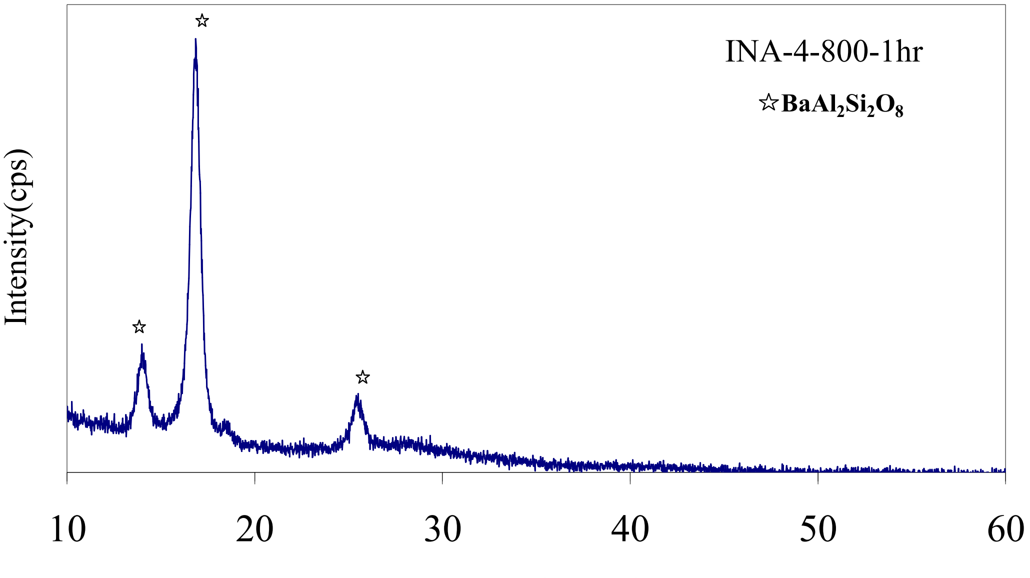

Figure 4.45 XRD pattern of INA-4 glass sample heat-treated at 800 °C for 1 hr

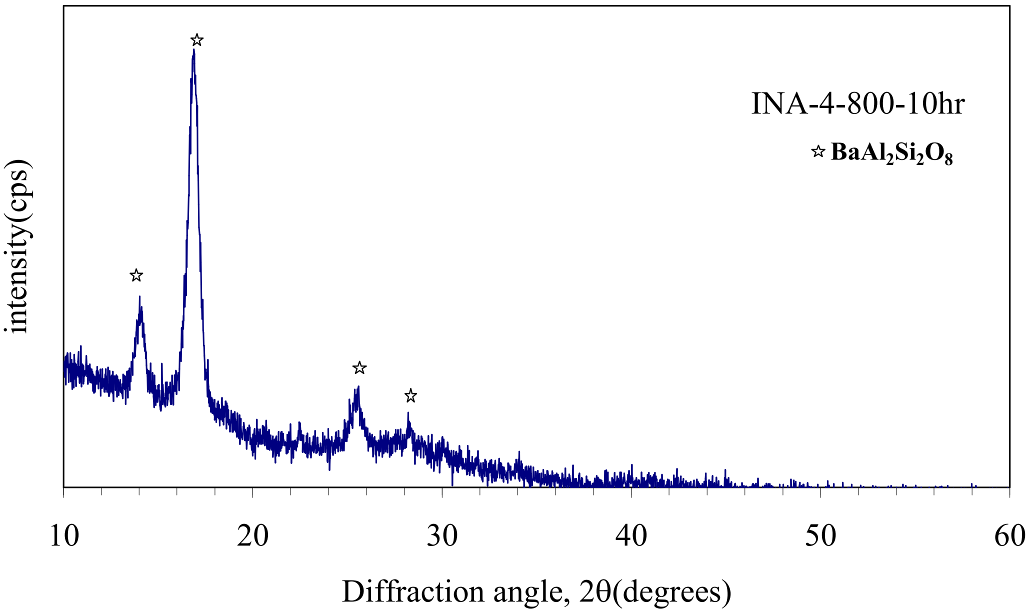

Figure 4.46 XRD pattern of INA-4 glass sample heat-treated at 800 °C for 10 hrs

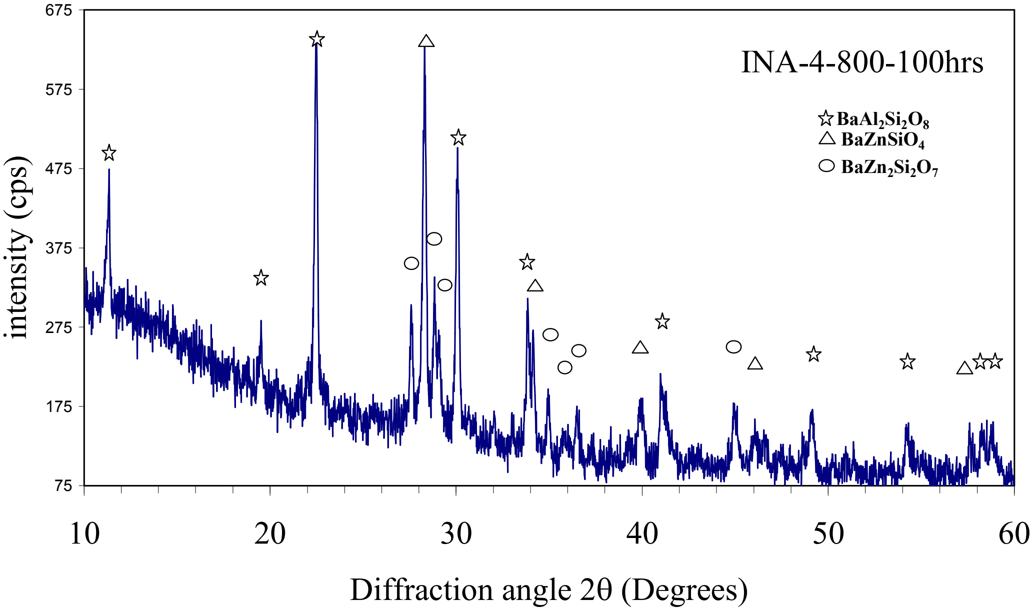

Figure 4.47 XRD pattern of INA-4 glass sample heat-treated at 800 °C for 100 hrs

When INA-4 sample is heat treated at 800 °C for various time durations i.e. 1, 10 and 100 hrs (figs. 4.45, 4.46 and 4.47), formation of various crystalline phases take place. When glass sample INA-4 is heat treated at 800 °C for 1 hr formation of hexagonal $BaAl_2Si_2O_8$ (HC, ICDD card no. 77-0185) takes place. TEC value of this formed HC phase is in accordance with the TEC value of our as formed glass sample i.e. 8.2.X $10^{-6}/^{o}C$. This pattern remains same when we heat treat this glass for 10 hrs at 800°C. Heating at the same temperature i.e. at 800 °C for 100 hrs leads to the formation of two more phases i.e. $BaZnSiO_4$ (Hexagonal, ICDD card no. 42-0335) and $BaZn_2Si_2O_7$ (ICDD card no. 10-0058) along with $BaAl_2Si_2O_8$ phase. Nucleation of single $BaAl_2Si_2O_8$ phase at 800 °C for 1 hr and 10 hrs indicate that the glass matrix is very stable and tight. However, 10 hrs diffractogram indicates that the glass matrix is in highly strained condition as base line is not smooth. However, prolong time heat treatment (100 hrs) provide conducive condition for the relaxation of glass matrix by getting the other phases nucleated as mentioned above. High temperature heat treatment leads to nucleation of several other phases as heat treatment time is increased.

When INA-4 glass sample is given further heat treatment up to 850 °C for 1 hr, formation of $BaAl_2Si_2O_8$ (HC, ICDD card no. 77-0185), $Ba_2Zn_3Si_3O_{11}$ (ICDD card no. 23-0844) and $Ba_3B_6Si_2O_{16}$ (ICDD card no. 06-0351) takes place (fig. 4.48). On increasing the time duration for heat treatment at same temperature i.e. heating at 850 °C for 10 hrs leads to the formation of $BaAl_2Si_2O_8$ (HC, ICDD card no. 12-0726), SiO_2 (stishovite, ICDD card no. 45-1374), $BaZnSiO_4$ (Hexagonal, ICDD card no. 42-0335) and BaB_2O_4 (rhombohedral, ICDD card no. 15-0862) occurs (fig. 4.49). We may say here that on increasing the heat treatment duration phase $Ba_2Zn_3Si_3O_{11}$ is getting converted into $BaZnSiO_4$. This may be because of the volatile nature of Zn. In the similar manner phase $Ba_3B_6Si_2O_{16}$ might be converted into BaB_2O_4 and SiO_2 phases.

On giving further heat treatment i.e. at 900 °C for 1 hr all the above formed phases are getting dissolved except $BaAl_2Si_2O_8$ (HC, ICDD card no. 77-0185) and formation of $Ba_2Zn_3Si_3O_{11}$ (ICDD card no. 23-0844) again comes into picture (fig. 4.50).

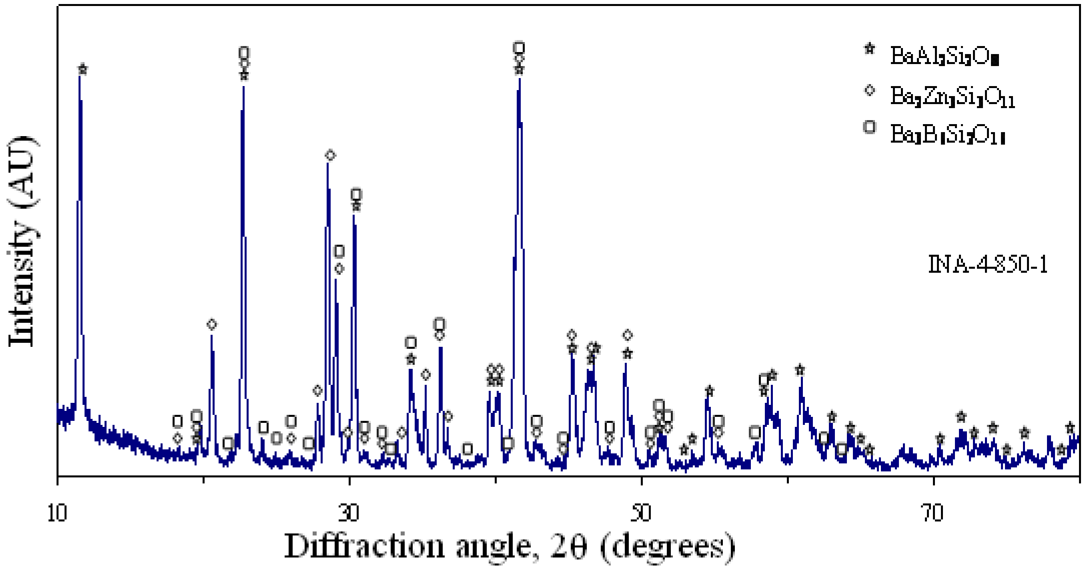

Figure 4.48 XRD pattern of INA-4 glass sample heat-treated at 850 °C for 1 hr

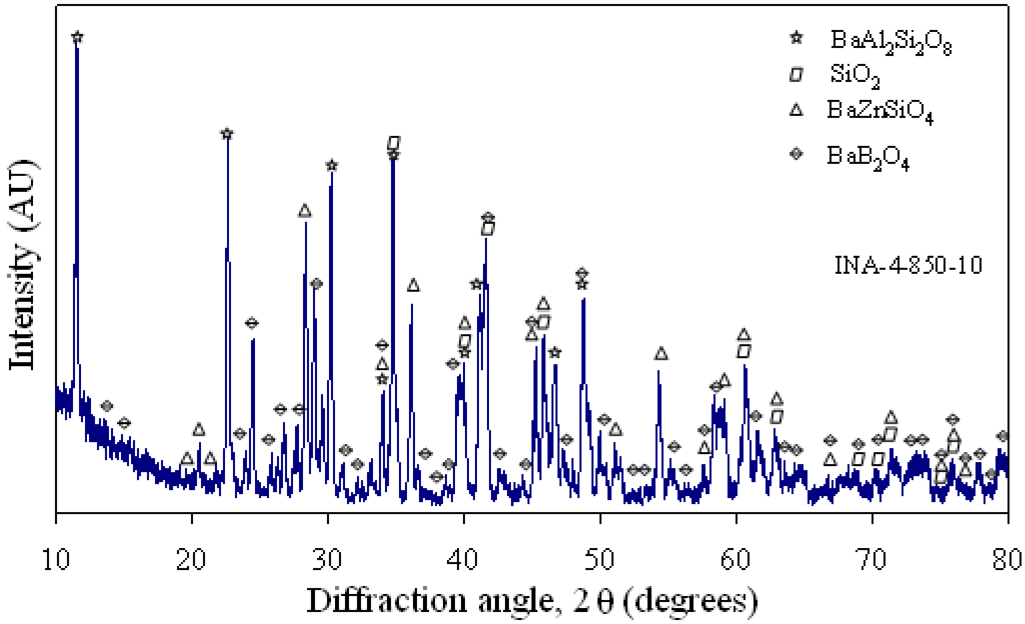

Figure 4.49 XRD pattern of INA-4 glass sample heat-treated at 850 °C for 10 hrs

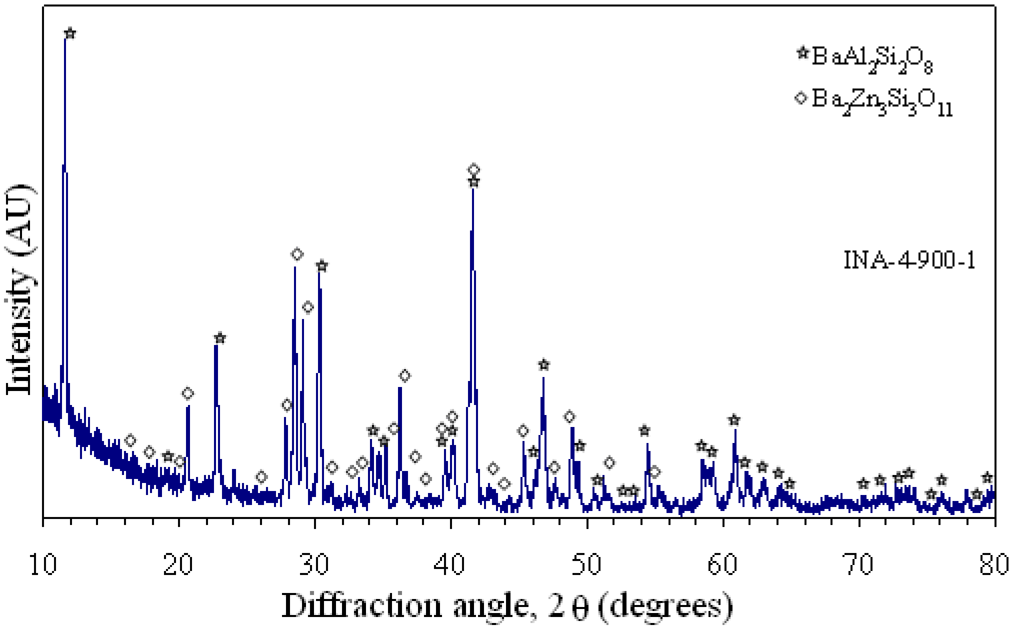

Figure 4.50 XRD pattern of INA-4 glass sample heat-treated at 900 °C for 1 hr

Figure 4.51 SEM micrographs of INA-4 glass sample heat treated at 800 °C for 1 hr

Figure 4.51 shows the SEM micrograph of INA-4 glass sample heat treated at 800 °C for 1 hr. All formed structures in INA glass series indicate that crystalline phase has nucleated as spherulite structure. These features are also common for glasses containing Al_2O_3 but the size of spherulite becomes smaller. This indicates the addition of Al_2O_3 makes the nucleation process sluggish. Though in fig. 4.51 these crystals are not clearly visible but in the background smaller size of spherulite structure can be seen which may appear more pronounced if the timing of etching is increased. As Al_2O_3 content was increased, the structure becomes more complex. It gets distorted and tries to acquire ellipsoidal shape (fig. 4.51). Though the density of such crystal is lower but the transformation mechanism changes. However, higher temperature heat treatment leads to nucleation of other phases. This nucleation starts from matrix and follows spherical contour as segregation of phases proceeds (fig. 4.52).

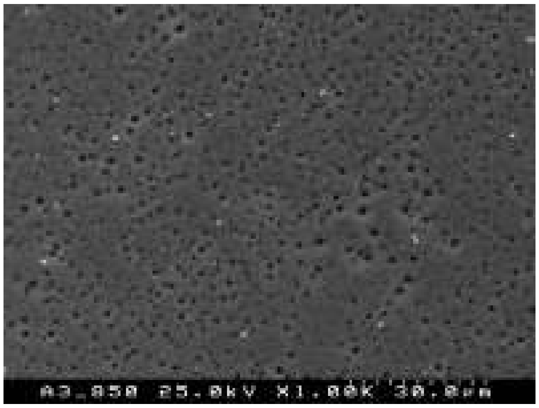

Figure 4.52 SEM micrograph of INA-4 sample heat treated at 850 ^{o}C for 1 hr

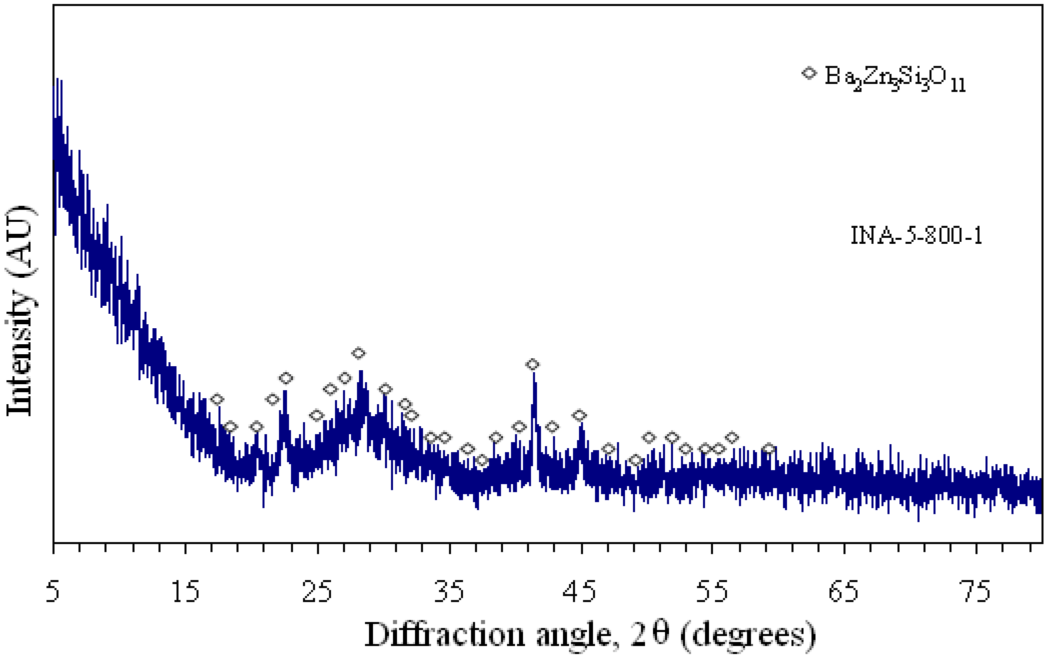

Figure 4.53 XRD pattern of INA-5 glass sample heat-treated at 800 ^{o}C for 1 hr

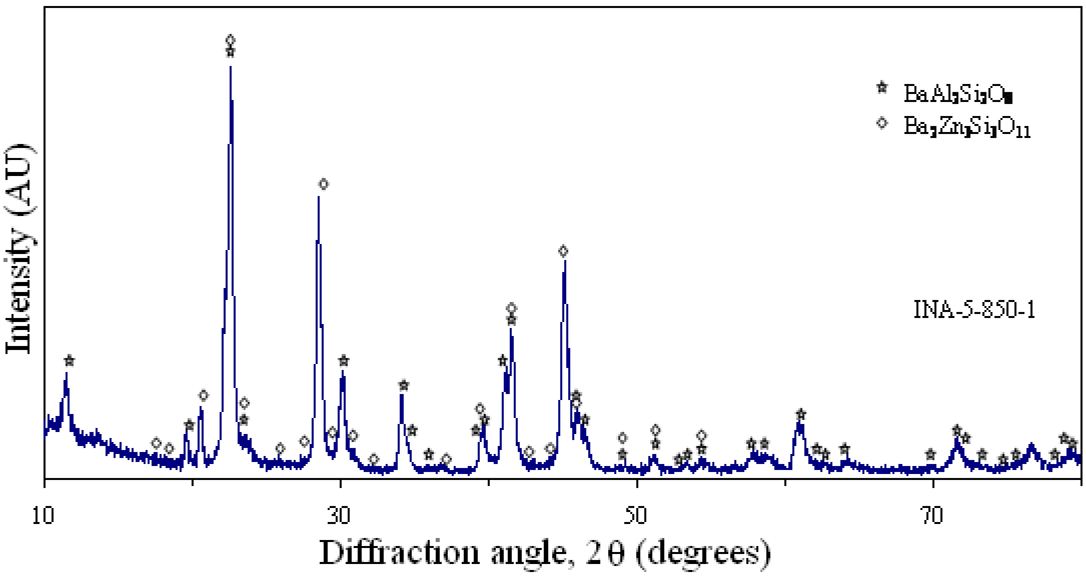

Figure 4.54 XRD pattern of INA-5 glass sample heat-treated at 850 °C for 1 hr

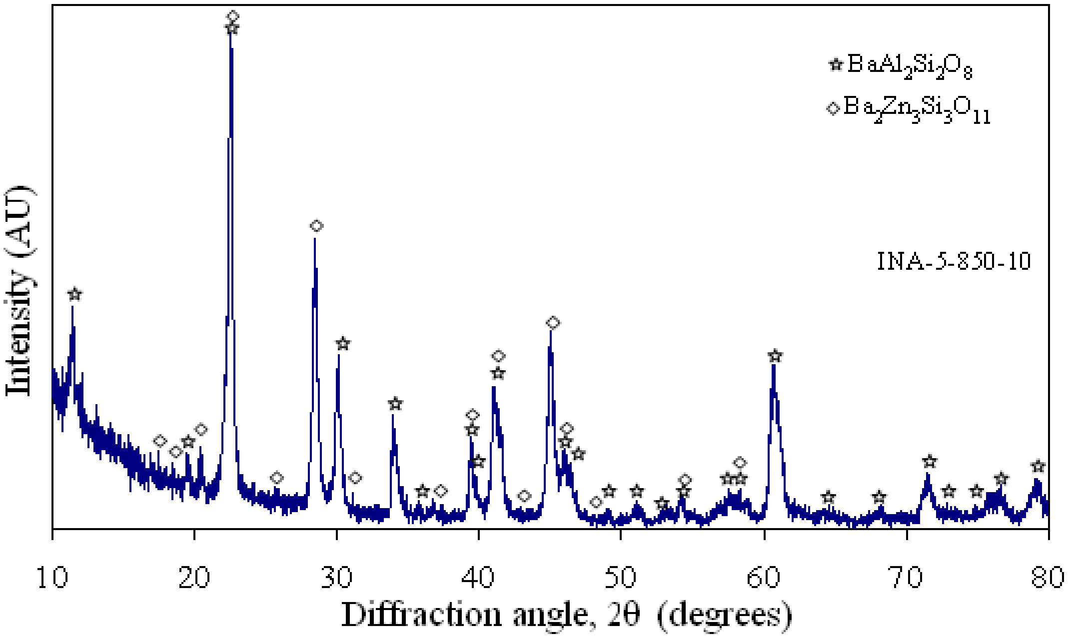

Figure 4.55 XRD pattern of INA-5 glass sample heat-treated at 850 °C for 10 hrs

As the alumina content in INA-5 sample is maximum and alumina hinders the formation of crystallites, most of the sample remains amorphous and only one phase i.e $Ba_2Zn_3Si_3O_{11}$ (ICDD card no. 23-0844) segregates during the heat treatment of 800 °C for 1 hr for this sample (fig. 4.53). When this glass sample is given further heat treatment i.e. 850°C for 1 hr and 10 hrs formation of $BaAl_2Si_2O_8$ (HC, ICDD card no. 77-0185) and $Ba_2Zn_3Si_3O_{11}$ (ICDD card no. 23-0844) takes place (figs. 4.54 and 4.55). When this sample is further heat treated for 900 °C for 1 hr time duration because of volatile nature of Zn earlier formed phase $Ba_2Zn_3Si_3O_{11}$ is converted into $BaZnSiO_4$ (Hexagonal, ICDD card no. 42-0335) phase (fig. 4.56).

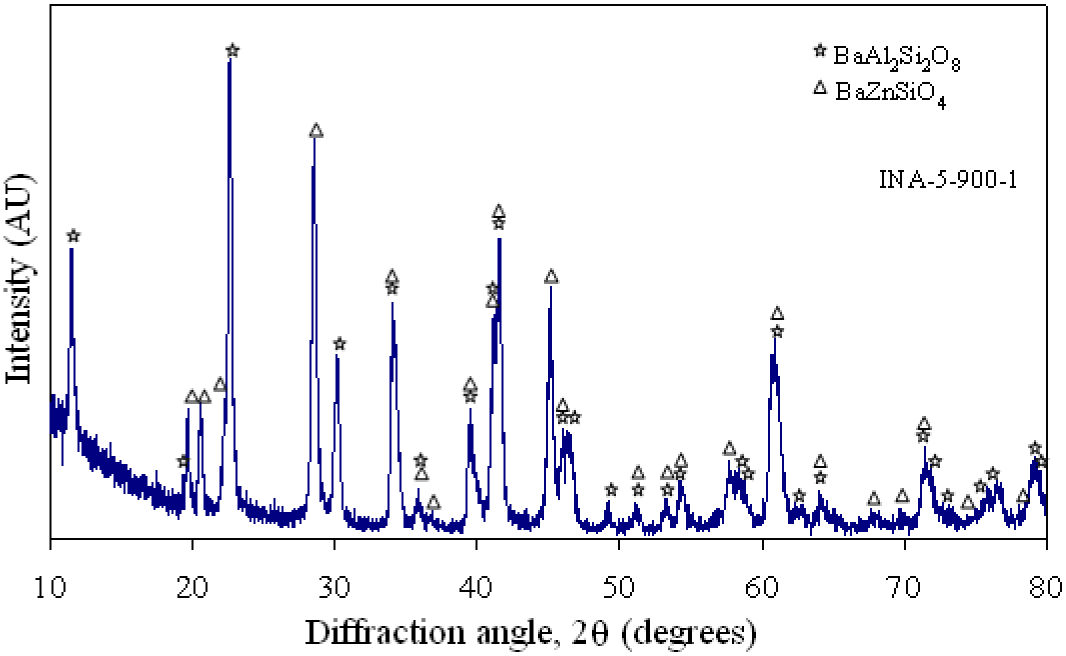

Figure 4.56 XRD pattern of INA-5 glass sample heat-treated at 900 °C for 1 hr

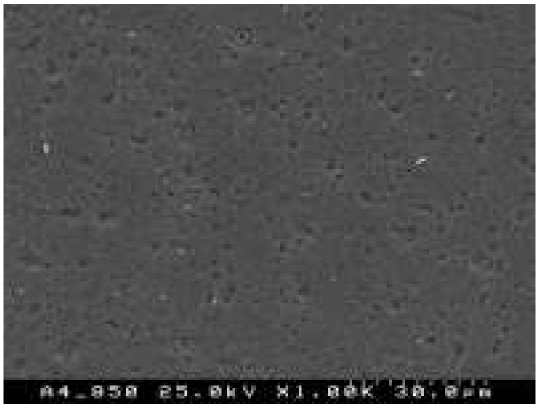

Figure 4.57 SEM micrograph of INA-5 sample heat treated at 850 °C for 1 hr

Figures 4.57 is the SEM micrographs of INA-5 glass sample which is heat treated at 850 ^{o}C for 1 hr time duration. In samples INA-4 and INA-5 crystalline growth is hindered because of increased amount of Al_2O_3. If these samples are heat treated for long time duration crystalline growth may take place. Since Al_2O_3 provides stability to glass, it hinders the nucleation process thus making glass more suitable for higher temperature application.

4.1.4 Conductivity Measurement

Conductivity measurement of INA series is done at room temperature by plotting graph between real and imaginary values of impedance obtained by LCR meter. The values of resistivity calculated are given in table 4.9.

Table 4.9 Resistivity values of INA series

Sample ID	Resistivity (MΩcm)
INA-1	1.60
INA-2	0.40
INA-3	0.24
INA-4	5.40
INA-5	1.20

It is clear from above data that sample INA-4 has maximum resistivity value as compared to all the other samples present in this series. This is because of higher activation energy of INA-4 glass. It is fulfilling the basic requirement of a glass, which can act as a sealant in SOFC.

4.2 INL Series

This series comprises of four samples i.e. $40SiO_2$-$30BaO$-$20ZnO$-$(10-x)B_2O_3$–xLa_2O_3 (x= 2.5, 5.0, 7.5, 10.0).

4.2.1 Differential Thermal Analysis

Thermal analysis of INL glass series samples was done by differential thermal analysis at various heating rates of 10°C/min, 20°C/min, 30°C/min and 40°C/min from 50°C to 1000°C by taking α-alumina as the reference sample where the amount of sample taken was approximately 20 mg. The plots obtained by DTA of INL-1, INL-2, INL-3 and INL-4 series are as shown in figures below from 4.58 to 4.61 respectively.

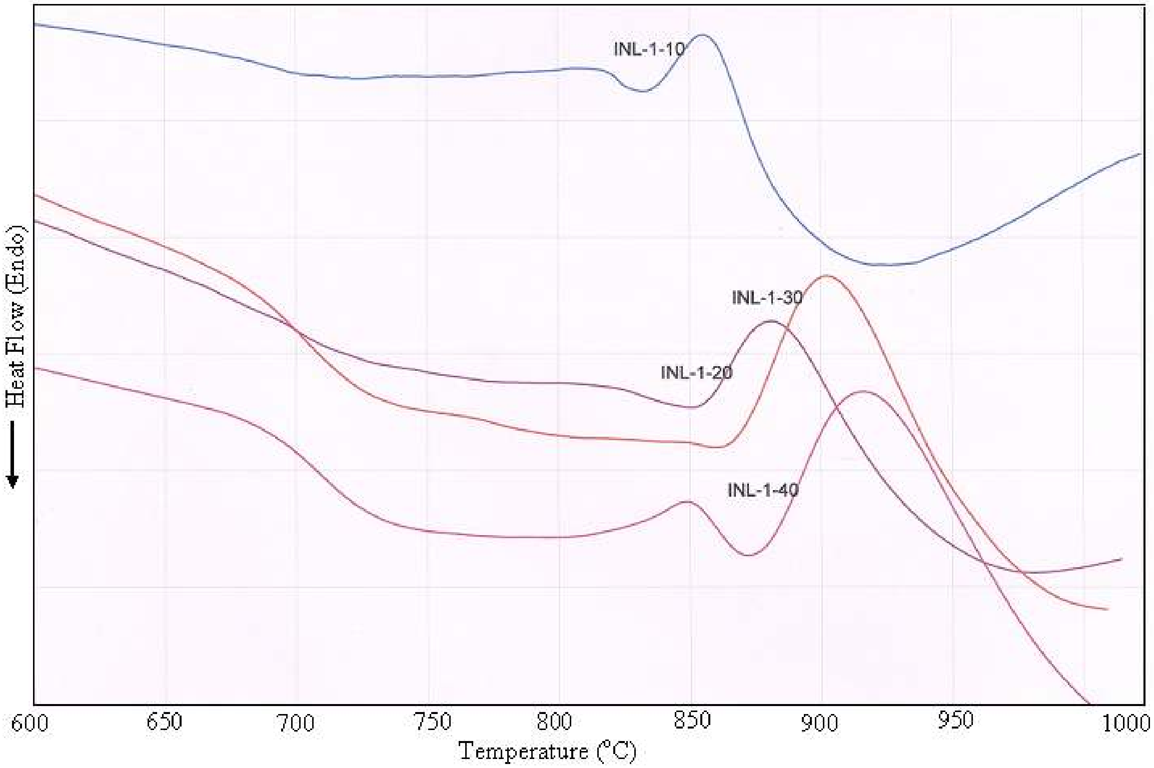

Figure 4.58 DTA plot of INL-1 glass sample at 10, 20, 30, 40 °C/min from 600-1000°C

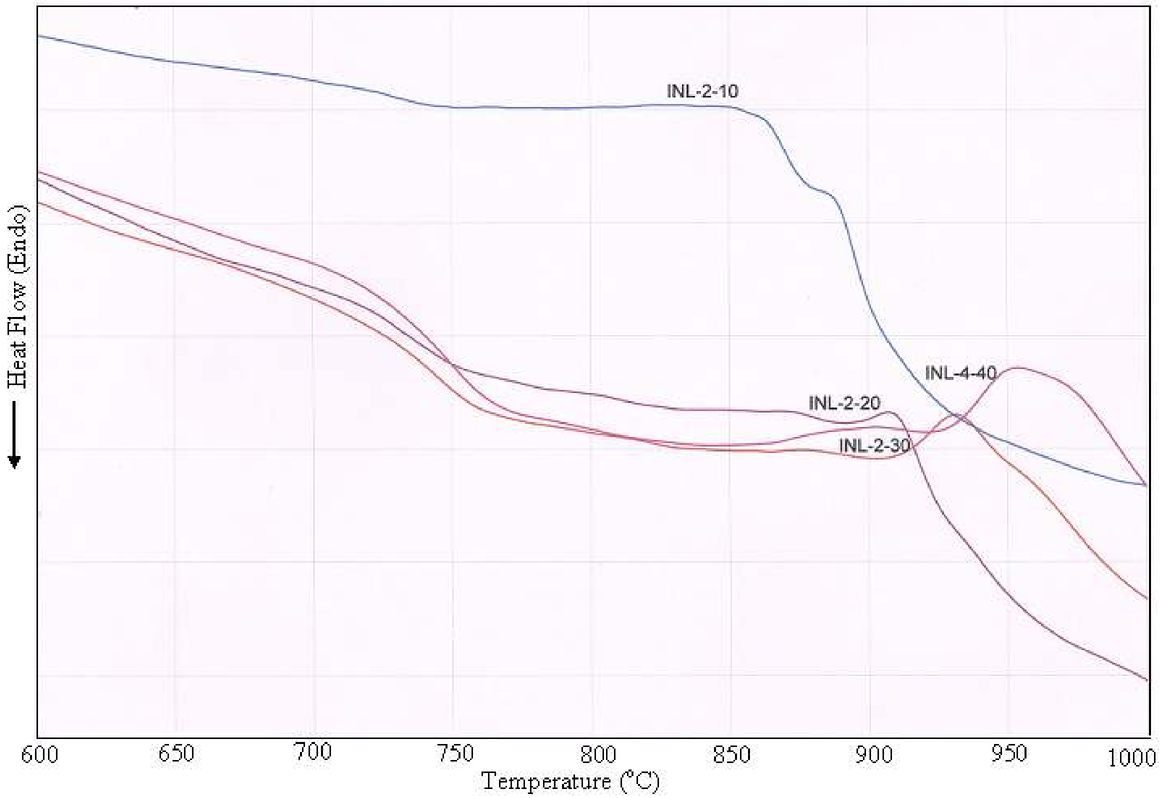

Fig 4.59 DTA plot of INL-2 glass sample at 10, 20, 30, 40 °C/min from 600-1000°C

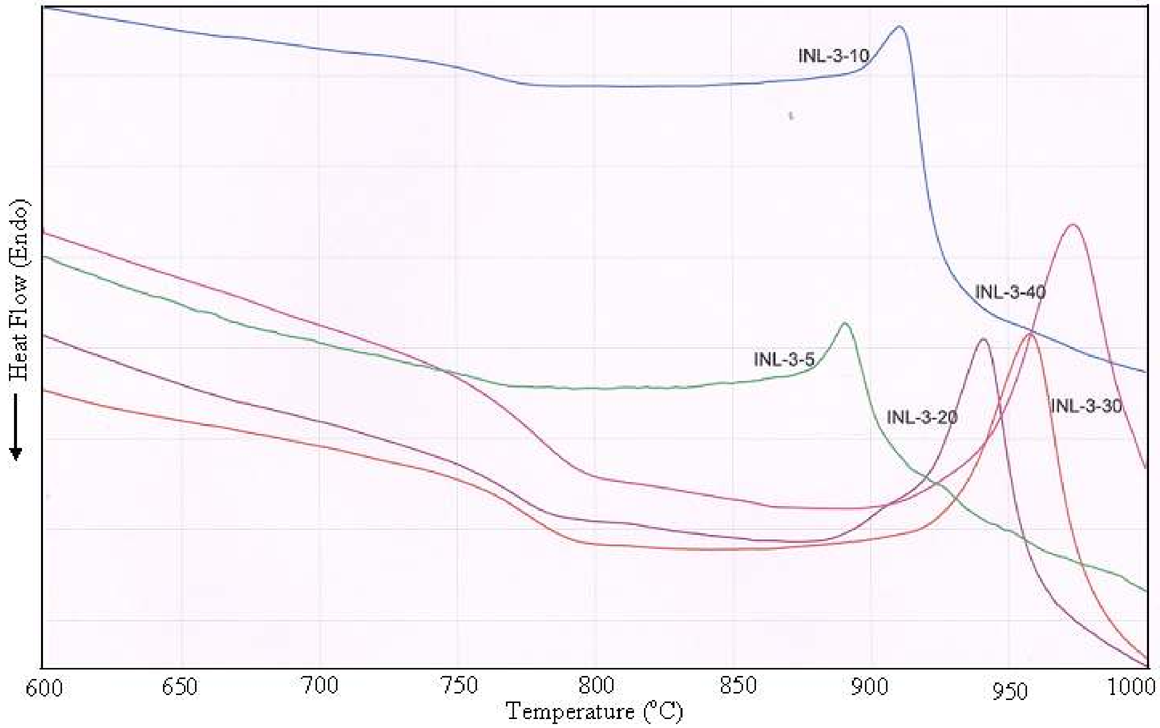

Figure 4.60 DTA plot of INL-3 glass sample at 5, 10, 20, 30, 40 °C/min from 600-1000°C

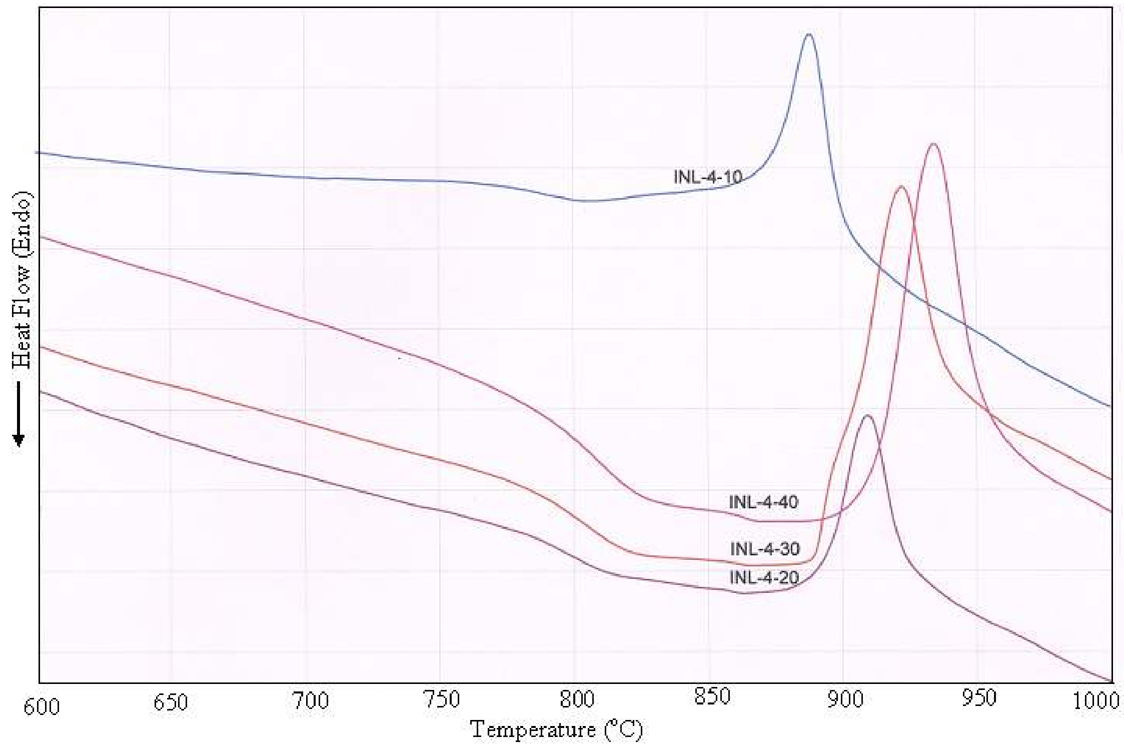

Figure 4.61 DTA plot of INL-4 glass sample at 10, 20, 30, 40 °C/min from 600-1000°C

The values of transition temperature, crystallization temperature and peak crystallization temperature obtained by DTA at various heating rates are given in table 4.10. It is observed from the above figures that when lanthanum content is increased from 2.5% to 5.0%, the peaks gets diffused. This broad crystallization exotherm might be attributed due to overlapping of two exothermic crystallization peaks. On the other hand, these two exothermic peaks are clearly resolved where intermediate oxide is not present (fig. 4.1). The increasing trend in T_g, T_c and T_m values with increasing intermediate oxides can be explained as it has two fold effect i.e. the ratio of SiO_2/B_2O_3 increases. Secondly, intermediate cation La^{3+} may have higher oxidation number which convert more non bridging oxygen into bridging oxygen. The activation energy of crystallization for the formation of phases is 246 kJ/mol in pure sample. As La^{3+} content was varied from 2.5% to 5.0% (mol) the activation energy decreases from 239 to 122 kJ/mol. It clearly indicates that the three dimensional connectivity of glass decreases with the addition of La^{3+} with respect to B^{3+} cation. Moreover, the openness in glass matrix leads to easy diffusion of the ions from the glass to form crystalline phases. When lanthanum content was varied from 2.5% to 5.0% it goes at tetrahedral site which does not provide strength to the matrix or it can also be said that lanthanum is acting as network modifier. On the other hand, when lanthanum content is increased from 5.0% to 10%, it provides strength to the matrix and acts as network former, as it is clear from the sharpness of peaks which increased in case of INL-3 and INL-4 samples. Basically, high content of La_2O_3 reduces the tendency of phase separation as observed in pure sample.

Table 4.10 T_g, T_c and T_{pc} values of INL series

COMPOSITION	$T_g(^oC)$	$T_c(^oC)$	$T_{pc}(^oC)$
INL-1-10	707	835	857
INL-1-20	727	855	881
INL-1-30	731	866	902
INL-1-40	734	874	916
INL-2-10	748	797	843
INL-2-20	750	896	908
INL-2-30	760	907	931
INL-2-40	765	928	954
INL-3-5	770	870	890
INL-3-10	777	893	911
INL-3-20	786	905	941
INL-3-30	792	921	958
INL-3-40	795	940	974
INL-4-10	805	870	889
INL-4-20	811	886	911
INL-4-30	820	890	922
INL-4-40	824	904	935

As discussed in section 4.1.1. the shifting of peak maxima with increase in heating rate is as explained on the basis that with decrease in heating rate, number of nucleation sites gets increased and hence peak maxima will come at low temperature. Out of four synthesized glass samples of INL series, sample INL-3 shows better results as compared to other samples present in series as it has minimum change in weight percent (table 4.11). The graphical representation of INL-3 sample is shown in figure 4.62.

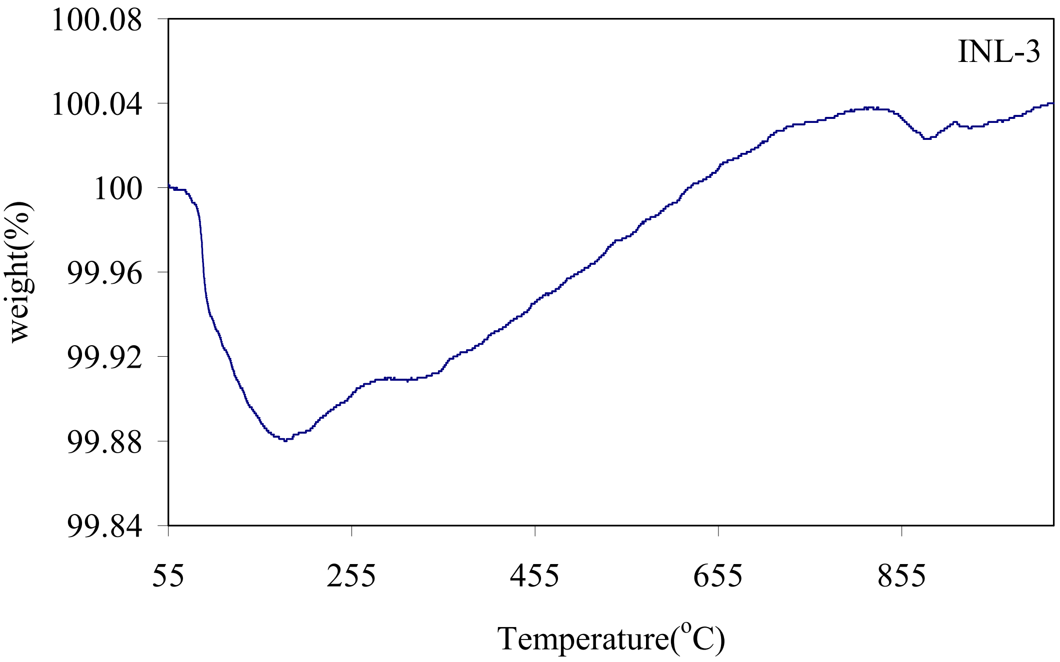

Figure 4.62 Change in weight % of INL-3 sample

Table 4.11 change in weight % in INL glass samples

Sample ID	Change in weight (%)
INL-1	-0.2045
INL-2	0.097
INL-3	0.04
INL-4	0.1

The negative value of weight change is because of the fact that Zn being volatile in nature comes out from the matrix while heating. The endothermic peak just before exothermic indicate that when zinc is migrating from the matrix, the remaining glass tries to get it stabilize by absorbing heat. Moreover, the loss is not much. As the lanthanum content is increased it tends to decrease the loss of Zn from the matrix by absorbing it in the glassy network. It also increases the compactness of the glass matrix. The vacancy existing in the glass matrix is eliminated by absorbing oxygen from the atmosphere because of this there is weight gain in samples INL-2, INL-3 and INL-4. The endothermic peak gets flattened as the lanthanum content is increased. It is well documented in literature that the intermediate oxides such as Al_2O_3, La_2O_3, Y_2O_3 etc. plays dual role in glasses. The role of intermediate oxides depends on the constituents of glasses and their chemical nature i.e whether it works as the modifier or the former in the glass matrix. Because of minimum percentage weight loss value for INL-3 sample it is selected for further study. Activation energy (E_a) value is also calculated from DTA data using Kissinger equation as given in equation (i) and its graphical representation is given in figure 4.63.

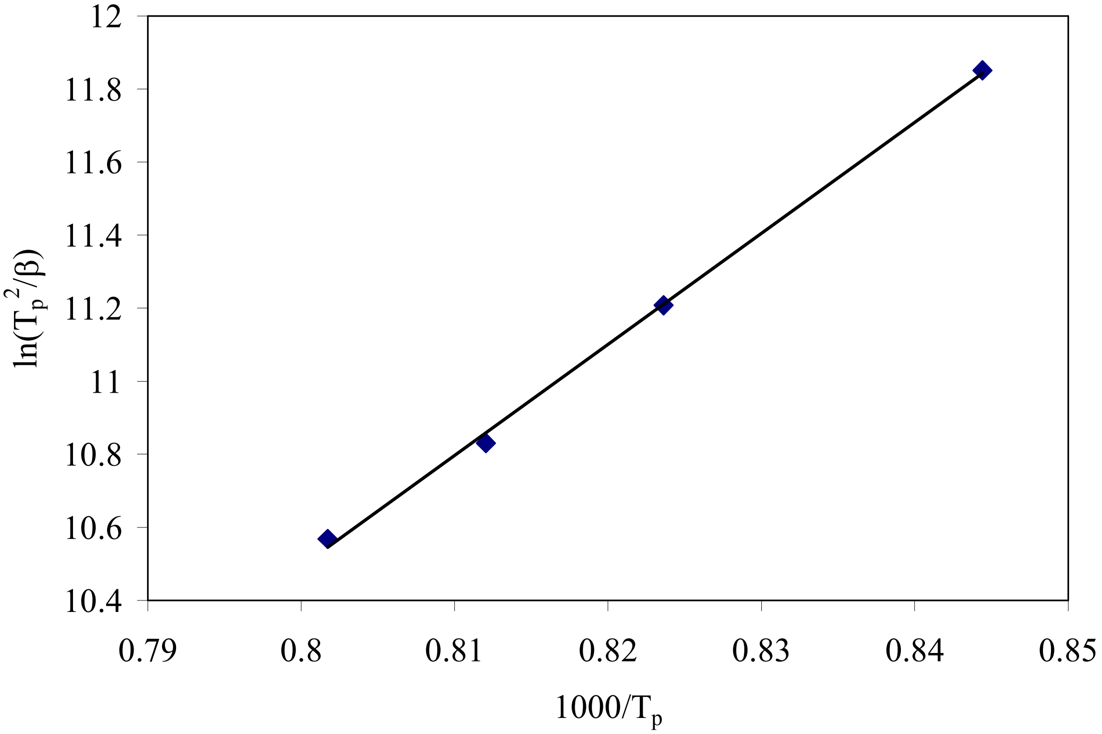

Figure 4.63 Plot of $\ln(T_p^2/\beta)$ vs. $10^3/T_p$ for INL-3 glass powder

Values of activation energy of peak crystallization E_a obtained by least square fitting of experimental data obtained by DTA is as shown in table 4.12.

Table 4.12 activation energy values of INL glass samples determined by DTA

Sample ID	E_a(kJ/mol)
INL-1	239
INL-2	122
INL-3	253
INL-4	343

The large change in activation energy is due to formation of various crystalline phases induced in the glass samples. Because of diffused system INL-2 sample has minimum value of activation energy.

4.2.1.1 Thermal Stability Parameter (S)

Thermal stability (ΔT) as defined in equation (iii) has been calculated for this series also. Larger is the difference in T_c and T_g, glass is most thermally stable (section 4.1.1.2). Similarly value of thermal stability parameter is given in equation (iv). The calculated values of ΔT and S are given in table 4.13 below.

Table 4.13 Values of ΔT and S from DTA data for INL glass series

Sample ID	Thermal Stability (ΔT)	Thermal stability parameter (S)
INL-1	90	4.2
INL-2	72	5.0
INL-3	110	5.5
INL-4	70	2.6

This is clear from the values calculated from DTA data for INL glass series that glass sample INL-3 has maximum value of thermal stability parameter. Hence this glass sample can be designated as the most stable glass among the whole chosen series.

4.2.1.2 Fragility index (F)

The fragility index is calculated as given in equation (v) in section 4.1.1.3. The calculated value of fragility index is as given in table 4.14 below.

Table 4.14 Values of Fragility Index for INL glass series from DTA data

Sample ID	Fragility Index (F)
INL-1	12.83
INL-2	6.39
INL-3	12.92
INL-4	17.02

The above calculated data indicates that INL-4 glass approaches the limit for kinetically strong-glass-forming liquids as this glass has maximum value of activation energy. The fragility index further strengthens the hypothesis that the higher concentration of La_2O_3 in glass leads to act as a glass network former.

4.2.2 Thermal Dilatometric Analysis

Thermal dilatometric analysis is done on polished flat glass frits from 20°C to the softening temperature of glass at a scan rate of 5°C/min. The graphical representation of INL series obtained by dilatometer is shown in figure 4.64.

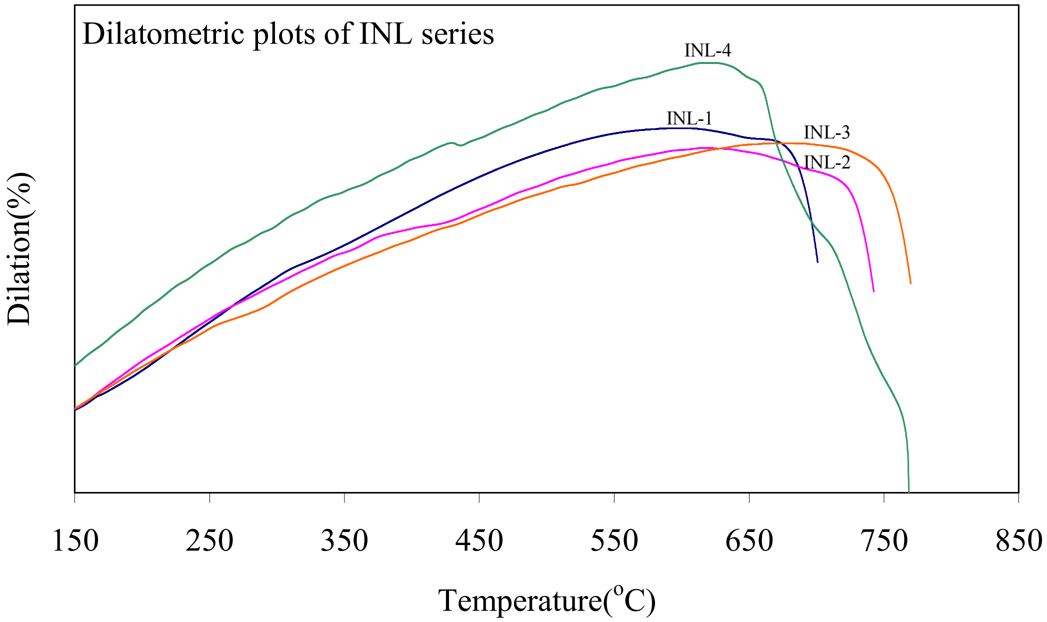

Figure 4.64 Plot of dilatometer of INL series glass samples

The softening temperature (T_s) of glass frits increases with increase in lanthanum content. The results given by Sohn et al. [36] clearly show that T_g, T_s and T_c values increases with the addition of La_2O_3. Their results confirm that La_2O_3 doped glasses are more rigid at high temperatures and hence an increase in the TEC value of glasses was observed. The TEC value depends on rigidity of glass matrix. It might be possible that the addition of La_2O_3 in glass composition increases the covalent character, since the electronic configuration of boron is (2s, 2p) and in case of lanthanum the electronic configuration is (5d, 6s). The involvement of d orbitals in bond formation always tends to the directionality in bonding [41]. Another study done on La_2O_3 says that La_2O_3 controls the viscosity [37]. The softening temperature and thermal expansion coefficient values are given in table 4.15.

Table 4.15 T_s and TEC values obtained from dilatometer for INL series

Sample ID	T_s(°C)	TEC (X 10^{-6}/K) (200-600°C)
INL-1	700.9	8.28
INL-2	742.4	8.17
INL-3	769.9	8.17
INL-4	768.4	8.29

4.2.3 XRD of $40SiO_2$-$30BaO$-$20ZnO$-$(10-x)B_2O_3$-xM_2O_3 (M= La, x= 2.5,5.0,7.5,10.0)

After confirming the amorphous nature of INL glass series, INL glass samples are given heat-treatment at various temperatures and for different time durations. The presence of barium aluminum silicate in these glasses occurs due to the uptake of alumina from alumina crucible during melting process. First of all the INL-1 glass sample is given heat treatment at 850°C for 20 hrs (fig. 4.65). There occurs formation of barium aluminum silicate ($BaAl_2Si_2O_8$) (hexacelsian, ICDD card no. 77-0185), barium lanthanum oxide silicate ($Ba_4La_6O(SiO_4)_6$) (hexagonal, ICDD card no. 27-0037), zinc silicate ($ZnSiO_3$) (rhombohedral, ICDD card no. 34-0575) and barium aluminum oxide ($BaAl_2O_4$) (hexagonal, ICDD card no. 73-0202). Since the ionic radii of Ba^{2+} (1.43A°) and La^{3+} (1.22A°) is close to each other as compared to Zn^{2+} (0.83A°), there is possibility of formation of barium lanthanum silicate compound, as these two ions (Ba^{2+} and La^{3+}) will replace each other. As La^{3+} will replace Ba^{2+}, it may absorb oxygen to have a net neutrality of charge and because of this it gains weight when TGA was done. Due to long time heat treatment i.e. at 850°C for 20 hrs, nucleation of different crystalline phases occurs. Thermodynamically any phase which will nucleate first will have enthalpy of formation less as compared to other phases.

When INL-1 sample is given further heat treatment i.e. at 900°C for 1 hr duration time formation of barium aluminum silicate $Ba(Al_2Si_2O_8)$ (hexacelsian, ICDD card no. 88-1048, HC), barium zinc silicate ($Ba_2Zn_3Si_3O_{11}$) (BZS, ICDD card no. 23-0844), zinc silicate ($ZnSiO_3$) (hexagonal, ICDD card no. 34-0575) and barium aluminum oxide ($BaAl_2O_4$) (hexagonal, ICDD card no. 73-0202) takes place (fig.4.66). $BaAl_2Si_2O_8$ and $Ba(Al_2Si_2O_8)$ are isomorphs of each other. At higher temperature Zn^{2+} migrates from glassy matrix and replaces La^{3+}. Kinetically at higher temperatures Zn^{2+} being the smaller ion will migrate easily to form stable compound. Moreover, the X-Ray diffraction pattern of INL-1 glass heat treated at 900°C for 1 hr shows that glass matrix is in strained condition because of the dissolution of initially nucleated phase and formation of new phases. It seems that with an increase in temperature of heat treatment formation of BZS phase is taking place by replacing $Ba_4La_6O(SiO_4)_6$ phase and the rest of the phases remains as such.

In the similar manner when INL-2 glass sample is given heat treatment at 850 °C for 20 hrs time duration, formation of barium aluminum silicate ($BaAl_2Si_2O_8$) (hexacelsian, ICDD card no. 77-0185), barium lanthanum oxide silicate ($Ba_4La_6O(SiO_4)_6$) (hexagonal, ICDD card no. 27-0037), zinc silicate ($ZnSiO_3$) (rhombohedral, ICDD card no. 34-0575) and barium aluminum oxide ($BaAl_2O_4$) (hexagonal, ICDD card no. 73-0202). These phases are same as formed in sample INL-1 when heat treated at 850 °C for 20 hrs. Figure 4.67 shows the X-ray diffratogram of INL-2 sample heat treated at 850 °C for 20 hrs. In this case lanthanum is in glass matrix and provides strength to the glass matrix.

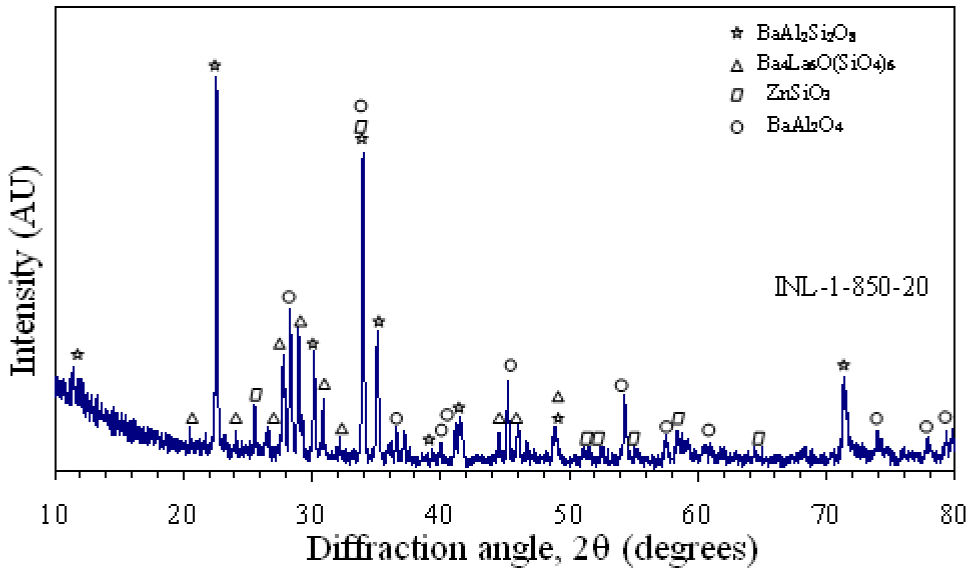

Figure 4.65 XRD pattern of INL-1 glass sample heat-treated at 850 °C for 20 hrs

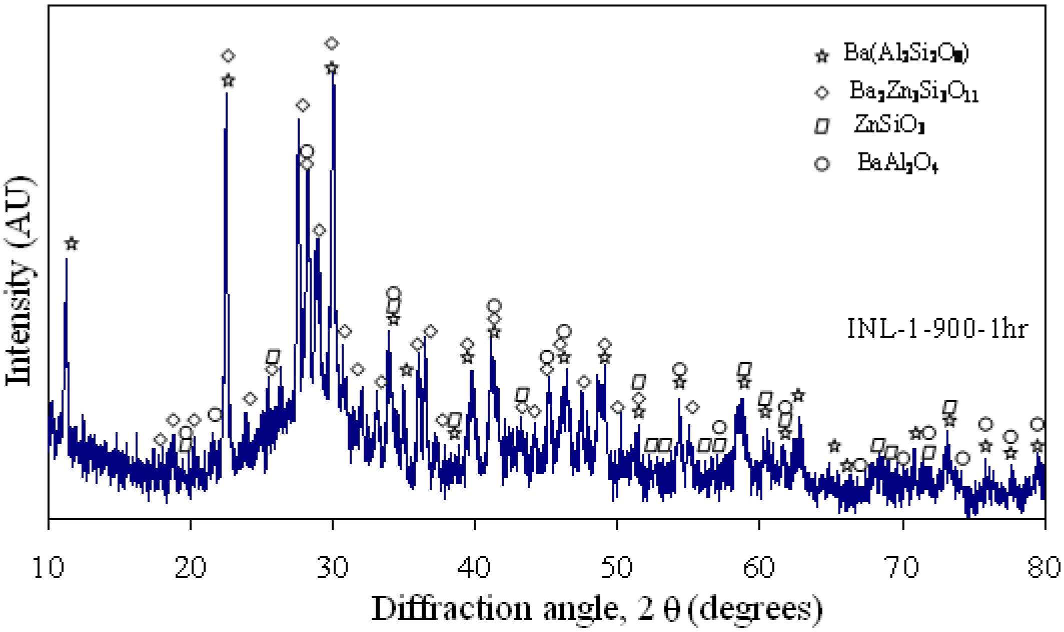

Figure 4.66 XRD pattern of INL-1 glass sample heat-treated at 900 °C for 1 hr

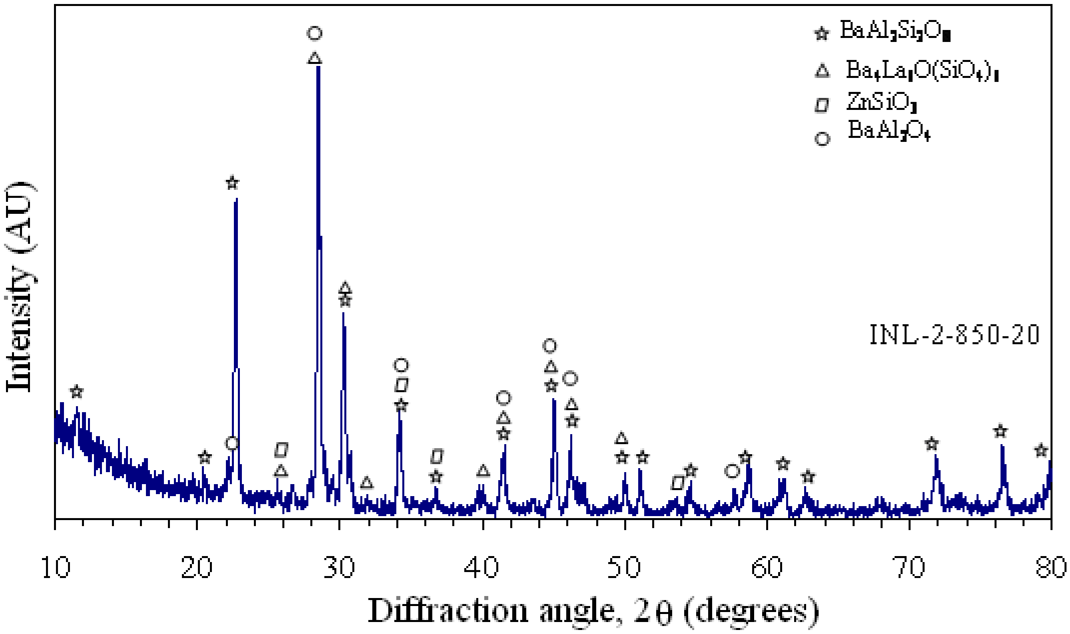

Figure 4.67 XRD pattern of INL-2 glass sample heat-treated at 850 °C for 20 hrs

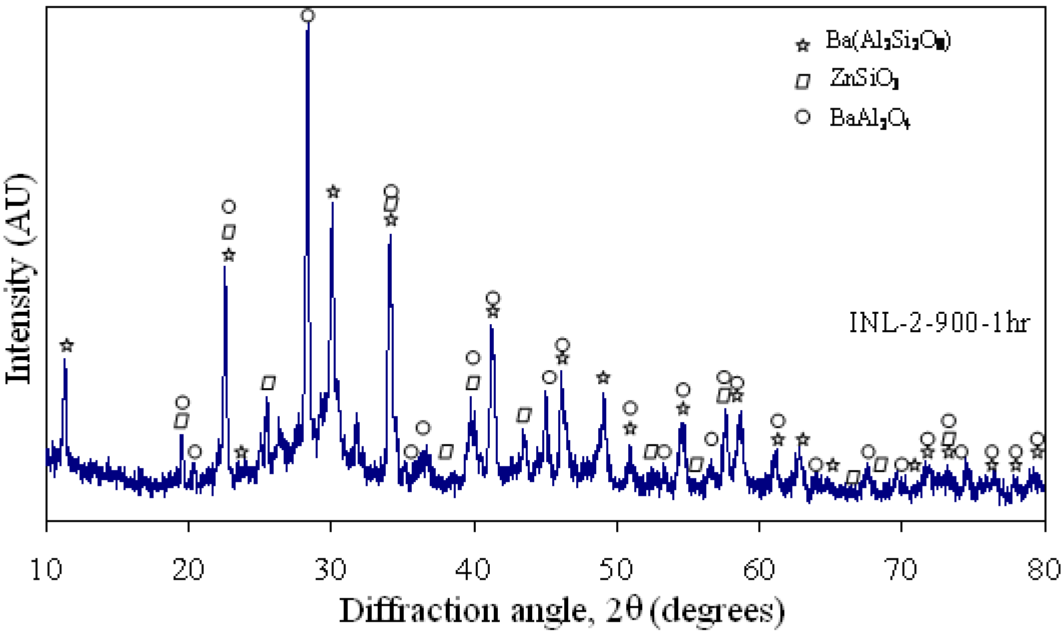

Figure 4.68 XRD pattern of INL-2 glass sample heat-treated at 900 °C for 1 hr

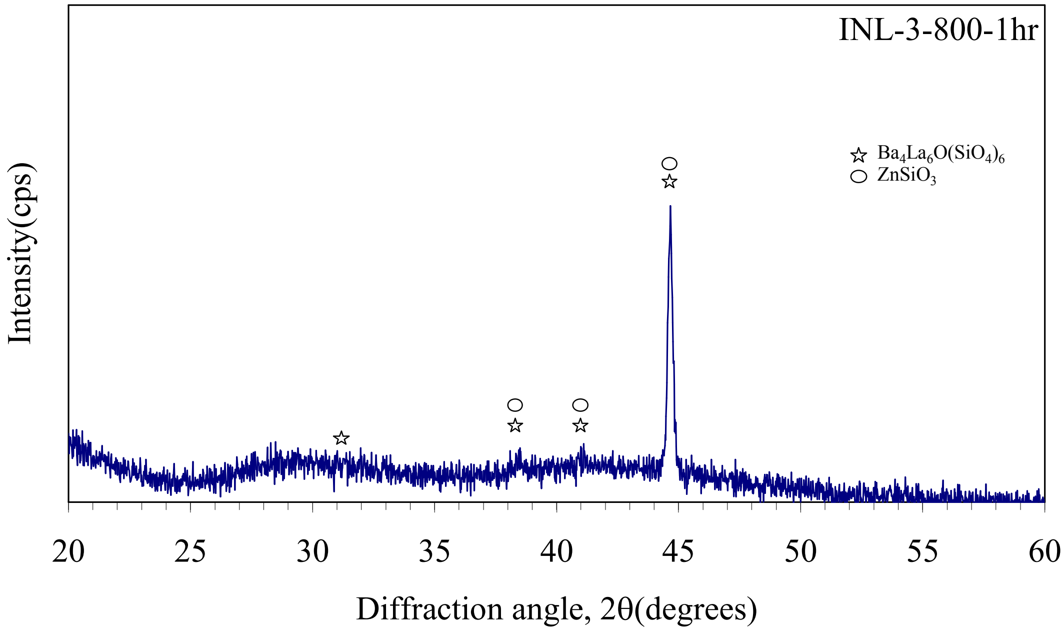

Figure 4.69 XRD pattern of INL-3 glass sample heat-treated at 800 °C for 1 hr

After giving heat treatment at high temperature i.e. at 900 ^{o}C for 1 hr $Ba_4La_6O(SiO_4)$ gets dissolved and three phases i.e. barium aluminum silicate $Ba(Al_2Si_2O_8)$ (hexacelsian, ICDD card no. 88-1048, HC), zinc silicate ($ZnSiO_3$) (hexagonal, ICDD card no. 34-0575) and barium aluminum oxide ($BaAl_2O_4$) (hexagonal, ICDD card no. 73-0202) are left (fig.4.68). It is clearly visible from the X-Ray diffraction pattern of INL-2 sample that the shifting of the peaks at lower 2θ angle with broadening and splitting in peaks, indicate more disordering in crystallization phases. Similar type of behavior is seen in INL-2 glass sample as we have observed in INL-1 glass sample. When INL-2 glass sample is heat treated at 900^{o}C formation of $Ba(Al_2Si_2O_8)$ takes place and this phase tries to transform into $BaAl_2Si_2O_8$. On providing sufficient time to heat treatment, formation of $Ba_4La_6O(SiO_4)$ also takes place which is an isomorph of $BaAl_2Si_2O_8$ in INL-2 glass sample. However, by looking at the X-RD pattern it seems that matrix is in strained condition because nucleation is hindered or it is also possible that crystallites of very fine size and in small amount may be nucleating which causes straining effect and is not being observed by X-RD.

Because of minimal loss in weight% value of INL-3 glass sample among the INL series, this glass is studied in detail. INL-3 glass sample is given heat treatment at 800 ^{o}C for 1, 10 and 100 hrs time durations. This temperature is selected on the basis of transition temperature values obtained from DTA analysis. The X-ray diffraction pattern of INL-3 samples are as shown in 4.69, 4.70 and 4.71 heat-treated at 1, 10, 100 hrs respectively.

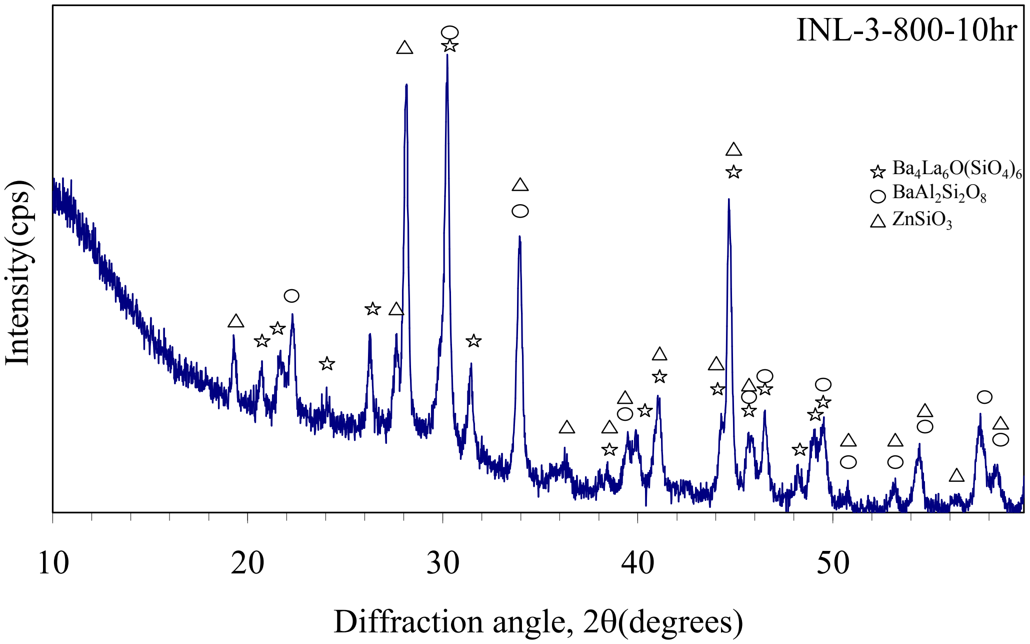

Figure 4.70 XRD pattern of INL-3 glass sample heat-treated at 800 °C for 10 hrs

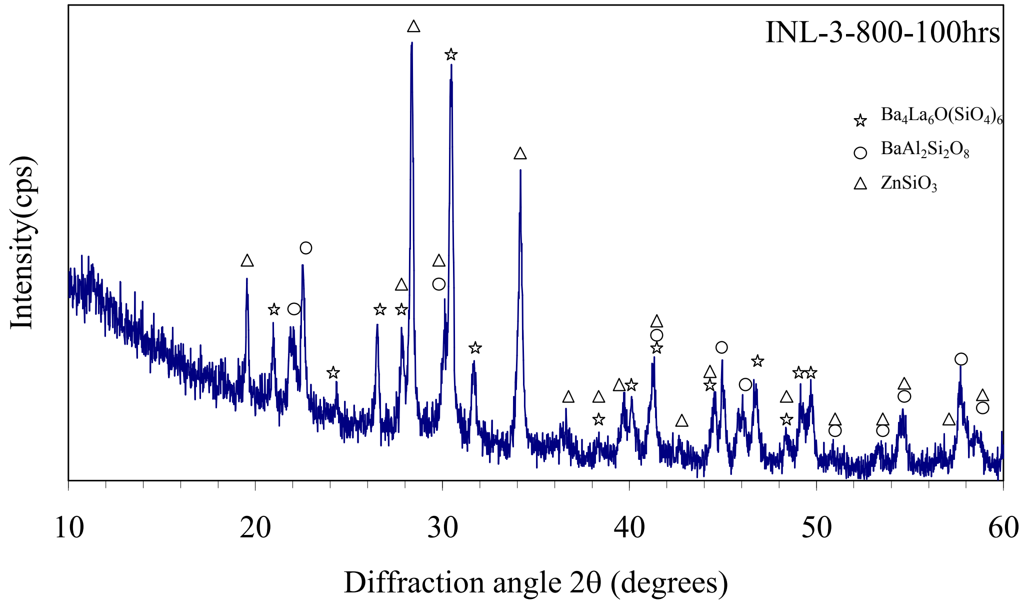

Figure 4.71 XRD pattern of INL-3 glass sample heat-treated at 800 °C for 100 hrs

When glass sample INL-3 is heat-treated at 800 °C for 1 hr time duration, formation of hexagonal (barium lanthanum oxide silicate) $Ba_4La_6O(SiO_4)_6$ (ICDD card no. 27-0037) phase takes place. Formation of small amount of monoclinic (zinc silicate) $ZnSiO_3$ phase (ICDD card no. 70-0851) also occurs. This result indicates that since in the beginning the viscosity of the sample is high, the nucleation of other phases is hindered. This causes the nucleation of the solid solution phase comprising of bigger crystalline phase having bigger lattice. When the same glass sample is heat-treated further at 800 °C for 10hrs time duration a new phase i.e. hexagonal (barium aluminum silicate) $BaAl_2Si_2O_8$ (ICDD card no. 77-0185) also appears along with $Ba_4La_6O(SiO_4)_6$ and $ZnSiO_3$. All these three phases, which are present during 10 hrs heat-treatment, are also present in 100 hrs time duration heat-treatment. This indicates that system is stable at 800 °C for larger duration as no other phase(s) nucleates.

When further heat treatment is given to these glass samples i.e. at 850 °C for 20 hrs, there occurs formation of barium aluminum silicate ($BaAl_2Si_2O_8$) (hexacelsian, ICDD card no. 77-0185), barium lanthanum oxide silicate ($Ba_4La_6O(SiO_4)_6$) (hexagonal, ICDD card no. 27-0037), zinc silicate ($ZnSiO_3$) (rhombohedral, ICDD card no. 34-0575) and barium aluminum oxide ($BaAl_2O_4$) (hexagonal, ICDD card no. 73-0202) phases as shown in fig. 4.72.

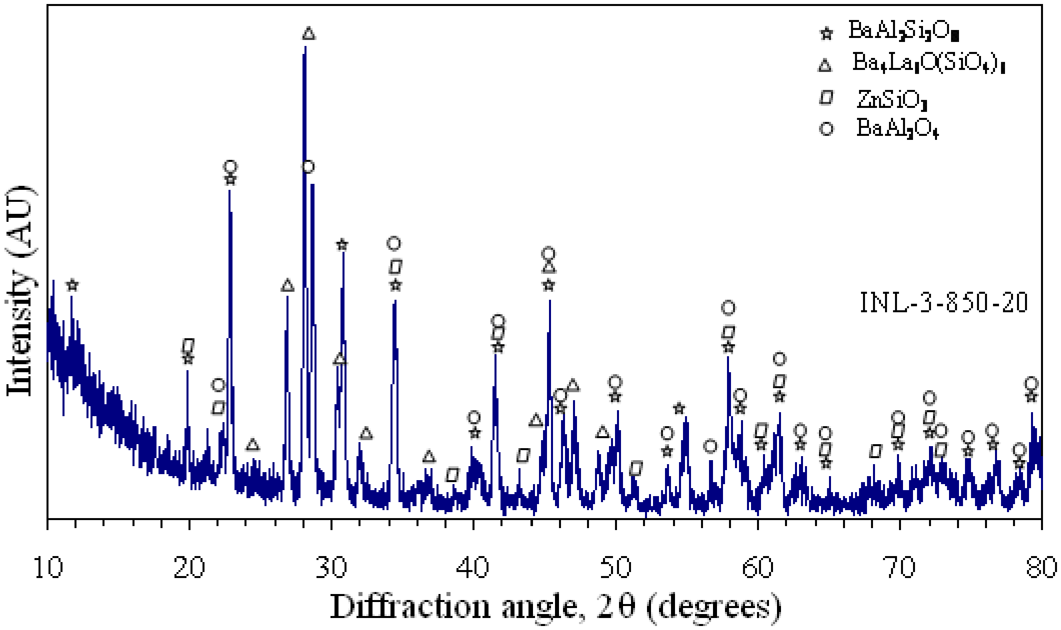

Figure 4.72 XRD pattern of INL-3 glass sample heat-treated at 850 °C for 20 hrs

After giving further heat treatment at 900 °C for 1 hr, the phases as we get in INL-3 glass sample heat treated at 850 °C for 20 hrs remains as such i.e. barium aluminum silicate ($BaAl_2Si_2O_8$) (hexacelsian, ICDD card no. 77-0185), barium lanthanum oxide silicate ($Ba_4La_6O(SiO_4)_6$) (hexagonal, ICDD card no. 27-0037), zinc silicate ($ZnSiO_3$) (rhombohedral, ICDD card no. 34-0575) and barium aluminum oxide ($BaAl_2O_4$) (hexagonal, ICDD card no. 73-0202) (fig. 4.73). Contrary to INL-1 and INL-2 glass samples, in INL-3 glass sample the concentration of lanthanum is sufficient to induce the crystallization of $Ba_4La_6O(SiO_4)_6$ phase in the glass matrix. The nucleation of this phase occurs at the initial stage of heat treatment i.e. at 800 °C when sample INL-3 is heat treated for 1 hr.

When INL-4 glass sample of INL series is given heat treatment at 850 °C formation of barium aluminum silicate ($BaAl_2Si_2O_8$) (hexacelsian, ICDD card no. 77-0185), barium lanthanum oxide silicate ($Ba_4La_6O(SiO_4)_6$) (hexagonal, ICDD card no. 27-0037), zinc silicate ($ZnSiO_3$) (rhombohedral, ICDD card no. 34-0575) and barium aluminum oxide ($BaAl_2O_4$) (hexagonal, ICDD card no. 73-0202) (fig. 4.74) takes place.

When INL-4 glass sample is given further heat treatment at 900 °C for 1 hr formation of barium aluminum silicate ($BaAl_2Si_2O_8$) (hexacelsian, ICDD card no. 77-0185), barium lanthanum oxide silicate ($Ba_4La_6O(SiO_4)_6$) (hexagonal, ICDD card no. 27-0037), zinc silicate ($ZnSiO_3$) (rhombohedral, ICDD card no. 34-0575) and barium aluminum oxide ($BaAl_2O_4$) (hexagonal, ICDD card no. 73-0202) (fig. 4.75) takes place. This is similar as observed in INL-4 glass sample heat treated at 850 °C for 20 hrs.

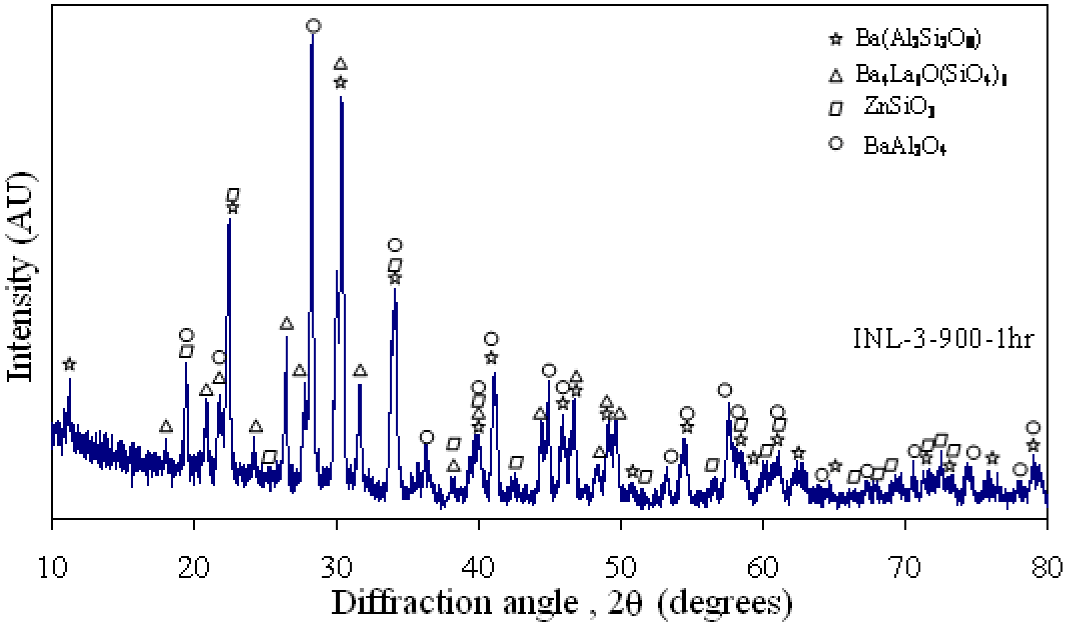

Figure 4.73 XRD pattern of INL-3 glass sample heat-treated at 900 °C for 1 hr

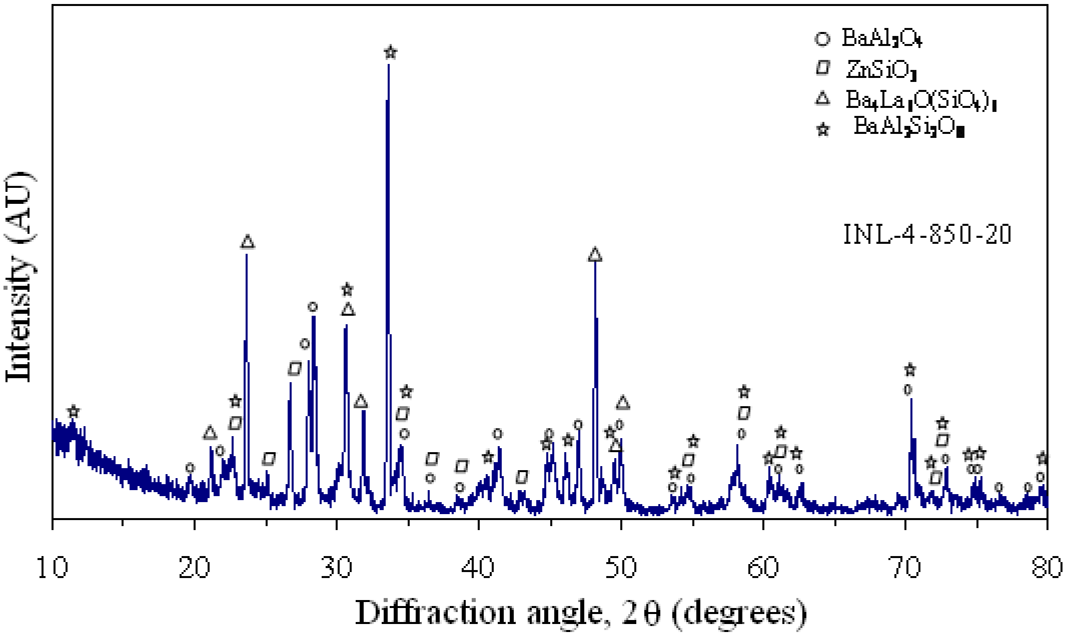

Figure 4.74 XRD pattern of INL-4 glass sample heat-treated at 850 °C for 20 hrs

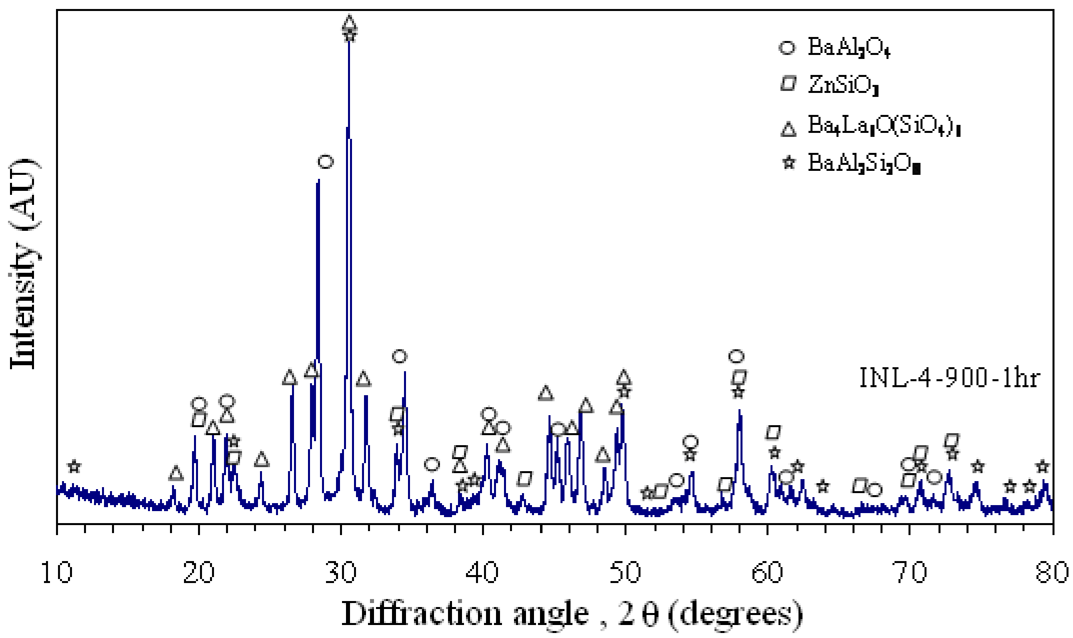

Figure 4.75 XRD pattern of INL-4 glass sample heat-treated at 900°C for 1 hr

In INL-4 glass sample lanthanum amount is on higher side and because of this the formation of $Ba_4La_6O(SiO_4)_6$ phase occurs even when sample INL-4 is heat treated at 900°C for 1 hr. There is a solid solution phase of barium lanthanum silicate; even then it maintains its identity at higher temperature heat treatment. In this series, initially $ZnSiO_3$, $BaAl_2Si_2O_8$, $Ba_4La_6O(SiO_4)_6$ and $BaAl_2O_4$ phases are formed. As the heat treatment time duration increases $Ba_4La_6O(SiO_4)_6$ phase is dissolving especially when La_2O_3 content is up to 5 mol%. As the content of La_2O_3 increases all these phases again come into picture. However, the volume fraction of $Ba_4La_6O(SiO_4)_6$ phase decreases with the increase in heat treatment time duration at higher temperatures. In all the samples the volume fraction of $BaAl_2O_4$ phase is increasing with the increase in temperature.

4.2.4 Conductivity Measurement

Conductivity measurement of INL glass samples is done by plotting real and imaginary values of impedance taken by LCR meter. The obtained values are as given in table 4.16.

Table 4.16 Resistivity values of INL series

Sample ID	Resistivity (MΩcm)
INL-1	0.24
INL-2	1.2
INL-3	0.7
INL-4	2.4

From the above values it is clear that all the values lie in the required range (2kΩcm) of resistivity for a glass to act a good sealant.

4.3 INM-Series

This series include four samples i.e. $40SiO_2$-30BaO-20ZnO-(10-x)B_2O_3–xMn_2O_3 (x= 2.5, 5.0, 7.5, 10.0).

4.3.1 Differential Thermal Analysis

Differential thermal analysis of manganese doped glass samples was done at 10 °C/min, 20 °C/min, 30 °C/min and 40 °C/min heating rates from 50 °C to 1000 °C by taking α-alumina as reference sample and sample amount taken was approximately 20 mg. DTA plots of INM-1, INM-2, INM-3 and INM-4 glass samples are given in figures 4.76, 4.77, 4.78, and 4.79 respectively.

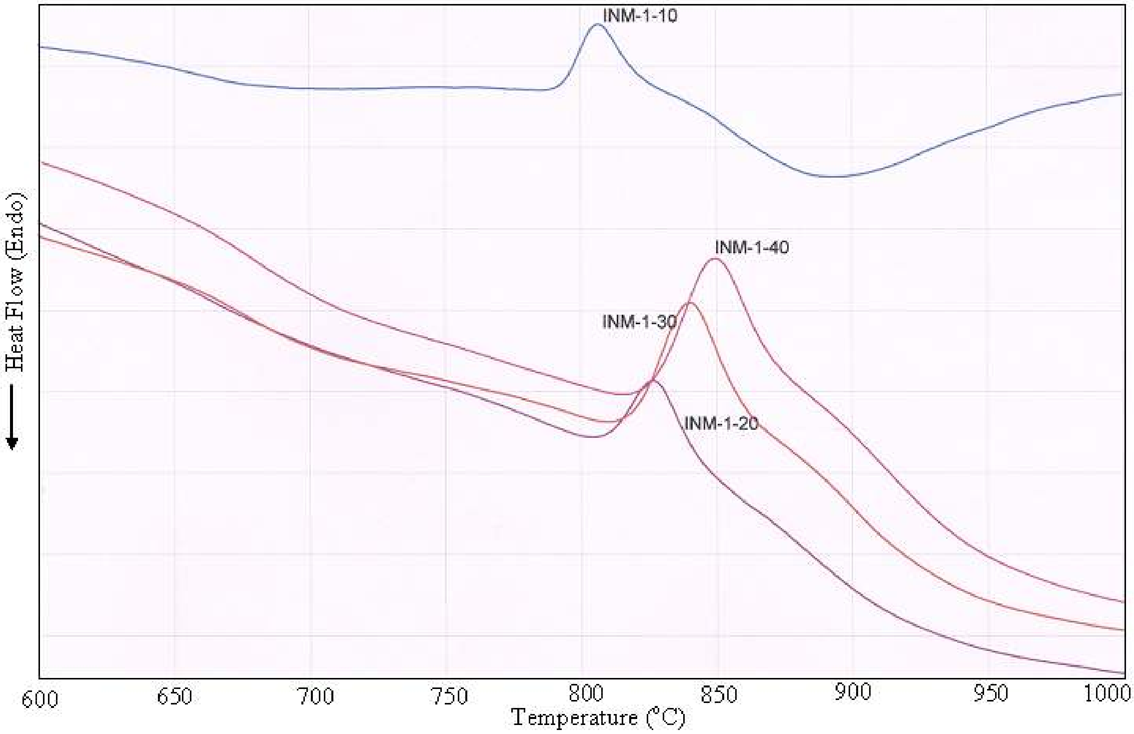

Figure 4.76 DTA plot of INM-1 glass sample at 10, 20, 30, 40 °C/min from 600-1000°C

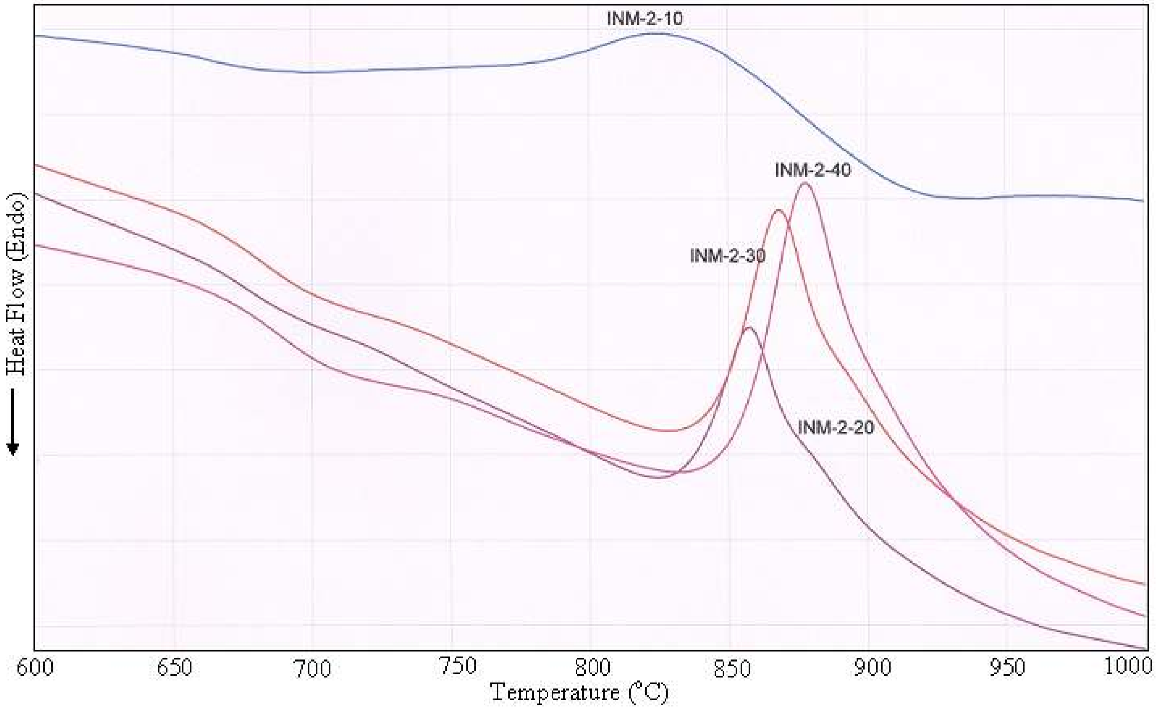

Figure 4.77 DTA plot of INM-2 glass sample at 10, 20, 30, 40 °C/min from 600-1000°C

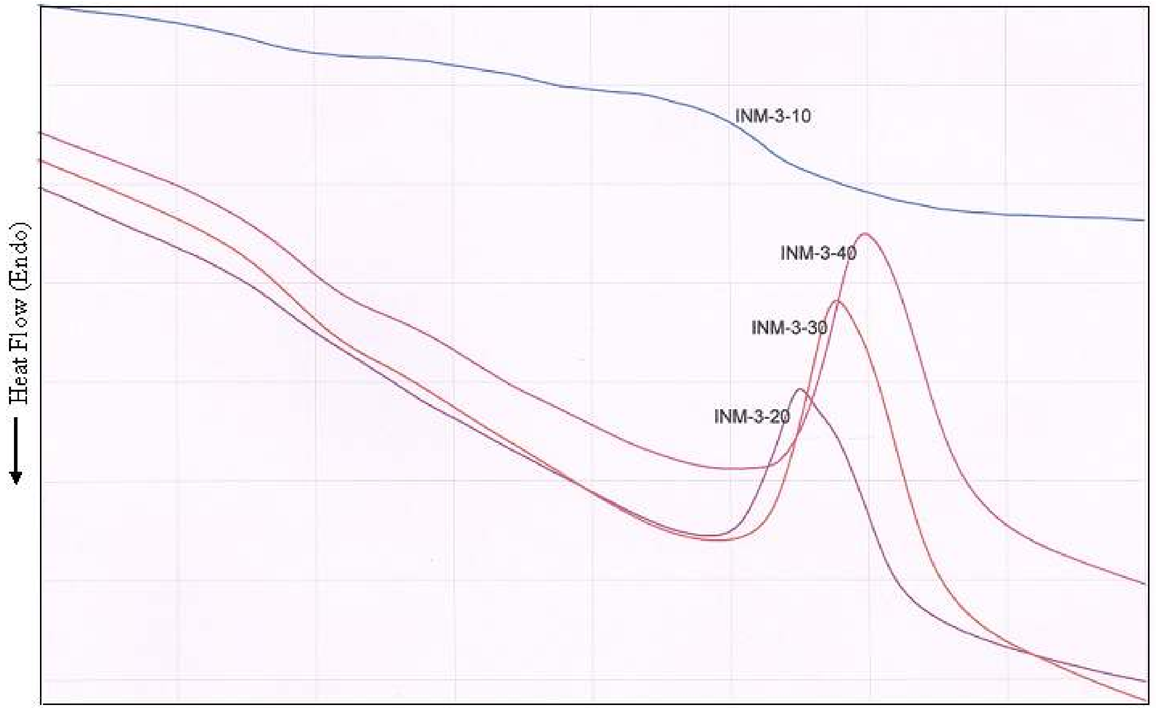

Figure 4.78 DTA plot of INM-3 glass sample at 10, 20, 30, 40 °C/min from 600-1000°C

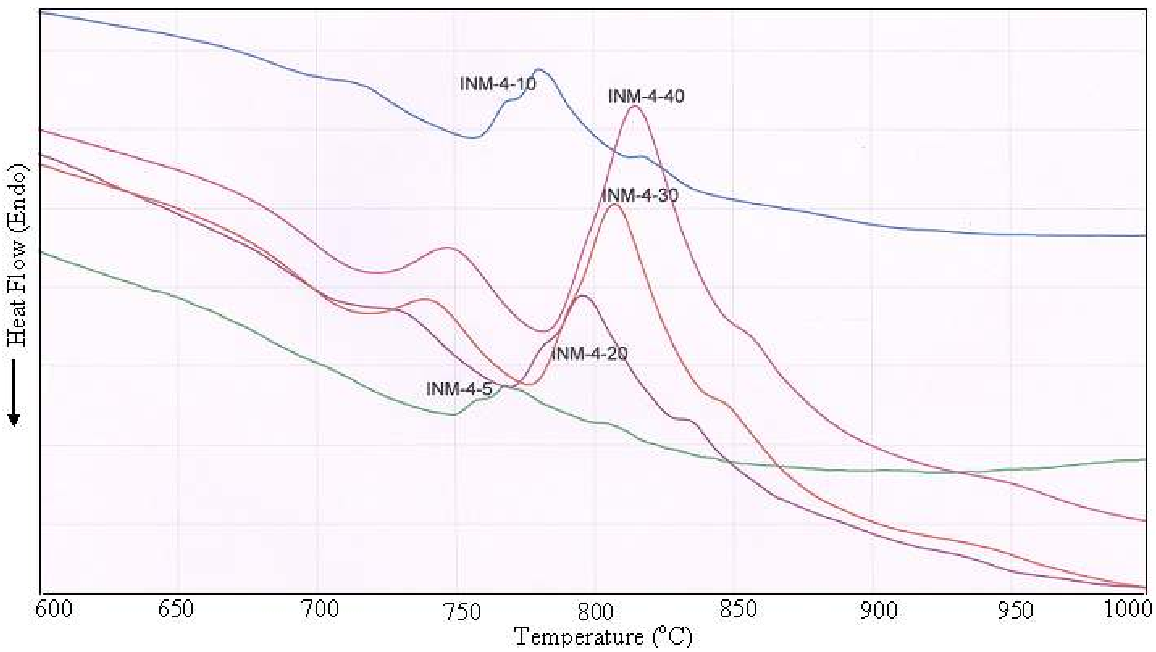

Fig. 4.79 DTA plot of INM-4 glass sample at 5, 10, 20, 30, 40 °C/min from 600- 1000°C

The values of T_g, T_c and T_{pc} as obtained by differential thermal analyzer at various heating rates are given in table 4.17.

Table 4.17 T_g, T_c and T_{pc} values of INM series

COMPOSITION	T_g(°C)	T_c(°C)	T_{pc}(°C)
INM-1-10	676	791	806
INM-1-20	688	809	827
INM-1-30	700	816	840
INM-1-40	708	823	850
INM-2-10	685	780	829
INM-2-20	691	830	857
INM-2-30	700	839	868
INM-2-40	707	844	877
INM-3-10	699	790	833
INM-3-20	700	851	874
INM-3-30	708	858	889
INM-3-40	710	870	899
INM-4-5	660	747	770
INM-4-10	666	756	780
INM-4-20	686	770	796
INM-4-30	692	777	807
INM-4-40	700	783	815

The explanation of shifting of peak maxima is already explained in section 4.1.1. In all the DTA plots, two exothermic peaks were observed, but these are not clearly resolved. This effect is prominent in INM-1 sample. As the percentage of Mn_2O_3 increases in the glass up to 7.5 mol% the exothermic peaks becomes sharp, which indicates that with the addition of Mn_2O_3 phase separation tendency is hindered which is higher in pure glass (INA-1). Basically high content of network modifier leads to nucleation at different places as compared to glass former in the glass matrix. Due to different sites, phases in the matrix have different kinetics that induces phase separation in glass. As the percentage of Mn_2O_3 increases in the matrix it may act as network former. The higher oxidation states of Mn cations in the glass matrix are readily possible due to transition states of Mn. In addition to this the higher Mn oxidation states also reduces the size of Mn cation. The smaller size cation increases the cross link density in glass matrix [48]. Moreover, higher oxidation states of intermediate oxides convert the non bridging oxygen into bridging oxygen. Conclusively, the addition of Mn_2O_3 increases the connectivity of glass network. Therefore, in comparison to pure sample (INA-1), T_g, T_c and T_{pc} increases in INM-1, INM-2 and INM-3 glass samples. On the other hand, further addition of Mn_2O_3 in glass leads to decrease the thermal properties of INM-4 glass. The DTA curve of INM-4 sample even has 3 exothermic peaks. It means that, in this glass where B_2O_3 is absent, Mn_2O_3 remains in lower oxidation state say Mn^{3+} may acts as a glass modifier. Due to this reason, the tendency of phase separation is increased in INM-4 sample.

Out of four synthesized glass samples of INM series, sample INM-4 shows better results as compared to other samples present in series as it has minimum change in weight% (table 4.18). The graphical representation of INM-4 sample is as shown in figure 4.80.

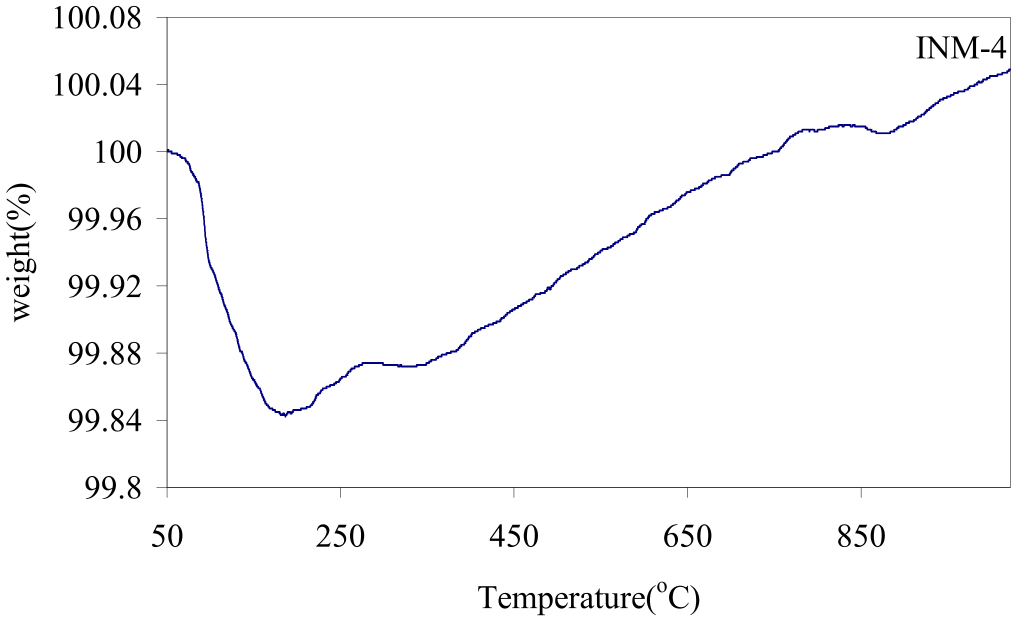

Figure 4.80 Change in weight % of INM-4 sample

Table 4.18 change in weight % in INM samples

Sample ID	Change in weight (%)
INM-1	-0.201
INM-2	0.084
INM-3	-0.304
INM-4	0.05

Based on minimum change in weight%, sample INM-4 is selected for further characterization. The values of activation energy of INM glass series is also calculated using DTA data by the use of Kissinger equation as discussed in section 4.1.1 is as given in fig. 4.81.

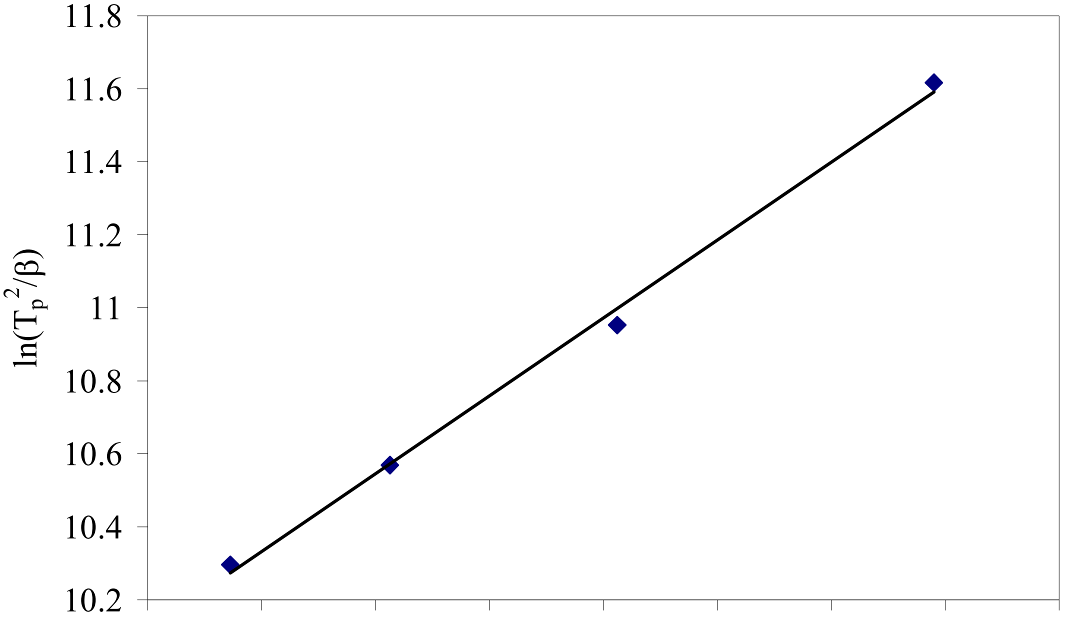

Figure 4.81 Plots of $\ln(T_p^2/\beta)$ vs. $10^3/T_p$ for INM-4 glass powder

The activation energy values of peak crystallization temperature as obtained by least square fitting of experimental data for samples INM-1 to INM-4 is given in table 4.19.

Table 4.19 Activation energy values of INM glass samples determined by DTA

Sample ID	E_a(kJ/mol)
INM-1	315
INM-2	281
INM-3	200
INM-4	355

It is clear from the data obtained by activation energy that sample INM-4 is most stable as it has minimum change in weight% and maximum activation energy. The large difference in activation energy is explained on the basis of formation of various crystalline phases in different glass samples.

4.3.1.1 Thermal Stability Parameter (S)

Thermal stability (ΔT) is calculated as we have already defined in equation (iii). Larger is the difference in T_c and T_g, glass is most thermally stable (section 4.1.1.2). Similarly value of thermal stability parameter is given in equation (iv). The calculated values of ΔT and S are given in table 4.20 below.

Table 4.20 Values of ΔT and S from DTA data for INA glass series

Sample ID	**Thermal Stability (ΔT)**	**Thermal stability parameter (S)**
INM-1	115	1.7
INM-2	85	2.6
INM-3	90	2.3
INM-4	106	2.8

This is clear from the values calculated from DTA data for INM glass series that glass sample INM-4 has maximum value of thermal stability parameter. Hence this glass sample can be designated as the most stable glass among the whole chosen series.

4.3.1.2 Fragility index (F)

The fragility index is calculated as given in equation (v) in section 4.1.1.3. The calculated value of fragility index is as given in table 4.21 below.

Table 4.21 Values of Fragility Index for INA glass series from DTA data

Sample ID	Fragility Index (F)
INM-1	17.34
INM-2	15.17
INM-3	10.74
INM-4	20.10

The above calculated data indicates that INM-1, INM-2 and INM-4 glasses approaches the limit for kinetically strong-glass-forming liquids.

4.3.2 Thermal Dilatometric Analysis

Thermal dilatometric analysis is done on polished flat glass frits from 30 ^{o}C to the softening temperature of glass at a scan rate of 5 ^{o}C/min. The graphical representation of INM series obtained by dilatometer is as shown in figure 4.82.

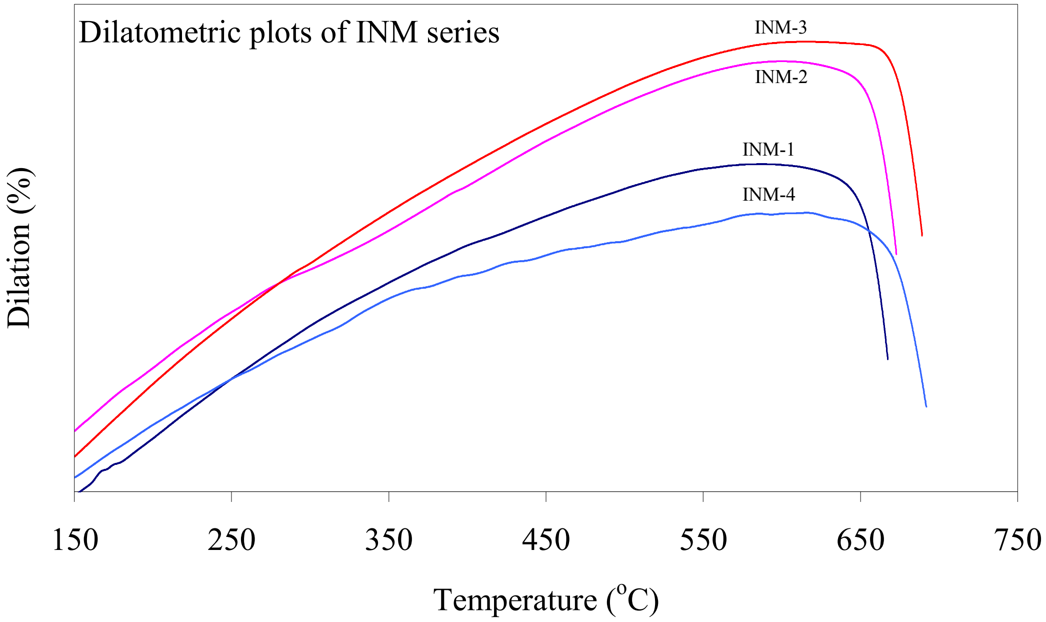

Figure 4.82 Plot of Dilatometer of INM series

It is observed from the above figure that with the increase in manganese content softening temperature (T_s) value goes on increasing. This may be explained on the basis of decrease in B_2O_3 content because of formation of boron-oxygen triangle which loosened the Si-O network. More is the value of B_2O_3, lesser is the softening temperature value. The experimental values obtained by dilatometer of softening temperature and TEC are as given in table 4.22.

Table 4.22 T_s and TEC values obtained from dilatometer for INM series

Sample ID	T_s(°C)	TEC (X 10^{-6}/K) (200-600°C)
INM-1	667	8.11
INM-2	673	8.20
INM-3	689	8.29
INM-4	692	7.96

TEC value remains almost constant for samples INM-1, INM-2 and INM-3. There is a slight decrease in the value of TEC in INM-4 glass sample. From DTA curve of INM-4 glass sample, it is clear that too much amount of Mn_2O_3 induces the phase separation in the glass and it may be the reason for decrease in TEC value of this glass sample.

4.3.3 XRD of $40SiO_2$-$30BaO$-$20ZnO$-$(10-x)B_2O_3$-xM_2O_3 (M= Mn, x= 2.5,5.0,7.5,10.0)

After confirming the amorphous nature of INM glass samples these samples are given heat treatments at different temperatures for different time durations. When INM-1 sample is heat treated at 800 °C for 1 hr time duration formation of barium aluminum silicate ($BaAl_2Si_2O_8$) HC, (hexacelsian, ICDD card no. 88-1048), barium zinc silicate ($BaZnSiO_4$) (hexagonal, ICDD card no. 42-0335), barium manganese oxide ($Ba_3Mn_2O_8$) (hexagonal, ICDD card no. 23-1026), barium aluminum oxide ($Ba_4Al_2O_7$) (orthorhombic, ICDD card no. 41-0165) and zinc borate ($Zn_4O(BO_2)_6$) (cubic, ICDD card no. 72-1316) takes place (fig. 4.83).

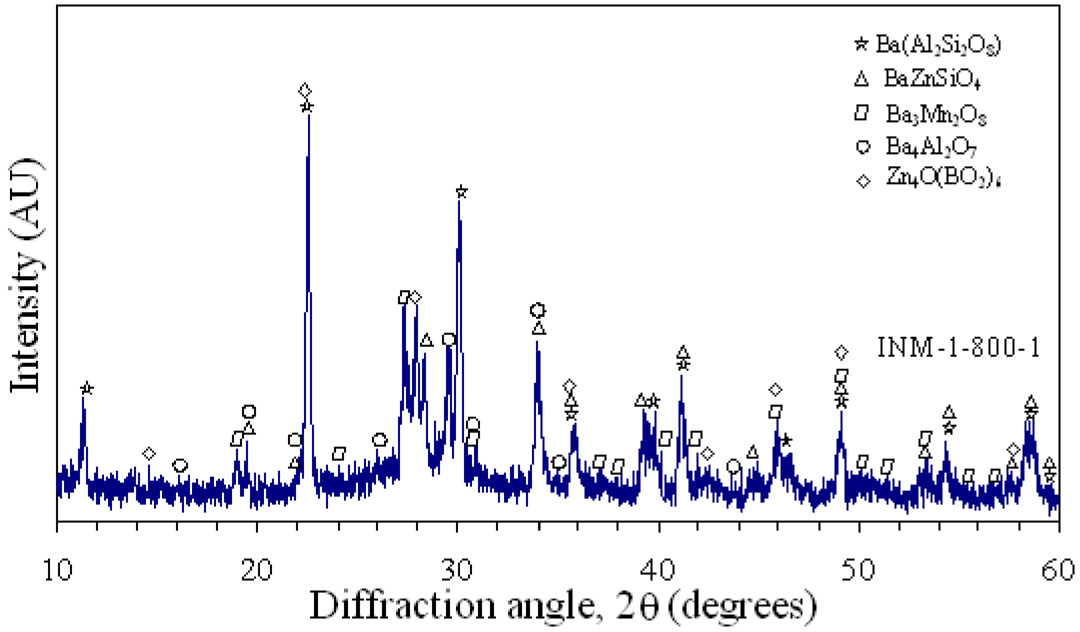

Figure 4.83 XRD pattern of INM-1 glass sample heat-treated at 800 °C for 1 hr

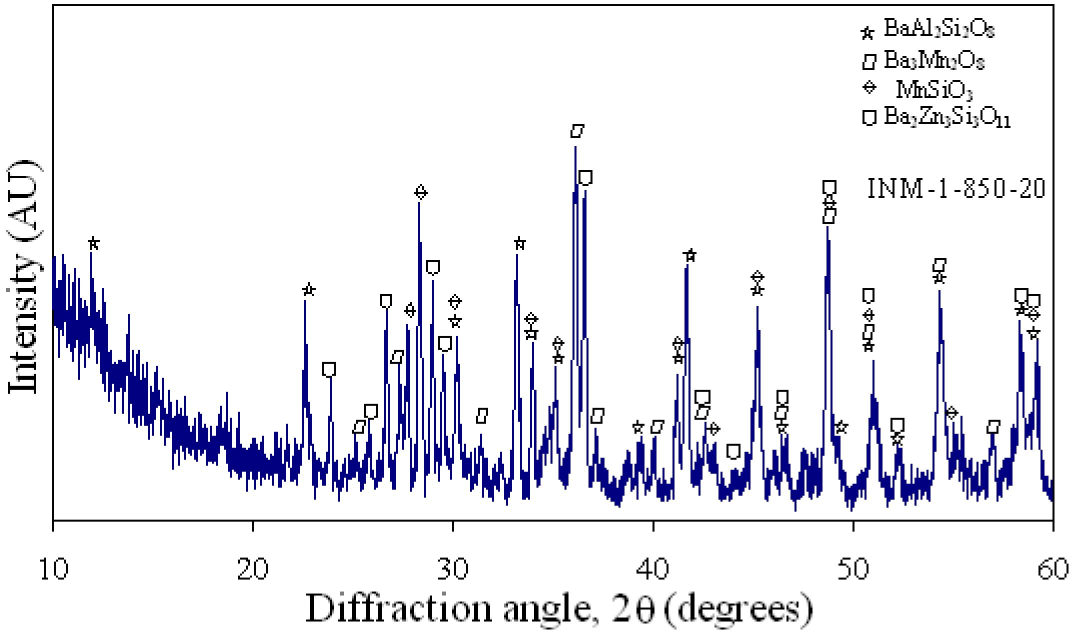

Figure 4.84 XRD pattern of INM-1 glass sample heat-treated at 850 °C for 20 hrs

When INM-1 glass sample is given further heat treatment at 850 °C for 20 hrs formation of barium aluminum silicate ($BaAl_2Si_2O_8$) HC, (hexacelsian, ICDD card no. 77-0185), barium zinc silicate ($Ba_2Zn_3Si_3O_{11}$) (BZS, ICDD card no. 23-0844), barium manganese oxide ($Ba_3Mn_2O_8$) (hexagonal, ICDD card no. 23-1026) and manganese silicate

($MnSiO_3$) (monoclinic, ICDD card no. 26-1249) takes place (fig. 4.84). $BaZnSiO_4$ phase seems to be converted into $Ba_2Zn_3Si_3O_{11}$ phase. Bansal et al. [38] have reported that initially higher symmetric phase may be formed like hexagonal, orthorhombic. As the heat treatment progresses, these phases gets rearranged or dissolved in the matrix to pave the way to form the more stable phases.

On giving further heat treatment i.e. at 900 °C for 1 hr the phase formed in INM-1 sample are barium aluminum silicate ($BaAl_2Si_2O_8$) HC, (hexacelsian, ICDD card no. 77-0185), barium zinc silicate ($Ba_2Zn_3Si_3O_{11}$) (BZS, ICDD card no. 23-0844) and barium zinc silicate ($BaZn_2Si_2O_7$) (ICDD card no. 10-0058) (fig. 4.85).

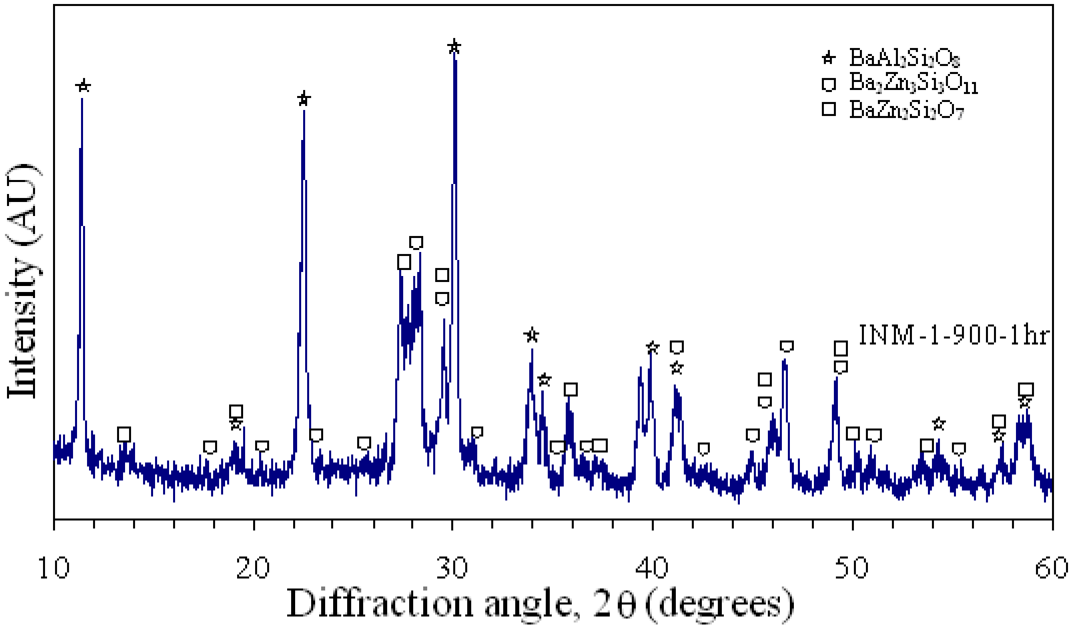

Figure 4.85 XRD pattern of INM-1 glass sample heat-treated at 900 °C for 1 hr

Considering the fact that thermal energy provides sufficient energy for the nucleation of crystalline phases in the glass matrix. The X-ray analysis of the INM-1 glass heat treated at different temperature for different duration indicates that glass matrix is not very strong. Small time duration provides sufficient time for nucleation of different phases. The nucleation of large number of phases even at low temperature indicate that activation energy required for nucleation of these phases is low as compared to other glass series studied here. Moreover, these nucleated phases will have coefficient of thermal expansion differently. If these are intact in the glass matrix for large duration it can provide good properties as a sealant to cope up the expansion of different components of SOFC. As the time of heat treatment is increased, these phases get dissolved and nucleation of other phases occurs. This tendency may lead to reactivity of the glasses more with other components of SOFC. At higher temperature heat treatment 900 °C for 1 hr further indicates that the phases nucleated at 800°C after 10 hrs heat treatment are not stable. They further dissolve and more stable $BaAl_2Si_2O_8$, $Ba_2Zn_3Si_3O_{11}$ and $BaZn_2Si_2O_7$ phase nucleates. Since these silicates are the ultimate result of higher temperature heat treatment, they can be considered as stable one. Looking at the X-ray diffractogram it can be said that the matrix is not in a relaxed situation as at some places sharp XRD peaks are not observed.

When INM-2 glass is given heat treatment at 800 ^{o}C for 1 hr, formation of barium aluminum silicate ($BaAl_2Si_2O_8$) HC, (hexacelsian, ICDD card no. 88-1048), barium zinc silicate ($BaZnSiO_4$) (hexagonal, ICDD card no. 42-0335), barium manganese oxide ($Ba_3Mn_2O_8$) (hexagonal, ICDD card no. 23-1026), manganese ($MnSiO_3$) (monoclinic, ICDD card no. 26-1249), manganese silicon oxide silicate ($MnSiO(SiO_4)$) (monoclinic, ICDD card no. 88-1232) and kyanite (Al_2SiO_5) (triclinic, ICDD card no. 83-1567) takes place (fig. 4.86). The glass matrix is in strained condition (2θ around 28°) as phases nucleated are not stable because of nucleation of large number of phases.

On giving further heat treatment i.e. at 850 ^{o}C for 20 hrs to INM-2 glass sample barium aluminum silicate ($BaAl_2Si_2O_8$) HC, (hexacelsian, ICDD card no. 77-0185), barium zinc silicate ($Ba_2Zn_3Si_3O_{11}$) (BZS, ICDD card no. 23-0844), barium manganese oxide ($Ba_3Mn_2O_8$) (hexagonal, ICDD card no. 23-1026) and manganese silicate ($MnSiO_3$) (monoclinic, ICDD card no. 26-1249) were formed (fig. 4.87). In this case $BaZnSiO_4$ phase seems to get converted into $Ba_2Zn_3Si_3O_{11}$ phase, $MnSiO(SiO_4)$ and Al_2SiO_5 phases get dissolved. Long hour heat treatments provide sufficient time for dissolution of metastable phases and nucleation of stable phases. This provides stability in glass matrix as number of crystalline phases are reduced.

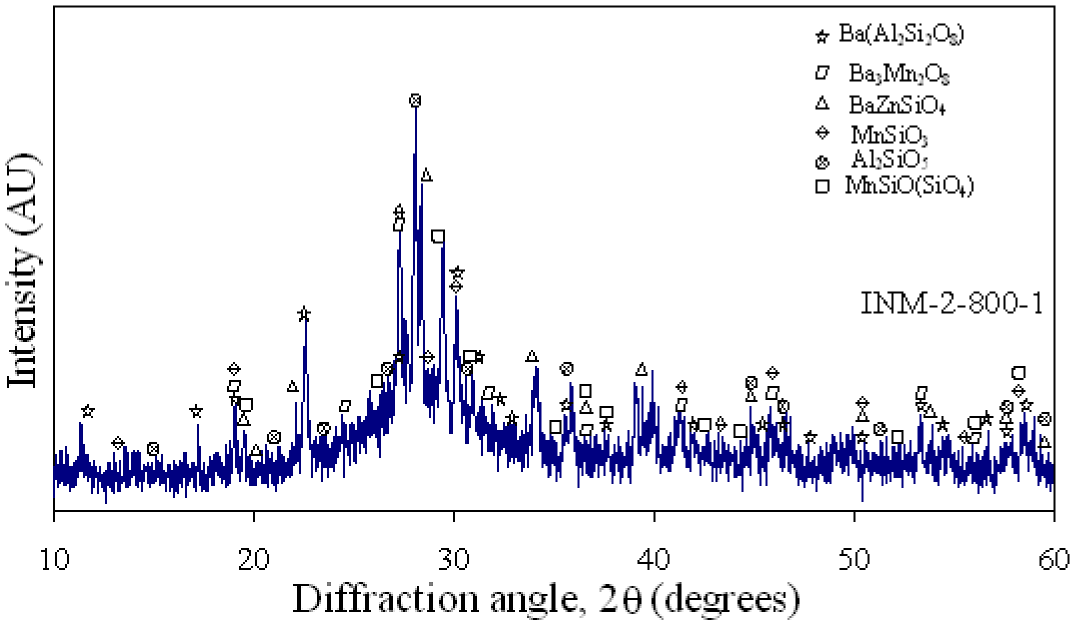

Figure 4.86 XRD pattern of INM-2 glass sample heat-treated at 800 °C for 1 hr

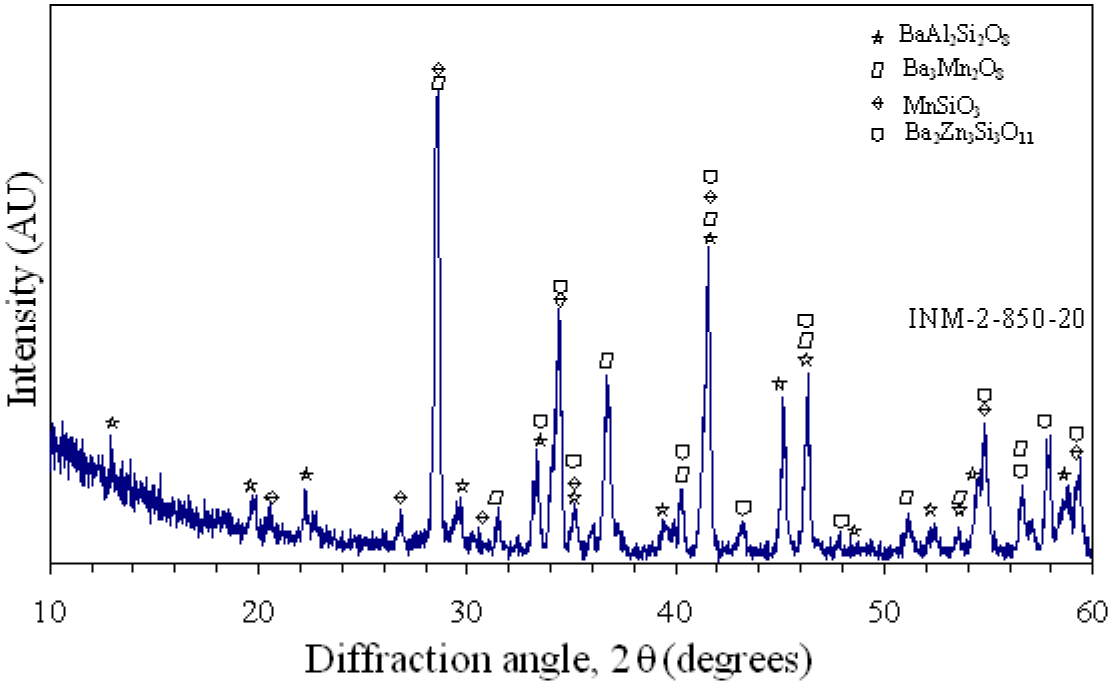

Figure 4.87 XRD pattern of INM-2 glass sample heat-treated at 850 °C for 20 hrs

Formation of barium zinc silicate ($BaZn_2Si_2O_7$) (ICDD card no. 10-0058), barium aluminum oxide ($BaAl_2O_4$) (hexagonal, ICDD card no. 82-1350) and quartz (SiO_2)

(hexagonal, ICDD card no. 70-2537) takes place when INM-3 glass sample is given heat treatment at 900 °C for 1 hr time duration (fig. 4.88). $Ba_2Zn_3Si_3O_{11}$ phase again transforms to $BaZn_2Si_2O_7$ phase, $BaAl_2Si_2O_8$ phase gets converted into $BaAl_2O_4$ phase and SiO_2 nucleates as a new phase. Here also peak stability is observed. This indicates that because of fluid nature of glass there is competition between different phases to nucleate.

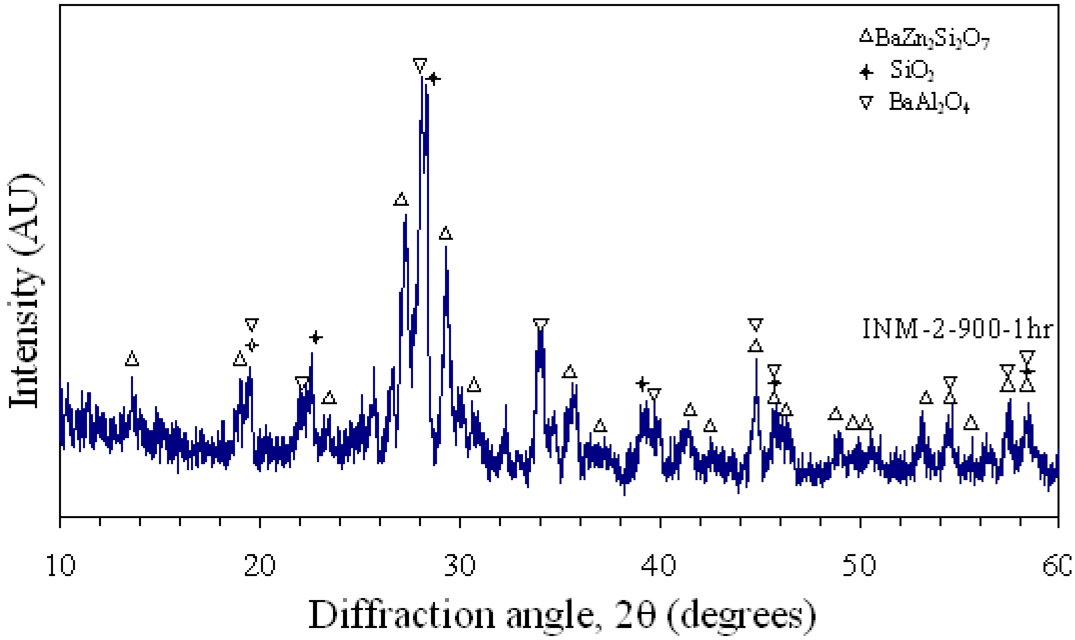

Figure 4.88 XRD pattern of INM-2 glass sample heat-treated at 900 °C for 1 hr

Heat treatment at 800 °C for 1 hr to INM-3 glass sample leads to the formation of barium aluminum silicate ($BaAl_2Si_2O_8$) HC, (hexacelsian, ICDD card no. 88-1048), barium zinc silicate ($BaZnSiO_4$) (hexagonal, ICDD card no. 42-0335), barium manganese oxide ($Ba_3Mn_2O_8$) (hexagonal, ICDD card no. 23-1026), manganese ($MnSiO_3$) (monoclinic, ICDD card no. 26-1249), manganese silicon oxide silicate ($MnSiO(SiO_4)$ (monoclinic, ICDD card no. 88-1232) and kyanite (Al_2SiO_5) (triclinic, ICDD card no. 83-1567) phases (fig. 4.89).

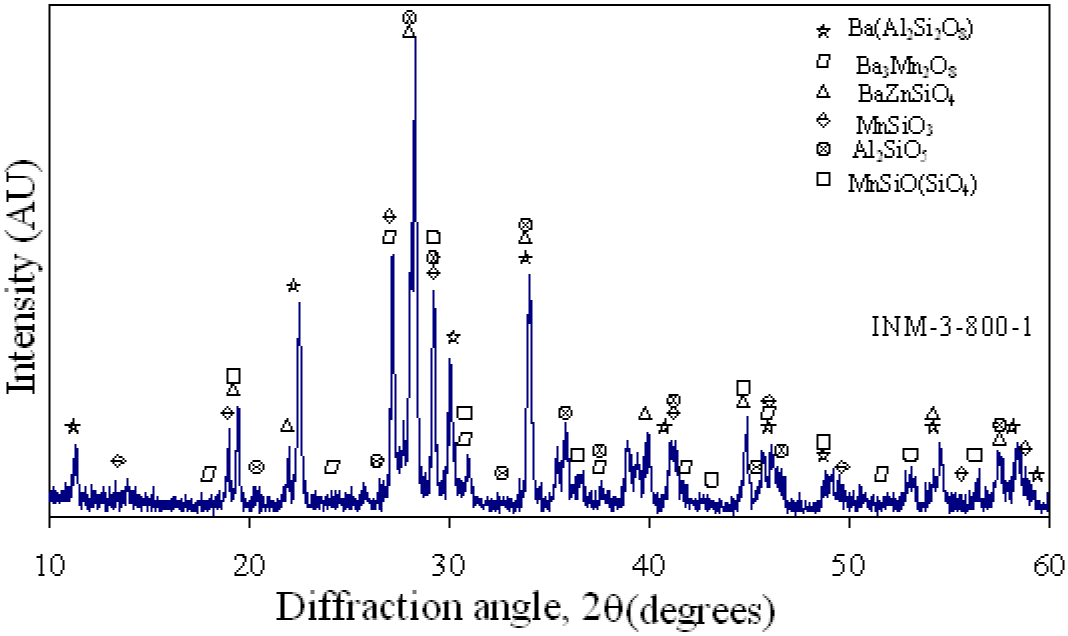

Figure 4.89 XRD pattern of INM-3 glass sample heat-treated at 800 ^{o}C for 1 hr

When heat treatment at 850 ^{o}C for 20 hrs is given to INM-3 glass sample formation of barium aluminum silicate ($BaAl_2Si_2O_8$) HC, (hexacelsian, ICDD card no. 77-0185), barium zinc silicate ($Ba_2Zn_3Si_3O_{11}$) (BZS, ICDD card no. 23-0844), barium manganese oxide ($Ba_3Mn_2O_8$) (hexagonal, ICDD card no. 23-1026) and manganese silicate ($MnSiO_3$) (monoclinic, ICDD card no. 26-1249) were observed (fig. 4.90). $BaZnSiO_4$ phase gets converted into $Ba_2Zn_3Si_3O_{11}$ phase and $MnSiO(SiO_4)$ phase gets converted into $MnSiO_3$ phase.

When INM-3 glass is further heat treated at 900 ^{o}C for 1 hr formation of barium aluminum oxide ($BaAl_2Si_2O_8$) (hexacelsian, ICDD card no. 77-0185), barium zinc silicate ($BaZnSiO_4$) (hexagonal, ICDD card no. 42-0335) and barium manganese aluminum silicate ($Ba_{0.96}Mn_{0.75}Al_{0.25}Si_{1.9}O_6$) (monoclinic, ICDD card no. 49-0943) takes place (fig. 4.91). $Ba_2Zn_3Si_3O_{11}$ phase get converted into $BaZnSiO_4$ phase and $Ba_3Mn_2O_8$ and $MnSiO_3$ phases gets converted into $Ba_{0.96}Mn_{0.75}Al_{0.25}Si_{1.9}O_6$ phase by taking alumina from the crucible.

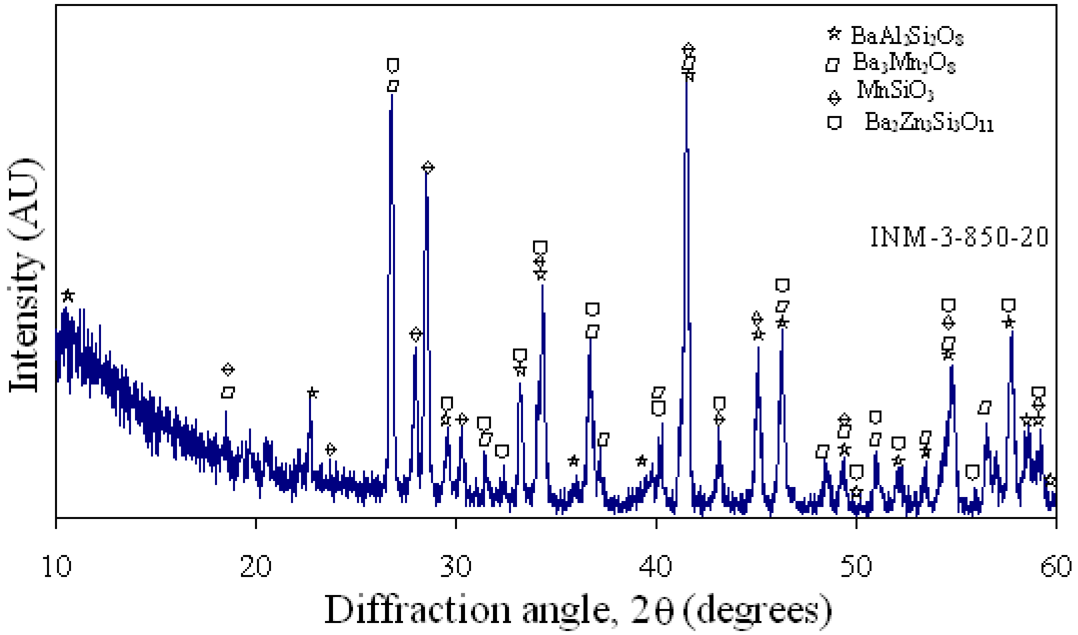

Figure 4.90 XRD pattern of INM-3 glass sample heat-treated at 850 °C for 20 hrs

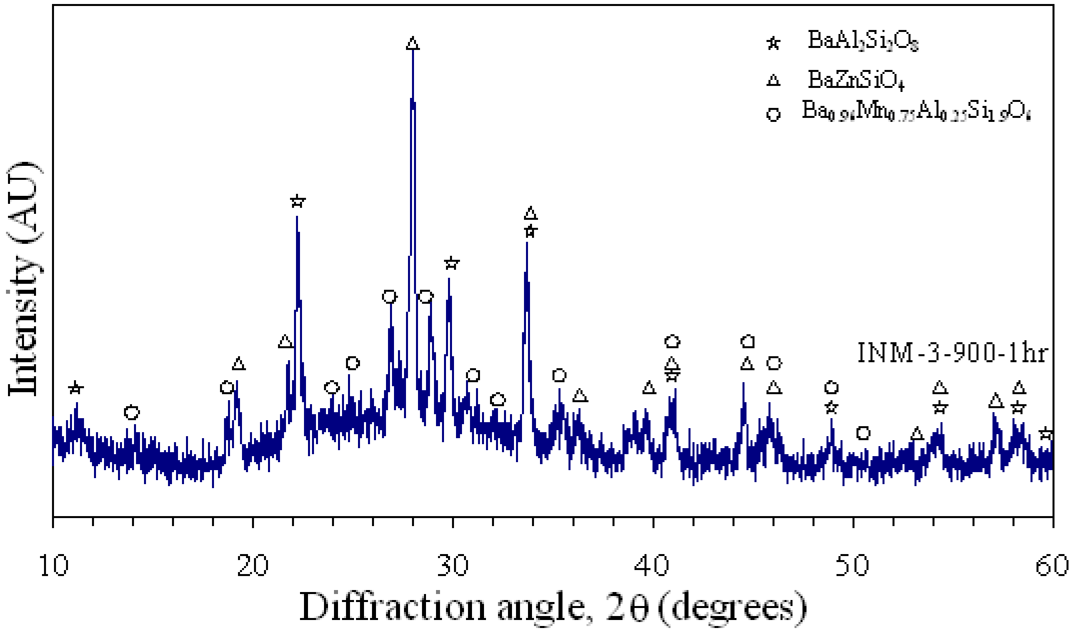

Figure 4.91 XRD pattern of INM-3 glass sample heat-treated at 900 °C for 1 hr

When glass sample INM-4 is given heat-treatment at 1, 10 and 100 hrs duration formation of various phases takes place. The X-ray diffraction patterns obtained during heat-treatments of 1, 10 and 100 hrs are as given in figures 4.92, 4.93 and 4.94 respectively.

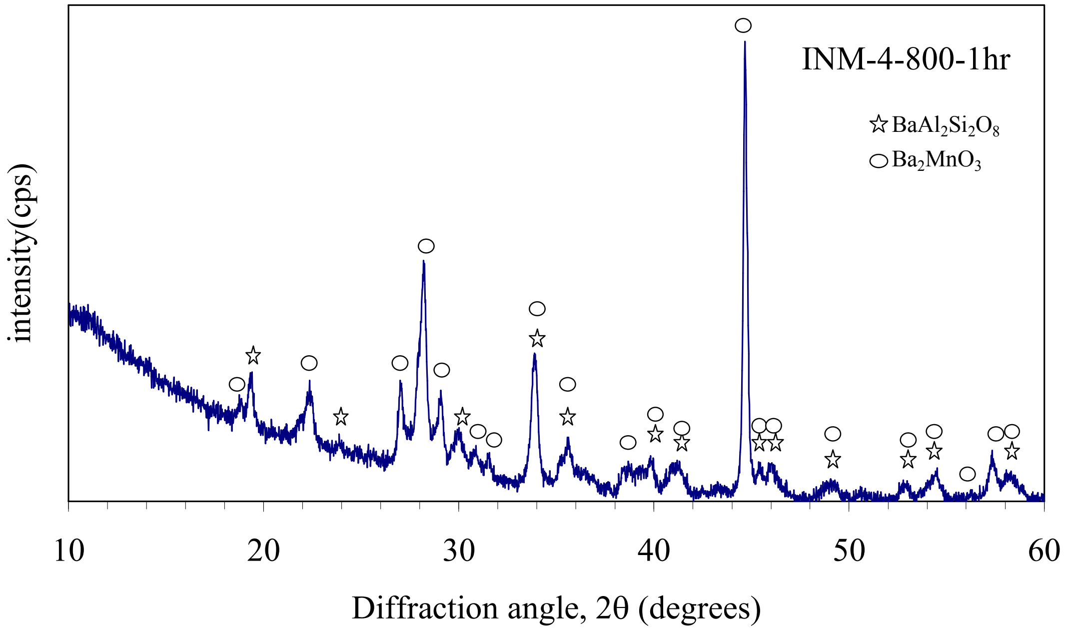

Figure 4.92 XRD pattern of INM-4 glass sample heat-treated at 800 ^oC for 1 hr

Among the all glass samples of INM series in which nucleation of different crystalline phases occur at low temperature annealing even for shorter duration of time (1 hr.), this glass (INM-4) shows different behaviour as number of phases nucleated is only two i.e. $BaAl_2Si_2O_8$ and Ba_2MnO_3. These phases seems to be thermodynamically stable and are not changing even after long hour heat treatment.

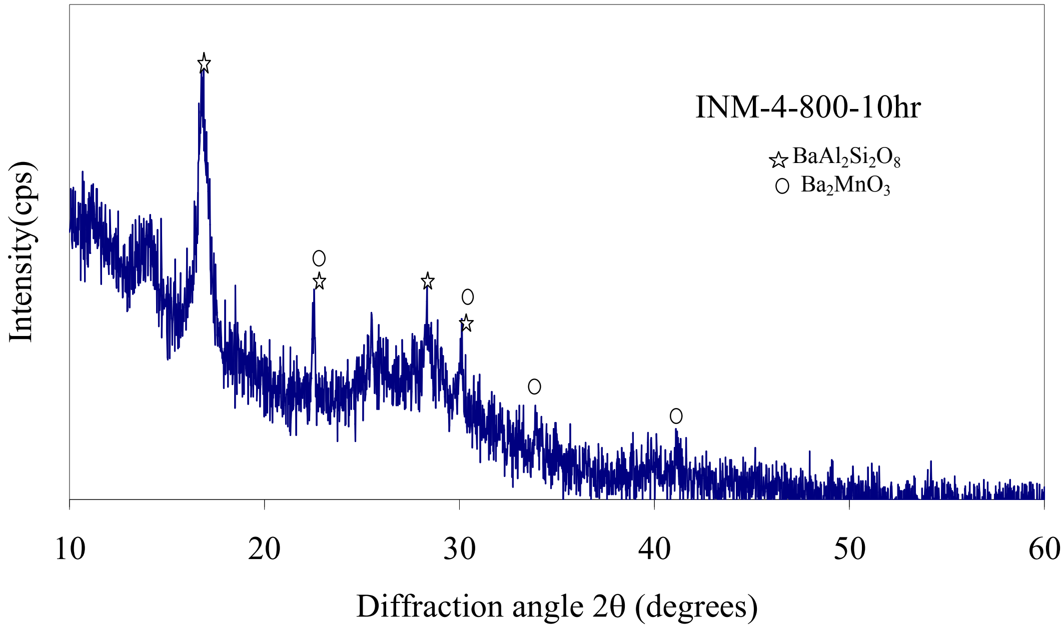

Figure 4.93 XRD pattern of INM-4 glass sample heat-treated at 800 °C for 10 hr

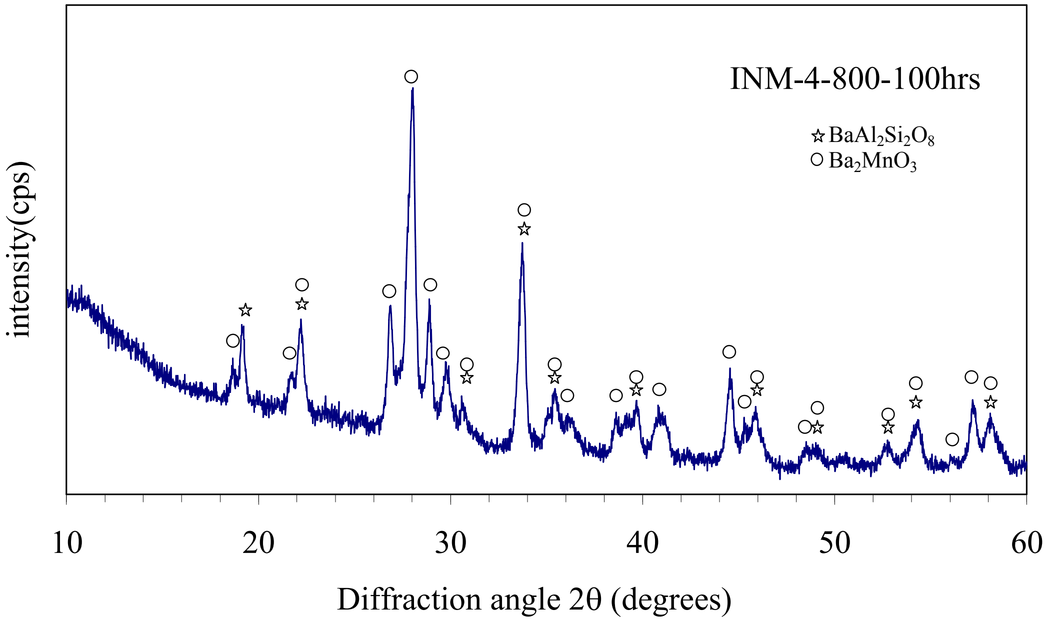

Figure 4.94 XRD pattern of INM-4 glass sample heat-treated at 800 °C for 100 hrs

There occurs the formation of hexagonal (Barium Aluminum Silicate) $BaAl_2Si_2O_8$ (ICDD card no. 77-.185) and monoclinic (Barium Manganese Oxide) Ba_2MnO_3 (ICDD card no. 72-0193). Formation of polymorphs of barium aluminum silicate is unexpected as no Al_2O_3 was incorporated in the batch. Evidently, chemical interactions between alumina and the glass melt took place due to unavoidable uptake of the former from the crucible during melting. EDS analysis of the glass frits confirmed the presence of alumina in the amount of 5–7 wt% and ZnO 16 wt% whereas no deviation was observed for other constituents of glass. However, atomic absorption spectroscopy (AAS) indicated that Al_2O_3 and ZnO are 6% and 15%, respectively. The wet chemical analysis also confirmed the observed variation in the composition of glass which is for Al_2O_3 and ZnO (6% and 15%, respectively) and no variation was observed for SiO_2, BaO and B_2O_3.

4.3.4 Scanning Electron Microscopy (SEM)

Figure 4.95 (a & b) shows the SEM images of INM-4 glass sample when it is heat treated at 800 ^oC for 10 hrs time duration at low and high magnification. It is clear from these micrographs that nucleation of crystalline phase in the glass matrix have occurred. These are uniformly distributed throughout the matrix. The crystallite size is observed to vary from 2µm to 8µm. These nucleated phases are faceted in nature which is typical characteristics of brittle substances. The important features observed is that all the nucleated phases grow uniformly in all the direction. These nucleated polygonal phases grow uniformly. The polygonal phases grow first in the close packed direction at different planes. The faceted hexagonal features are of hexagonal barium aluminium silicate ($BaAl_2Si_2O_8$) as can be seen in the structure.

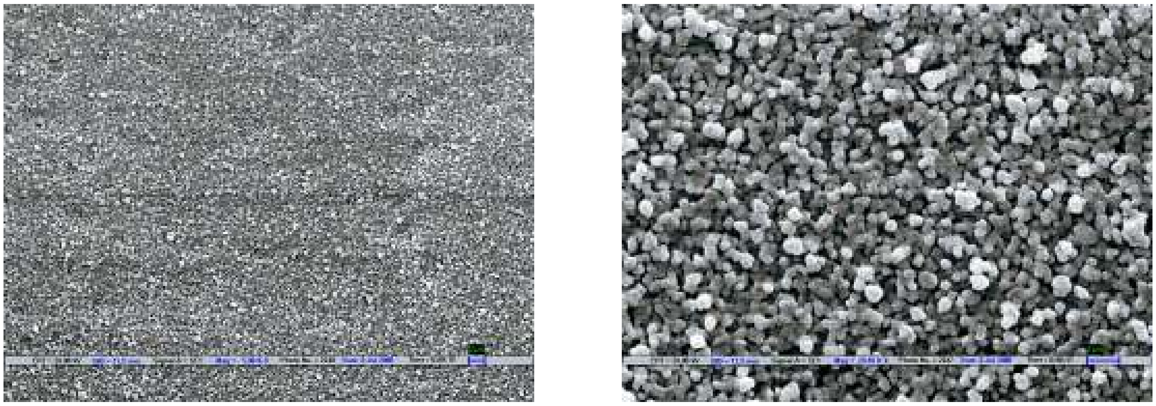

Figure 4.95 (a & b) SEM micrograph of INM-4 glass heat treated at 800 ^oC for 10hrs

4.3.5 Conductivity Measurement

Conductivity measurement of the INM glass series has been done at room temperature by plotting the graph between real and imaginary values of impedance obtained by LCR meter. The obtained results are as given in table 4.23.

Table 4.23 Resistivity values of INL series

Sample ID	Resistivity (MΩcm)
INM-1	0.28
INM-2	0.08
INM-3	0.27
INM-4	0.02

From the above-obtained data, it is observed that sample INM-1 and INM-3 has maximum value of resistivity.

4.4 INY Series

This series include four samples i.e. $40SiO_2$-30BaO-20ZnO-(10-x)B_2O_3–xY_2O_3 (x= 2.5, 5.0, 7.5, 10.0).

4.4.1 Differential Thermal Analysis

Thermal analysis of INY glass series samples was done by differential thermal analyzer at various heating rates of 10°C/min, 20°C/min, 30°C/min and 40°C/min from 50 °C to 1000 °C by taking α-alumina as the reference sample and amount of sample taken was approximately 20 mg. The plots obtained by DTA of INY-1, INY-2, INY-3 and INY-4 series are as shown in figures below from 4.96 to 4.99 respectively.

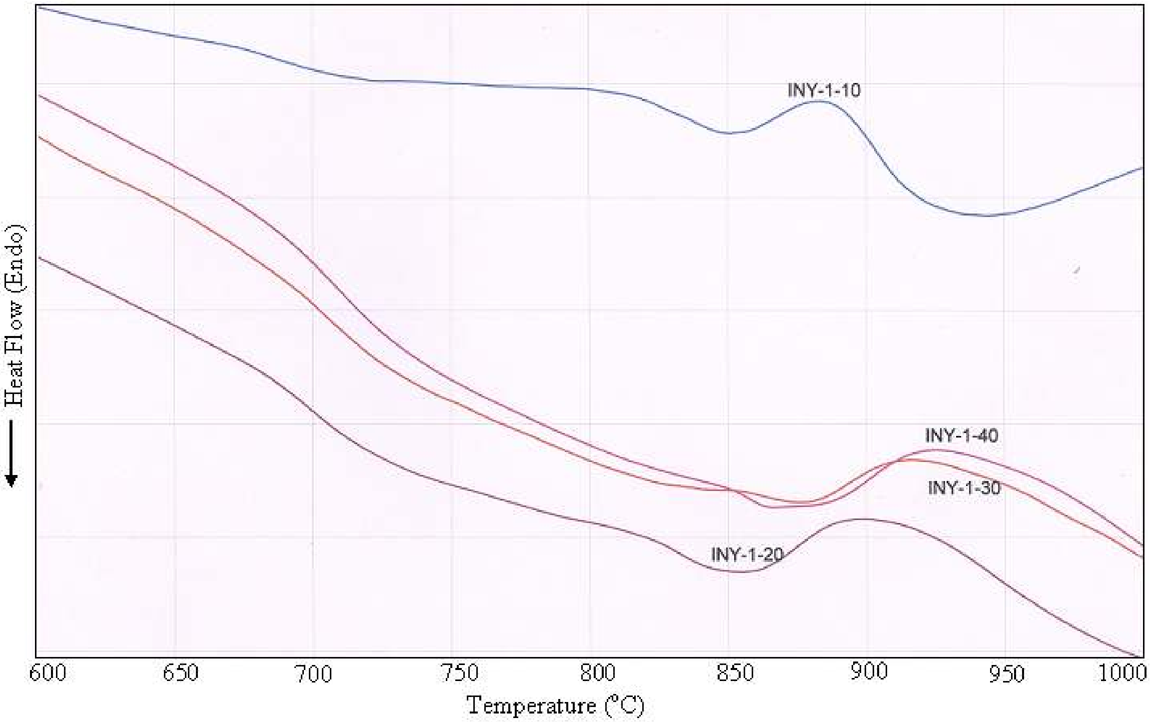

Figure 4.96 DTA plot of INY-1 glass sample at 10, 20, 30, 40 °C/min from 600-1000°C

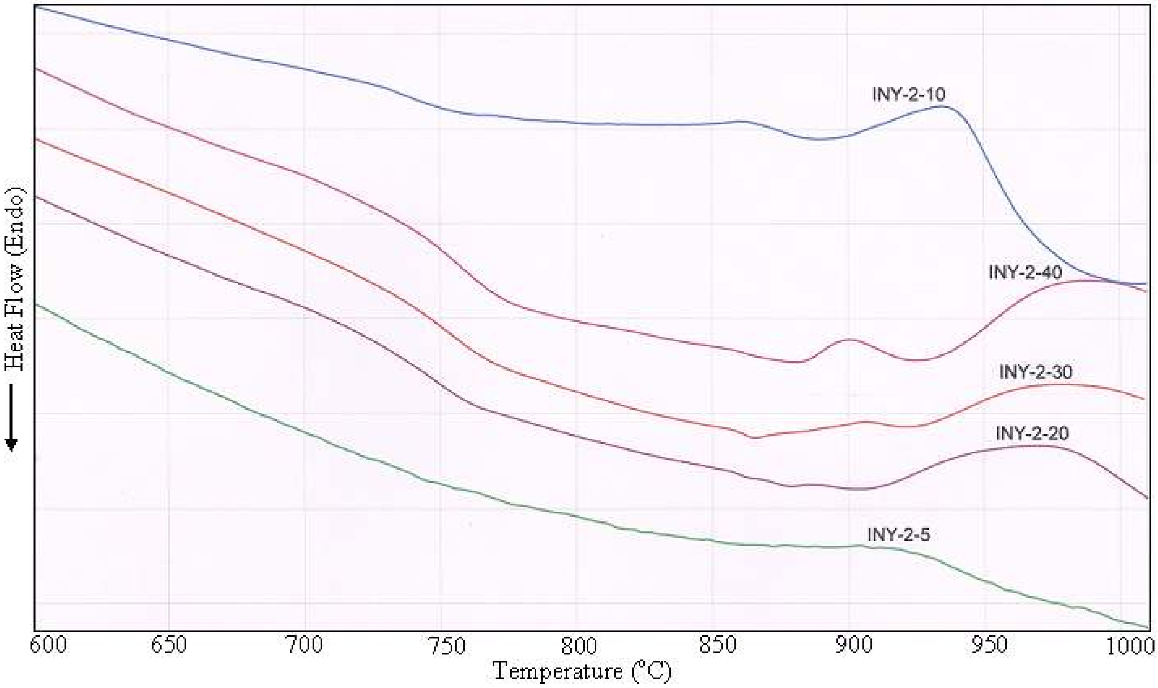

Fig. 4.97 DTA plot of INY-2 glass sample at 5, 10, 20, 30, 40 °C/min from 600-1000°C

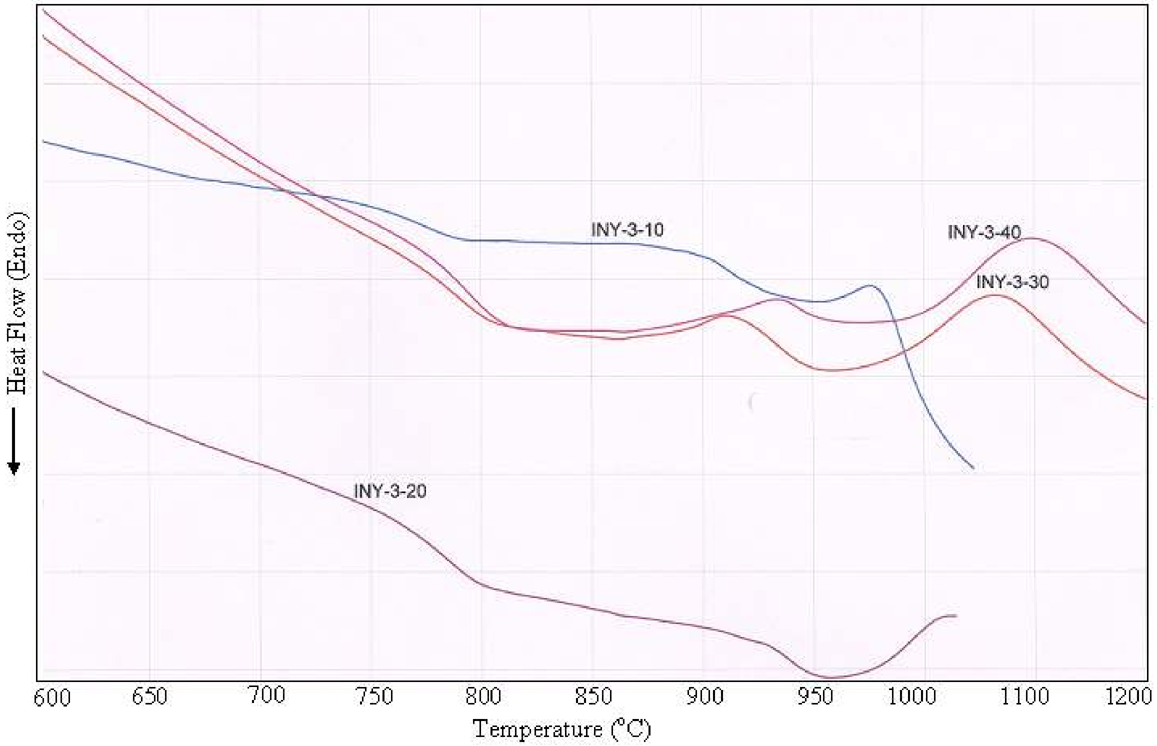

Figure 4.98 DTA plot of INY-3 glass sample at 10, 20, 30, 40 °C/min from 600-1000°C

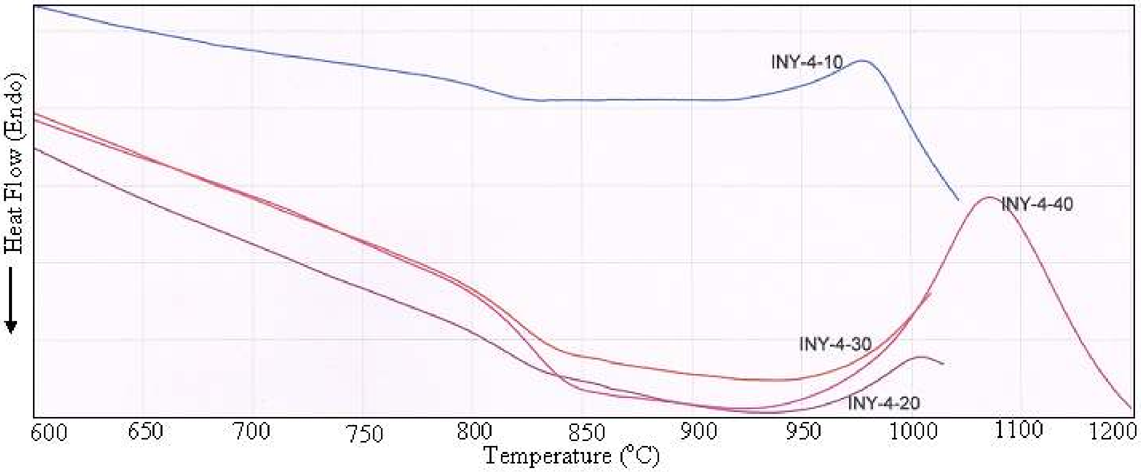

Figure 4.99 DTA plot of INY-4 glass sample at 10, 20, 30, 40 °C/min from 600-1000°C

The values of transition temperature, crystallization temperature and peak crystallization temperature obtained by DTA at various heating rates are given in table 4.24. Figures 4.96-4.99 and table 4.24 reflect a systematic increase in T_g, T_c and T_{pc} of the as cast glasses as the Y_2O_3 increases with respect to B_2O_3. As the amount of Y_2O_3 increases in the glasses while substituting equivalent amount of glass formers (B_2O_3), the intermediate oxide (Y_2O_3) might have worked as network former. Therefore, the number of non-bridging oxygen created by the modifiers (BaO, ZnO) in glass matrix might be converted into bridging oxygen by Y_2O_3. Due to this reason, the T_g, T_c and T_{pc} increases in the present glass sample with addition of Y_2O_3. Moreover, Yttrium being larger size metal as compared to B^{3+} offer higher coordination number [39], so it can act as network former. However, the field strength of Y^{3+} ions is less than B^{3+} ions. It is well documented in literature [40] that the higher content of alkaline earth oxides (30mol%) in present sample owing to the existence of large number of non bridging oxygen ions; intermediate cations can attain a higher coordination number of 6 instead of 3 [40]. Basically, intermediate oxides (Al^{3+}, Al^{6+}, Cr^{3+} and Cr^{6+} etc.) in glass matrix plays dual role due to their different oxidation states. Such multiple oxidation states that can simultaneously be presented in the glass matrix depends on the modifier-former properties, size of the ions, their field strength and their mobility [41]. Apart from this, the higher oxidation states leads to smaller size of the cation which causes a tightening effect of glass network with a consequent increase in T_g value. Moreover, the smaller cation size also increase the cross-link density [42].

Table 4.24 T_g, T_c and T_{pc} values of INY series

COMPOSITION	$T_g(^oC)$	$T_c(^oC)$	$T_{pc}(^oC)$
INY-1-10	705	851	883
INY-1-20	717	856	898
INY-1-30	730	879	909
INY-1-40	734	890	924
INY-2-5	740	870	910
INY-2-10	755	893	937
INY-2-20	762	911	973
INY-2-30	766	92	978
INY-2-40	776	930	988
INY-3-10	758	951	977
INY-3-20	769	956	1010
INY-3-30	771	975	1034
INY-3-40	777	996	1049
INY-4-10	786	922	980
INY-4-20	791	960	1004
INY-4-30	798	964	1020
INY-4-40	809	967	1035

The explanation of shifting of peak maxima is as explained in section 4.1.1. In order to check the stability of the glass with respect to temperature, all four glasses were investigated using TGA. A typical TGA curve of INY-2 glass is given in figure 4.100. A fully resolved peak is observed at nearly 865^{o}C which belongs to the crystallization peak as observed in DTA analysis of the same glass (table 4.24). However, the TGA curve of the entire glass sample is not following any trend. INY-1 glass sample exhibit weight loss when glass was investigated in the range of 50-1000^{o}C. It indicates that the glass is having lot of strain and get relaxed during the experiment. At higher addition (10mol%) Y_2O_3 again creates some stress and strain within glass matrix as compared to INY-2 and INY-3 glass samples. It is also verified from the activation energy data as given in table 4.26. Out of four synthesized glass samples of INY series, sample INY-2 shows better results as compared to other samples present in series as it has minimum change in weight percent (table 4.25). The graphical representation of INY-2 sample is as shown in figure 4.100.

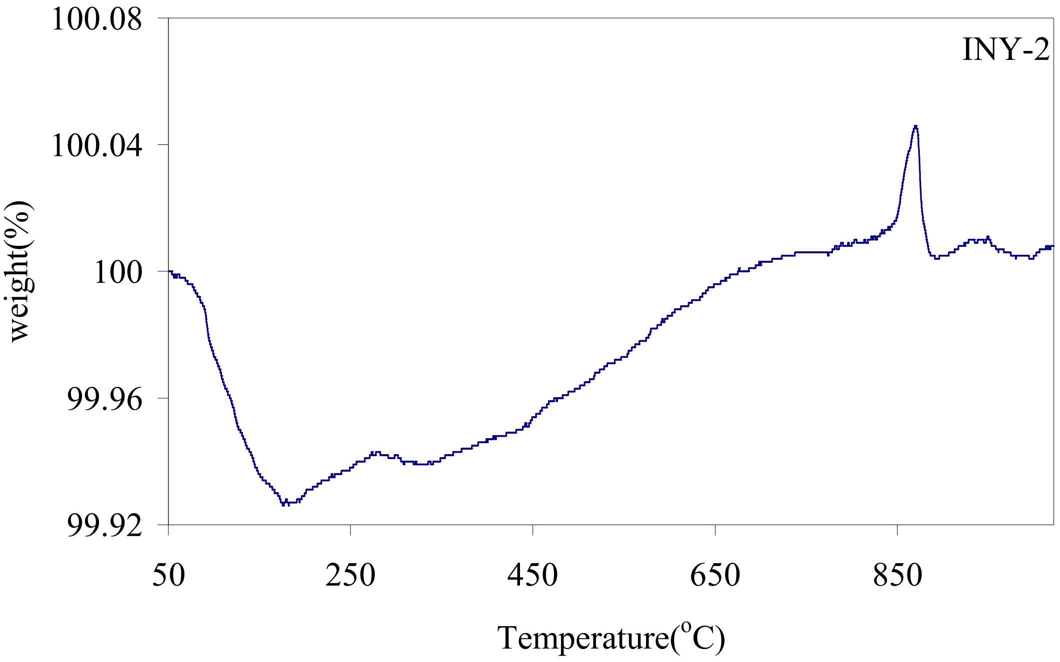

Figure 4.100 Change in weight % of INY-2 sample

Table 4.25 change in weight % in INY glass samples

Sample ID	Change in weight (%)
INY-1	-1.283
INY-2	0.008
INY-3	0.174
INY-4	-0.029

Because of minimum percentage weight loss INY-2 sample is selected for further study. Activation energy (E_a) value of peak crystallization temperature is also calculated from

DTA data using Kissinger equation as given in equation (i) and its graphical representation is given in figure 4.101.

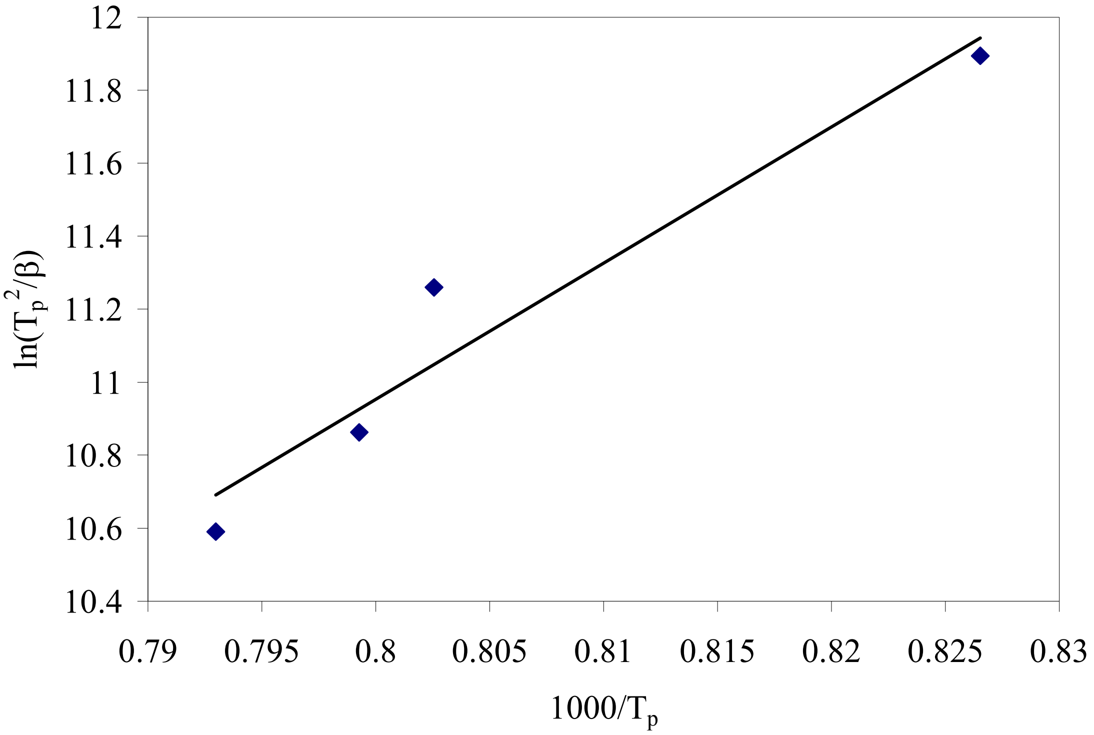

Fig. 4.101 Plot of $\ln(T_p^2/\beta)$ vs. $10^3/T_p$ for INY-2 glass powder

Values of activation energy of peak crystallization temperature E_a obtained by least square fitting of experimental data obtained by DTA is as shown in table 4.26.

Table 4.26 Activation energy values of INA glass samples determined by DTA

Sample ID	E_a(kJ/mol)
INY-1	369
INY-2	574
INY-3	240
INY-4	326

Glass sample INY-2 has maximum value of activation energy as compared to other samples present in the series. Above glass transition temperature the structure of glass becomes relaxed and diffusion of ions is easier. However, the competition among various cations, which are present in glass matrix, reduces the diffusion rate of the ions.

Therefore, in case of INY-2 glass sample, where Y_2O_3 (5%) and B_2O_3 (5%) has higher competition which needs sufficient power from the surroundings to nucleate the crystalline phases [43]. It confirms the maximum stability of this sample.

4.4.1.1 Thermal Stability Parameter (S)

Thermal stability (ΔT) is calculated as we have already defined in equation (iii). Larger is the difference in T_c and T_g, glass is most thermally stable (section 4.1.1.2). Similarly value of thermal stability parameter is given in equation (iv). The calculated values of ΔT and S are given in table 4.27 below. The thermal stability parameter (S) reflects the resistance to devitrification of the glassy matrix. The big difference in T_c-T_g is related to delay the nucleation process. It is also manifested from the XRD pattern of the INY-3 and INY-4 glasses which are even heat treated at 900^oC. On the other hand the stability factor (S) is higher in INY-2 glass than other glasses of this series. These calculations show the similarity with the activation energy of the glasses. Interestingly, the TGA data of this particular glass shows the minimum weight change in temperature range of 50-1000^oC. Therefore, based on the above mentioned results, it is concluded that INY-2 sample exhibits higher thermal stability with higher activation energy of crystallization. Hence, this glass was further investigated for crystallization kinetic study to check their suitability as a probable good sealing candidate.

Table 4.27 Values of ΔT and S from DTA data for INA glass series

Sample ID	**Thermal Stability (ΔT)**	**Thermal stability parameter (S)**
INY-1	145.25	4.7
INY-2	138.52	5.9
INY-3	192.37	4.8
INY-4	156.54	5.5

This is clear from the values calculated from DTA data for INY glass series that glass sample INY-2 has maximum value of thermal stability parameter. Hence this glass sample can be designated as the most stable glass among the whole chosen series.

4.4.1.2 Fragility index (F)

The fragility index is calculated as given in equation (v) in section 4.1.1.3. The calculated value of fragility index is as given in table 4.28 below.

Table 4.28 Values of Fragility Index for INA glass series from DTA data

Sample ID	Fragility Index (F)
INY-1	19.70
INY-2	29.19
INY-3	12.16
INY-4	16.08

The above calculated data indicates that INY-1, INY-2 and INY-4 glasses approach the limit for kinetically strong-glass-forming liquids.

4.4.2 Thermal Dilatometric Analysis

Thermal dilatometric analysis is done on polished flat glass frits from 30 °C to the softening temperature of glass at a scan rate of 5 °C/min. The graphical representation of INY series obtained by dilatometer is as shown in figure 4.102.

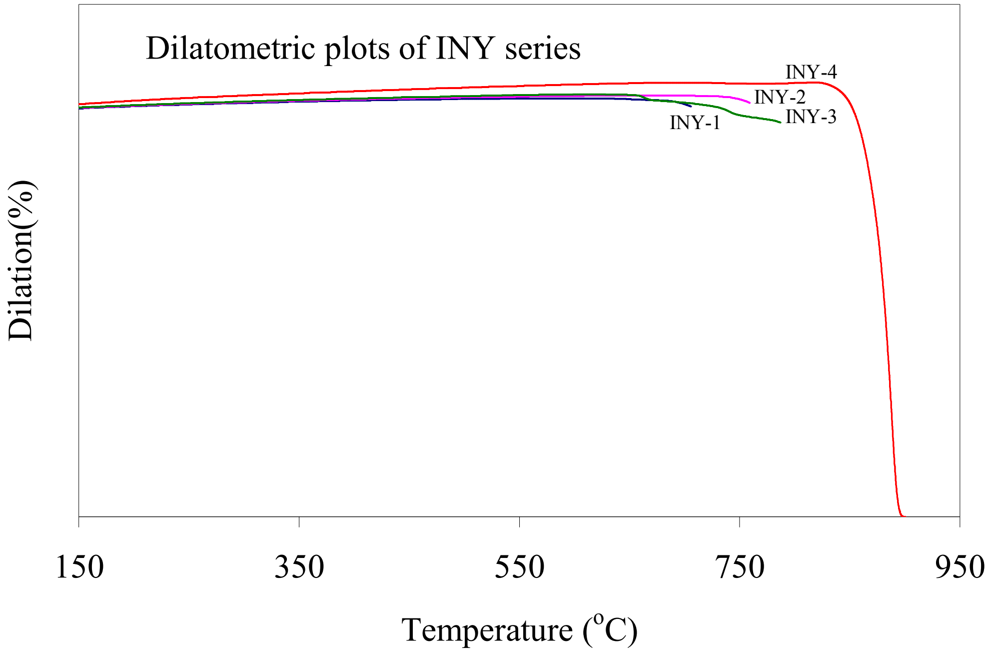

Figure 4.102 Plot of dilatometer of INY series glass samples

The softening temperature of glass frits increases with increase in yttrium content. The softening temperature and thermal expansion coefficient values are given in table 4.29.

Table 4.29 T_s and TEC values obtained from dilatometer for INY series

Sample ID	T_s(°C)	TEC (X 10^{-6}/K) (200-600°C)
INY-1	705	7.9
INY-2	759	8.1
INY-3	787	8.2
INY-4	900	8.5

These values are in close proximity. However, the high TEC is observed for INY-4 sample. As mentioned in lanthanum series, the change in thermal expansion coefficient could be explained on the basis of change of bond characteristic towards covalent at the local level. Additionally, the addition of Y_2O_3 in glass composition might have induced some trace of crystallinity during quenching of the glasses which is manifested from the XRD pattern of these glasses before heat treatment. The XRD pattern of as cast glass has sharp hump instead of broad hump, in general, manifestation of amorphous nature.

4.4.3 XRD of $40SiO_2$-30BaO-20ZnO-(10-x)B_2O_3-xM_2O_3 (M= Y, x= 2.5, 5.0, 7.5, 10)

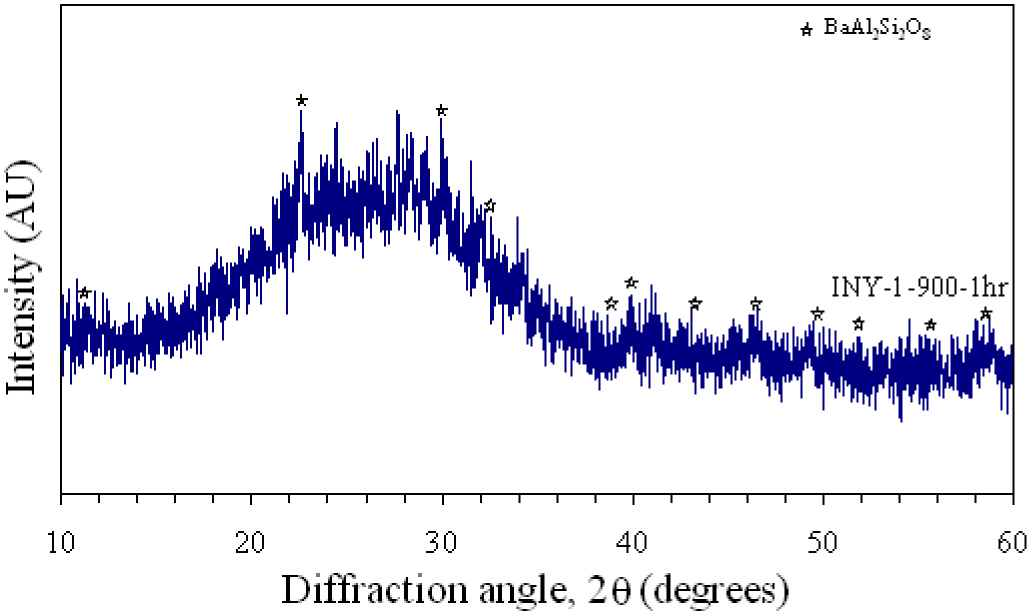

Figure 4.103 XRD pattern of INY-1 glass sample heat-treated at 900 °C for 1 hr

When INY-1 glass sample is given heat treatment at 900 °C for 1 hr time duration only barium aluminum silicate ($BaAl_2Si_2O_8$) (hexacelsian, ICDD card no. 88-1048) phase nucleates in a very minute amount (fig. 4.103) and yttria remains in the glass matrix at this temperature. In the initial composition of glass Al_2O_3 was absent. However, possibility of picking from crucible during melting exists which was also observed in all other glass samples. As shown in figure 4.103 the major phase precipitates in glass INY-2 after heat treatment at 900°C for 1 hr is hexacelsian. Drummond et al. [32] have reported that hexacelsian is a metastable phase and precipitate in the early stage of the heat treatment in $BaO-SiO_2-Al_2O_3$ systems.

Other higher temperatures were not selected for annealing for this composition as SOFC operating temperature is around 800 °C. Moreover, the glass matrix seems to be stable one as nucleation is a delayed process even after heat treatment at higher temperature.

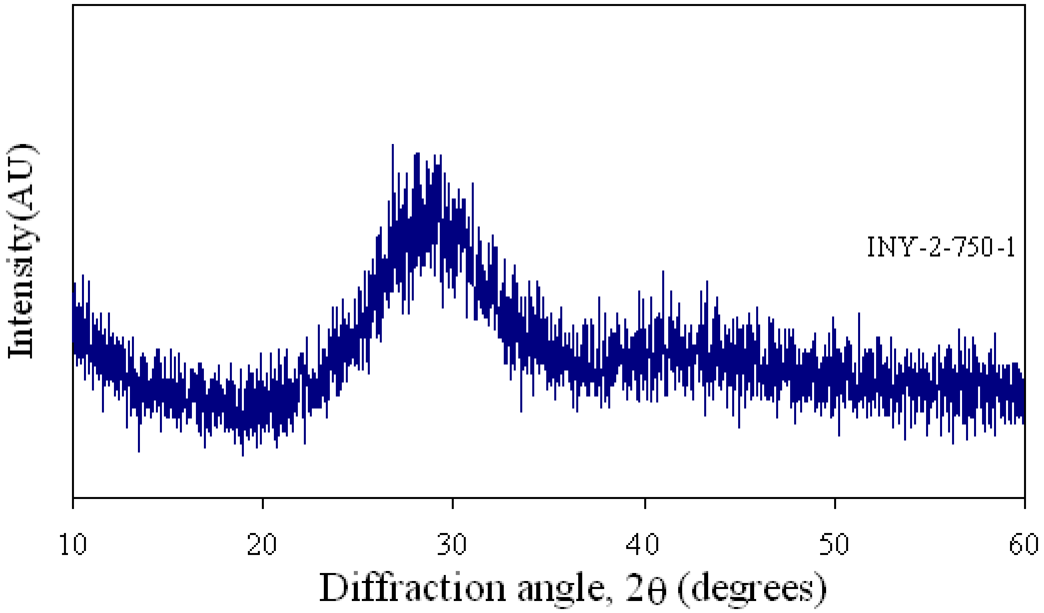

Figure 4.104 XRD pattern of INY-2 glass sample heat-treated at 750 °C for 1 hr

Since the thermal behavior of INY-2 glass is better as compared to other glasses of this series, it is essential to know the nucleation kinetics in this composition. Therefore, a systematic heat treatment was performed from lower temperature to higher temperature over a wide range of duration. When INY-2 glass sample is given heat treatment at 750 °C for 1 hr time duration, the sample remains amorphous (fig. 4.104). On giving further heat treatment i.e. at 800 °C for 1, 10, 100 hrs different phases gets nucleated. This temperature is selected on the basis of transition temperature values obtained in DTA.

The X-ray diffraction pattern of INY-2 samples are as shown in 4.105, 4.106 and 4.107 heat-treated at 1, 10, 100 hrs respectively.

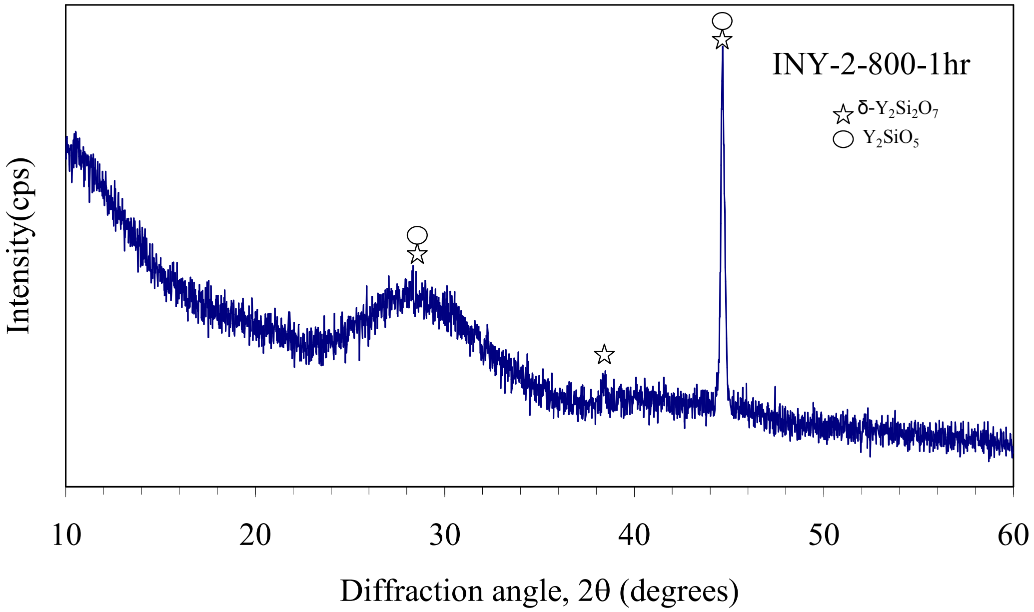

Figure 4.105 XRD pattern of INY-2 glass sample heat-treated at 800°C for 1 hr

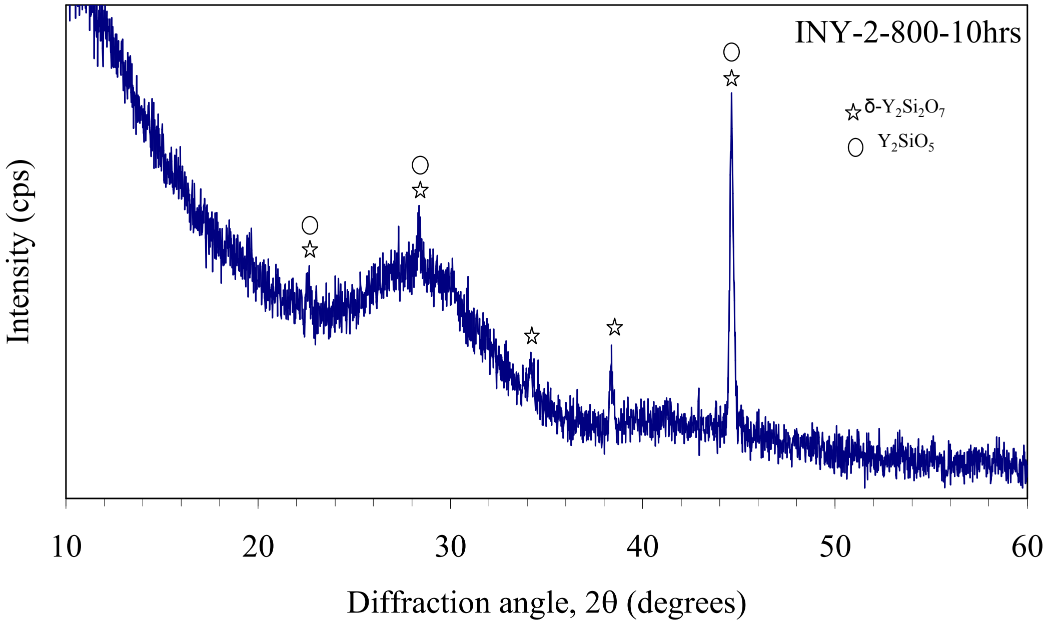

Figure 4.106 XRD pattern of INY-2 glass sample heat-treated at 800^{o}C for 10 hrs

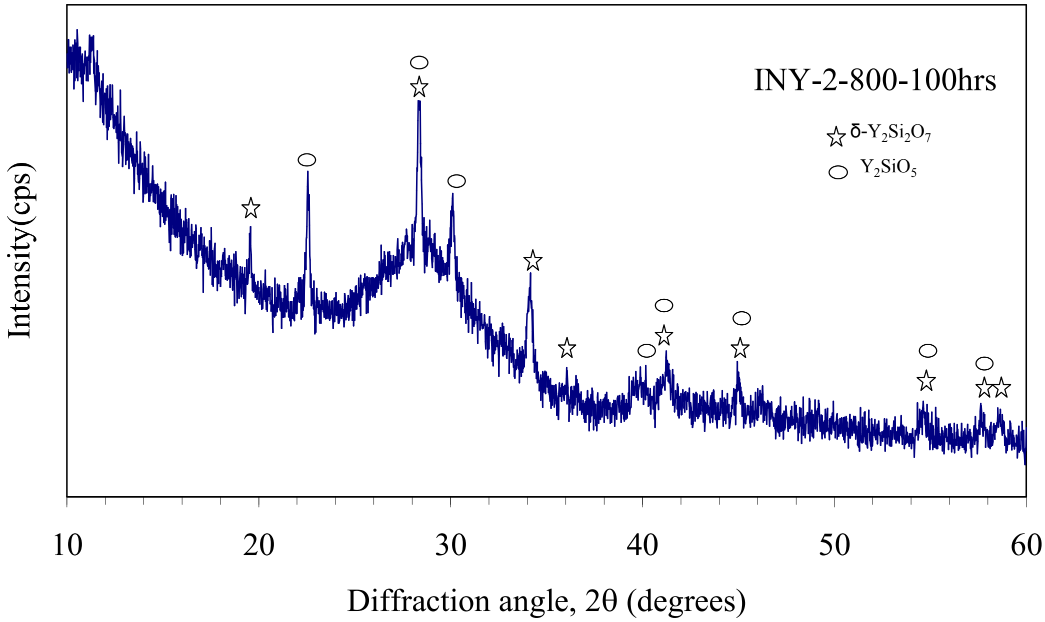

Figure 4.107 XRD pattern of INY-2 glass sample heat-treated at 800^{o}C for 100 hrs

When glass sample INY-2 is heat-treated at 800°C for 1 hr time duration, formation of yttrium silicate (δ-$Y_2Si_2O_7$) (orthorhombic, ICDD card no. 42-0168) phase starts nucleating. A small amount of yttrium silicate (Y_2SiO_5) (monoclinic, ICDD card no. 21-1458) phase formation also occurs. These two phases, which are present during 1 hr heat-treatment, are also present even in 10 and 100 hrs time duration heat-treatment. A careful observation of XRD (INY-2) clearly indicates that the nucleation and growth of $Y_2Si_2O_7$ and Y_2SiO_5 phases are very less as XRD peaks are embedded in large amorphous background. Moreover, both the phases might be metastable in nature. Bahat has reported [44] the heterogeneous nucleation of alkaline earth based glasses by wide variety of nucleating agents. According to Bahat initially higher symmetric phase (like hexacelsian) nucleated more readily from the glasses than the stable forms (monoclinic and triclinic). This can be explained by the simple structures of high symmetry modifications. The hexagonal forms are roughly build [45] of alternate double sheets of tetrahedral and a single layer of R^{2+} cations (R= Ba, Ca, Mg etc.) normal to the c axis. In contrast, the low symmetry forms [46] are made of three dimensional networks in which the Al and Si are atleast partially ordered in a special distribution. Due to these structural differences, the high symmetry forms have lower kinetic barrier for nucleation [38]. The higher temperature phases indicate that there is competition among Zn^{2+}, Ba^{2+} and Al^{3+} (uptake from crucible) with Y^{3+}. Y^{3+} tries to act as network former due to higher oxidation states at higher temperature and becomes part of glassy matrix. Zn^{2+} being volatile in nature will always try to come out and hence precipitate in glassy matrix as $Ba_2Zn_3Si_3O_{11}$ phase.

When this glass sample is given heat treatment at 900°C for 1 hr time duration δ-$Y_2Si_2O_7$ and Y_2SiO_5 phases gets dissolved and barium aluminum silicate ($BaAl_2Si_2O_8$) (hexacelsian, ICDD card no. 88-1048) and barium zinc silicate ($Ba_2Zn_3Si_3O_{11}$) (BZS, ICDD card no. 23-0844) nucleates (fig. 4.108). The long hour annealing at 800 °C indicate that the glass is stable and the dissolution and dissociation of phases do not occur. Moreover, considering its applicability in SOFC it can be said that this glass can provide good compatibility with system at high operational temperature (nearly 1000°C).

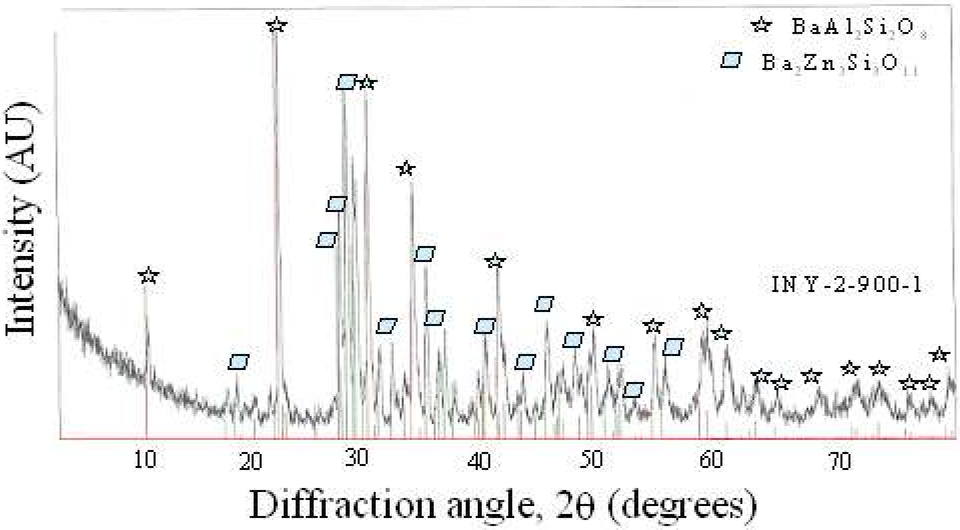

Figure 4.108 XRD pattern of INY-2 glass sample heat-treated at 900°C for 1 hr

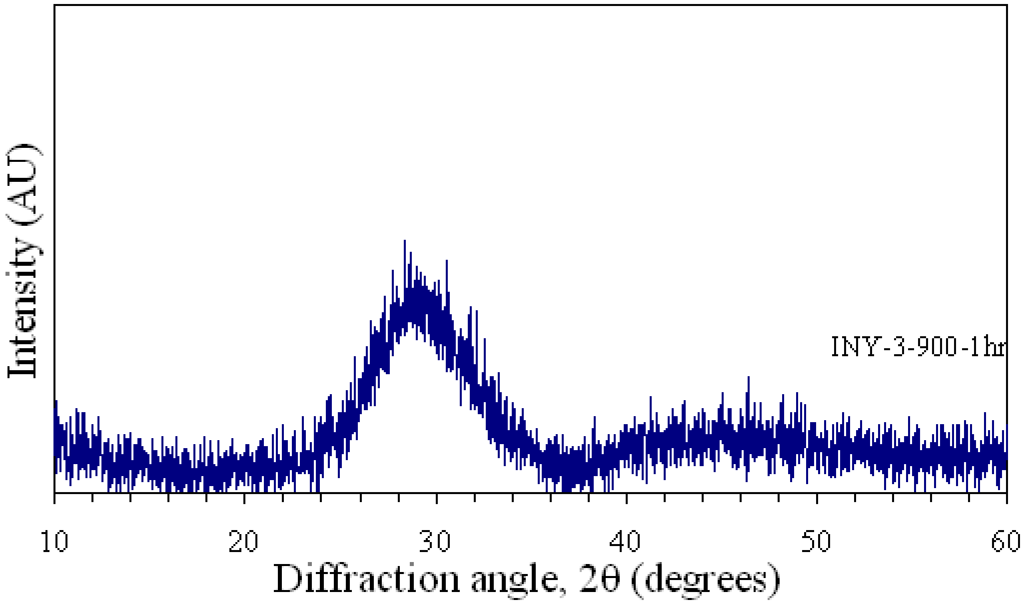

Figure 4.109 XRD pattern of INY-3 glass sample heat-treated at 900°C for 1 hr

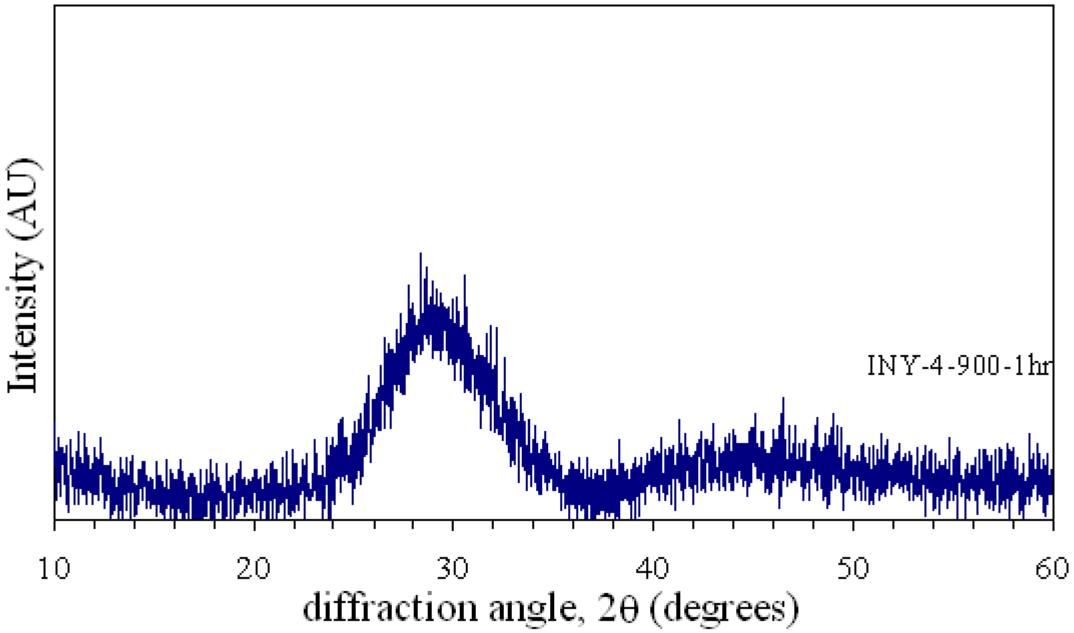

Figure 4.110 XRD pattern of INY-4 glass sample heat-treated at 900°C for 1 hr

When INY-3 and INY-4 samples were heated at 900°C for 1 hr it remains amorphous after heat treatment (fig. 4.109 and 4.110). Yttria amount is maximum (7.5 and 10%) in both these samples and it remains as such. Considering the fact that INY-3 and INY-4 glasses remain in glassy state even at higher temperature annealing (900°C for 1 hr) further heat treatment for higher duration was not done. Singh et al. [28] have reported the effect of Y_2O_3 on T_g, T_c and T_m of the glasses as well as their mechanical properties with higher thermal stability. The addition of high atomic number elements in general increased the rigidity of glass matrix [47].

4.4.4 Scanning Electron Microscope (SEM)

After analyzing the data of thermal analysis and X-Ray diffratogram it was concluded that INY-2 glass exhibits better properties, the microstructural analysis of this glass was done.

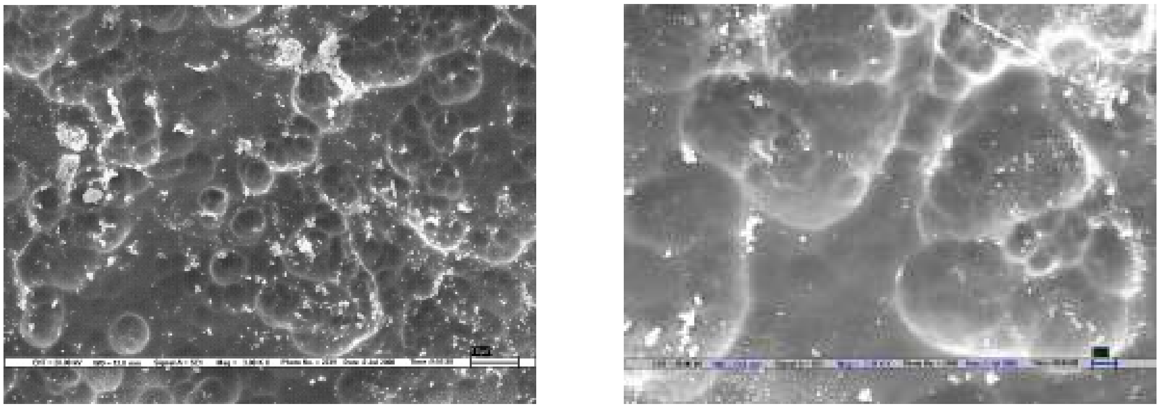

Fig. 4.111(a & b) SEM micrographs of INY-2 glass heat treated at $800^{o}C$ for 100 hrs

Figures 4.111 (a & b) shows the micrographs of INY-2 glass sample which is heat treated at $800^{o}C$ for 100hrs time duration. It is apparent from the micrographs that the nucleation phenomenon is very sluggish in nature. The structural features indicates that the crystallization phase come out from the glass matrix and grows. From the XRD pattern of this glass heat treated at $800^{o}C$ for 100 hrs shows that the crystalline phases are embedded in glassy matrix. The structural growth is continuous process and formed structure is like mushroom.

4.4.5 Conductivity Measurement

Conductivity measurement of INY glass samples is done by plotting real and imaginary values of impedance taken by LCR meter. The obtained values are as given in table 4.30.

Table 4.30 Resistivity values of INY series

Sample ID	Resistivity (MΩcm)
INY-1	0.48
INY-2	0.94
INY-3	0.44
INY-4	0.57

The obtained values of resistivity for INY series are very well fulfilling the required condition to use this glass series as a sealant. In above series INY-2 sample exhibits higher resistivity than other samples. It is again a manifestation that this sample shows higher thermal stability with higher activation energy for crystallization.

References

[1] H.E. Kissinger, Anal. Chem. 29 (1957) 1702.

[2] A. Hruby, Czech. J. Physlk B 22 (1972) 1187.

[3] S. Mahadevan, A. Giridhar, A.K. Singh, J. Non-Cryst. Solids 88 (1986) 11.

[4] M. Saad, M. Poulin, Mater. Sci. Forum 19&20 (1987) 11.

[5] R. Bohmer, K.L. Nagi, C.A. Angell, D.J. Plazek, J. Chem. Phys. 99 (1993) 4201.

[6] K. Chebli, J.M. Saiter, J. Grenet, A. Hamou, G. Saffarini, Physica B 304 (2001) 228.

[7] M.M. Wakkad, E.K. Shokr, S.H. Mohamed, J. Non-Cryst. Solids 265 (2000) 157.

[8] T.A. Viglis, Phys. Rev. B 47 (1993) 2882.

[9] R. Bohmer, C.A. Angell, in: R. Richert, A. Blumen (Eds.), Disorder Effects on Relaxation Processes, Springer, Berlin, 1994.

[10] A. Arora, E.R. Shaaban, K. Singh, O.P. Pandey, J. Non-Cryst. Solids 354 (2008) 3944.

[11] W.A. Johnson, R.F. Mehl, Trans. Am. Inst. Min. Met. Eng. 135 (1939) 416.

[12] M. Avrami, J. Chem. Phys. 8 (1940) 212.

[13] M. Avrami, J. Chem. Phys. 9 (1941) 177.

[14] J. Vázquez, C. Wagner, P. Villares, R. Jim!enez Garay, J. Non-Cryst. Solids 235 (1998) 548.

[15] Yi Qun Gao, W. Wang, F.Q. Zheng, X. Liu, J. Non-Cryst. Solids 81 (1986) 135.

[16] K. Matusita, S. Saka, J. Non-Cryst. Solids 38&39 (1980) 741.

[17] K. Matusita, T. Konatsu, R. Yorota, J. Mater. Sci. 19 (1984) 291.

[18] H. Yinnon, D.R. Uhlmann, J. Non-Cryst. Solids 54 (1983) 253.

[19] E. Tkalcec, S. Kurajica, H. Ivankovic, Thermochim. Acta 378 (2001) 135.

[20] V.N. Sigaev, E.V. Lopatina, P.D. Sarkisov, A. Marotta, P. Pernice, Thermochim. Acta 286 (1996) 25.

[21] Y.M. Sung, J. Mater. Sci. 31 (1996) 5421.

[22] N. Lahl, K. Singh, L. Singheiser, K. Hilpert, D. Bahadur, J. Mater. Sci. 35 (2000) 3089.

[23] A. Arora, A. Goel, E.R. Shaaban, K. Singh, O.P. Pandey, J.M.F Ferreira, Phys. B 403 (2008) 1738.

[24] J. Va´ zquez, C. Wagner, P. Villares, R. Jime´ nez-Garay, Acta Mater 44 (1996) 4807.

[25] M.J. Davis, P.D. Ihinger, Am. Miner. 83 (1998) 1008.

[26] K.A. Jackson, Liquid Metals and Solidification, vol. 174, ASM, 1958.

[27] K.A. Jackson, J.D. Hunt, Acta Met. 13 (1965) 1212.

[28] K. Singh, Neha Gupta, O.P. Pandey, J. Mater. Sci. 42 (2007) 6426.

[29] M.H. Lewis, J.M. Johnson, P.S. Bell, J. Am. Ceram. Soc. 62 (1979) 278.

[30] D. Turnbull, Contemp. Phys., 10 (1969) 473.

[31] C. Lara, M. J. Pauscal, A. Duran, J. Non-Cryst. Solids 348 (2004) 149.

[32] C. H. Drummond III and N. P. Bansal, Ceram. Eng. Sci. Proc. 11 (1990) 1072.

[33] M. J. Hyatt and N. P. Bansal, J. Mater. Sci. 31 (1996) 172.

[34] Y.-M. Sung, J. Mater. Sci. 35 (2000) 4913.

[35] N. A. Toropov, F. Y. Galakhov and I. A. Bondar, Izvest. Akad. Naak S.S.S.R, Otdel. Khim. Naak 5 (1954) 756.

[36] S. B. Sohn, S. Y. Choi, G. H. Kim, H. S. Sung and G. D. Kim J. A. Ceram. Soc. 87[2] 254 (2004)

[37] M. A. Matveev, G. M. Matveev and B. N. Frankel, Holon, Israel, 1975, p. 14.

[38] N. P. Bansal and M. J. Hyatt, J. Mater. Res. 4(5) (1989) 1257.

[39] J. D. Lee, Concise inorganic chemistry, 4th edition, Chapman and Hall, London, (1993) 683.

[40]S. Morimoto and N. Kuriyama, J. Cera. So. Jpn, 104 (5) (1996) 442.

[41] F. E. Diasty, F. A. A. Wahab and M. A. Baki, J. App. Phys. 100 (2006) 093511

[42] A. Aronne , S. Esposito, P. Pernice, Mater. Chem. Phys. 1997; 51(2): 163.

[43] R. G. Duan and K. M. Liang, J. Mater. Proc. Tech. 75 (1998) 235.

[44] D. Bahat, J. Mater. Sci. 4 (1969) 855

[45] T. Ito, R. Sadanaga, and Y. Takeuchi, X-Ray Studies on Polymorphism, Maruzen Co. Ltd., Tokyo, Japan, 1950.

[46] R.E. Newnham and H.D. Megaw, Acta Cryst., 13(1960) 303.

[47] J. A. Haidary, M.A. Haidari and S. Qrunfuleh Biomed. Mater. 3 (2008) 015005

[48] V. Kumar, A. Arora, O.P.Pandey and K. Singh, Int. J. Hyd. Eng. 33(1) (2008) 434.

Chapter 5

Interaction Study

Overview

An important aspect of glass sealants is their interaction with other components of SOFC. Fuel cells have operating temperature in the range of 800-1000 ^{o}C. In order to study the suitability of glasses as sealing material their interaction study with other components of SOFC is required. In this chapter the interaction study of some selected glasses with bismuth vanadate and 8YSZ (electrolyte) and Crofer 22 APU (interconnect) is described. For this study glass powder was sandwiched between bismuth vanadate and Crofer 22 APU and heated at 800 ^{o}C for 100 hrs. The reaction products at the interfaces were analyzed under scanning electron microscope. X-ray diffraction study was done for selected samples.

5.1 Introduction

In order to develop a suitable sealing material for a planer SOFC, several sealing materials have been tested. Among these glass and glass ceramic materials have been found to be most suitable as these can meet the requirement of an ideal sealant. These substances exhibit better mechanical properties as the process of nucleation of different crystalline phases and their volume fraction varies with variation in temperature. The controlled crystallization process when temperature is varied leads to have a different thermal expansion coefficient (TEC) of these phases which in turn dominates the behavior of glass when in contact with other components of SOFC. Moreover, the chemical composition of glass can be tailored so as to control the required physical properties such as TEC and viscosity. In this regard many glasses of different compositions have been developed [1-8].

In the present chapter some of the selected glass samples of different compositions have been used to see their behavior when in contact with other components of SOFC. In order to join dissimilar materials such as Crofer 22 APU as an interconnect and bismuth vanadate and 8YSZ as electrolyte, the present study has been taken. This type of study has been done by other researchers [9-12] but considering the requirement where tolerance limit has its own importance because of the thermo mechanical stress, the development of different categories of glasses are being done. This is a preliminary study with the present glass system which will open a new area for the study in detail.

5.2 Interconnects

The interconnect connects the anode side of one single cell with the cathode side of the adjacent single cell, thus preventing the fuel and oxidant gases from mixing. The interconnect is sometimes designated as bipolar plate, or separator, emphasizing the different polarities of anode and cathode which it connects or the gas separation, respectively. The availability of a suitable material for the interconnect is of key importance for solid oxide fuel cell (SOFC) development [13].

The interconnect has to meet the following requirements:

- high electronic and low ionic conductivities (electrical conductivity $>1 \mathrm{Scm}^{-1}$);
- chemical stability under the reducing and oxidizing conditions at the anode and cathode sides of the cell at temperatures of up to 1000 ^{o}C
- gas tightness;
- thermal expansion coefficient matching with that of other cell components;
- low costs.

Ceramic and metallic interconnects are the most widely used substances. The ceramic interconnect materials used are $LaCrO_3$ base perovskites. They are used for tubular cell configurations as well as for monolithic and planar design of SOFC. There is a general trend towards using metallic interconnects in planar cells due to their relatively low costs, easy working potential, as well as high electrical and thermal conductivity. In recent years metallic materials have gained more and more attention as possible replacements for ceramics as construction materials for interconnects in SOFCs [14, 15]. Metals and alloys offer a number of advantages over ceramic materials in planar designs [16, 17]. Compared to the La-chromite-based ceramics, metallic materials are easier, and therefore cheaper to fabricate, they are less brittle, easier to machine and they can be joined using a number of standard welding and brazing techniques. Additionally, they possess higher electrical and thermal conductivities than most ceramic materials. If one has to consider resistance to high temperature corrosion [16] as the most important interconnector property, alloys of the type Ni-Cr-Al, Co-Cr-Al and especially Fe-Cr-Al would be the materials to select. The materials most frequently studied for SOFC interconnect application are based on the binary alloy system, Fe-Cr. Thus, the interconnects should have TEC in the range of $11–12 \times 10^{-6}$ K^{-1} in order to fulfill the requirement for other components of SOFC from application point of view.

Crofer 22 APU completely fulfills the requirements for suitability with other cell components as it has thermal expansion coefficient in the range 12 X 10^{-6}/K which is in compatibility with the widely used 8YSZ (yttria stabilized zirconia) electrolyte material which has TEC value in the range 10.8 X 10^{-6}/K. In the present study Crofer 22 APU is used as an interconnect material which is widely used commercially and for the research purpose too. The composition of Crofer 22 APU is given in table 5.1 below.

Table 5.1 Composition of Crofer 22 APU (interconnect)

Element	Wt. % composition
Cr	22.6
Fe	76.6
Mn	0.4
Si	0.017
Ti	0.06
P	0.013

5.3 Electrolytes

The ionic conductivity is a critical property of a solid electrolyte which determines the efficiency and operating temperature of electrochemical cells. Solid electrolyte must have high ionic conductivity at the operating temperature to allow efficient transfer of ions from the cathode to anode and also a low electronic conductivity to prevent electron leakage across the cell.

Solid compounds that exhibit the high ionic conductivity are termed as solid electrolytes. Solid electrolytes have either mobile anions or cations, which due to their high degree of disorder are free to move throughout the structure. The maximum ionic conductivity of these materials lies between 0.1 and 10 ohm^{-1} cm^{-1}. Thus, these materials are intermediate in between normal crystalline solids and liquid electrolytes. Different solid electrolytes can be broadly categorized as follows:

(i) Crystalline Electrolytes
(ii) Glass Electrolytes
(iii) Polymer Electrolytes

5.3.1 Characteristics of Solid Electrolytes

Good electrolyte is supposed to have crystal structures with open channels, layers so as to provide pathways for easy ionic transport via hopping mechanism. High conducting electrolytes are required to fulfill the following conditions:

a) Availability of large number of free ions
b) Large number of vacancies for hopping

c) Same energies of the occupied and vacant sites

d) Three dimensional networking through open channels for the migration of ions

e) High polarizability of the anion framework

The performance of electrolytes depends upon the number of above mentioned parameters. Various electrolyte materials which are currently in use as a solid electrolyte in different devices are discussed below:

5.3.1.1 Zirconia-based Oxide Ion Conductors

In pure ZrO_2, ionic conductivity is very low because of presence of low concentration of the oxide ion vacancies and interstitial oxide ions. However, when yttria is added, the conductivity increases significantly. Yashima *et al.* [18] surveyed the phase diagrams of doped zirconia systems, including ZrO_2-Y_2O_3 [19] and ZrO_2-Sc_2O_3 [20]. The dopant Sc^{3+} (0.81 Å), which has the closest ion radius to the host ion, Zr^{4+} (0.80 Å), shows the highest conductivity and higher doping level as compared to yttrium doping. For electrolytes, high electrolyte strength and toughness are also desirable in addition to high ionic conductivity especially for its applications in solid oxide fuel cell.

5.3.1.2 Ceria-Based Oxide Ion Conductors

CeO_2 doped with CaO, Y_2O_3, Sm_2O_3, Gd_2O_3 and a number of other rare earth oxides have high oxygen ion conductivity. However, the ionic conductivity regime is rather narrow. Ceria-based oxide ion conductors are reported to have purely ionic conductivity at high oxygen partial pressures. However, in reducing environments, ceria based systems lose oxygen and develop electronic conductivity behavior at 800 ^oC [21].

5.3.1.3 Bi_2O_3-Based Oxide Ion Conductors

Electrolyte material such as doped bismuth oxide exhibit superior ionic conductivity over YSZ and CeO_2 based electrolytes at lower temperature [22]. The coefficient of thermal expansion is very important factor while fabricating electrochemical devices. The value of TEC in Bi_2O_3 based oxide ion conductors comes out to be 11 X 10^{-6}/K at operating temperature of 25-730 ^oC [23]. The electrolyte material which is selected to study the interaction properties has composition $Bi_4V_{2-x}Ti_xO_{11}$. In earlier studies, most of the research work has been carried out with titanium (IV) substitution [24-26] on V^{5+} sites. But in the present study, Ti^{3+} was used to study the effect on phase stabilization and conductivity measurement. However, it might be possible that Ti^{3+} gets converted into

Ti^{4+} (most stable state) during processing of the sample under experimental conditions. Ti^{4+} has better ionic conductivity value as compared to the other doped samples. The conductivities a value of selected electrolyte at 300 °C is summarized in table 5.2.

Table 5.2 The ionic conductivity of $Bi_4V_{2-x}Ti_xO_{11-\delta}$ ($0.1 \leq x \leq 0.4$)

Composition	$\sigma_{300}{}^{o}C$ (S/cm)
x = 0.1	9.59×10^{-6}
x = 0.2	1.62×10^{-5}
x = 0.3	1.72×10^{-5}
x = 0.4	2.66×10^{-5}

Based on the better properties of $Bi_4V_{2-x}Ti_xO_{11}$ (x= 0.4), this electrolyte is selected to check its chemical compatibility with our glass samples.

5.4 Experimental procedure

The interaction among these three components (Crofer 22 APU-glass sealant-bismuth vanadate) was studied by sandwiching glass sealant between interconnect (Crofer 22 APU) and electrolyte (bismuth vanadate) (fig. 5.1). For this study finely powdered glass was mixed in 2% PVA (poly vinyl alcohol) to form a paste. This paste was applied uniformly over the surfaces of interconnect and electrolyte to be joined together. The entire assembly was joined together to have a sandwitch of electrolyte, glass sealant and Crofer 22 APU as shown in fig 5.1. The entire assembly was kept under pressure of 2 kg load to have a contact till the paste dries out. This combination of glass sealant sandwiched between electrolyte and interconnect was placed in high resistance furnace in air and given a heat treatment for 100 hrs at a temperature of 800 °C. After the heat treatment the system was mounted in acrelic media using hardener. This was done to keep the mass intact. After that the sample was carefully polished as is being done for other substance. The surface was etched by 2% HF for 30 sec and analysed under optical microscope (Nikon eclipse MA-100). Once the structural visibility was confirmed it was sputter coated with carbon for SEM studies.

Figure 5.1 Glass sealant sandwiched between Crofer 22 APU and bismuth vanadate

Similarly a thin coating of 8YSZ was applied on glass using PVA as binder. The assembly was also given heat treatment at 800 ^oC for 5 to 36 hrs and also at 850^oC for 36 hrs. Only X-Ray diffraction study of this was done to find out the formation of different phases.

5.5 Results and Discussion

Among all the glass series studied in this work it was observed that INL and INY exhibit better thermal and physical properties as shown in table 5.3 below:

Table 5.3 Thermal and Physical properties of INL-3 and INY-4 glass samples

Sample ID	T_g (^oC)	TEC (X 10^{-6}/K)	% change in weight (50-1000 ^oC)
INL-3	770	8.2	0.04
INY-2	740	8.1	0.008

As is evident form the table INL-3 glass sample in INL series and INY-2 glass sample in INY series exhibit better coefficient of thermal expansion i.e.8.2X10^{-6}/K and 8.1X10^{-6}/K respectively. These samples exhibit lowest change in weight % value as compared to the other glasses present in the series which is basic requirement for using these glasses as sealant material. In order to see the feasibility of using them in actual unit, it is essential to find out their long term behavior when these glasses are in contact with other constituents of SOFC materials. In this current section interaction study of only these glasses with electrolyte and interconnect is being presented.

In the present study $Bi_4V_{2-x}Ti_xO_{11}$ is selected as electrolyte for the interaction phenomenon as it exhibits better ionic conductivity at low temperature as has been reported in literature [27-30]. The conductivity of this particular sample has maximum value at 300 ^oC which is of the order of 2.66X10^{-5} S/cm (about 24 times higher than that of the base compound $Bi_4V_2O_{11}$), for x=0.4. Because of its better properties i.e. high value of ionic conductivity bismuth vanadate (titanium doped) is used to study the interaction with glass samples. Crofer 22 APU is widely used as an interconnect material to study the interaction behavior with other components of fuel cell such as anode, cathode and sealant. The major reason for the wide use of Crofer 22 APU as interconnect in SOFC is its compatible thermal expansion coefficient (TEC) value with the widely used YSZ (yttria stabilized zirconia) as electrolyte. It has thermal expansion coefficient value in the range 12 X $10^{-6}/^{o}C$, which is very near to that of YSZ electrolyte (~10.8 X $10^{-6}/^{o}C$) [31, 32]. Because of thermal expansion match in Crofer 22 APU interconnect adhere well with YSZ electrolyte and hence is widely used.

5.5.1 Interaction study of INL-3 glass sample with interconnect and electrolyte

As described earlier heat treatment at 800 ^{o}C for 100 hrs was given to composite (fig. 5.1) for some selected samples. After the heat treatment the system was studied under SEM and the micrographs were recorded. SEM images of INL-3 glass interfaces are given in figures 5.2-5.5. Figure 5.2 shows the SEM micrograph of interconnect (Crofer 22 APU)-glass sealant (INL-3)-electrolyte (bismuth vanadate). It is clear from the figure 5.2 that the glass starts crystallizing at 800 ^{o}C and its volume fraction increases due to long hour (100hrs) holding but there is no appreciable interaction between interconnect and sealant because of their TEC mismatch. The TEC of INL-3 glass is 8.2 X $10^{-6}/^{o}C$ whereas thermal expansion coefficient value of Crofer 22 APU is 12 X $10^{-6}/^{o}C$ [33]. Both these materials did not show any diffusion behavior. Figure 5.3 shows the micrograph of the glass-interface-electrolyte zone where diffusion layer at the interface can be seen. This is observed at sealant and electrolyte junction. It is apparent from this structure that both glass and electrolyte phases are diffusing in each other. Careful examination at this interface reveals that fluid flow condition at 800 ^{o}C for long hours heat treatment has been achieved. The flow curvature observed within the interface indicates that both are trying to make a compatable band with each other. The area at glass side at the interface has different appearance. This indicates that in the beginning the inter diffusion phenomenon is at higher rate. Once the steady state is achieved, the interface form compound which has low melting point as compared to glass and electrolyte. This river flow pattern observed is a proof of liquid state reaction at the interface (fig. 5.3 b).

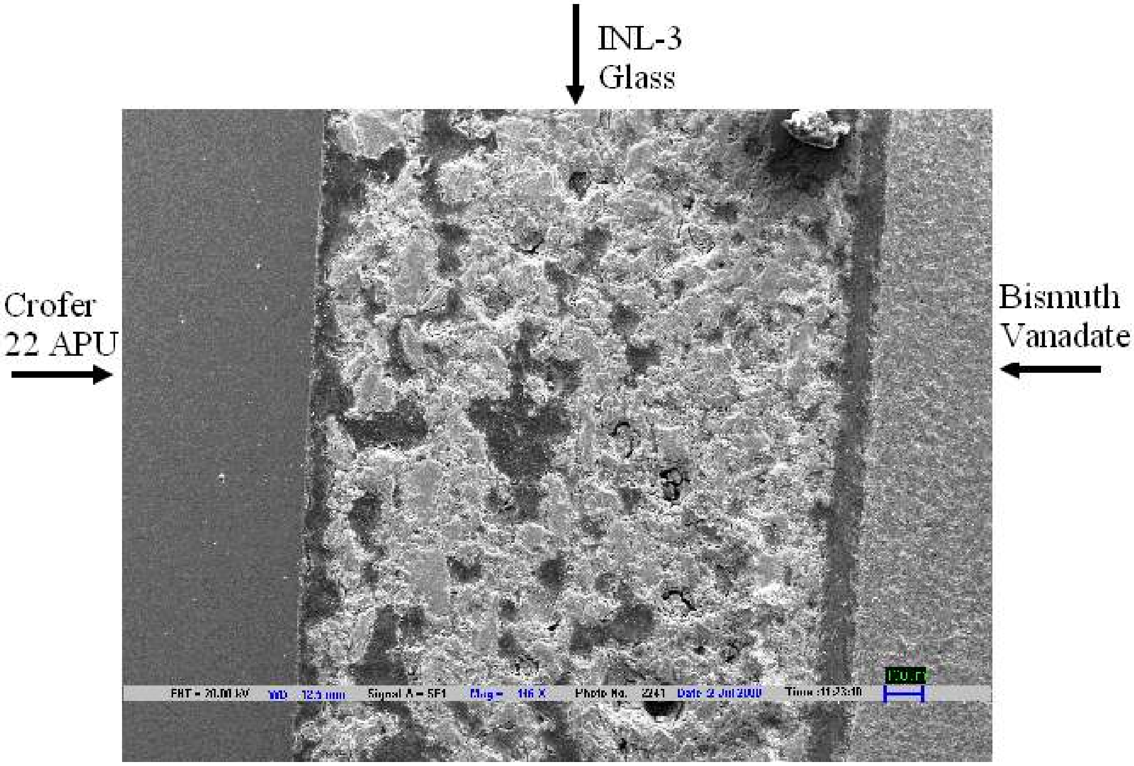

Figure 5.2 SEM micrograph of INL-3 glass sample heat treated at 800 °C for 100 hrs along with electrolyte (bismuth vanadate) steel Crofer 22 APU) sealant

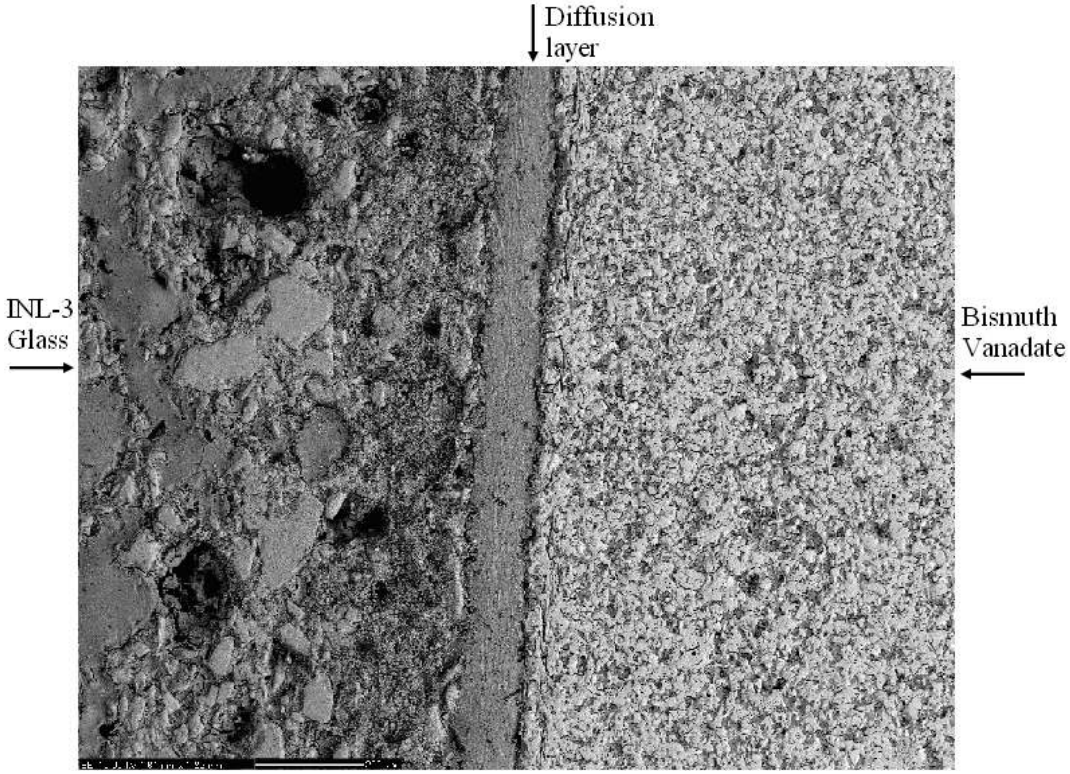

Figure 5.3(a) SEM micrograph of sealant (INL-3) and electrolyte (bismuth vanadate)

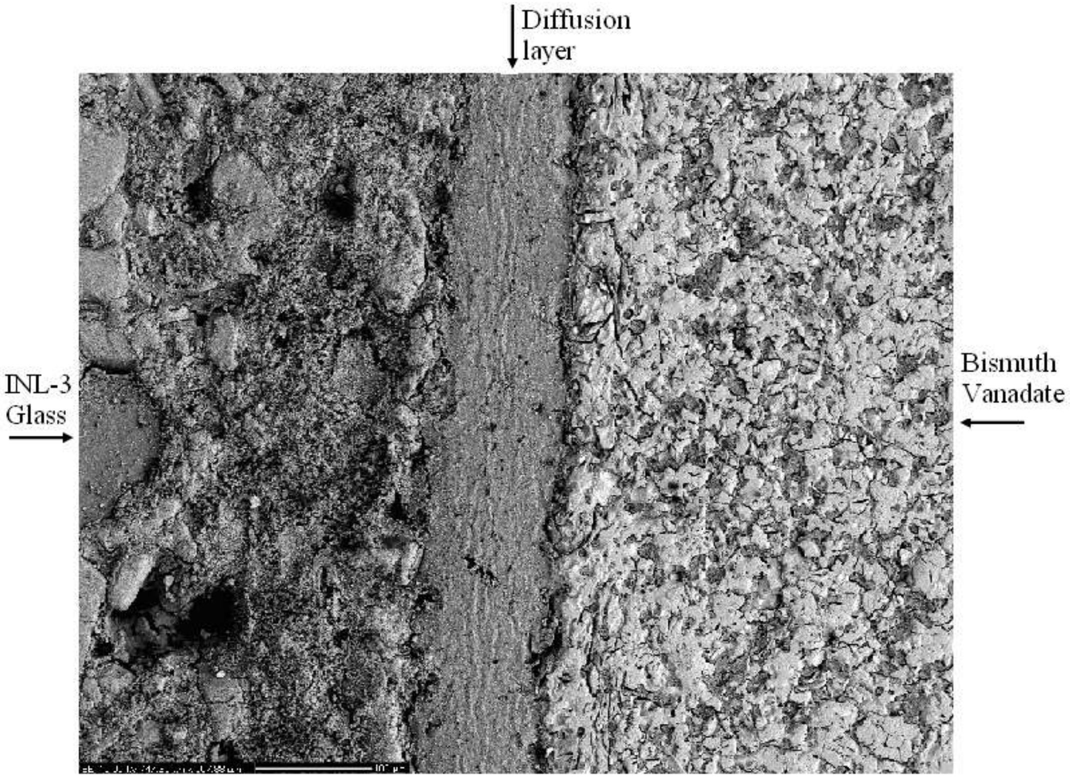

Figure 5.3(b) Higher magnification SEM micrograph of sealant (INL-3) and electrolyte (bismuth vanadate)

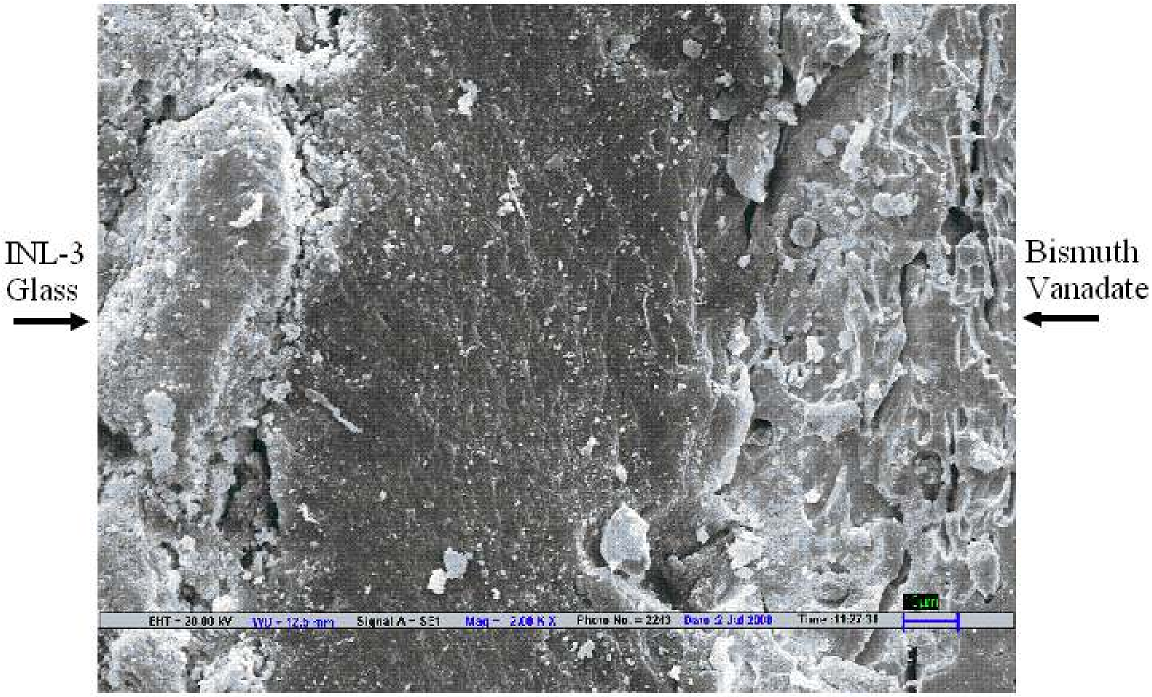

Figure 5.3(c) SEM micrograph of sealant (INL-3) and electrolyte (bismuth vanadate)

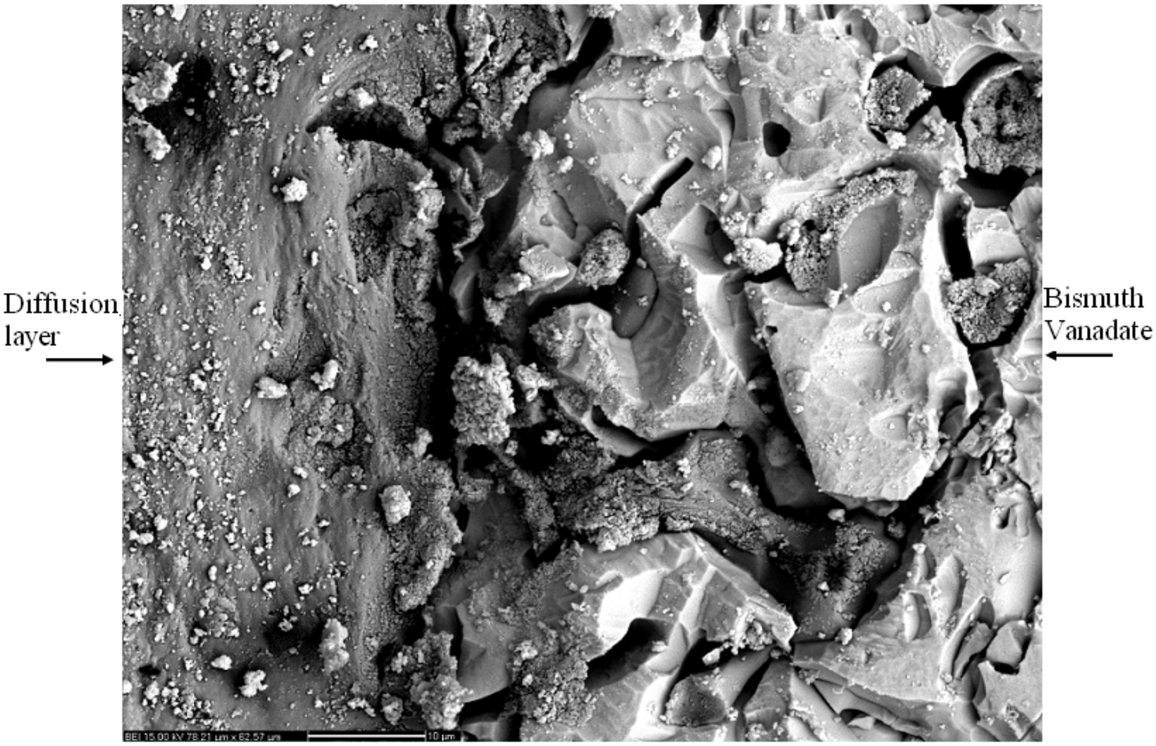

Figure 5.4 SEM micrograph of diffusion layer of INL-3 glass sample and electrolyte

Higher magnification micrograph (fig. 5.3c) shows that the interfacial layer is compact in nature and dense. However, the electrolyte has developed more cracks. These cracks are developed because of thermal mismatch. Moreover, within the electrolyte material different structures along the crack boundary is seen. This is only feasible when the molten fluid is flowing through these cracks. This indicates that even at long duration interaction study the reactivity at interface is not completed (fig. 5.4).

At the same time Crofer-glass interface is smooth in nature. At the interface glass gets melted to fill the voids existing at the interface. The lamellar fluid flow morphology at interface is proof of the observation. Higher magnification micrograph indicate that glass has not bonded with Crofer completely (fig. 5.5b). This phenomenon can be seen as most pronounced one in fig. 5.5c where cracks at the interface can be seen. It is obvious that such type of structure may arise because of thermal mismatch. The reaction product of electrolyte, glass and Crofer can be seen in figure 5.6 where the morphology is totally different.

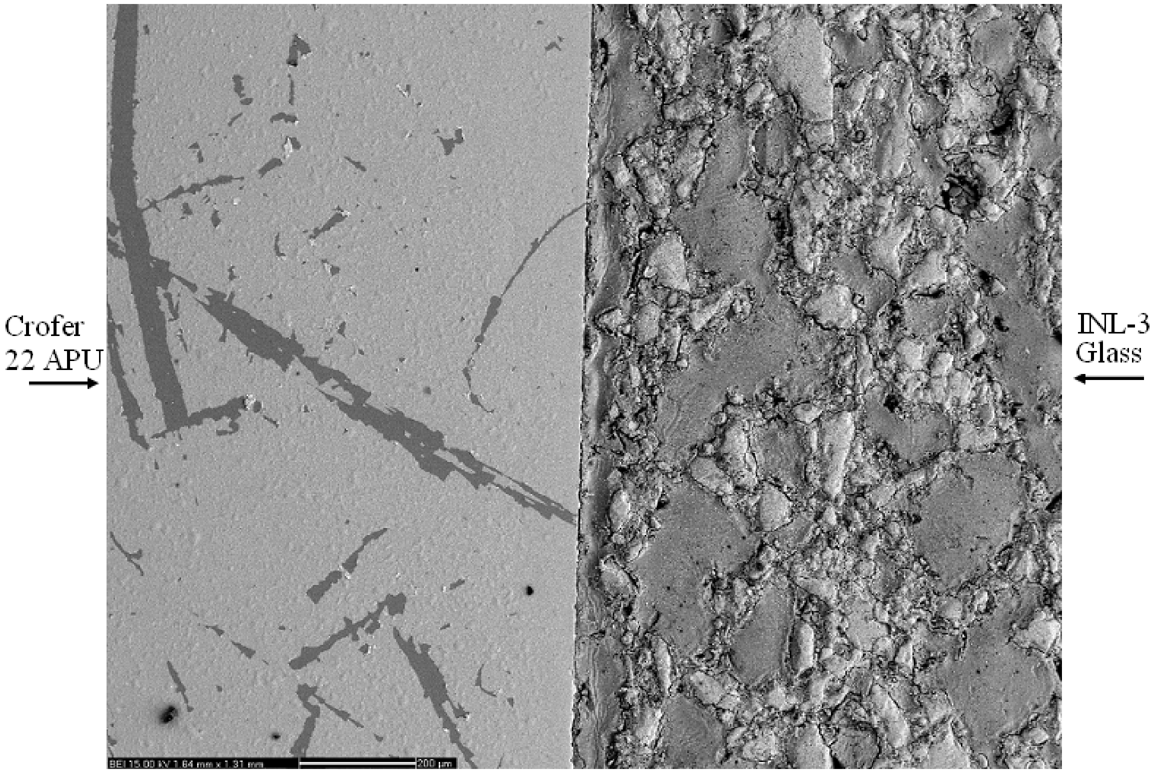

Figure 5.5 (a) SEM micrograph of interconnect (Crofer 22 APU) and sealant (INL-3)

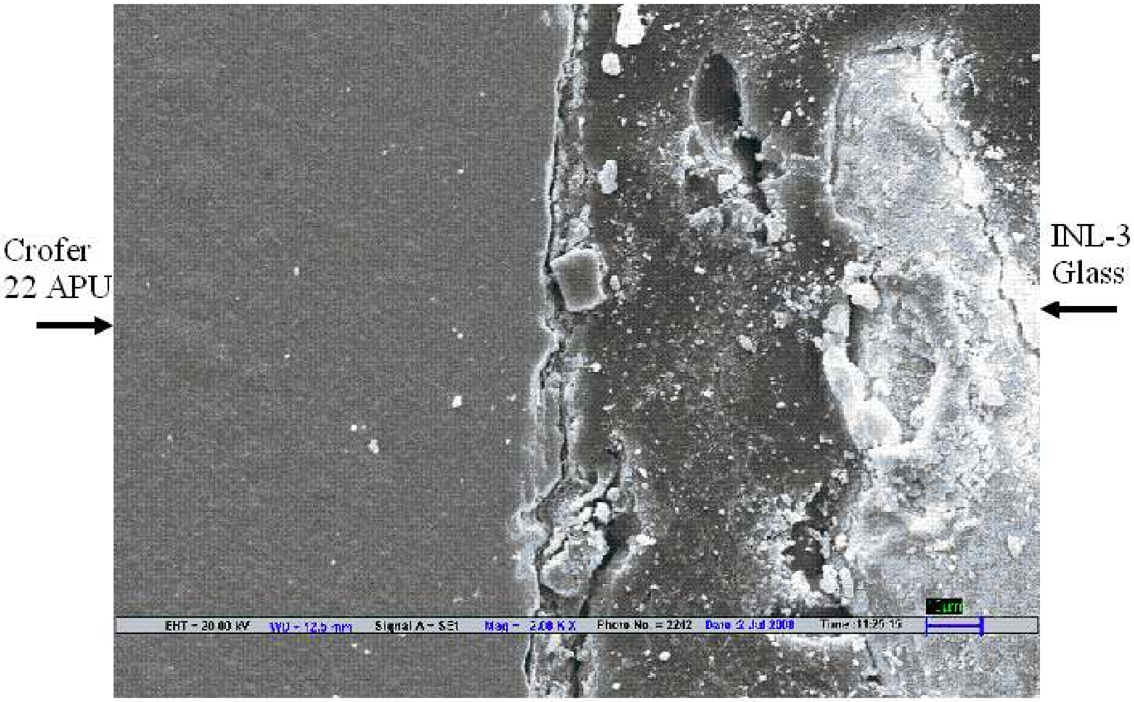

Figure 5.5 (b) SEM micrograph of interconnect (Crofer 22 APU) and sealant (INL-3)

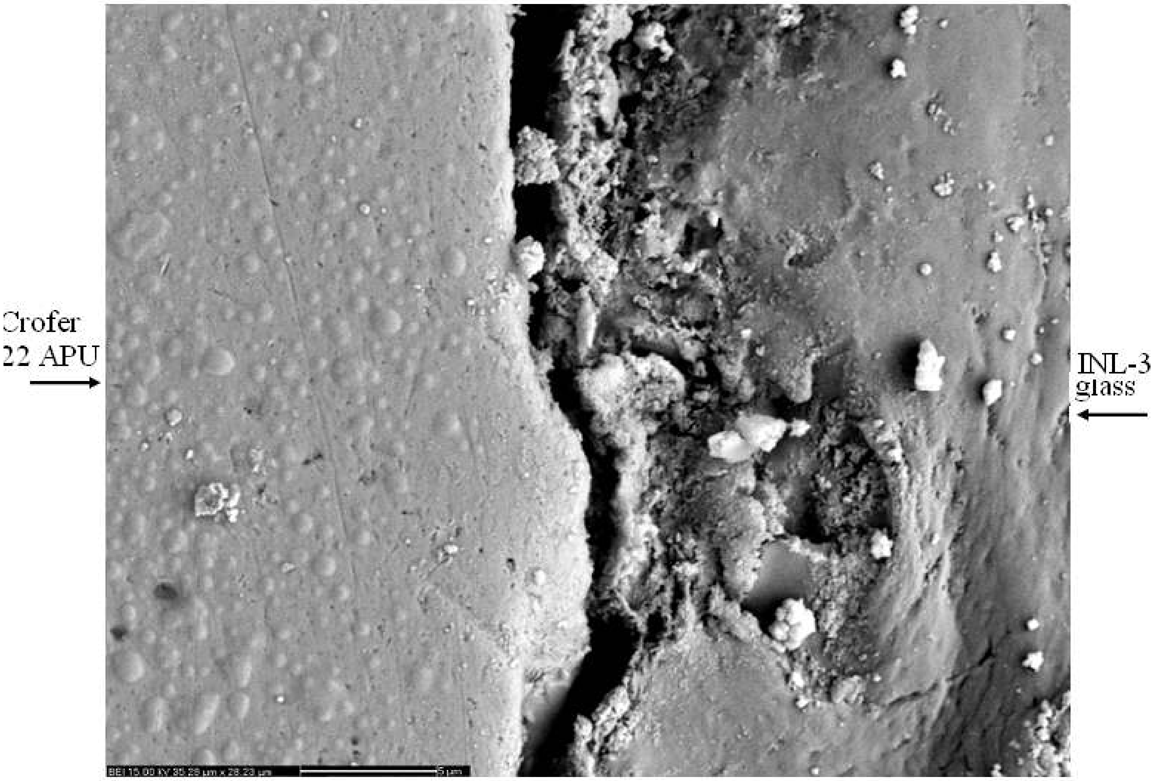

Figure 5.5 (c) SEM micrograph of interconnect (Crofer 22 APU) and sealant (INL-3)

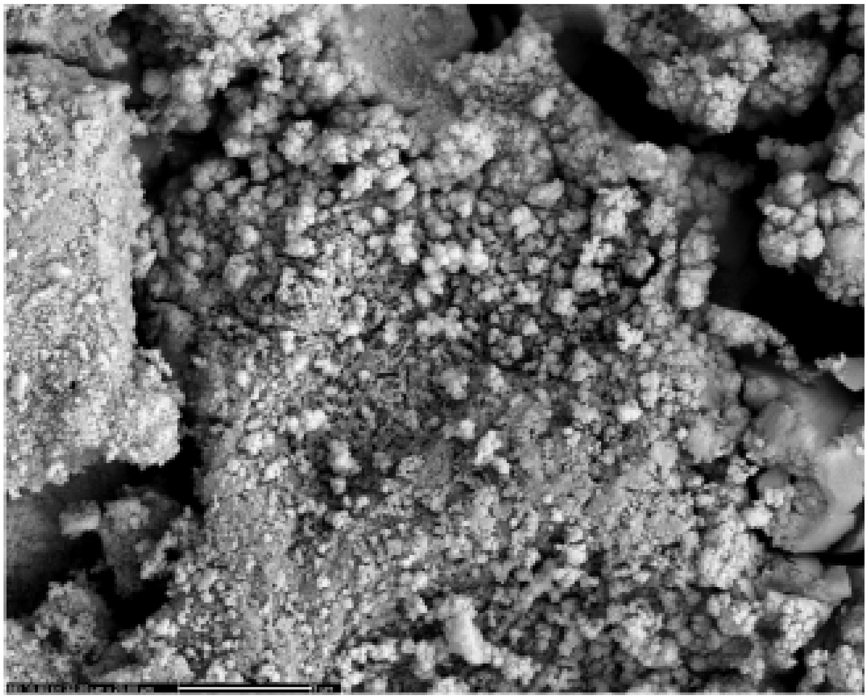

Figure 5.6 SEM micrograph of sealant (INL-3)

5.5.2 Interaction study of INY-2 glass sample with Interconnect (Crofer 22 APU) and Electrolyte (Bismuth Vanadate)

Figure 5.7 shows the SEM micrograph of interconnect (Crofer 22 APU)-glass sealant (INY-2)-electrolyte (bismuth vanadate). Figures 5.8 (a-d) shows the SEM micrographs of glass sealant-diffusion layer-electrolyte at low and high magnifications. Figures 5.9 (a-c) shows the SEM images of interconnect-glass sealant at low and high magnification. Figure 5.10 (a-c) shows the SEM micrographs of INY-2 glass heat treated at 800^{o}C for 100 hrs time duration at low and high magnifications.

The structural features of the heat treated composite give two basic information. The crofer-glass interface is not bonded rigidly. The cracks developed in the glassy matrix at the interface indicate a thermal mismatch. However, the glass is not completely crystallized which is good for achieving good bonding characteristics. Secondly the diffusion has occurred at both the interfaces (fig. 5.7). The glass sealant and electrolyte interface indicate that the interdiffusion of glass and electrolyte substance has occurred. A thin layer has formed at the interface. This layer has formed due to melting at the interface (fig. 5.8a). When glassy matrix is analyzed around the interface it gives the information that melting inside the glass matrix has occurred upto a long distance whereas this is not existing in the electrolyte matrix. The area in the glassy matrix near the interface has completely dissolved leading to the formation of fine crystalline structure (fig. 5.8a). As proceeded away from the interface big chunk of mass having flow pattern which a typical characteristic of structure derived from liquid state can be seen. Even in this area faceted structure of glass which has not reacted can be seen (fig. 5.8a). The interfacial crack due to thermal mismatch is observed towards electrolyte matrix (fig. 5.8a). The higher magnification micrograph indicates that electrolyte matrix around interface is more in strained condition causing multiple cracks (fig. 5.8b). However, the interfacial layer is very rigid. When analyzed at different places, it was observed that the interface has appearance of river bed pattern indicating that solidification derived from liquid mass has occurred. The reaction has initiated from electrolyte and the liquid mass has migrated inside the glassy matrix like tributary of river. Since melting has occurred from electrolyte side the development of cracks at the surface of electrolyte can be seen (fig. 5.8c). However, these cracks have appeared in both sides of interface (fig. 5.8d). The cracks appearing in electrolyte matrix is because of solidification shrinkage (fig. 5.8d); as is apparent from flow pattern.

When the interconnect and glassy matrix interface is analyzed the structure gives different appearance (fig. 5.9a). Crofer is not at all reacting with glass. The flow pattern existing at the interface in glassy matrix indicates that it is derived from liquid state. The migration of liquid starts from the electrolyte glass interface and it flows through channels existing in the glassy matrix. Since fine glass powders of micron size were kept along with binder, it is possible that evaporation of binder may provide interconnecting channels. The binder existing at Crofer 22 APU- glass interface has evaporated leading to formation of drain. This is filled by liquid. Moreover, glass frits are also visible within the solidified mass. The micro cracks existing are because of solidification shrinkage (fig. 5.9a). Higher magnification micrograph (fig. 5.9b) reveals that no bonding has occurred at the interface. Moreover, crofer has also reacted with glass/ electrolyte products as can be seen in figure 5.9c. The appearance of cracks at the interface indicates that thermal expansion coefficient of both phases are different (thermal mismatch). Analysis of glassy phase indicates that it has also reacted even at the middle of zone in between crofer and electrolyte (fig. 5.10a). Micro cracks appear because of this reaction. Fine glass powders have reacted first creating liquid interface. The cracks observed are due to solidification shrinkage at the interface of glass powders. When solidified mass existing in between glass powders were analyzed, it was observed that within this mass lot of cracks exist (fig. 5.10b). Structure of this liquid derived mass when visualized at higher magnification also reveals cracks-indicating poor compatibility of the system (fig. 5.10c).

Since it was not possible to do EPMA of these phases, it is difficult to derive any conclusive remark. However, one basic information from this analysis can be derived is that the system is not compatible.

In order to see the interfacial reactivity of these glasses with YSZ where sufficient literature exists for its compatibility, a separate study was done [34-36]. However, X-ray study was done to see the formation of different phases which is presented in next section.

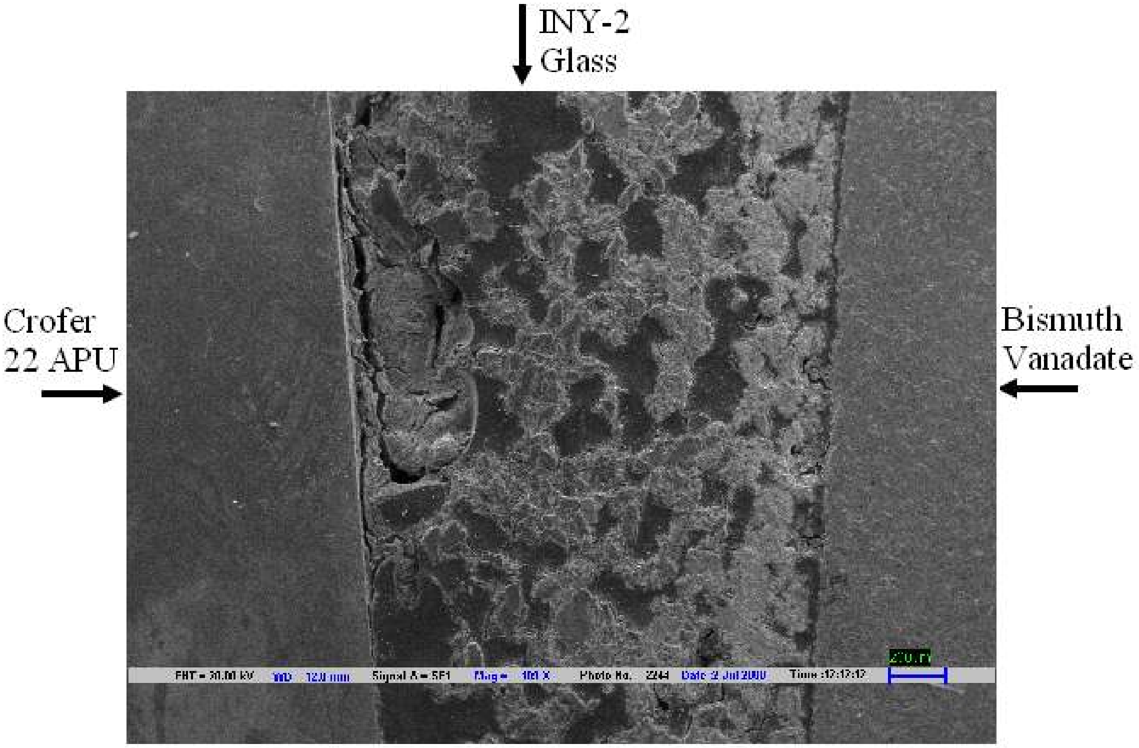

Figure 5.7 SEM micrograph of INY-2 glass sample heat treated at 800 ^oC for 100 hrs along with electrolyte (bismuth vanadate) steel (Crofer 22 APU)

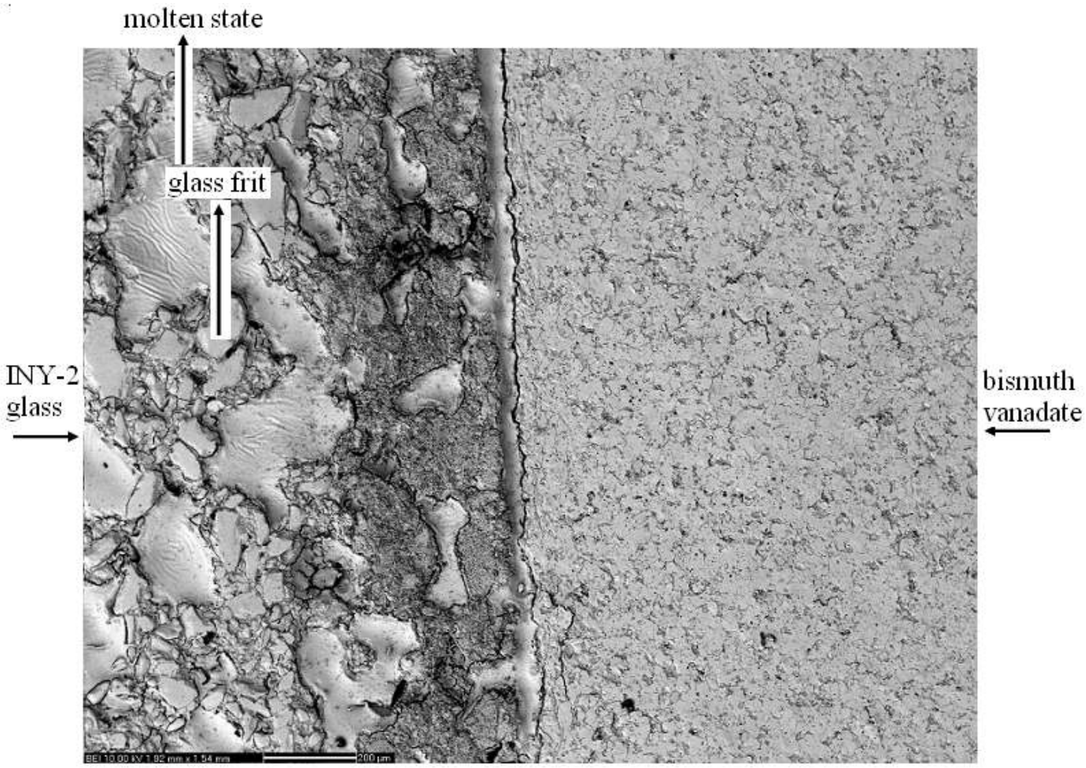

Figure 5.8 (a) SEM micrograph of sealant (INY-2) and electrolyte (bismuth vanadate) heat treated at 800 ^{o}C for 100 hrs

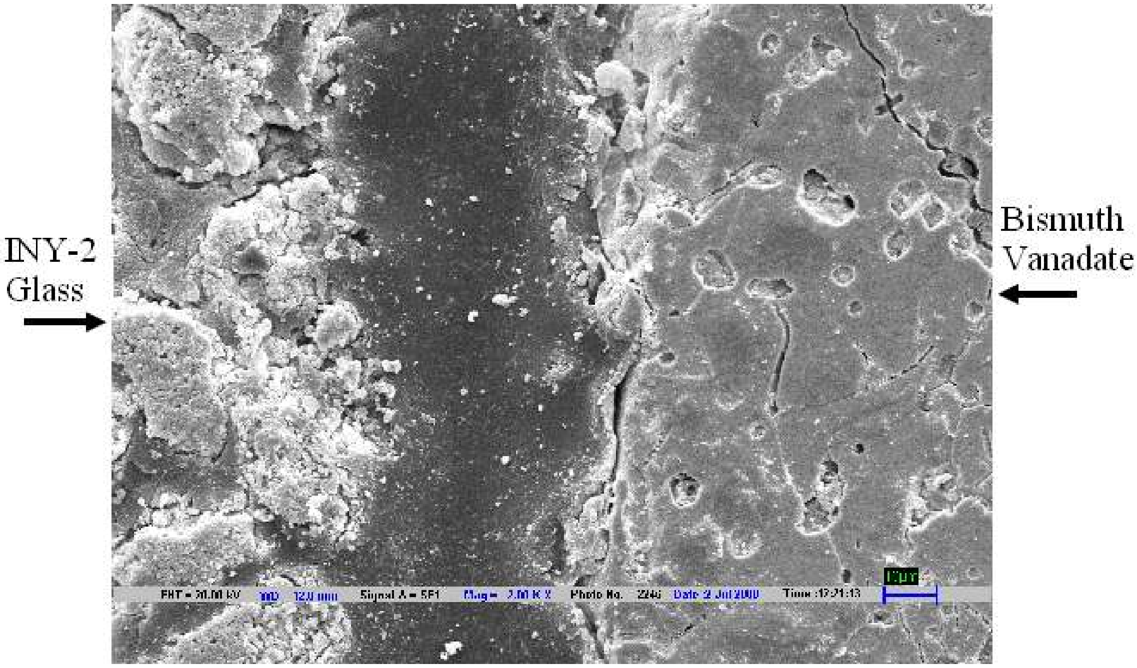

Figure 5.8 (b) SEM micrograph of sealant (INY-2) and electrolyte (bismuth vanadate) heat treated at 800 ^{o}C for 100 hrs

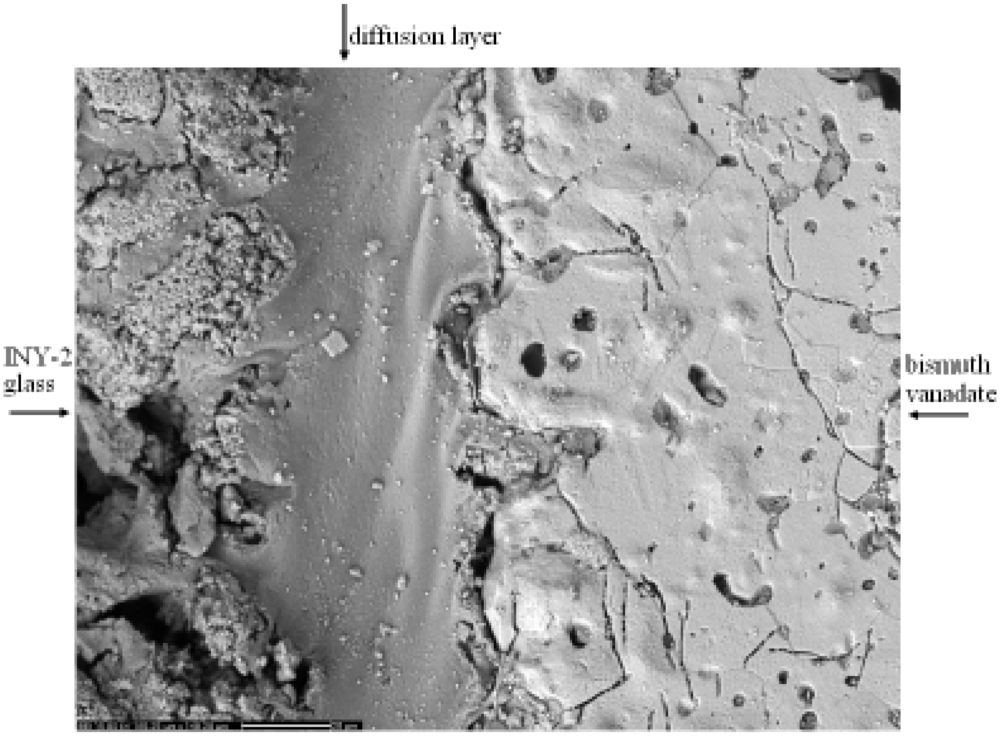

Figure 5.8 (c) SEM micrograph of sealant (INY-2) and electrolyte (bismuth vanadate) heat treated at 800 ^{o}C for 100 hrs

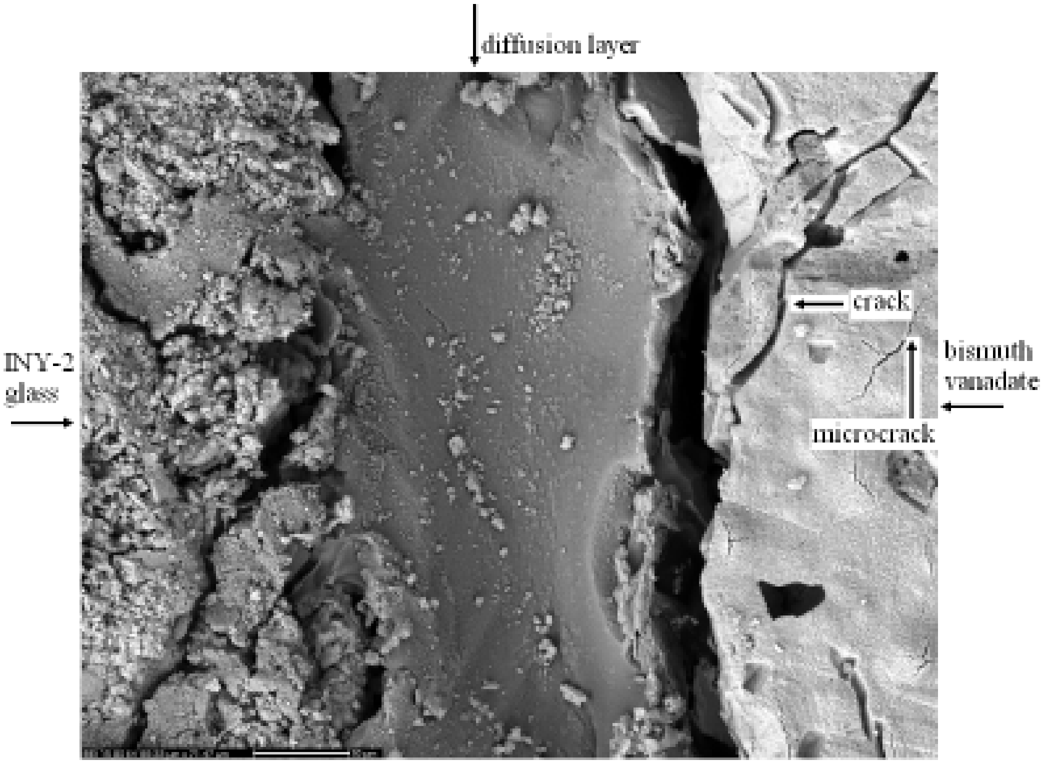

Figure 5.8 (d) SEM micrograph of sealant (INY-2) and electrolyte (bismuth vanadate) heat treated at 800 ^{o}C for 100 hrs

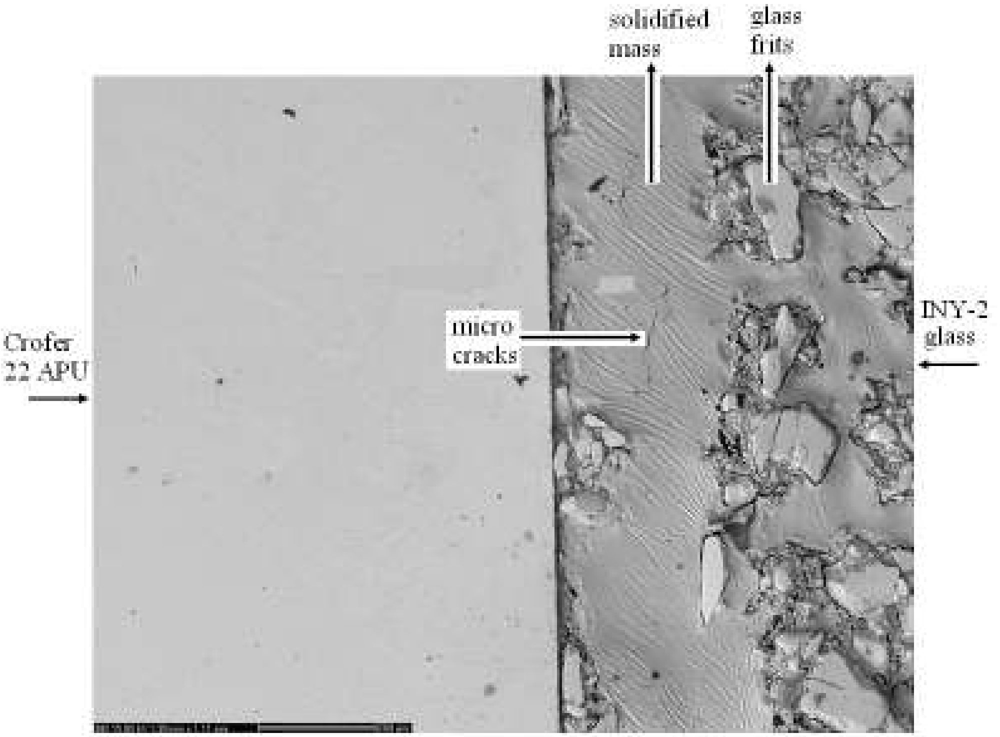

Figure 5.9 (a) SEM micrograph of interconnect (Crofer 22 APU) and sealant (INY-2) heat treated at 800 °C for 100 hrs

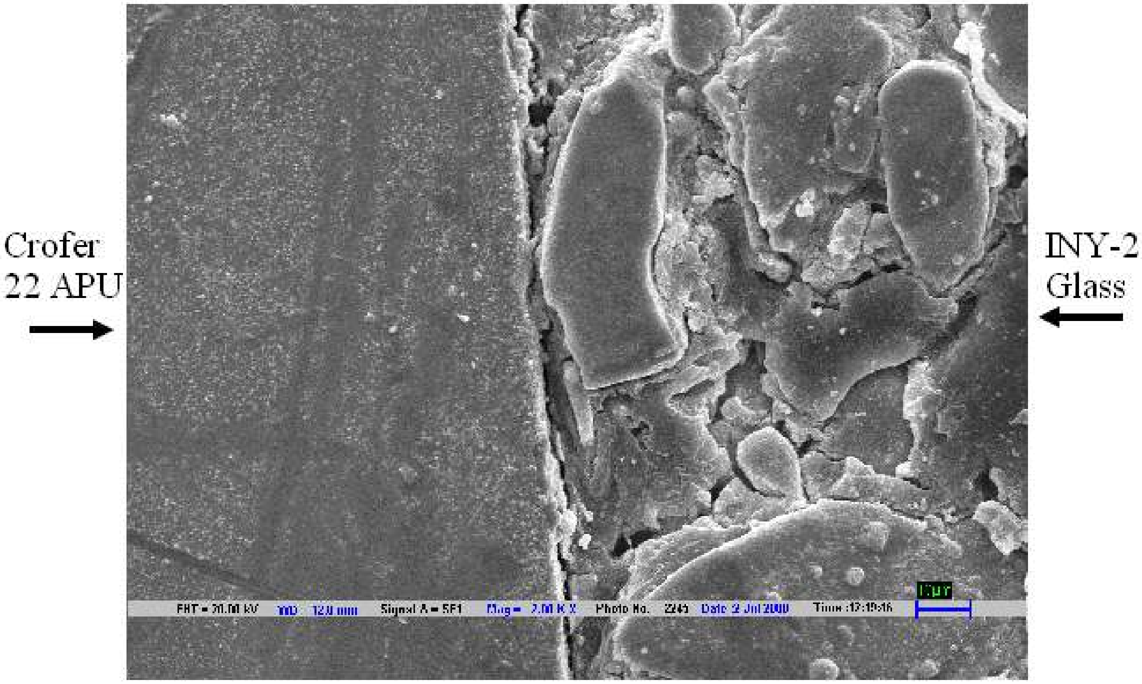

Figure 5.9 (b) SEM micrograph of interconnect (Crofer 22 APU) and sealant (INY-2) heat treated at 800 °C for 100 hrs

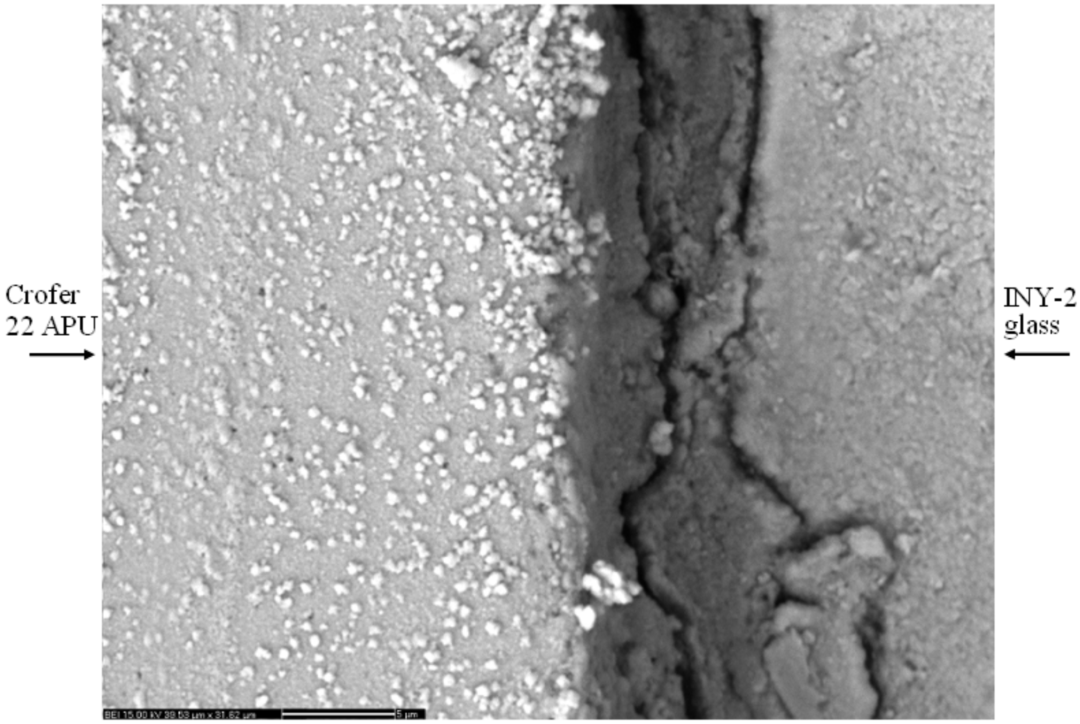

Figure 5.9 (c) SEM micrograph of interconnect (Crofer 22 APU) and sealant (INY-2) heat treated at 800 °C for 100 hrs

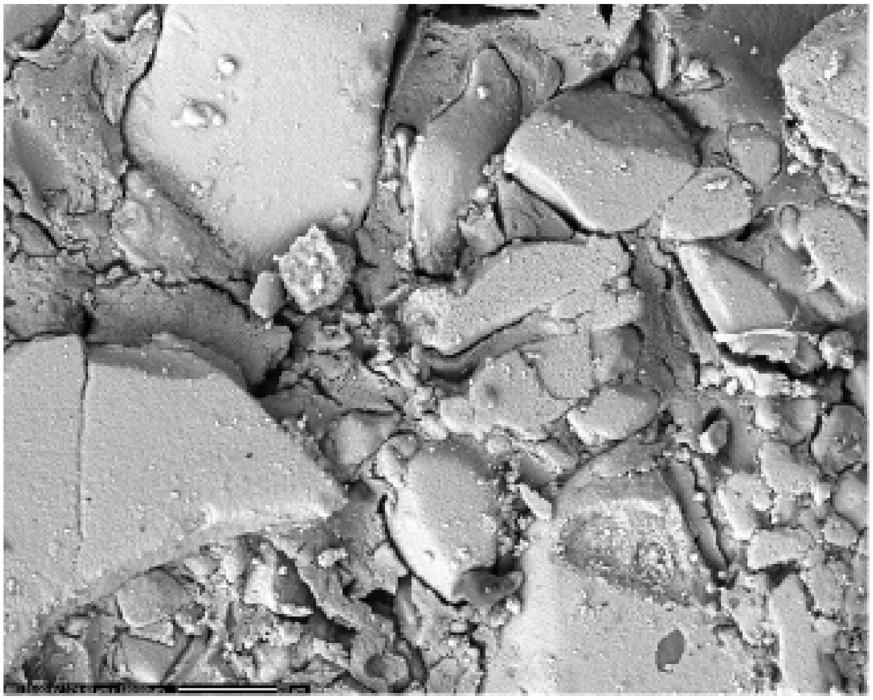

Figure 5.10 (a) SEM micrograph of sealant (INY-2) heat treated at 800 °C for 100 hrs

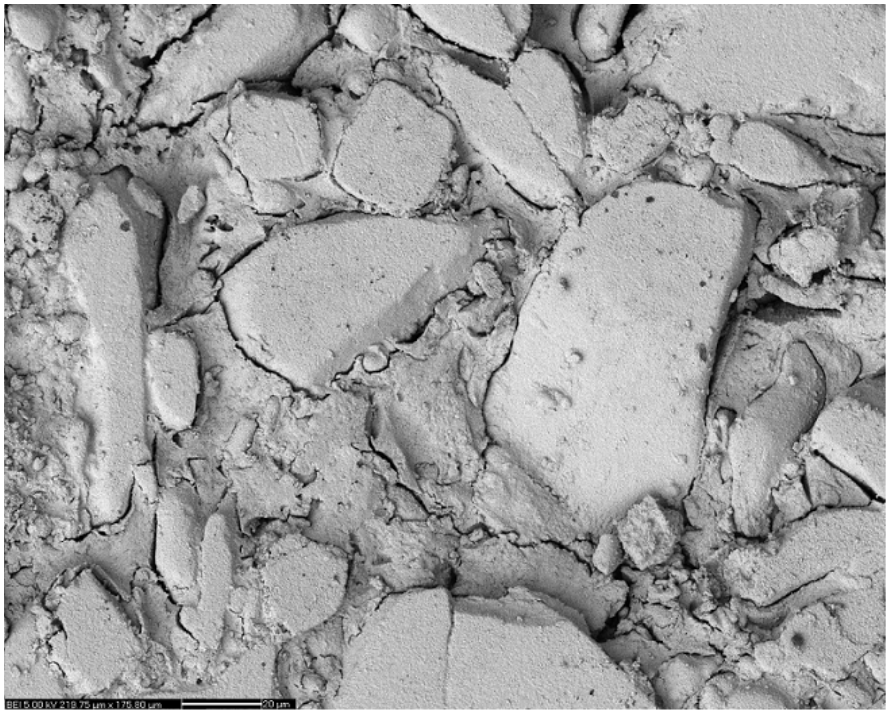

Figure 5.10 (b) SEM micrograph of sealant (INY-2) heat treated at 800 ^{o}C for 100 hrs

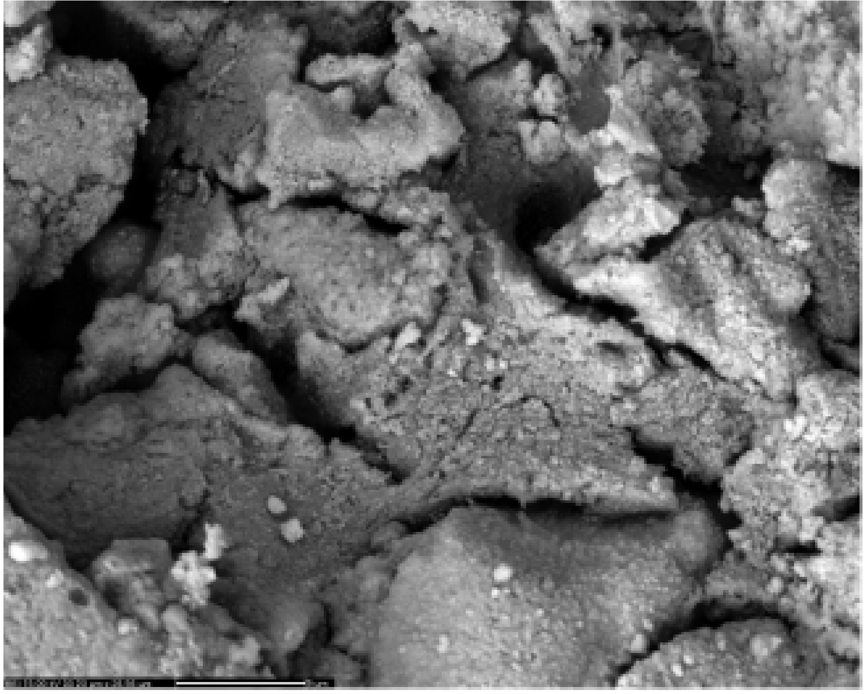

Figure 5.10 (c) SEM micrograph of sealant (INY-2) heat treated at 800 ^{o}C for 100 hrs

5.5.2.1 X-Ray Diffractograms of INY-2 glass sample with YSZ (electrolyte)

8YSZ was taken in pellet form and finely crushed INY-2 glass paste was applied on the surface of it. As described earlier the entire assembly was heated at 800°C for different duration. After that its X-ray diffraction is taken. When INY-2 glass sample was heat treated with YSZ (electrolyte) at 800 °C for 5 hrs time duration formation of zirconium yttrium oxide ($Zr_{0.82}Y_{0.18}O_{1.91}$)(tetragonal, ICDD card no. 82-1245), barium aluminum oxide ($BaAl_2Si_2O_8$) (hexagonal, ICDD card no. 77-0185), barium aluminum oxide ($BaAl_2O_4$)(hexagonal, ICDD card no. 82-1349), quartz (SiO_2)(86-1565) and barium silicate (Ba_3SiO_5)(tetragonal, ICDD card no. 26-0180) takes place (fig. 5.11).

When INY-2 glass sample with YSZ is further heat treated at 800 °C for 36 hrs time duration formation of zirconium yttrium oxide ($Zr_{0.82}Y_{0.18}O_{1.91}$)(tetragonal, ICDD card no. 82-1245), barium aluminum silicate, Ba($Al_2Si_2O_8$) (hexagonal, ICDD card no. 88-1048) and barium zinc silicate ($BaZnSiO_4$) (hexagonal, ICDD card no. 42-0335) takes place (fig. 5.12).

When INY-2 glass sample with YSZ is given heat treatment at 850 °C for 36 hrs time duration formation of zirconium yttrium oxide ($Zr_{0.82}Y_{0.18}O_{1.91}$)(tetragonal, ICDD card no. 82-1245), barium aluminum silicate, Ba($Al_2Si_2O_8$) (hexagonal, ICDD card no. 88-1048) and barium zinc silicate ($Ba_2Zn_3Si_3O_{11}$) (hexagonal, ICDD card no. 42-0335) takes place (fig. 5.13).

It is apparent from this study that the equilibrium phases appear as was observed during heat treatment. This study indicates that there is not much variation in structure th ough long hours heating was done. The report of similar work existing in literature also supports our findings [37]. The analysis indicate that glass and 8YSZ system is more compatable as compared to $Bi_4V_{2-x}Ti_xO_{11}$ system where the interfacial reaction over a long distance was observed.

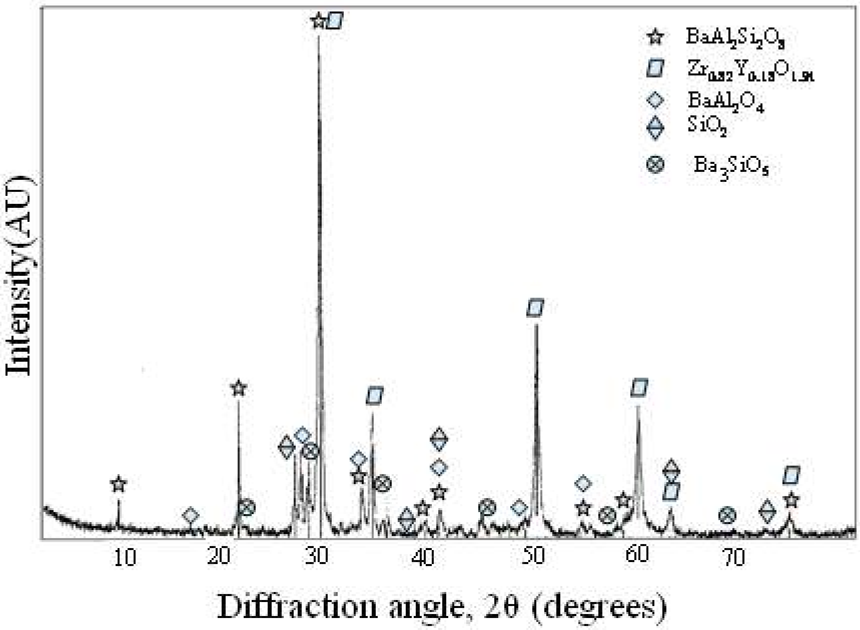

Figure 5.11 Glass sample INY-2 with 8YSZ heat treated at 800 °C for 5 hrs

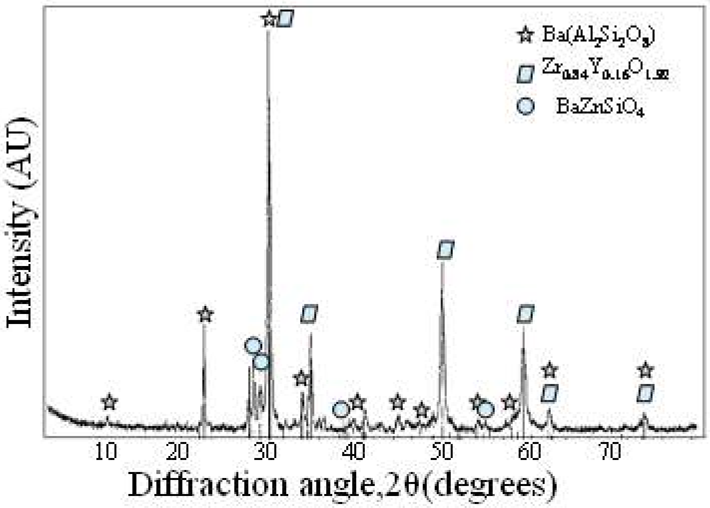

Figure 5.12 Glass sample INY-2 with 8YSZ heat treated at 800 °C for 36 hrs

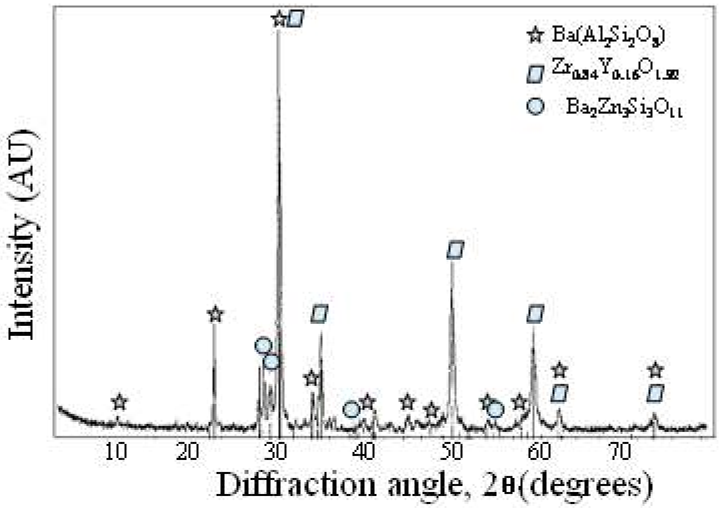

Figure 5.13 Glass sample INY-2 with 8YSZ heat treated at 850 °C for 36 hrs

References

[1] K. Ley, M. Krumplet, R. Kumar, J. Meiser, I. Bloom, J. Mat. Res. 11 (1996) 1489.

[2] S.-B. Sohn, S.-Y. Choi, G.-H. Kim, H.-S. Song and G.-D. Kim, J. Non-Cryst. Solids 297 (2002) 103.

[3] C. Lara, M. J. Pauscal, A. Duran, J. Non-Cryst. Solids 348 (2004) 149.

[4] N. Lahl, K. Singh, L. Singheiser, K. Hilpert, D. Bahadur, J. Mater. Sci. 35 (2000) 3089.

[5] D. Bahadur, N. Lahl, K. Singh, L. Singheiser, K. Hilpert, D. Bahadur, J. Electrochem. Soc. 151 (2004) A558.

[6] N. Lahl, K. Singh, L. Singheiser, K. Hilpert, D. Bahadur, J. Electrochem. Soc. 149 (2002) A607.

[7] C. Lara, M. J. Pascual, J. M. Prado, A. Duran, Solid State Ionics 170 (2004) 201.

[8] C. Lara, M. J. Pascual, R. Keding and A. Dur´an, J. Power Sources 157 (2006) 377.

[9] K. D. Meinhardt, J. D.Vienna, T. R. Armstrong, L. R.. Pederson, U. S. Pat. 6430966 (Aug. 13, 2002).

[10] S.-B. Sohn, S.-Y. Choi, G.-H. Kim, H.-S. Song and G.-D. Kim, J. Am. Ceram. Soc., 87 [2] (2004) 254.

[11] Z. Yang, J. W Stevenson and K. D. Meinhardt, Solid State Ionics 160 (2003) 213.

[12] Z. Yang, G. Xia, K. D. Meinhardt, K. Scott Weil and J. W. Stevenson, J. Mat. Eng. and Perf. 13 (2004) 327.

[13] Handbook of Fuel Cells – Fundamentals, Technology and applications, Interconnects, K. Hilpert, W. J. Quadakkers and L. Singheiser Volume 4, Part 8, pp 1037–1054 In (ISBN: 0-471-49926-9).

[14] H. P. Buchkremer, U. Dieckmann, L. De Haart, H. Kabs, U. Stimming and D. St¨over, in ‘Solid Oxide Fuel Cells’ (SOFC V), U. Stimming, S. C. Singhal, H. Tagawa and W. Lehnert (Eds), The Electrochemical Society Proceedings Series, Pennington, NJ, PV 97-40, p. 160 (1997).

[15] W. K¨ock, H. Martinz, H. Greiner and M. Janousek, in ‘Solid Oxide Fuel Cells’ (SOFC IV), M. Dokiya, O. Yamamoto, H. Tagawa and S. C. Singhal (Eds), The Electrochemical Society Proceedings Series, Pennington, NJ, PV 95-1, p. 841 (1995).

[16] P. Kofstad, ‘High Temperature Corrosion’, Elsevier Applied Sciences/Chapman and Hall, London (1988).

[17] W. Wersing, E. Ivers-Tiffee, M. Schiessl and H. Greiner, in ‘Proc. Int. Symp. Solid Oxide Fuel Cells’, O. Yamamoto, M. Dokiya and H. Tagawa (Eds), Nagoya, Japan, pp. 33–42 13–14 Nov. (1989).

[18] M Yashima. M. Kakihana and M Yoshimura, Solid State Ionics*,* 86/88 (1996) 1131.

[19] R. A. Miller, J. L. Smialek and R. G. Garlik, in Science and Technology of Zirconia, eds. A. H. Heuer and L. W. Hobbs, Advances in Ceramics, vol. 3*,* American Ceramics Society, Columbus, OH, 19 8 1, p. 24 1.

[20] R. Ruh, H. J. Garnett, R. F. Donagala and V. A. Patel, J. Am. Ceram. Soc.*,* 60 (1977) 399.

[21] H.L. Tuller and A.S. Nowick, J. Electrochem. Soc., 126 (1979) 209.

[22] S. J. Skinner and J. A. Kilner, Materials Today (31-37), March, 2003.

[23] E.M. Levin and R. S.Roth, Polymorphism of bismuth sesquixide. II. Effect of oxide additions on the polymorphism of Bi_2O_3, Journal of Research of the National Bureau of Standards-A, 68A (1964) 189.

[24] R.N. Vannier, G.Mairesse, F.Abraham, and G. Nowogrocki, Journal of Solid State Chemistry, 103 (1993) 441.

[25] P. Hagenmuller and W. Van Gool, “Solid Electrolytes”, Academic Press, New York/San Francisco/London (1978).

[26] R.N. Vannier, G. Mairesse, F. Abraham, and G. Nowogrocki, Solid State Ionics, 80 (1995) 11.

[27] Y. L. Yang, L. Qiu, W. T. A. Harrison, R. Christoffersen and A. J. Jacobson, J. Mater. Chem., 7(2) (1997) 243.

[28] L. Qiu, Y. L. Yang and A. J. Jacobson J. Mater. Chem., 1997, 7(2), 249.

[29] C.K. Lee, C.S. Ong, Solid State Ionics, 117 (3) (1999) 301.

[30] Ravi Kant, K. Singh, O.P. Pandey, Int. J. Hydrogen Energy, 33(1) (2008)455

[31] R. Maenner, E. Ivers-Tiff~e, W. Wersing, W.Kleinlien, Proc. 2nd Eur. Ceram. Soc. Conf. (Euro-Ceramics II), eds.: G. Ziegler, H. Hausner, Deutsche Keramische Gesellschaft (1991), p. 2085.

[32] F. Tietz, G. Stochniol, A. Naoumidis, Proc. 5th Eur. Conf. on Advanced Materials,

Processes and Applications (Euromat '97), eds.: L. A. J. L. Sarton, H. B. Zeedijk, Netherlands Society for Materials Science (1997), Vol. 2, p. 271.

[33] F. Tietz, in: Proc. 9th CIMTEC - World Ceramic Congress and Forum on New Materials, ed. P. Vincenzini, Techna Publishers S.r.l., Faenza, Italy, Vol. 24: Innovative Materials in Advanced Energy Technologies (1999), p. 61.

[34] Ruifang Wang, Zhe Lu, Chaoqian Liu, Ruibin Zhu, Xiqiang Huang, Bo Wei, na Ai and Wenhui Su, J. Alloys Comp. 432 (2007) 189.

[35] F. Smeacetto, M. Salvo, M. Ferraris, V. Casalegno, P. Asinari and A. Chrysanthou, J. Eur. Ceram. Soc. 28 (2008) 2521.

[36] S. Ghosh, P. Kundu, A.D. Sharma, R. N. Basu, H. S. Maiti, J. Eur. Ceram. Soc. 28 (2008) 69.

[37] S. Ghosh, A.D. Sharma, P. Kundu, S. Mahanty and R. N. Basu, J. Non-Cryst. Solids xxx(2008)xxx-xxx

Chapter 6

Conclusions and future scope

Overview

The present chapter summarizes the results of various experiments described in previous chapters. The effect of different substitutions has led to a spectrum of new properties in the glass. Their role as network former and network modifier has led to certain conclusions. The summary of all the results of different series is described in this chapter. At the end the suggestion for future work on the basis of results obtained in this work is given.

Glass sealant is an essential part of planar SOFC. Various sealing materials have been tested in real working conditions of the SOFCs. However, glass and glass ceramics meet most of the requirements. In the present study, glasses of the series $40SiO_2$-30BaO-20ZnO-(10-x)B_2O_3-xM_2O_3, x =0, 2.5, 5.0, 7.5, 10; (M=Al, La, Mn, Y) were selected on the basis of earlier study. The as prepared glasses are characterized using various experimental techniques such as XRD, DTA/TGA, Dilatometer, SEM and conductivity measurement to check their suitability to be used as sealing materials. Sixteen glasses were prepared by conventional casting and splat quenching technique. All the glasses exhibit amorphous nature when characterized by XRD. The addition of intermediate oxides to replace network former B_2O_3 in the above series leads to increase the T_g, T_c and T_{pc} in all the samples. In the present glasses the amount of modifier is high owing to the existence of a large number of non-bridging oxygen ions. M^{3+} cations can attain a co-ordination number of 6, so non-bridging oxygen gets converted into bridging oxygen with the addition of M_2O_3 by replacing B_2O_3 in these samples. Therefore the conversion of non bridging oxygen to bridging oxygen leads to increase in T_g, T_c and T_m of these glasses. The crystallization peak maximum is seen to increase with increase in heating rate. The thermal data show that the sample INA-4 shows maximum activation energy value and hence is most stable sample for future investigation. Theoretical calculation done by taking DTA data for the calculation of thermals stability of glass sample shows that INA-4 exhibits highest thermal stability as compared to other glass samples of the present series.

Dilatometer data of present glass series conclude that the values of TEC obtained in this series are very near to the specified range which is the requirement of SOFC. The crystallization kinetic studies of INA-1 sample formation of hexacelsian phase ($BaAl_2Si_2O_8$) is observed when heat treated at 850 ^oC, which was also confirmed by DTA/ Dilatometer, because the TEC value of hexacelsian phase is in the same range that is obtained in dilatometer study. The microstructures of INA-1 sample which have been given heat treatment at 800 ^oC and 850 ^oC at heating rate of 5 ^oC/min indicates that two crystalline phases nucleates simultaneously in such a way that one phase nucleates epitaxially and another phase grows laterally. However, with passage of time the nucleation of another solid solution phase occurs in the matrix as faceted phase. The growth phenomenon continues till they merge in each other. At higher temperature heat treatment metastable solid solution phase which nucleates in the glass matrix is further converted into crystalline phase within the glass matrix. Further heat treatment at 850 °C for 10 hours shows the peak splitting which is an indication of internal distortion in the system. Crystallization in the glass appears to start from the periphery of the glass, thus giving the signs of the dominance of surface crystallization mechanism for the crystallization process which occurs as time proceeds. When the sample is given heat treatment for higher temperature i.e. for 900 °C it indicates that the nucleation of other phase is restricted with addition of Al_2O_3 in higher concentration. In sample INA-3 crystallization process starts uniformly and crystalline growth is taking place in lateral and epitaxial direction. The feature resembles with dendritic structure which is stable one. Nucleation of single $BaAl_2Si_2O_8$ phase in INA-4 sample at 800 °C for 1 hr and 10 hrs indicate that the glass matrix is very stable and tight. However, 10 hrs diffractogram indicates that the glass matrix is in highly strained condition as base line is not smooth. On increasing the heat treatment duration $Ba_2Zn_3Si_3O_{11}$ is converted into $BaZnSiO_4$. All formed structures in INA glass series indicate that crystalline phase has nucleated as spherulite structure. These features are also common for glasses containing Al_2O_3 but the size of spherulite becomes smaller. This indicates the addition of Al_2O_3 makes the nucleation process sluggish. As the alumina content in INA-5 sample is maximum and alumina hinders the formation of crystallites, most of the sample remains amorphous and only one phase segregates. When this sample is further heat treated for 900 °C for 1 hr time duration because of volatile nature of Zn earlier formed phase $Ba_2Zn_3Si_3O_{11}$ is converted into $BaZnSiO_4$. In samples INA-4 and INA-5 crystalline growth is hindered because of increased amount of Al_2O_3. If these samples are heat treated for long duration crystalline growth may take place. Since Al_2O_3 provides stability to glass, it hinders the nucleation process thus making glass more suitable for higher temperature application.

In INL glass series DTA data shows the increasing trend in in T_g, T_c and T_m values. The intermediate cation La^{3+} may have higher oxidation number which converts more non bridging oxygen into bridging oxygen. When lanthanum content was varied from 2.5% to 5.0%, it acts as network modifier. On the other hand, when lanthanum content is increased from 5.0% to 10%, it provides strength to the matrix and acts as network former. High content of La_2O_3 reduces the tendency of phase separation as compared to pure sample where La_2O_3 is zero mol%. TGA data of INL series has negative value of change in weight % for INL-1 glass sample which is because of the fact that Zn being volatile in nature comes out from the matrix while heating. As the lanthanum content is increased it tends to decrease the loss of Zn from the matrix by absorbing it in the glassy network. It also increases the compactness of the glass matrix. Theoretical calculation done by taking DTA data to calculate the thermal stability of the glass samples in INL series shows that INL-3 glass sample has maximum value of thermal stability parameter. Dilatometer data shows that with increase in La content the value of TEC is increasing which depends on the rigidity of the glass matrix. It is possible that with the addition of La_2O_3, the covalent character in the glass composition is increasing.

XRD data of INL series confirms the presence of Al_2O_3 in these glass samples which is picked up from alumina crucible during melting process. The EDS and AAS (atomic absorption spectroscopy) studies confirmed that alumina uptake is around 5-7%. Sample INL-1 heat treated at 900 ^oC for 1 hour shows that with an increase in temperature of heat treatment formation of BZS phase is taking place by replacing $Ba_4La_6O(SiO_4)_6$ phase and the rest of the phases remains as such. Sample INL-2 when heat treated at 850 ^oC for 20 hrs indicates that lanthanum is in glass matrix which provides strength to the glass matrix. After a heat treatment of 900 ^oC to INL-2 glass sample, the shifting of peaks at lower angle with broadening and splitting in peaks occurs. This indicates the disordering in the crystalline phases. When INL-2 glass sample is heat treated at 900^oC formation of $Ba(Al_2Si_2O_8)$ takes place and this phase tries to transform into $BaAl_2Si_2O_8$. From XRD pattern it seems that matrix is in strained condition because nucleation is hindered or it is also possible that crystallites of very fine size and in small amount may be nucleating.

Heat treatment results of INL-3 glass sample at 800 ^oC indicate that in the beginning the viscosity of the sample is high due to which and the nucleation of other phases is hindered. This causes the nucleation of the solid solution phase comprising of bigger crystalline phase having bigger lattice. All the formed phases which nucleate after 10 hrs heat treatment remains as such when heat treatment duration is increased to 100 hrs. This concludes that the system is very stable at 800 ^{o}C as no other phases nucleate. Contrary to INL-1 and INL-2 glass samples, in INL-3 glass sample the concentration of lanthanum is sufficient to induce the crystallization of $Ba_4La_6O(SiO_4)_6$ phase in the glass matrix. The nucleation of this phase occurs at the initial stage of heat treatment i.e. at 800 ^{o}C when sample INL-3 is heat treated for 1 hr. Nucleation of this phase again occurs in INL-4 glass sample also. In this series, initially $ZnSiO_3$, $BaAl_2Si_2O_8$, $Ba_4La_6O(SiO_4)_6$ and $BaAl_2O_4$ phases are formed. As the duration of heat treatment is increased $Ba_4La_6O(SiO_4)_6$ phase is dissolving especially when La_2O_3 content is up to 5 mol%. As the content of La_2O_3 increases all these phases again come into picture. However, the volume fraction of $Ba_4La_6O(SiO_4)_6$ phase decreases with the increase in heat treatment duration at higher temperatures. In all the samples the volume fraction of $BaAl_2O_4$ phase is increasing with the increase in temperature.

The DTA plots in INM series shows two exothermic peaks. This effect is prominent in INM-1 sample. As the %age of Mn_2O_3 increases in the glass up to 7.5 mol% the exothermic peaks become sharp which indicates that with the addition of Mn_2O_3 phase separation tendency is hindered. As the %age of Mn_2O_3 increases in the matrix it act as network former. Conclusively, the addition of Mn_2O_3 increases the connectivity of glass network. DTA data shows that T_g, T_c and T_{pc} increases in INM-1, INM-2 and INM-3 glass samples. On the other hand, further addition of Mn_2O_3 in glass leads to decrease in the thermal properties of INM-4 glass. The DTA curve of INM-4 sample even has 3 exothermic peaks. It means that, in this glass where B_2O_3 is absent, Mn_2O_3 remains in lower oxidation state which acts as glass modifier. Due to this reason, the tendency of phase separation is increased in INM-4 sample. TGA data shows that INM-4 glass sample is showing minimum weight change in temperature range of 50-1000 ^{o}C so it may act as stable sample among the INM series. Theoretical calculations shows that INM-4 sample has maximum value of stability parameter among the whole INM series.

Dilatometer data shows that with the increase in manganese content softening temperature (T_s) value goes on increasing. This is because decrease in B_2O_3 content lead to formation of boron-oxygen triangle which loosened the Si-O network. More is the value of B_2O_3, lesser is the softening temperature value.

XRD data of INM-1 glass sample when heat treated at 850 ^{o}C for 10 hrs shows transition of $BaZnSiO_4$ phase to $Ba_2Zn_3Si_3O_{11}$ and as the heat treatment progresses, these phases get rearranged or dissolved in the matrix to pave the way to form the more stable phases. The nucleation of large number of phases even at low temperature indicate that activation energy required for nucleation of these phases is low as compared to other glass series studied here. If these are intact in the glass matrix for large duration it can provide good properties as a sealant to cope up the expansion of different components of SOFC. As the time of heat treatment is increased, these phases get dissolved and nucleation of other phases occurs. This tendency may lead to reactivity of the glasses more with other components of SOFC.

Looking at the X-ray diffractogram it can be said that the matrix is not in a relaxed situation. When INM-2 glass is given heat treatment at 800 ^{o}C for 1 hr the glass matrix is in strained condition as phases nucleated are not stable because of nucleation of large number of phases. When INM-2 glass is heat treated at 850 ^{o}C for 20 hrs it provides sufficient time for dissolution of metastable phases and nucleation of stable phases. This provides stability in glass matrix as number of crystalline phases is reduced. When INM-3 glass sample is given heat treatment at 900 ^{o}C for 1 hr time duration $Ba_2Zn_3Si_3O_{11}$ phase again transforms to $BaZn_2Si_2O_7$ phase, $BaAl_2Si_2O_8$ phase gets converted into $BaAl_2O_4$ phase and SiO_2 nucleates as a new phase. INM-4 glass shows different behavior as number of phases nucleated is $BaAl_2Si_2O_8$ and Ba_2MnO_3. These phases seem to be thermodynamically stable and are not changing even after long hour heat treatment. Formation of polymorphs of barium aluminum silicate is unexpected as no Al_2O_3 was incorporated in the batch. Evidently, chemical interactions between alumina crucible and the glass melt took place due to unavoidable uptake of the former from the crucible during melting. When INM-4 glass sample is heat treated at 800 ^{o}C for 10 hrs time duration nucleation of crystalline phase in the glass matrix has occurred. These phases are uniformly distributed through out the structure and thus provide strength to this sample.

In INY series DTA data shows that there is a systematic increase in T_g, T_c and T_{pc} of the as cast glasses as the Y_2O_3 increases with respect to B_2O_3. As the amount of Y_2O_3 increases in the glasses while substituting equivalent amount of glass formers (B_2O_3), the intermediate oxide (Y_2O_3) might have worked as network former. Therefore, the number of non-bridging oxygen created by the modifiers (BaO, ZnO) in glass matrix might be converted into bridging oxygen by Y_2O_3. Due to this reason, the T_g, T_c and T_{pc} increases in the present glass sample with addition of Y_2O_3. Moreover, Yttrium being larger size metal as compared to B^{3+} offer higher coordination number so it can associates more NbO created by modifier (ZnO, BaO) in glass matrix. The TGA curve of the entire glass sample is not following any trend. INY-1 glass sample exhibit weight loss when glass was investigated in the range of 50-1000°C. It indicates that the glass is having lot of strain and get relaxed during the experiment. At higher addition (10 mol%) Y_2O_3 again creates some stress and strain within glass matrix as compared to INY-2 and INY-3 glass samples which is also clear from the activation energy data of the present series. TGA data of INY series shows that there is minimum weight loss in INY-2 glass sample so it is considered as the most stable sample in INY series. Thermal analysis data also shows that INY-2 glass sample has maximum value of thermal stability parameter among the INY series. The value of activation energy is also maximum for INY-2 glass sample. Dilatometer data shows that the addition of Y_2O_3 in glass composition might have induced some trace of crystallinity during quenching of the glasses which is manifested from the XRD pattern of these glasses before heat treatment. The XRD pattern of as cast glass has sharp hump instead of broad hump, in general, manifestation of amorphous nature. When INY-1 glass sample is given heat treatment at 900 °C for 1 hr yttria remains as such in the network. The major phase that precipitates in glass INY-2 after heat treatment at 900 °C for 1 hr is hexacelsian. The glass matrix seems to be stable one as nucleation is a delayed process even after heat treatment at higher temperature. When INY-2 glass sample is given heat treatment at 750 °C for 1 hr time duration, the sample remains amorphous. On giving further heat treatment i.e. at 800 °C for 1, 10, 100 hrs different phases gets nucleated. This concludes the stability of INY-2 glass sample. A careful observation of XRD (INY-2) clearly indicates that the nucleation and growth of $Y_2Si_2O_7$ and Y_2SiO_5 phases are very less as XRD peaks are embedded in large amorphous background which is a positive sign to use this sample as a sealant in SOFC. Y^{3+} here is acting as network former and becomes part of glassy matrix. Zn^{2+} being volatile in nature will always try to come out and hence precipitate in glassy matrix as $Ba_2Zn_3Si_3O_{11}$ phase. The long hour annealing at 800 °C indicate that the glass is stable and the dissolution and dissociation of phases do not occur. Moreover, considering its applicability in SOFC it can be said that this glass can provide good compatibility with system at high operational temperature (nearly 1000^{o}C).

Micrographs of INY-2 glass sample which is heat treated at 800^{o}C for 100 hrs time duration shows that nucleation phenomenon is very sluggish in nature. The structural features indicates that the crystallization phase come out from the glass matrix and grows. In INY series INY-2 sample exhibits higher resistivity than other samples. It is again a manifestation that this sample shows higher thermal stability with higher activation energy for crystallization.

The range of resistivity of glass sealant to qualify for SOFC application should be more than 2 KΩcm. The values of resistivity for our as prepared glass series lie well above this range. For glass samples having Al_2O_3 as intermediate the maximum value of resistivity is 5.4MΩ for INA-4 glass sample. In lanthanum doped series the value of resistivity is 2.4 for INL-4 glass sample.

After analyzing all the four series it is concluded that INL-3 and INY-2 samples of INL and INY series are showing best results in TGA (change in % weight), DTA (thermal stability), dilatometer (thermal expansion coefficient) and XRD and SEM (nucleation phenomenon) when heat treated at various temperatures for different time durations. These glasses were selected for interaction study. After giving 100 hrs heat treatment at 800 ^{o}C to the entire assembly (Crofer 22 APU-glass-electrolyte) it is concluded that sample INL-3 does not have any appreciable interaction with interconnect because of its TEC mismatch. After long hour heat treatment a liquid state reaction is taking place at the interface. Because of thermal mismatch cracks are observed at glass and electrolyte interface. The reactivity of electrolyte and glass is not completed even at long hour heat treatment. At the interface of interconnect and glass lamellar fluid flow is observed. Considering INY-2 glass sample under similar condition i.e. heating at 800 ^{o}C for 100 hrs in the form of assembly (Crofer 22 APU-glass-bismuth vanadate), it is concluded that sample INY-2 does not adhere with interconnect because of TEC mismatch and no bond formation among these two materials occurs. But the glass was not completely crystallized even after long hour heat treatment which is a very good property to use this glass as a glass sealant in SOFC. At the interface of glass and electrolyte interdiffusion has occurred. Reaction at the interconnect and glass interface is not observed. After long hour heat treatment melting is occurring in electrolyte and development of cracks is observed at its surface. It is concluded that because of thermal expansion mismatch in all the three materials, this system is not compatible as formation of cracks occurs.

Interaction among glass and YSZ indicates that equilibrium phases are observed after giving heat treatment to the system but not much variation in the structure is observed. It is concluded that YSZ is more compatible with the present glass sample (INY-2) as compared to bismuth vanadate.

After discussing all the glass series independently, it is concluded that out of four selected samples (INA-4, INL-3, INM-4 and INY-2) INL-3 and INY-2 samples are giving suitable results for its use in SOFC as a sealant material. These two glasses are thermally and microstructurally very stable.

It is hereby concluded that INL-3 will show best results when it used at 800 ^{o}C for long hour duration which is clear from its change in weight %, activation energy, thermal stability and dilatometer data. Similarly INY-2 glass sample is giving best results i.e. very less change in weigh %, very high activation energy, thermal stability and TEC value for its use in SOFC at 1000 ^{o}C as a sealant.

Future scope of the work

Details in interaction, thermal and structural studies of lanthanum and yttrium series of all glass composition exhibits high TEC and phase stability even at high temperature. These glasses are more stable as compared to other glasses comprising of aluminum and manganese. For more promising and favorable results the study of interaction of glass sealant with 8YSZ and Crofer 22 APU should be done for 100 and 1000 hrs. The new reaction surfaces or the interface thus formed should be analyzed. Apart from this, new glass series comprising of yttrium and lanthanum should be developed and studied in detail. The interaction study among the INL series with 8YSZ can be done. Moreover, it is essential to test the seal under real SOFC stacking unit under operating environment.